Hot tearing of Mg-Ca binary and Mg-Ca-Zn ternary alloys

Doctoral Thesis

(Dissertation)

to be awarded the degree

Doctor of Engineering (Dr.-Ing.)

submitted by

Jiangfeng Song

from Chongqing/VR China

approved by the Faculty of Natural and Materials Science,

Clausthal University of Technology

Date of oral examination

26.01.2016

Dean

Prof. Dr. rer. nat. Winfried Daum

Chairperson of the Board of Examiners

Prof. Dr.-Ing. Dieter Meiners

Supervising tutor:

Prof. Dr.-Ing. Babette Tonn

Reviewer:

Prof. Dr.-Ing. Karl Ulrich Kainer

Name, Vorname

Song, Jiangfeng

Datum:

04.05.2016

EIDESSTATTLICHE ERKLÄRUNG

Hiermit erkläre ich an Eides Statt, dass ich die bei der Fakultät für Natur- und Materialwissenschaften der Technischen Universität Clausthal eingereichte Dissertation selbständig und ohne unerlaubte Hilfe verfasst und die benutzten Hilfsmittel vollständig angegeben habe.

Unterschrift

Name, Vorname | Datum:

Song, Jiangfeng | 04.05.2016

EIDESSTATTLICHE ERKLÄRUNG

Hiermit erkläre ich an Eides Statt, dass die eingereichte Dissertation weder in Teilen noch in Ihrer Gesamtheit einer anderen Hochschule zur Begutachtung vorliegt oder vorgelegen hat und dass ich bisher noch keinen Promotionsversuch unternommen habe.

Unterschrift

Abstract

Hot tearing is known as one of the most fatal solidification defects commonly encountered during casting practice. Although it has been investigated for decades, it is still not fully understood yet. As most of the Mg alloys are first prepared by casting, their ingots must have superior quality with less casting defects for the further processing. Hence their castability, especially the resistance to hot tearing must be an important casting characteristic to be investigated. Due to the extensive potential biodegradable and automotive applications of binary Mg-Ca and Mg-Zn-Ca ternary alloys, it is of great importance to investigate their hot tearing behaviour.

In the present work, the crack susceptibility coefficient (CSC) of binary Mg-Ca alloys was predicted using thermodynamic calculations based on Clyne and Davies model. The predicted CSC was compared with the experimental hot tearing susceptibility (HTS). The HTS of binary Mg-Ca alloys and Mg-Ca-Zn alloys were investigated with a constrained rod casting (CRC) apparatus equipped with a load cell and data acquisition system. The initiation of hot tearing was monitored during solidification. The effects of mould temperatures (250 ^{0}C and 450 ^{0}C) on hot tearing were also investigated. The formed tears were evaluated using X-ray tomography and the crack volumes were measured. Microstructures and fracture surfaces were investigated using XRD, OM and SEM. Residual strain at the junction area were measured by neutron diffraction. Besides, the solidification process as well as hot tearing indicator (HTI) was simulated with ProCAST.

The experimental results show that HTS decreases with increase in initial mould temperature from 250 to 450 ^{0}C. The initiation of hot cracks was monitored during experiments and it corresponds with a force drop or a sudden change of force increment on the force-temperature-time curves. The critical solid fraction at which hot cracks form is determined according to the thermodynamic calculation with the Pandat software using the Scheil model. The microstructures and fracture surfaces of Mg-Ca alloys and Mg-Ca-Zn alloys show that the hot tears propagate along the dendritic region or grain boundaries through thin film rupture and liquid metal embrittlement of solid bridges. The results also show that the grain size, second phases, freezing range and the amount of eutectic are important factors to HTS. The HTS of binary Mg-Ca alloys and ternary Mg-Ca-Zn alloys is simulated using the stress model (HTI) implemented in the ProCAST software. The HTI is defined as the accumulated plastic strain in the last stage of solidification. The predictions of HTI were validated with the experimental measurements.

List of symbols and abbreviations

f_l	Liquid fraction
t_V	Vulnerable time period where hot tearing may develop
t_R	Time available for the stress-relief process
f_s	Solid fraction
t_{cr}	Time when feeding becomes inadequate
t_{coh}	Time when solid fraction at the coherency point
$\dot{\varepsilon}_{\max}$	Maximum strain rate
G	Temperature gradient
λ_2	Secondary dendrite arm spacing
β	Shrinkage factor
μ	Viscosity
ΔT_0	Solidification interval
Δp_{max}	Maximum pressure drop the mushy zone can bear
v_T	Velocity
T	Temperature
$\dot{\varepsilon}_{nuc}$	Critical strain rate to nucleate
$\dot{\varepsilon}_{prop}$	Critical strain rate to propagate
e	Liquid film thickness
h	Gauge length
λ	Half the grain size
a	Length of the tear
p_c	Cavitation pressure
p_m	Metallostatic pressure
K	Permeability of the mushy zone

η_L	Viscosity of the liquid
$\dot{\varepsilon}_{crit}$	Critical strain rate
d	Grain size
L	Length of mushy zone
γ	Surface tension
V	Velocity of solidification front velocity
f_v	Cavity fraction
$\frac{\partial f_v}{\partial t}$	Contribution to the cavity
d	Cavity diameter
σ	Stress
γ_e	Surface tension of liquid metal
E	Young's modulus of the mush
Q	Activation energy
R	Gas constant
d_{crit}	Critical diameter of cavity
b	Final grain diameter
D_{crit}	Critical diameter
w_{crack}	Maximum crack width
f_{length}	Crack length factor
$f_{location}$	Crack location factor
Φ	Maximal diameter of middle column where hot cracks occurred
s^{-1}	Per second
wt.%	Weight percent
e_{ht}	Hot tearing indicator
$\bar{\varepsilon}_{ht}^{p}$	Critical accumulated effective plastic strain

$\dot{\varepsilon}^{p}$	Effective plastic strain rate
t_C	Time when the coherency temperature is reached
t_S	Time when the solidus temperature is reached
:	The dyadic tensor
BN	Boron nitride
T_{mould}	Mould temperature
TC	Thermocouple
T_i	Hot tearing initiation temperature
f_{si}	Hot tearing initiation solid fraction
ε_{hkl}	Lattice strain
d_{hkl}	Lattice spacing of planes
θ_{hkl}	Diffraction angle
d_{hkl}^{0}	Lattice spacing in the stress-free materials
θ_{hkl}^{0}	Diffraction angle in the stress-free materials
FR	Freezing range
T_s	Solidus temperature
ΔT_s	Susceptible freezing range
f_{le}	Fraction of eutectic liquid at eutectic temperature
f_i	Fraction of intermetallic
T_l	Liquidus temperature
$T_{0.9}$	Temperature at solid fraction of 0.9
$T_{0.99}$	Temperature at solid fraction of 0.99
f_{lt}	Liquid fraction at the onset of $Mg_6Ca_2Zn_3$ formation
CSC	Crack susceptibility coefficient
HTS	Hot tearing susceptibility

XRD	X-ray diffraction
OM	Optical microscopy
SEM	Scanning electron microscopy
HTI	Hot tearing indicator
RDG	Rappaz, Drezet, and Gremaud's criterion
HSC	Hot tearing susceptibility coefficient
CRC	Constrained rod casting
PSM	Permanent star-shaped mould
HTS_{PSM}	Hot tearing susceptibility of permennant star-shaped mould
HCS	Hot cracking susceptibility
HTI	Hot tearing index
LVDT	Linear variable differential transformer
BL	Brightness level
PC	Personal computer
PSN	Particle stimulated nucleation
DC	Direct chill
OPS	Oxide Polishing Suspensions
EDX	Energy Dispersive X-ray Spectroscopy
FWHM	Full width of half maximum
HTC	Heat transfer coefficient

Table of contents

Abstract i

List of symbols and abbreviations ii

Table of contents vi

1 Introduction 1

2 Literature review 3

2.1 Hot tearing models 3

2.1.1 Clyne and Davies' Model 3

2.1.2 Katgerman's Model 4

2.1.3 RDG Criterion 4

2.1.4 Suyitno's Criterion 5

2.1.5 Model assessment 6

2.2 Experimental methods used to evaluate the hot tearing 7

2.2.1 Ring mould 7

2.2.2 Constrained rod casting (CRC) tests 8

2.2.3 Instrumented constrained rod casting tests 11

2.2.4 Other methods 14

2.3 Factors influencing hot tearing 16

2.3.1 Intrinsic factors 16

2.3.2 External factors – casting parameters 18

2.4 Hot tearing of magnesium alloys 19

2.4.1 Binary alloys 19

2.4.2 Ternary alloys 21

2.4.3 Other alloys 23

2.5 Mg-Ca and Mg-Zn-Ca alloys 24

2.6 Numerical simulation of hot tearing 25

2.6.1 Simulation methods 25

2.6.2 A new 3-D granular model 27
3 Motivations and objectives 29
4 Experimental procedure and simulation 30
4.1 Experimental procedure 30
4.1.1 Casting 30
4.1.2 Hot tearing apparatus 31
4.1.3 Typical hot tearing curves 32
4.1.4 Evaluation of the hot tears 33
4.1.5 Characterization of microstructure and fracture surface 34
4.1.6 Residual strain measurement 34
4.2 Numerical simulation by ProCAST 36
4.2.1 Geometry and mesh 36
4.2.2 Materials properties 37
4.2.3 Boundary and initial conditions 37
4.2.4 Simulation results analysis 37
5 Results 38
5.1 Hot tearing of Mg-xCa binary alloy 38
5.1.1 Chemical composition 38
5.1.2 Experimental hot tearing tendency 38
5.1.3 Numerical simulation 54
5.2 Hot tearing of Mg-0.5Ca-xZn ternary alloy 57
5.2.1 Chemical composition 57
5.2.2 Experimental hot tearing tendency 57
5.2.3 Hot tearing behaviour of Mg-0.5Ca-4Zn-0.2Zr alloys 69
5.2.4 Numerical simulation of hot tearing tendency 70
5.3 Hot tearing of Mg-2Ca-xZn ternary alloy 71
5.3.1 Chemical composition 71
5.3.2 Experimental hot tearing tendency 72

5.4 Hot tearing of Mg-xCa-4Zn ternary alloy 87
5.4.1 Chemical composition 87
5.4.2 Experimental hot tearing tendency 87
6 Discussion 97
6.1 Hot tearing behaviour of Mg-Ca binary alloys 97
6.1.1 Comparison with thermodynamic prediction 97
6.1.2 Effect of Ca on HTS of Mg-Ca binary alloys 99
6.1.3 Tearing in the middle of the rod at T_{mould} = 450 ^{0}C 101
6.1.4 Effect of mould temperature 102
6.2 Hot tearing behaviour of Mg-Ca-Zn alloys 103
6.2.1 Effect of Zn and Ca content on hot tearing behaviour of Mg-Ca-Zn alloys 103
6.2.2 Residual strain 113
6.2.3 Tearing at load screw at T_{mould} = 450 ^{0}C 114
6.2.4 Effect of mould temperature 115
6.2.5 Effect of grain refinement 116
6.3 Hot tearing mechanisms 117
6.3.1 Solidification and hot tearing 117
6.3.2 Tear initiation and propagation 118
6.3.3 Tear healing 122
6.3.4 Micropores 124
7 Summary 126
8 Acknowledgements 128
9 References 129
10 Publication list during doctoral study 139
Curriculum Vitae 140

1 Introduction

In comparison with Al alloys and steel, Mg alloys have attracted increasing interest in industrial applications, due to their high specific strength [1]. The majority of Mg alloys were prepared by conventional casting processes [2]. Thus, defect free castings are highly desirable for the subsequent processing and service. Hot tearing or hot cracking is often a major casting defect and has a significant impact on the quality of casting products [3]. Therefore, it is of great importance to investigate the hot tearing behaviour of Mg alloys.

Hot tearing is a complex solidification phenomenon which is still not fully understood [4]. Such cracking occurs above the solidus temperature due to the obstructed contraction of solidifying alloys, often at hot spots where the casting solidifies last or at areas with sudden changes of cross section [5]. Industrial and fundamental studies of this phenomenon show that hot tears initiate when the liquid flow through the mushy zone becomes insufficient to fill initiated cavities. Normally the volume fraction of solid at this stage is in the range of 85-95% and the solid phase is organized in a continuous network of grains [6].

In the past decades, many hot tearing criteria, experimental set-ups, and simulation models were developed to characterize the hot tearing susceptibility (HTS). The hot tearing criteria were reviewed by D. G. Eskin et al. [7]. It is stated that the existing hot tearing criteria based on different principles have limited applicability to commercial casting processes, due to their probabilistic character. Generally, in order to assess the HTS, constraint is designed in all the developed experimental setups [6]. Important hot tearing factors, such as temperature and stresses, were monitored during solidification [8]. Meanwhile, the application of numerical simulation techniques in metal casting provides insight into interpreting and understanding hot tearing. Numerical simulation has been used to reduce the time required in new product design cycles and as a tool for quality assurance [9].

Hot teaing behaviour is affected by many factors. Numorous studies proved that HTS is composition dependent [10-12]. Different alloying element, freezing range, grain size, and eutectic result in different hot tearing behaviour [13, 14]. Besides, casting parameters, such as initial mould temperature, pouring temperature, and casting speed also play an important role on hot tearing behaviour [7, 15, 16].

Hot tearing behaviour of several binary Mg alloys, including Mg-Al [4, 8, 17], Mg-Zn [18], Mg-Y [19] and Mg-Gd [20], have been investigated. Results revealed that HTS is

composition dependent. In addition, hot tearing behaviour of the ternary Mg-Zn-Y [21, 22], Mg-Ca-Al [23], Mg-Sr-Al [5, 24], Mg-Zn-Al [25, 26] and commercial AZ31 [27], AZ91 [27, 28], and AM60 [27, 29] alloys has also been investigated.

Calcium plays a quite important role in tailoring the mechanical properties of magnesium alloys for structural as well as medical applications [30-32]. Owing to the fact that both Mg and Ca have an excellent biocompatibility, Mg-Ca alloys are being considered as the potential degradable biomaterials [33]. Mg-Zn-Ca ternary alloys have a great potential for both biodegradable and automotive applications [34, 35]. Both *in vitro* and *in vivo* studies showed that the designated Mg-Zn-Ca ternary alloys are biocompatible and have satisfactory mechanical properties and corrosion resistance [36-38]. Previous investigations also showed that Mg-Zn-Ca alloys have excellent creep resistance [35, 39].

Due to the extensive potential applications of Mg-Ca and Mg-Zn-Ca alloys, it is of great importance to investigate their hot tearing behaviour. Consequently, in the present work, the hot tearing behaviour of Mg-Ca and Mg-Zn-Ca alloys were investigated. Solification and hot tearing indicator (HTI) of Mg alloys were simulated with ProCAST.

2 Literature review

2.1 Hot tearing models

Hot tearing was numerously investigated since 150 years ago. Many theories and criteria are proposed to predict the occurrence of hot tearing. These hot tearing criteria, as reviewed by D.G. Eskin [6, 7], can be conditionally divided into two categories: nonmechanical and mechanical. The nonmechanical criteria dealt with the vulnerable temperature range, phase diagram, and process parameters such as pouring temperature and mould temperature. The mechanical criteria are derived mainly from the mechanical behaviour of semi-solid, such as the critical stress, critical strain, and critical strain rate.

2.1.1 Clyne and Davies' Model

In 1975, T. W. Clyne and G. J. Davies [10, 40, 41] proposed a hot tearing theory, which considers the critical time when the structure is most vulnerable to cracking during solidification. Four stages were proposed that may happen in the vicinity of the hot spot (which will in general be the region most vulnerable):

(i) Strain accommodation by solid movement (mass feeding, $0.1 < f_l < 0.6$). This involves cooperative rearrangement of the growing solid dendrites.

(ii) Strain accommodation by liquid movement (liquid feeding, $0.1 < f_l < 0.6$). This involves liquid flow, which is expected to assist stress relief by liquid healing of cracks and continuous inter-dendritic feeding.

(iii) Interdendritic separation ($0.01 < f_l < 0.1$). This requires the liquid to be distributed as an interdendritic film. Hot tearing mainly happens at this stage.

(iv) Interdendritic bridging ($f_l < 0.01$). The integrity of the interdendritic film will become impaired and regions of solid cohesion will be established between adjacent dendrites. If this occurs to a sufficient extent, the interdendritic separation can be prevented, thus there will be no hot crack.

Thus, the crack susceptibility coefficient (CSC) is defined as:

$$CSC = \frac{t_V}{t_R} = \frac{t_{0.99} - t_{0.9}}{t_{0.9} - t_{0.4}} \qquad 2\text{-}1$$

where t_V is the vulnerable time period where hot tearing may develop and t_R is the time available for the stress-relief process where mass and liquid feeding occur. $t_{0.99}$ corresponds

the time when the local solid fraction (f_s) is 0.99. $t_{0.9}$ corresponds the time when f_s is 0.9 and $t_{0.4}$ corresponds the time when f_s is 0.4.

However, Clyne and Davies' criterion is sometimes found to be inconsistent with the casting practice [3]. The criterion does not show any sensitivity to the casting speed and position within the billet volume. Generally, increasing casting speed leads to high HTS [7].

2.1.2 Katgerman's Model

Katgerman [42] proposed a model to predict hot tearing susceptibility (HTS) based on Clyne and Davies' criterion and also took casting speed into consideration. The HTS is defined as:

$$HTS = \frac{t_V}{t_R} = \frac{t_{0.99} - t_{cr}}{t_{cr} - t_{coh}} \qquad 2\text{-}2$$

where t_{cr} is the time when feeding becomes inadequate; t_{coh} is the time when f_s at the coherency point.

This model is proved sensitive to both alloy composition and casting speed. However, the definition of coherency temperature is unclear. The coherency temperature was simply defined as the temperature where the dendritic network starts to form. Whether the coherency point derived from shear or tension is not specified in the criterion.

2.1.3 RDG Criterion

A mechanical hot tearing criterion proposed by Rappaz, Drezet, and Gremaud [11] in 1999, is so called RDG criterion. This criterion is based on the maximum strain rate ($\dot{\varepsilon}_{\max}$) the mushy zone can sustain before the hot crack occurs. Thus, the hot cracking sensitivity (HCS) is defined as $\dot{\varepsilon}_{\max}^{-1}$. The criterion is only an indicator of the hot tearing initiation, but not for the hot tearing propagation.

RDG model is proposed based on columnar grain structure. The HCS can be obtained as $\dot{\varepsilon}_{\max}^{-1}$ through the calculations. The maximum strain rate can be finally written as:

$$\dot{\varepsilon}_{max} = \frac{G^2\lambda_2^2}{180(1+\beta)B\mu\Delta T_0^2}\Delta p_{max} - \frac{v_T G\beta A}{(1+\beta)B\Delta T_0} \qquad 2\text{-}3$$

where G is the temperature gradient; λ_2 is the secondary dendrite arm spacing; β is the shrinkage factor; μ is the viscosity; ΔT_0 is the solidification interval; Δp_{max} is the maximum pressure drop the mushy zone can bear; v_T is the velocity. The two integrals A and B depend only on the nature of the alloy and its solidification path, i.e. on the relationship between f_s

and T. They are also extremely sensitive to the choice of integral limits. The HCS can be obtained as $\dot{\varepsilon}_{\max}^{-1}$ through the calculations.

Braccini et al. [43] and Grandfield et al. [44] proposed modifications to the RDG model, which give the expression of critical strain rate in both columnar and equiaxed grains for hot tearing nucleation and propagation.

In Braccini et al.'s model, an improved description of the rheology of the mush that surrounds the area where cavities initiate was introduced. The critical strain rate to nucleate ($\dot{\varepsilon}_{nuc}$) and propagate ($\dot{\varepsilon}_{prop}$) a hot tear in an equiaxed structure is respectively defined as:

$$\dot{\varepsilon}_{nuc} = \left(1 - \frac{e}{h}\right)\left(\frac{\frac{2}{3p_c} - p_m}{K(T, f_s)}\right)^{1/m} + \frac{e}{h}\frac{2\kappa}{\lambda^2}\frac{p_c}{\eta_L} \qquad 2\text{-}4$$

$$\dot{\varepsilon}_{prop} = \left(1 - \frac{e}{h}\right)\left[\frac{\lambda - a}{\lambda}\left(\frac{\frac{2}{3p_c} - p_m}{K(T, f_s)}\right)\right]^{1/m} + \frac{e}{h}\frac{2\kappa}{(\lambda - a)^2}\frac{p_c}{\eta_L} \qquad 2\text{-}5$$

where e is the liquid film thickness; h is the gauge length; λ is half the grain size; a is the length of the tear; p_c is the cavitation pressure; p_m is the metallostatic pressure; K is permeability of the mushy zone; η_L is viscosity of the liquid.

In Grandfield's model, the capillary effects are introduced. Moreover, the pressure in the dissolved gas and equiaxed grain case are considered. The critical strain rate $\dot{\varepsilon}_{crit}$ for hot tear propagation in equiaxed structure is expressed as:

$$\dot{\varepsilon}_{crit} > \frac{d^2}{180(1+\beta)B\mu L^2}\left[p_m + \frac{4\gamma}{d(1-\sqrt[3]{f_{scoh}})}\right] - \frac{V\beta A}{(1+\beta)BL} \qquad 2\text{-}6$$

where d is the grain size; L is the length of mushy zone; γ is the surface tension; V is the velocity of solidification front velocity (growth velocity). Other parameters are the same as defined above.

2.1.4 Suyitno's Criterion

Suyitno et al. proposed a hot tearing criterion combining critical liquid feeding theory, deformation rate, and cavity formation [45]. This model can distinguish whether a hot tear or a micro-porosity appears under a certain strain rate. The contribution of feeding, shrinkage, and strain rate is compared, in order to decide whether the cavity is formed or not. This model is based on the following assumptions: the grain had equiaxed microstructure, the cavity formed at triple junctions between grains, and feeding only occured in the casting direction.

Initally, the contribution of feeding, shrinkage and deformation to the cavity are calculated, expressed as:

$$\frac{\partial f_v}{\partial t} = -\left(\frac{\rho_s}{\rho_l} - 1\right)\frac{\partial f_l}{\partial t} + \left(\frac{\rho_s}{\rho_l}\right) f_s \dot{\varepsilon} - \frac{\partial (f_l \mu)}{dx} - \frac{\partial (f_l v)}{dy} \quad 2\text{-}7$$

where f_v is cavity fraction. The first and second terms on the right side are the contributions of shrinkage and deformation respectively. The third and fourth terms are the contributions of feeding in horizontal and vertical directions respectively. The third term is taken as zero according to the assumption that feeding only occurs in the casting direction.

$\frac{\partial f_v}{\partial t}$ is a net result of shrinkage, deformation, and feeding. In case it is positive, the cavity will form which may finally result in a hot tear. Whether the cavity propagates as a crack depends on the stress developed in the mush. The relation between cavity diameter (d) and stress (σ) is:

$$d = 4\gamma_e \frac{E}{\pi \sigma^2} \quad 2\text{-}8$$

where γ_e is surface tension of liquid metal. E is Young's modulus of the mush.

The stress developed in the mush can be calculated from:

$$\sigma = \sigma_0 \exp(\alpha f_s) \exp\left(\frac{mQ}{RT}\right) (\dot{\varepsilon})^m \quad 2\text{-}9$$

where σ_0 and α are material constants; Q is the activation energy; R is the gas constant; m is the strain rate sensitivity coefficient.

By assuming the cavity shape is circular, the critical diameter of cavity (d_{crit}) is determined by:

$$\pi d_{crit}^2 = \sqrt{3} b^2 \int_o^t \varepsilon \dot{d} \tau \quad d_{crit} = b\sqrt{\frac{\sqrt{3}}{\pi} \int_o^t \varepsilon \dot{d} \tau} \quad 2\text{-}10$$

where b is the final grain diameter. If the diameter of cavity d is larger than a critical diameter d_{crit}, a hot tear will appear. Otherwise only micro-porosity will develop.

2.1.5 Model assessment

These models have been evaluated by Suyitno et al. [46] and Katgerman et al. [3]. Only the criterion from Suyitno adequately responds to all tested parameters, such as casting speed, ramping rate, grain size, position of tear in a billet and casting practice. Suyitno's criterion gives a precise prediction of hot tearing appearance under which solid fraction and strain rate. However, it adapts more to the well-investigated alloy systems. As in those alloy systems, the

parameters are easy to find. However, in other alloy systems, the parameters such as Young's modulus of the mush, surface tension between liquid and solid, and permeability of the mush, are rarely available. In addition, these parameters need to be determined experimentally. However, the existing experimental techniques are not reliable [3]. Consequently, the widespread utilization of this criterion is limited.

On the contrary, the parameters needed for the prediction with Clyne and Davies' criterion can be easily obtained. All parameters can be calculated from commonly used thermodynamic softwares, i.e. Pandat and Panengine. As mentioned earlier, the criterion shows no sensitivity to casting speed. However, the criterion is successful in predicting the compositional dependence of hot tearing [3, 46]. Therefore, if the compositional dependence of hot tearing is of great interest, Clyne and Davies' criterion is still a good choice. Previous studies showed that the predictions with the model were in good agreement with the experimental results in Mg-Zn [47] and Mg-Y [19] binary alloys.

2.2 Experimental methods used to evaluate the hot tearing

Many techniques have been developed to investigate hot tearing behaviour of alloys. Normally, stress induced from constraints is incorporated in all the methods. Different apparatuses use different constraints to induce stress. Main apparatuses developed in recent years are summarized in this section. The methods to evaluate HTS are summarized as well.

2.2.1 Ring mould

Ring mould is a simple and classic method to assess HTS and used by many researchers [26, 48-51]. The setup normally consists of a ring and a core, both concentrically resting on a flat plate. Schematic mould of crack rings is shown in Fig. 2-1 [26]. The core is made with a slight taper in order to be separated easily after casting. The ring, core and flat plate are made of materials with low thermal expansion coefficients and much higher melting points than those of the tested alloys. The molten metal is poured into the annular space between the ring and the core. During solidification, the core resists solidification shrinkage and thermal contraction of the solidifying alloy. Consequently, a tensile stress is imposed onto the solidifying alloy. If the stress on the solidifying body exceeds its strength, hot tearing occurs.

Average length of all cracks on the top, bottom, outside, and inside surfaces was regarded as hot tearing susceptibility by Singer et al. [48]. The severity of hot tearing (hot tearing susceptibility coefficient, HSC) in Wang et al.'s report [26] is expressed as:

$$HSC = \frac{108 - D_{crit}}{108} \qquad 2\text{-}11$$

where D_{crit} is the critical diameter of the round steel block, 108 mm is the diameter of the mould.

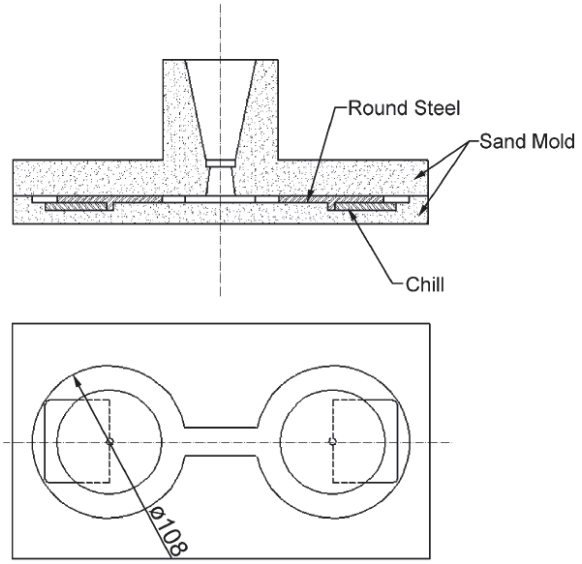

Fig. 2-1 Mould of crack-rings [26]

2.2.2 Constrained rod casting (CRC) tests

Constrained rod casting (CRC) utilizes another kind of constraint to introduce stress. In CRC mould, the ends of the bar solidify first and the central part solidifies later. The ends of the bar are anchored at the end of the mould to prevent free shrinkage. The central part is then placed under tensile stress along the axial direction of the bar. Cracks will form perpendicular to the bar axis. This test implies sideways movement to conserve mass if tearing does not occur [52].

There are mainly two types of constrained rod casting moulds, as shown in Fig. 2-2. Both moulds are reviewed by Eskin et al. [6]. One CRC mould contrains casting rods with different lengths (Fig. 2-2 (a)). The other mould consists of casting rods with different diameter (Fig. 2-2 (b)).

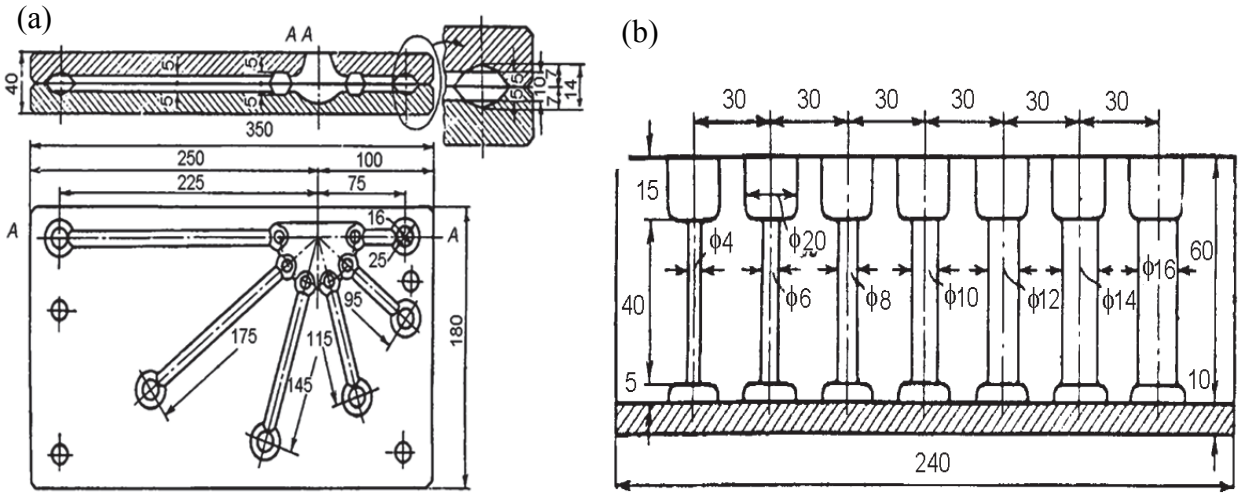

Fig. 2-2 Constrained rod casting mould with variation of casting (a) length and (b) diameter [6]

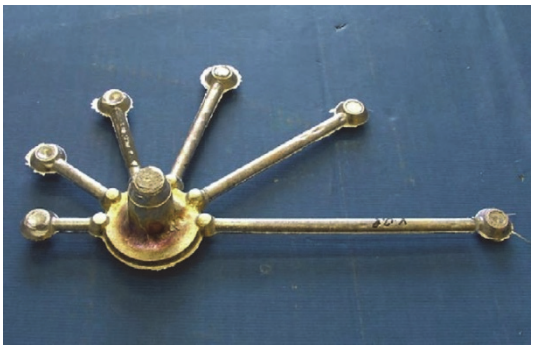

Fig. 2-3 Casting of PSM [22]

The first type (Fig. 2-2 (a)) is called permanent star-shaped mould (PSM). It consists of several bars with different length. A typical casting of PSM is displayed in Fig. 2-3 [22]. Severity of hot tearing is expressed as HTS_{PSM}. The PSM castings were optically examined and a number was assigned to represent the severity. The number with a value between 0 and 1 was assigned by examining each rod according to the following scheme: 1 for completely broken rods; 0.5 for obviously cracked rods; 0.25 for rods with cracks detectable only with the magnifying glass; and 0 if no cracks were observed. The final HTS_{PSM} is the average value of all the rods. $HTS_{PSM} = 6$ is the theoretical upper limit if all six rods are completely broken. While $HTS_{PSM} = 0$ represents the "best case" if the alloy is not susceptible to hot tearing under the given casting conditions.

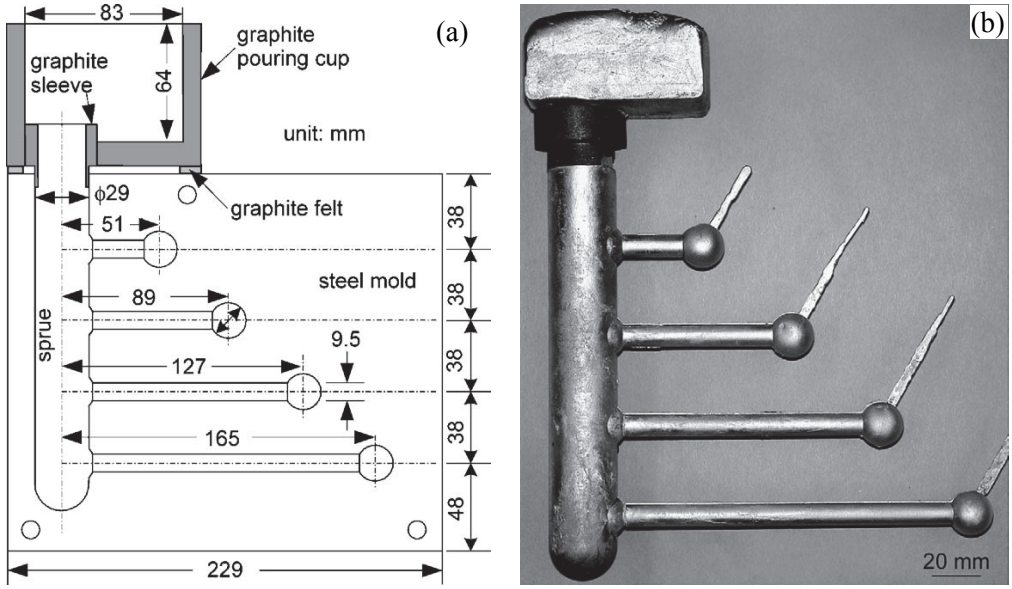

Fig. 2-4 Another constrained mould casting, (a) schematic mould, (b) casting [17]

Another commonly used constrained rod mould of the first type is shown in Fig. 2-4 [17]. Both the mould and the casting are shown. A modified and improved evaluation method of HTS is developed by Cao et al. [17] in this mould, as shown in

Fig. 2-5. The hot cracking susceptibility (HCS) was defined as:

$$HCS = \sum w_{crack} f_{length} f_{location} \quad 2\text{-}12$$

In the above equation, crack width factor w_{crack} is the maximum crack width measured in mm. Crack length factor f_{length} is set as 4 for the longest rod, 8 for the second longest rod, 16 for the third longest rod, and 32 for the shortest rod. Crack location factor $f_{location}$ is 1 for cracking at the sprue end, 2 at the ball end and 3 in the middle of the rod. This advanced evaluation method is more quantitative than the former one, owing to more factors (f_{length} and $f_{location}$) are taken into consideration. Additionally, crack width length instead of ranking the crack with a number is more reasonable.

For the second type, as shown in Fig. 2-2 (b), the hot-crack resistance of each alloy is evaluated by the hot crack grade [53]. It is expressed as:

$$HTS = \Phi^2 \quad 2\text{-}13$$

where Φ is the maximal diameter of middle column where hot cracks occurred. Higher value of the hot crack grade indicates a high HTS of the alloy.

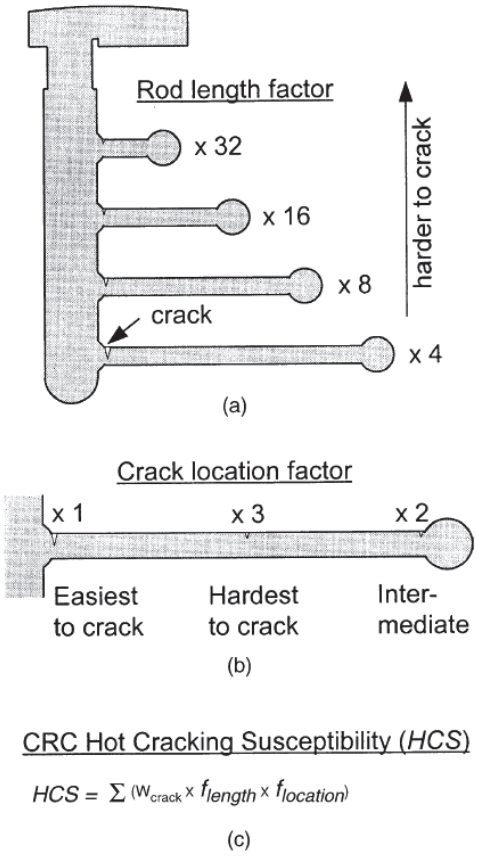

Fig. 2-5 Determination of crack sensitivity method: (a) rod length factor, (b) crack location factor, (c) equation of calculating hot cracking susceptibility [17]

2.2.3 Instrumented constrained rod casting tests

Recently, apparatuses that are more sophisticated have been developed, which can provide more information for better understanding of hot tearing. Efforts are made on simultaneously monitor the temperature, load, and/or displacement during solidification process. These recorded data help to understand the hot tearing initiation and propagation better.

Zhen et al. [54] developed an instrumented hot tearing setup. It can monitor the temperature and load evolution during solidification process. With the recorded temperature and load, onset temperature of hot tearing can be read on the curve. This apparatus is used in this study, detailed description of which can be found in Section 4.1.2. In this set-up, the mould is based on the first type of CRC mould (Fig. 2-2). It is simplified to contain only one rod. In addition, the constrained rod was designed to be a taper. This successfully eliminates the impact of friction between the inner wall of the mould and solidifying casting. In practice, the friction becomes a challenge on measuring the real contraction stress. This friction can result in unrepeatable and confusing data.

Crack volume is used as the index of HTS in Zhen et al.'s apparatus. Hot tearing index (HTI) is expressed as follows:

$$HTI = crack\ volume \quad 2\text{-}14$$

The crack volume is more accurate, as it takes the depth of crack as well as the complexity of the crack pattern into account [8]. Normally, the volume of cracks was measured by a wax penetration method. However, this wax method can only measure the volume of open cracks. More recently, X-ray tomography technique was introduced to measure the crack volume, which can measure both the open and closed crack volume [19, 20].

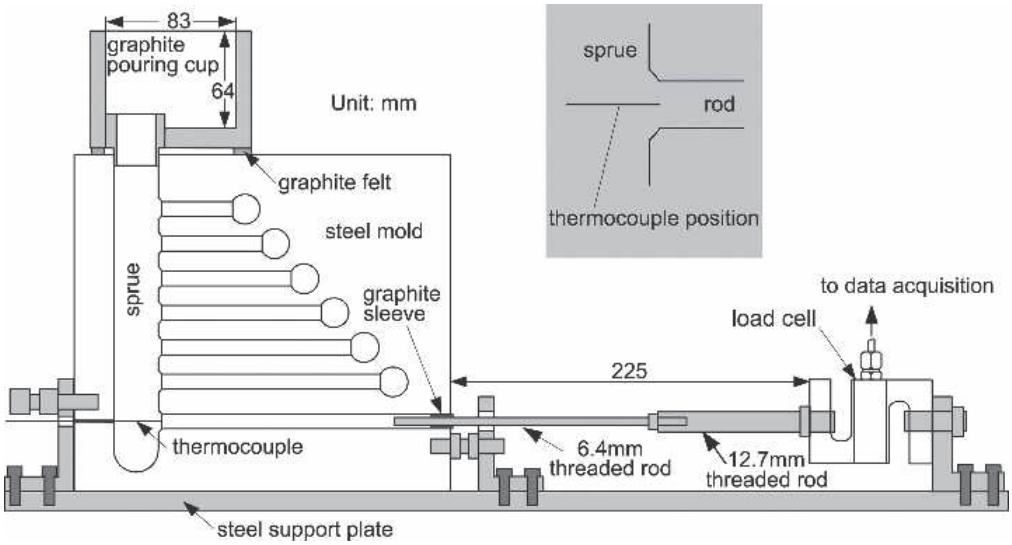

Fig. 2-6 Instrumented CRC mould from Cao et al. [24]

Cao et al. [24] also modified the original CRC mould (Fig. 2-4). A temperature and load acquisition units were instrumented on the original CRC mould, as shown in Fig. 2-6. An additional rod (the bottom rod) equipped with load cell was designed to record the stress development. A thermocouple was embedded at the junction area between the rod and the sprue to record the temperature. The location of thermocouple is near the potential place of the crack. The diameter of the bottom rod is kept constantly at 8.7 or 7.9 mm. The mould is equipped with a graphite pouring cup and a graphite sleeve. This can maximize the reproducibility and minimize the interference of the increased tension near the sprue end of the rods. After pouring the melt into the mould, the temperature, time and load are recorded with a data acquisition system. Assessment of HTS is the same as described in Fig. 2-5.

Displacement of casting sample during solidification is also of great interest in hot tearing behavior investigation. Recently, Metal Processing Institute at WPI and CANMET Materials Technology Laboratory developed an instrumented constrained rod mould [14, 55], as shown

in Fig. 2-7. The mould is designed to measure the load/time/temperature or displacement/time/temperature during solidification simultaneously. The mould has two arms. Both arms are designed as a taper to decrease friction between the mould and the casting. The right arm is designed to access hot tearing. The left arm is used to record the temperature and load/displacement data. The end of the left arm is connected to a rod, which has one end embedded in the arm and the other end connected to a load cell or linear variable differential transformer (LVDT). The LVDT is unrestrained and can move horizontally and freely. The load cell offers a resistance to the contraction and finally results in hot cracking. The tests are reproducible and reliable [14]. The hot tearing index is defined as the crack area, which is calculated using image processing software (Image J).

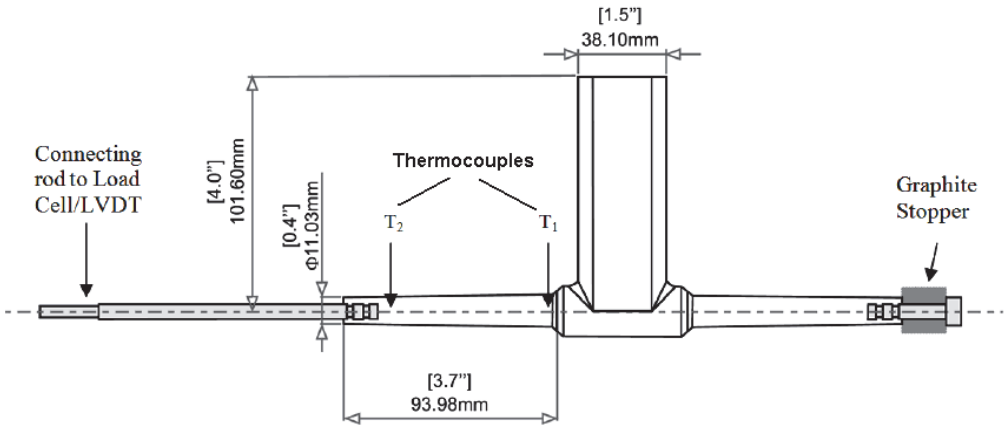

Fig. 2-7 Instrumented CRC mould from WPI and CANMET Materials Technology Laboratory [14]

Another apparatus for measuring tensile stress during solidification was developed by Instone et al. [56]. The designed apparatus is shown in Fig. 2-8. The apparatus contains a restrained bar casting which incorporates a feeder located in the centre of the bar. The setup provided constraint through anchoring the cast bar ends. Information on development of stress, strain accommodation and hot cracking behaviour of the mushy zone were also collected. This setup can monitor both the load and displacement, as shown in Fig. 2-8 (b). Image density of the radiographs was used as hot tearing index. Standard image editing software was used to measure the mean brightness level (BL) of a rectangular area. This rectangular area contains both the hot tear ($BL_{\text{Hot Tear}}$) area and the adjacent tear free area ($BL_{\text{No Tear}}$). Hot tearing was then quantified as:

$$HTI = \frac{BL_{No\,Tear} - BL_{Hot\,Tear}}{BL_{No\,Tear}} \qquad 2\text{-}15$$

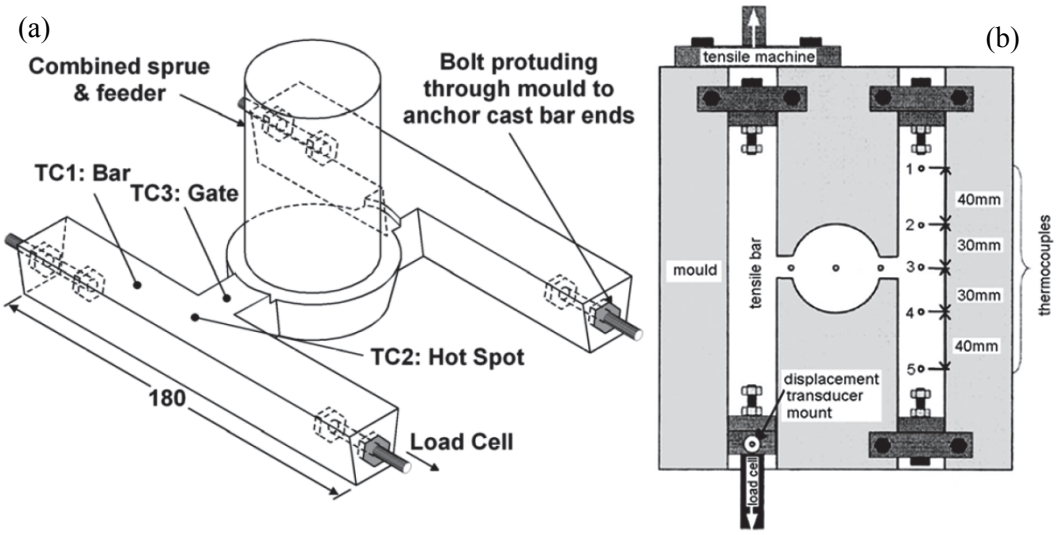

Fig. 2-8 Instrumented test rig, (a) schematic diagram [52], (b) plane view of the mould [56]

2.2.4 Other methods

Recently, *in situ* observation of hot tearing formation has drawn extensive attention of related researchers [57, 58]. Farup et al. [57] used a video camera attached to the microscope to observe hot tearing formation of succinonitrile-acetone. Tearing mechanisms were clarified. However, due to the difference between organic alloys and metal alloys, the developed hot tearing mechanisms are not fully applicable to metal alloys.

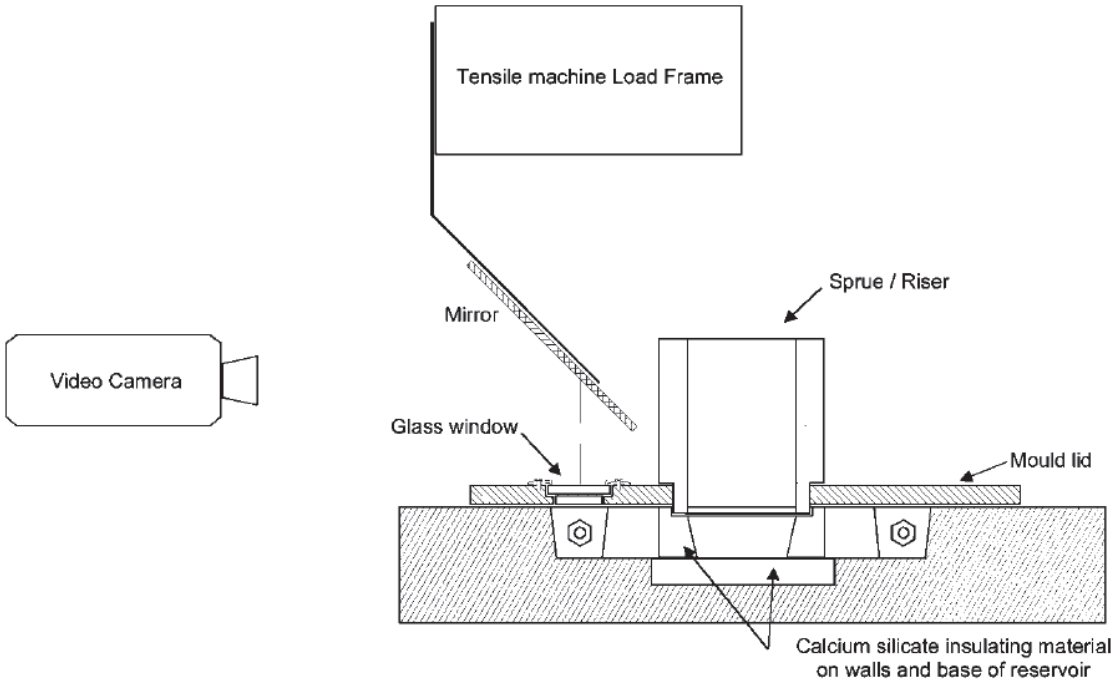

Fig. 2-9 Schematic of *in situ* observation of hot tearing by video camera [58]

Davidson et al. [58] modified the test rig (Fig. 2-8). The new setup enables *in situ* observation of hot tearing formation of Al-Cu alloys by video camera. Schematic of *in situ* observation

setup is shown in Fig. 2-9. A mirror angled at 45 ° was positioned above the glass window. A video camera with a long focal length lens was used to record the images to digital tape at the standard 25 frames s^{-1} interlaced. The image was transferred to a PC using a codec that compressed the image data spatially but not temporally. In this way, there was no contamination of image detail from one frame to the next.

Lately, highly focused and intense X-ray beams available at synchrotron facilities and in the laboratory have started to play an important role on the investigation of semi-solid alloys. In terms of deformation behavior, the utilization of X-ray microtomography allows for detailed 3D observation. For instance, 3 D liquid/solid configurations, the propagation of tears and the interactions of hot tears with the microstructure can be observed. In order to obtain a sequence of incremental 3D displacement fields of a deforming specimen, both digital image post-processing of tomography images and volumetric digital image correlation are applied. *In situ* observation on deformation of semi-solid Al-Cu alloys under tensile stress was carried out [59, 60]. The apparatus is shown in Fig. 2-10. This apparatus allows *in situ* observation of tensile test at different solidification range (f_s range from 0.35 to 0.98). This approach is not capable of observing *in situ* formation of hot tears. However, important information about deformation mechanisms at high solidification range (most susceptible to hot tearing) is provided.

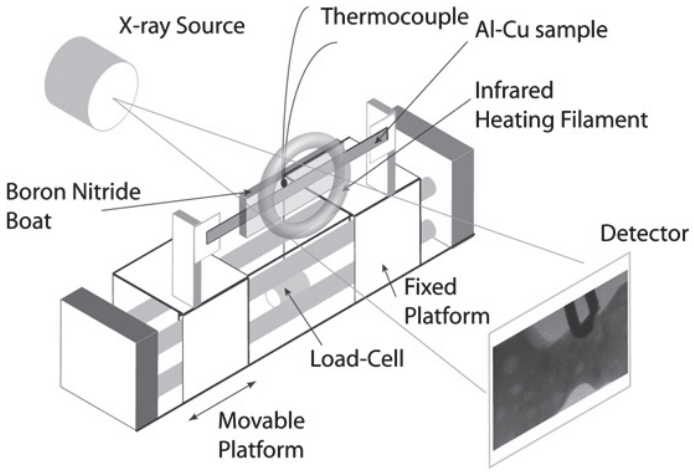

Fig. 2-10 Schematic of the semi-solid deformation apparatus [59]

Puncreobutr et al. [61] used fast *in situ* synchrotron X-ray tomographic microscopy experiments to study the solidification defects. The influence of Fe-rich intermetallics on solidification defect formation of commercial A319 alloy (Al-7.5Si-3.5Cu, wt.%) with 0.2 and 0.6 wt.% Fe are investigated. The *in situ* semi-solid deformation experiments show that β-Al_5FeSi intermetallics increase hot-tearing susceptibility. This is due to the presence of a large

fraction of β-intermetallics, which strongly blocks the interdendritic channels and induces porosity formation. The porosity formation is owing to permeability reduction and hydrogen super saturation in the local subdivided domain.

However, the *in situ* observation of semi-solid deformation by synchrotron is mainly restricted in Al alloys or steel. Utilization of *in situ* observation on semi-solid deformation of magnesium alloys still needs to be developed.

2.3 Factors influencing hot tearing

The phenomenon of hot tearing in metal castings has been experimentally investigated for many years with reference to factors that influence the hot tearing [10, 23]. The variables are either related to properties of alloys or processing parameters. Freezing range, amount of eutectic, and mechanical properties of semi-solid have a significant influence on HTS. Furthermore, grain size and grain morphology also affects the hot tearing behaviour. The processing parameters include pouring temperature and initial mould temperature.

2.3.1 Intrinsic factors

2.3.1.1 Freezing range

Generally, the larger the freezing range, the more the alloy is prone to hot tearing. Freezing range changes with alloying elements as well as alloying composition.

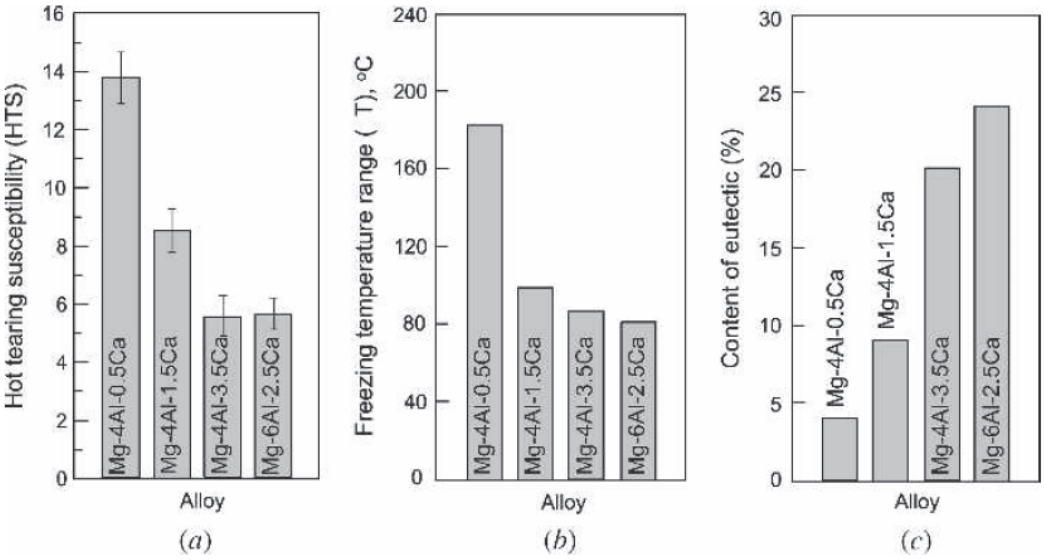

Fig. 2-11 Correlations between hot tearing susceptibility and freezing range and amount of eutectic: (a) hot tearing susceptibility, (b) freezing range, and (c) amount of eutectic [23]

In Cao et al.'s [23] research, freezing range was found to have a good correlation with HTS, as shown in Fig. 2-11. Wang et al [21] also found that high vulnerable freezing range ($T_{0.9}$-

$T_{0.99}$, which is the temperature at solid fraction of 0.9 and 0.99, respectively) results in high HTS in Mg-Zn-Y alloys.

2.3.1.2 Eutectic

It is commonly acknowledged that formation of hot tearing is due to lack of feeding at the last stage of solidification. As long as there is sufficient liquid which can freely feed the solid phase, no hot tear will appear [7]. Therefore, at this point of view, high amount of eutectic liquid is beneficial for hot tearing resistance. In general, amount of eutectic increases with alloying composition. Alloying elements also affect the amount of eutectic. As shown in Fig. 2-11 (a) and (c), it is revealed that HTS decreases with amount of eutectic [23]. Similar results can also be found in Mg-Gd alloys [20].

2.3.1.3 Strength and ductility of semi-solid alloys

The examination of mechanical properties of alloys during solidification is, of course, essential for studying hot tearing phenomena. Most of the attempts were staged to examine and study the failure (hot tearing) of the semi-solid mush under external or internally-induced stresses [6]. Mechanical properties of alloys at semi-solid state are tested either by remelting or by solidification approaches. Strength and ductility profiles of numerous Al alloys were summarized in Eskin et al.'s review [6]. The mechanical properties of semi-solid Al alloys were found to be highly dependent on the alloying elements and alloying composition.

Strength and ductility properties of semi-solid Mg alloys are still limited. Abedi et al. [62] tested the tensile deformation of semi-solid wrought AZ31. Results showed that ductility increased with testing temperature ranging from 300 °C to 500 °C. The high ductility values above the melting point (462 °C) of γ-intermetallic phase ($Mg_{12}Al_{17}$) were observed. This was attributed to the effect of liquid phase on stress relaxation, cavity retardation, and eventually grain boundary sliding accommodation.

2.3.1.4 Grain size and grain morphology

As reported in literature [12, 13, 63], both grain size and grain morphology have a great impact on hot tearing behaviour. Most of results show that grain refinement improves hot tearing resistance by better accommodating local strains. Moreover, grain refinement delays the onset of interdendritic feeding and reduces the liquid film thickness between grains (which increases the capillary pressures). Both of them reduce the HTS [63]. Viano et al. [12] studied effect of grain refinement on hot tearing behaviour of Al-Cu alloys. The HTS of Al-Cu alloys is reduced by grain refinement. However, it was also predicted with RDG model that the

refined grain size would decrease the permeability of the mush, which then leads to increased HTS [13]. The modelling suggests that grain refinement reduces the HTS until the grain morphology becomes globular [63]. Further grain refinement causes HTS to increase again. Evidence of increased HTS was not experimentally observed, probably because the grains were found to have dendritic equiaxed morphology. Thus, it is proposed that fine dendritic equiaxed grain morphology has the greatest resistance to hot tearing. It is commonly acknowledged that columnar and twinned columnar crystals are detrimental to hot tearing, due to the structure promoting easy initiation and propagation of hot cracking [13, 19, 20].

The morphology and size of grains depend on alloy elements and alloy composition of alloy as well as the processing parameters. Grain refinement achieved from alloying process is attributed to heterogeneous nucleation sites provided by intermetallic particles or alloying elements. With regard to the processing parameters, grain size decreases with cooling rate. With increasing solute composition, grain morphology tends to transit from columnar to equiaxed [19, 20, 64].

2.3.2 External factors – casting parameters

2.3.2.1 Pouring temperature

Clyne and Davies [41] utilized electrical resistance measurements to establish a relationship between the susceptibility of tearing and melt superheat. Results indicate that HTS depends on both the composition and the pouring temperature. High superheat results in a high HTS and the maximum HTS appears in alloys with a low content of solute. However, Bichler et al. [65] presented that the variation of pouring temperature does not have a significant effect on HTS in AZ91D alloy. Recently, Huang et al. [15] studied the effect of pouring temperature and mould temperature on HTS of AZ91. It is found that the pouring temperature can affect the HTS only when the mould temperature is low. In addition, HTS decreases with increase in pouring temperature first, and then increases with further increasing pouring temperature.

Pouring temperature affects the HTS in two contrary ways [14]. On one side, high pouring temperature might spread the hot spot, which is expected to reduce HTS. On the other side, high superheat might increase the liquid film life, which is expected to increase HTS.

2.3.2.2 Mould temperature

So far, all the literatures show that HTS decreases with increasing the mould temperature. Bichler et al. [65] investigated the effect the mould temperature, ranging from 140 - 380 °C, on HTS of AZ91D. It is observed that HTS decreases progressively with mould temperature.

Moreover, mould temperature is found to have a more significant impact on HTS than pouring temperature. Similar findings are also shown in Huang et al.'s [15] work. Investigations on Mg-Y [66], Mg-Al [8], Mg-Gd [20], and Mg-Zn [18] also reveal that high mould temperature improves hot tearing resistance. Among them, results of Mg-Gd alloys are shown in Fig. 2-12. Severity of hot tearing (HTS indicator) is represented by crack volume.

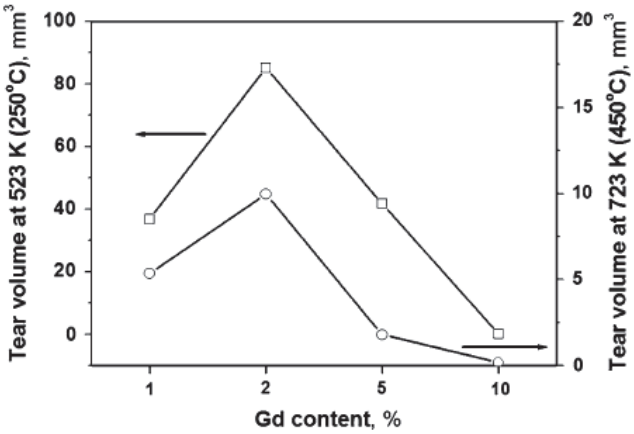

Fig. 2-12 Hot tearing severity of Mg-Gd alloys at different mould temperatures [20]

It is reported that high mould temperature provides good feeding and cracking refilling, which results in low HTS [14]. Besides, the thermal gradient at high mould temperature is low. Stress or strain accumulated during solidification highly depends on the thermal gradient. Consequently, low thermal gradient resulting from high mould temperature leads to low HTS.

2.4 Hot tearing of magnesium alloys

Hot tearing behaviours of Mg alloys can be also found in Wang et al.'s review [67]. HTS of binary, ternary, quaternary and some commercial alloys have been investigated. In the past decades, investigation on hot tearing behaviour of binary alloys has been carried out for Mg-Al [4, 8, 16, 17, 68, 69], Mg-Zn [16, 18, 70], Mg-Y [19, 66, 71], and Mg-Gd [20, 64] series. The hot tearing behaviours of ternary Mg-Al-Zn [25, 26], Mg-Al-Ca [23], Mg-Al-Sr [5, 24], and Mg-Zn-Y [21, 22] have also been investigated. Besides, HTS of several commercial Mg alloys have been investigated, such as, AZ91 [15, 65, 72], AE42 [73], AJ62X [73], and AXJ [74].

2.4.1 Binary alloys

2.4.1.1 Mg-Al

Cao et al. [17] investigated the HTS of binary Mg-Al alloys (from 0.25 to 8.0 wt.% Al) using a CRC mould. Results are presented in Fig. 2-13. The maximum HTS appeared at Mg-1 wt.%

Al. It is also observed that mould coating plays an important role on hot cracking. Crack susceptibility using a thick mould coating is lower than that with a regular thin mould coating. This is owing to coating reducing the cooling rate and perhaps providing a slightly more cushion effect for the shrinking rods. Both could result in reduced tension in the rods during solidification and hence a low HTS.

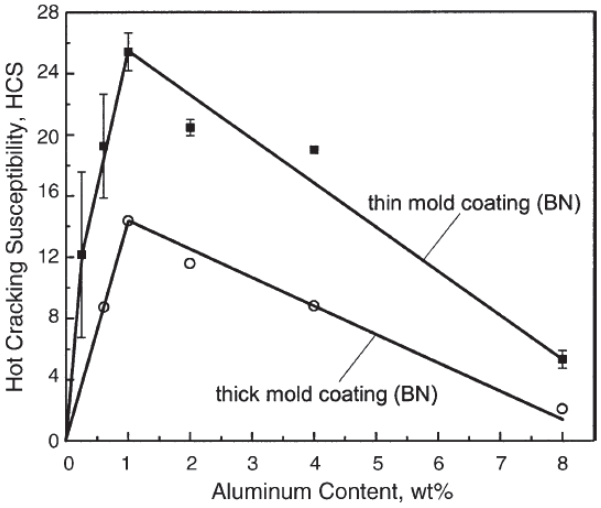

Fig. 2-13 Hot cracking susceptibility curves of binary Mg-Al alloys based on CRC testing [17]

Zhen et al. [8] also studied hot tearing behaviour of Mg-Al alloys. However, the mould used by Zhen et al. was a modified CRC mould, which can eliminate the effect of friction. Mg-1Al, Mg-3Al, Mg-6Al, and Mg-9Al (in wt.%) were studied. The Mg-1wt.% Al alloy was found to be most susceptible to hot tearing, thereby confirming Cao et al.'s [17] results.

2.4.1.2 Mg-Zn

Investigation on hot tearing behaviour of Mg-Zn alloys has been carried out with an instrumented CRC mould [18, 25]. Zn contents ranging from 0.5 - 12 wt.% were investigated in detail. Thermodynamic calculations of HTS based on Clyne and Davies' model were performed on Mg-Zn alloys. Maximum HTS was predicted at Mg-1.5 wt.% Zn. Experimental results also reveal HTS peak appears at Mg-1.5 wt.% Zn. It is also found that high mould temperature reduces HTS in Mg-Zn alloys.

2.4.1.3 Mg-Y

Hot tearing susceptibility of Mg-Y alloys at different mould temperatures was investigated [19, 66]. Yttrium contents ranging from 0.2 - 4 wt.% were studied. Mg-0.9 wt.% Y show the highest HTS among all. The high HTS of Mg-0.9 wt.% Y is due to its large grain size, large

solidification range, and small amount of eutectic. The increment in mould temperature from 250 to 450 °C significantly reduces the HTS of binary Mg-Y alloys.

2.4.1.4 Mg-Gd

Hot tearing characteristics of binary Mg-Gd alloys were investigated in an instrumented CRC mould apparatus by Srinivasan et al. [20]. HTS of Mg-1Gd, Mg-2Gd, Mg-5Gd, and Mg-10Gd were studied. The susceptibility increases with increase in Gd content, reaching a maximum at 2 wt.% Gd and then decreases with further increment of Gd content. The high susceptibility observed in Mg-2 wt.% Gd was attributed to cellular or columnar grain structure, which facilitates easy tear propagation. The results also indicate that the increase in mould temperature significantly reduce the HTS.

2.4.2 Ternary alloys

2.4.2.1 Mg-Al-Zn

Wang et al. [26] studied hot tearing behaviour of Mg-9Al-xZn (x=0, 0.2, 0.4, 0.6, 0.8, 1.0, and 1.2, wt.%) alloys using a ring mould. It is reported that HTS increases with Zn content within the whole investigated range. They thought that the inter-crystalline segregation of Zn and Al is the main contribution to the high HTS of Mg-9Al-xZn alloys. There are two effects of Zn on the solidification of Mg-9Al-xZn alloys. One is, it decreases the melting range of metals at grain boundaries, which increases existing time of liquid film. The other is, it increases the quantity of low melting point metal at grain boundaries. Both effects lead to low hot tearing resistance.

Hot tearing susceptibility of Mg-xZn-0.5Al (x=0.5, 1.5, 2.5, and 4, wt.%) alloys as well as Mg-1.5Zn-yAl (y=0.5, 3, and 6, wt.%) alloys were characterized by Zhou et al. [25]. It is revealed that, for Mg-xZn-0.5Al alloys, two peaks of HTS are obtained: one is at about 1.0 to 1.5 wt.% Zn, another is at about 3.0 wt.%. For Mg-1.5Zn-yAl ternary system, the HTS decreases with increasing Al content.

2.4.2.2 Mg-Al-Ca

Cao et al. [23] used a CRC mould to study the hot tearing behaviour of Mg-Al-Ca alloys. Fig. 2-14 shows the HTS of Mg-Al-Ca alloys as well as AZ91E. AZ91E is known to have a low HTS. For Mg-4Al-xCa (x=0, 0.5, 1.5, 2.5, and 3.5, wt.%) alloys, HTS decreases sharply with Ca content. For Mg-xAl-2.5Ca (x=4, 5, and 6, wt.%) alloys, the susceptibility to hot tearing does not change significantly as the Al content increases from 4 to 6 wt.%. Among all the investigated alloys, Mg-4Al-2.5Ca, Mg-4Al-3.5Ca, Mg-5Al-2.5Ca, and Mg-6Al-2.5Ca have

either similar or slightly lower susceptibility to hot tearing as compared to commercial alloy AZ91E. It is also found that freezing range and amount of eutectic play an important role on HTS of Mg-Al-Ca alloys.

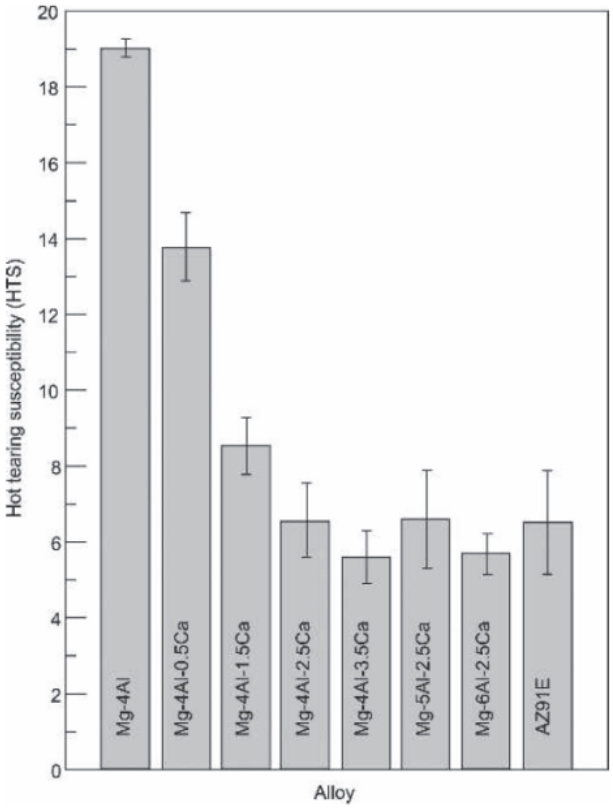

Fig. 2-14 Hot tearing susceptibility of ternary Mg-Al-Ca alloys evaluated by CRC, with commercial Mg alloy AZ91E included for comparison [23]

2.4.2.3 Mg-Al-Sr

Cao et al. [5, 24] also investigated HTS of Mg-Al-Sr alloys with the same mould as that used for Mg-Al-Ca alloys. Mg-xAl-1.5Sr and Mg-xAl-3Sr (both x= 4, 6, and 8, wt.%) alloys were investigated in detail. HTS of Mg-Al-Sr alloys are also compared with HTS of AZ91E. For both Mg-xAl-1.5Sr and Mg-xAl-3Sr alloy systems, HTS decreases with Al content. The decreasing trend of Mg-xAl-3Sr alloys is not as significant as for Mg-xAl-1.5Sr alloys. In addition, Mg-xAl-1.5Sr alloys show a higher HTS than Mg-xAl-3Sr alloys. The HTS of Mg-xAl-3Sr alloys is close to that of AZ91E.

2.4.2.4 Mg-Zn-Y

The influences of Y (0.2, 2 and 4, wt.%) additions on the hot tearing behaviour of Mg-1.5Zn alloys were investigated. Experiments were carried out using a CRC apparatus equipped with a load cell and data acquisition system [21]. The HTS of Mg-1.5Zn-xY alloys decreases with

increment in Y content at a mould temperature of 250 °C. The maximum HTS is obtained in Mg-1.5Zn-0.2Y alloy, which is due to its large grain size and solidification range.

The impact of Y additions on the HTS of Mg-3Zn-0.5Zr alloys was studied by Gunde et al. [22]. The permanent star-shaped mould was chosen for their study, as shown in Fig. 2-3. As the addition of Zr is mainly for grain refinement, the alloy is classified as Mg-Zn-Y alloys. In their study, the addition of a low content of Y (0.4 and 0.8 wt.%) results in a significant reduction of HTS. The reduced susceptibility is attributed to the effect of Y on the solidification path at the terminal period (f_s=0.9-0.98) of solidification. It increases the solidus temperature and thus shortens the solidification path, which in turn reduces the terminal freezing range. Via thermodynamic calculations, it is shown that this is caused by the formation of the ternary phase Mg_3YZn_6.

2.4.3 Other alloys

Investigation on hot tearing behaviour of AZ91 was carried out with a ring mould [72]. It is revealed that the temperature of hot tearing initiation is the practical solidifying end temperature (eutectic temperature) for AZ91. Moreover, eutectic is found to induce the hot tearing of AZ91 alloy. Effect of pouring temperature and mould temperature on HTS of AZ91 was also studied [15, 65]. The results suggest that increasing the mould temperature significantly reduces HTS of AZ91. Mould temperature above 340 °C can virtually eliminate hot tears through a morphological change of the alloys beta-phase regions, which enables liquid metal feeding of the casting at later stages of solid fraction and high fractions of solid. The effect of increasing the pouring temperature to reduce hot tearing was less pronounced than that of varying the mould temperature.

Hot tearing of AZ91D, AZ91E, AM50A, ITM (AX51, 0.8% Ca), AJ50x (0.2Ca, 0.5Sr), AS21, AS21x, AS41B, AE42, AJ51x, AJ52x, AJ53x, AJ62x, and AJ62Lx alloys were studied and the HTS of them were rated [73]. The setup for assessing HTS was the same as that shown in Fig. 2-4. The highest HTS is observed in the AE42 alloy and the lowest is found in the AJ62x alloys. Hot cracking behaviour of Ca containing Mg alloys was also compared in thin wall die casting [74]. The addition of Ca to AM50 increased the frequency and severity of hot cracking. Raising the Ca level to 1.7% (AXJ520) improved the casting rating, although not to the level of AM50. With even higher Ca additions, the hot cracking deteriorated again.

Effect of trace elements on hot tearing behaviour of commercial alloys was also studied [27, 29, 75]. The effects of Ca and Sr composite addition into AZ91D alloy on the hot cracking resistance were investigated [75]. Mechanisms were also determined. By adding Ca, the hot

cracking resistance of AZ91D alloy decreases. In contrast, adding Sr to Ca-containing AZ91D alloy effectively improved the hot tearing resistance. Li et al. [29] investigated the influence of Sr on HTS of AM60B. Only a small amount of Sr addition can improve the HTS of AM60B. Effect of RE on hot cracking behaviour of AZ31, AZ91, and AM60 was also studied [27]. Results show that RE increase HTS of those commercial alloys. This is due to a grain coarsening, eutectic temperature increment, and intermetallics induced by RE elements. Intermetallics are believed to block the feeding channel, which leads to high HTS.

2.5 Mg-Ca and Mg-Zn-Ca alloys

The alloying element Ca plays a quite important role on adjusting the mechanical properties of structural or medical magnesium alloys [30-32, 76]. It is found that Ca enhances the oxidation resistance of Mg-Ca and AZ31 alloys [77, 78]. Calcium is one of the solute grain refiner in Mg alloys, which is due to the effective grain growth restriction [79]. Addition of about 0.2 wt.% of Ca, can effectively refine the microstructure of Mg-Zn-Si and Mg-Al-Zn-Si alloys and therefore improve tensile strength [80]. The addition of Ca in AZ alloys improves the creep resistance due to the formation of thermal stable intermetallic Al_2Ca [30]. It is also found that Ca weakens the texture of extruded Mg-Ca-Zn alloys [81, 82]. The weakening of extrusion textures is related to the particle stimulated nucleation of recrystallization (PSN) and the particle retarded the growth of the dynamic recrystallization grains. As both Mg and Ca have an excellent biocompatibility, binary Mg-Ca alloys have attracted a considerable attention for biomaterial applications in recent years [33, 83]. Microstructure, mechanical properties, electrochemical behavior, and degradation kinetics of Mg-Ca implants are all affected by the amount of alloying element, i.e., Ca [83]. Thus, Mg-Ca alloys have shown to be very promising in development of biodegradable, biocompatible, metallic orthopedic implants.

Mg-Zn-Ca ternary alloys have a great potential for biodegradable and automotive applications [34, 35]. Zhang et al. [36-38] carried out a series of investigations on biodegradable ternary Mg-Zn-Ca alloys. The mechanical properties can be tailored by adjusting the ratio of Zn to Ca. Moreover, both *in vitro* and *in vivo* studies showed that the designated Mg-Zn-Ca ternary alloys are biocompatible and have a satisfactory corrosion resistance. Previous investigations also showed that Mg-Zn-Ca alloys have an excellent creep resistance [35, 39]. Their mechanical properties as well as corrosion resistance can be further improved by subsequent thermomechanical processing [84], heat treatments [85, 86], further alloying [39, 87], and surface treatment [88]. With addition of 0.6 wt.% Zr [39], the tensile strength and ductility of

Mg-1Ca-1Zn alloy are found to be superior to that of AZ91 alloy. Moreover, the creep resistance of Mg-1Ca-1Zn-0.6Zr alloy is also significantly higher than that of AZ91 alloy at temperatures up to 150 ^{0}C. These results indicate that Mg-1Ca-1Zn-0.6Zr alloy has a significant potential for automotive applications, especially at elevated temperatures.

2.6 Numerical simulation of hot tearing

The application of numerical simulation techniques in metal casting has provided insights into understanding the effects of alloy chemistry, thermal-fluid transport phenomena, and their relationship to the alloy microstructure and the formation of defects [89]. It can be used to reduce the time required for new product design cycles and as a tool for quality assurance. Because of the complex mechanisms acting during the solidification of metals, the prediction of a hot tearing phenomenon is not an easy task. The complexity of mushy zone makes the hot tear modeling even more demanding [90]. Several softwares are used to model hot tearing, such as ProCAST [66, 91, 92], MAGMAsoft [93-97], and ABAQUS [98], etc.

2.6.1 Simulation methods

2.6.1.1 ProCAST

The commercial numerical simulation software ProCAST simulates the process of casting and solidification based on finite elemental method. ProCAST has been extensively used in foundries to understand the physical phenomena occurred during solidification. In this software, there are two modules that can be used to predict hot cracking [92]. One is HCS, which is based on RDG model. The other is hot tearing inidicator (HTI), which is based on Gurson's constitutive model. According to the manual of ProCAST [92], HCS is only suitable for steady-state conditions, as encountered in continuous (or DC) casting. HTI should be used to compare different designs with the same alloy.

The HTI is a strain-driven model based upon the total strain which develops during solidification. The model computes the elastic and plastic strains at a given node when the fraction of solid is between the critical solid fraction (usually 50%) and 99%. It is assumed that the casting is isotropic (although at the final stage of the solidification, the castings may exhibit localized anisotropic behaviour). The HTI (e_{ht}) was obtained as follows:

$$e_{ht} = \bar{\varepsilon}_{ht}^{p} = \int_{t_c}^{t} \sqrt{\frac{2}{3}\dot{\varepsilon}^{p} : \dot{\varepsilon}^{p}}\, d\tau, \quad t_C \le t \le t_S \qquad 2\text{-}16$$

where $\bar{\varepsilon}_{ht}^{p}$ is the critical accumulated effective plastic strain for the initiation of hot tearing, $\dot{\varepsilon}^{p}$ is the effective plastic strain rate, t_C is the time when the coherency temperature is reached, and t_S denotes the time when the solidus temperature is reached, : is the dyadic tensor.

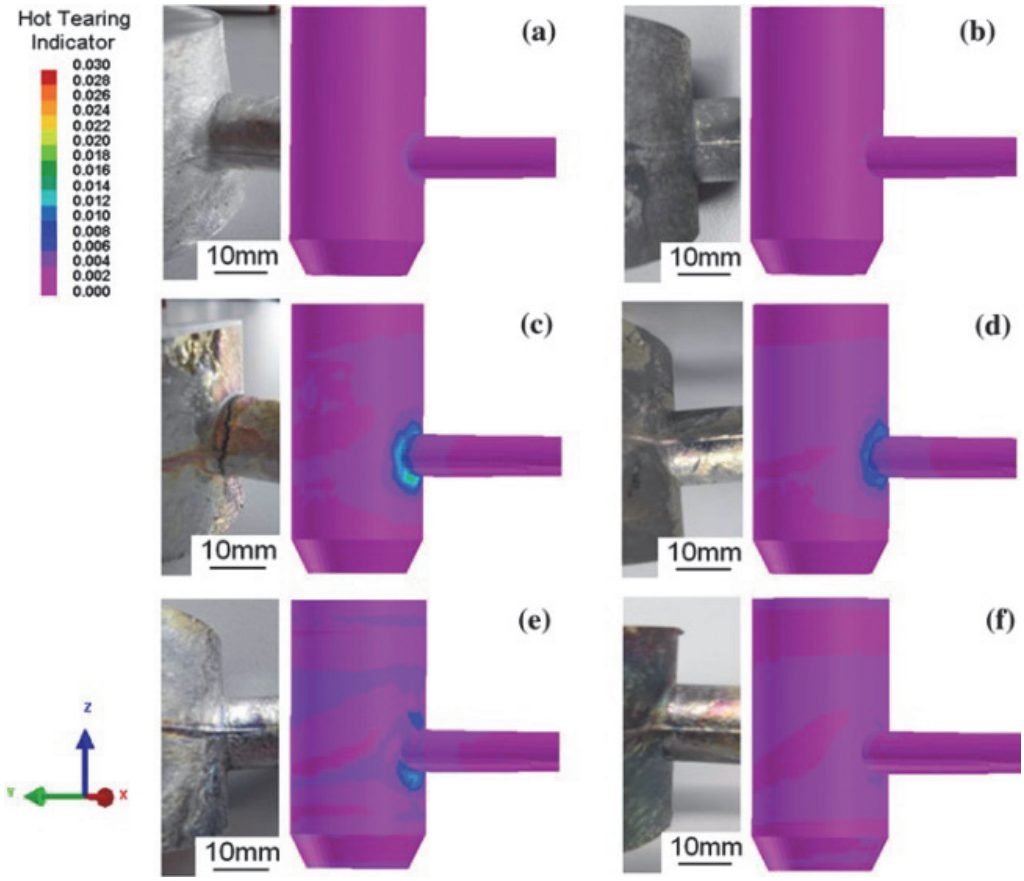

Fig. 2-15 Comparison between simulated HTI and experiments, (a), (b) Mg-0.2Y, (c), (d) Mg-1.5Y, and (e), (f) Mg-4Y, (a), (c), (e) T_{mould} =250 ℃, (b) (d) (f) T_{mould} =450 ℃ [66]

In fact, as shown by the above equation, HTI is the accumulated plastic strain in the semi-solid region that corresponds to the void nucleation. Therefore, it should provide a good indication for the susceptibility of the hot tearing occurred during solidification.

Wang et al. [9, 66] simulated the HTI of Mg-Y and Mg-Zn-Y alloys with ProCAST. The simulation and experimental results of Mg-Y alloys were compared in Fig. 2-15. Simulation results are in good agreement with experimental results. Zhu et al. [91] also used ProCAST to simulate hot tearing formation in binary Mg-Al alloys. Results show that the simulations agree well with the experimental results.

2.6.1.2 MAGMAsoft

A new viscoplastic deformation model was used to predict hot tears in an AZ91D magnesium alloy permanent mould casting with MAGMAsoft [94]. The predicted damage from the simulations was found to be in good agreement with the hot tears observed in the experiments, both in terms of location and severity. The simulation results corroborate that the hot tears form most likely at the junction between the horizontal bar and the vertical sprue. The simulation results also confirm that HTS decreases with increasing mould temperature. These results indicate that the damage calculated using the new viscoplastic deformation model is a reasonable predictor of hot tearing.

2.6.1.3 ABAQUS

ABAQUS is used to predict hot tearing in welding processes [98]. Novel steel sand casting experiments, which allow for simultaneous displacement and force measurements, are used to validate the model predictions. Good overall agreement is obtained. However, some uncertainty remains regarding the high temperature mechanical properties used in the simulations. Additional work is needed to verify the model for situations where significant hot tearing occurs. Such hot tearing significantly affects the subsequent deformation of a casting.

2.6.2 A new 3-D granular model

Recently, a 3-D granular hydromechanical coupled model has been developed to predict hot tear formation in solidifying alloys [60, 99]. This model is able to predict the overall response of semi-solid alloys to an externally applied strain before and after fracture initiation, while accounting for the localization of strains at grain boundaries. The results of a granular model have been compared with *in situ* X-ray tomographic observations made during the tensile deformation of a mushy Al–Cu alloy specimen, as shown in Fig. 2-16. Good agreement is obtained between modeling and experiments. It proves that the specimen continuously necks, allowing the liquid channels perpendicular to the tensile axis to open by feeding them with the liquid coming from neighbouring zones and from channels which are parallel to the tensile axis and tend to close. Once the liquid is no longer able to feed the deformed zone, cracks form in the structure. The granular model also demonstrates that the grain size has a large effect on the ‘overpressure’ required to overcome the capillary forces at the liquid–void interface. Because of this dependence, the HTS increases with increasing grain size.

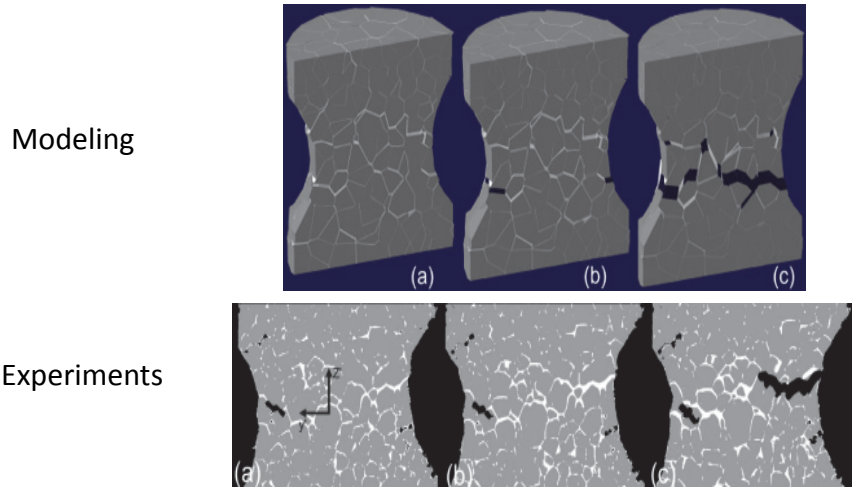

Fig. 2-16 Comparison between granular modelling and experiments, (a) t=405 s for modelling, t=486 s for experiments, (b) t= 729 s, and (c) t=1215 s [60]

3 Motivations and objectives

Investigations on the castability of magnesium alloys indicated that many alloy systems are often prone to hot tearing [72-74, 100]. Defect (hot tearing)-free Mg castings are desired for the subsequent processing and service. Thus, it is of great importance to study the hot tearing behaviour of Mg alloys. In the past decades, hot tearing of Al alloys, steel and some Mg alloys were extensively studied [3, 6, 23]. However, the mechniasms of hot tearing are still not fully understood.

Mg-Ca alloys are being considered as potential degradable biomaterials [33]. However, the past investigations indicated that the addition of Ca could deteriorate the castability of Mg alloys [74]. The mechanism for this behavior is still unclear and a systematic investigation on hot tearing susceptibility of Mg-Ca binary alloy is limited. Mg-Ca-Zn ternary alloys have great potential for biodegradable and automotive applications [34, 35]. The investigation on hot tearing behaviour of Mg-Ca-Zn alloys is still limited.

Therefore, the hot tearing behaviour of binary Mg-Ca and ternary Mg-Ca-Zn systems were investigated. The composition designation of binary Mg-Ca and ternary Mg-Ca-Zn alloys were based on the following priciples: binary Mg-Ca alloys were designed according to thermodynamic calculation results, while ternary Mg-Ca-Zn alloys were designed based on the hot tearing results of binary Mg-Ca alloys. Moreover, those ternary Mg-Ca-Zn alloys, which were used most often in other research investigations, were also taken into consideration.

The HTS of binary Mg-Ca and ternary Mg-Ca-Zn systems are investigated by experimental methods and numerical simulation. The objectives of this study are given as follows:

- Predict CSC of binary Mg-Ca alloys by thermodynamic calculation using the Clyne and Davies' model.
- Investigate HTS of binary Mg-Ca and ternary Mg-Ca-Zn alloys by an instrumented CRC mould apparatus.
- Study the effects of initial mould temperature, grain size, second phases, and eutectic on HTS of Mg-Ca-(Zn) alloys.
- Carry out computer simulations on temperature, solid fraction fields and HTI using casting simulation software ProCAST.
- Propose possible mechanisms of hot tearing in different Mg-Ca-(Zn) alloys.

4 Experimental procedure and simulation

4.1 Experimental procedure

4.1.1 Casting

In this study, Mg-xCa, Mg-0.5Ca-xZn, Mg-2Ca-xZn, Mg-xCa-4Zn and Mg-0.5Ca-4Zn-0.2Zr alloys were cast. Detailed nominal compositions are listed in Table 4-1. Pure Mg, pure Ca, Mg- 10 wt.% Ca master alloy, pure Zn, and Mg-33 wt.% Zr master alloys were used. The master alloy Mg-10 wt.% Ca was used for the preparation of low Ca content Mg alloys such as Mg-0.1Ca and Mg-0.2Ca alloys.

Table 4-1 Nominal compositions of tested alloys (wt.%)

Alloys	Zn	Ca	Zr	Mg
Mg-0.1Ca	-	0.1	-	Bal.
Mg-0.2Ca	-	0.2	-	Bal.
Mg-0.5Ca	-	0.5	-	Bal.
Mg-1Ca	-	1	-	Bal.
Mg-2Ca	-	2	-	Bal.
Mg-0.5Ca-0.5Zn	0.5	0.5	-	Bal.
Mg-0.5Ca-1.5Zn	0.5	1.5	-	Bal.
Mg-0.5Ca-4Zn	0.5	4	-	Bal.
Mg-0.5Ca-6Zn	0.5	6	-	Bal.
Mg-2Ca-0.5Zn	2	0.5	-	Bal.
Mg-2Ca-1.5Zn	2	1.5	-	Bal.
Mg-2Ca-4Zn	2	4	-	Bal.
Mg-2Ca-6Zn	2	6	-	Bal.
Mg-0.2Ca-4Zn	0.2	4	-	Bal.
Mg-1Ca-4Zn	1	4	-	Bal.
Mg-0.5Ca-4Zn-0.5Zr	0.5	4	0.5	Bal.

Approximately 350 g of Mg was melted in a mild steel crucible under a protective gas mixture of high pure Ar + 0.2% SF_6. Calcium, Zn, and/or the master alloys were added to magnesium melt at 700 ^{0}C and manually stirred for 2 min. Then the melt was heated to 750 ^{0}C, held at this temperature for 5 min, and cast into a constraint rod casting (CRC) mould. The mould

was coated with a thin layer of boron nitride (α-BN, hexagonal) and preheated to 250 ^{0}C or 450 ^{0}C, marked as T_{mould}=250 ^{0}C and T_{mould}=450 ^{0}C, respectively. The casting was extracted from the mould after it completely solidified. For each alloy the hot tearing test was carried out at least three times.

4.1.2 Hot tearing apparatus

The setup used in this study was previously developed at MagIC (Magnesium Innovation Center, Helmholtz Zentrum Geesthacht) [8], and is shown in Fig. 4-1. The setup consists of a CRC mould, a temperature monitor and measurement system, a contraction force measurement system with a load cell, and a data recording unit (as marked in Fig. 4-1 (a)). A similar apparatus can be found in the Cao et al.'s work [17]. However, the present CRC mould differs from the others as the rod portion of the mould was designed with a taper (diameter decreased from 12.5 mm at the junction to 10 mm at the end of the rod). This unique design successfully eliminated the influence of friction between the mould and casting rod, which ensures the collected contraction force data more reliable. Locations of three thermocouples (blue lines: TC 1, TC 2, and TC 3) are shown in Fig. 4-1 (b). All the thermocouples were inserted in steel tubes and firmly fixed on the mould.

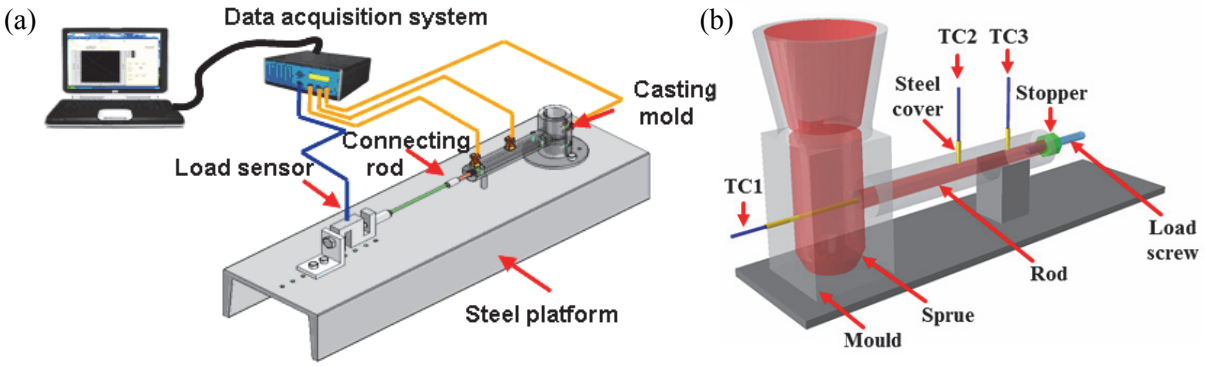

Fig. 4-1 Schematic diagram of the apparatus, (a) the complete appratus, (b) close-up of CRC mould (TC-Thermocouple).

The principle of the apparatus is to monitor the evolution of hot tearing using the measurement of the contraction stress and temperature. Due to the temperature difference, the casting at the rear end solidified at first and the surrounding Mg casting enwrapped the load screw. As the load screw was fixed, a constraint is generated in the axial direction of the casting rod. Consequently, a hot tear might occur as a result of such constraint. By analysing the force development during solidification, the characteristics of hot tearing including the initiation of hot tearing, the evolution and final size of the hot crack and so on can then be investigated. With the simultaneously recorded temperature, the corresponding solid fraction

during solidification process was estimated using Pandat software. Combining the force evolution and solidification process the hot tear mechanisms were identified.

4.1.3 Typical hot tearing curves

During casting procedure, temperature, force, and time were simultaneously recorded and used to generate the force-temperature-time curves. Fig. 4-2 displays two typical force-temperature-time curves. It is to be noted that the temperature data in these curves was taken from TC 1 (Fig. 4-1 (b)), which was placed near the hot spot at the sprue-rod junction. The detailed explanations of the force curves can be found elsewhere [19, 20]. A typical force curve can be divided into 4 stages:

I. A force drop or bumping at the very beginning of the force curve which could be due to pouring process [20]. As the melt flows toward the load cell and induces internal compression.
II. A increase in force afterwards due to the commencement of solidification. The casting begins to contract but the load cell restricts such contraction.
III. A force drop or a force increment change due to the formation and propagation of hot tear.
IV. A force increase after the hot crack propagation due to solid shrinkage during cooling.

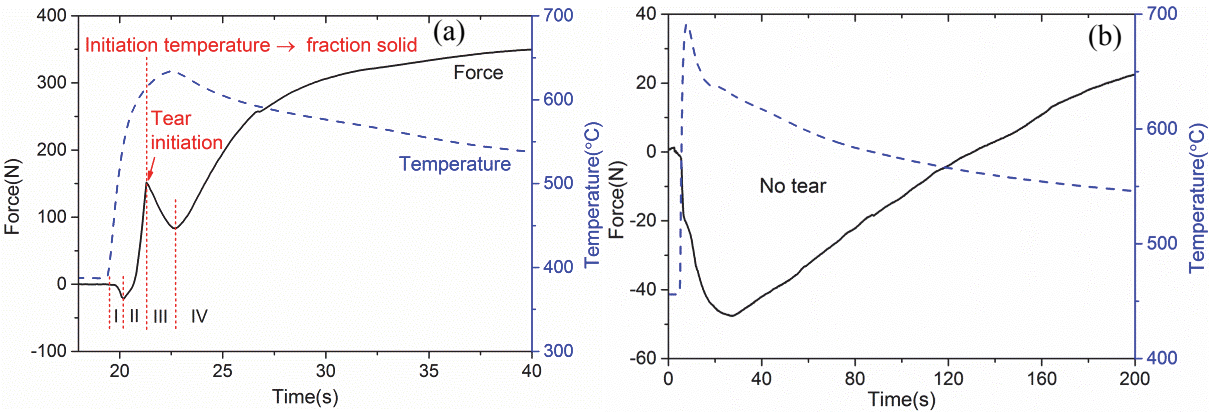

Fig. 4-2 Typical force-temperature-time curves, (a) hot tear, (b) no hot tear

Among them, the force drop during stage III is of great importance as it provides information about the initiation and propagation of hot tears. Therefore, the force drop was used to identifiy the hot tearing initiation, as shown in Fig. 4-2 (a). For some alloys, the force drop was invisible, indicating no hot tear initiated, as shown in Fig. 4-2 (b).

By locating the force drop position, the temperature of hot tearing initiation (T_i) is determined. The corresponding solid fraction (f_{si}) can be obtained from Pandat software using Scheil solidification model. The entire duration of force drop is regarded as tear propagation, as hot

tearing is a stress relieving process. After the termination of tear propagation, the force continues to increase due to the solidification and further cooling of the casting.

4.1.4 Evaluation of the hot tears

There are several ways to evaluate the hot tearing susceptibility. Normally, the size of a hot crack (either the total size or the width of crack) or equation based on the size of crack was used as the index of HTS [17, 28, 74]. However, large errors are inevitable because the depth of crack was not taken into account and the complexity of the crack pattern. Crack volume was introduced by Zhen et al. [8] to quantify the hot tearing tendency, which takes the three dimensions of the crack into consideration. Both wax penetration and X-ray tomography methods were used to measure the crack volume. It is well established from the previous investigation that X-ray micro-tomography is a reliable technique to analyse the hot crack [19]. There are two advantages of this technique: i. 3D images of the cracks can be obtained, which were later used to reconstruct the three dimensional crack distribution in the casting, ii. the complete crack volume, including both closed and open cracks, can be accurately quantified. The quantified crack volumes were used as an index of HTS.

Initially, the hot tears of the castings were photographed using digital camera and visually inspected, as shown in Fig. 4-3 (a). The macro view of the hot tearing provides an intuitive and initial impression on the severity of hot tearing.

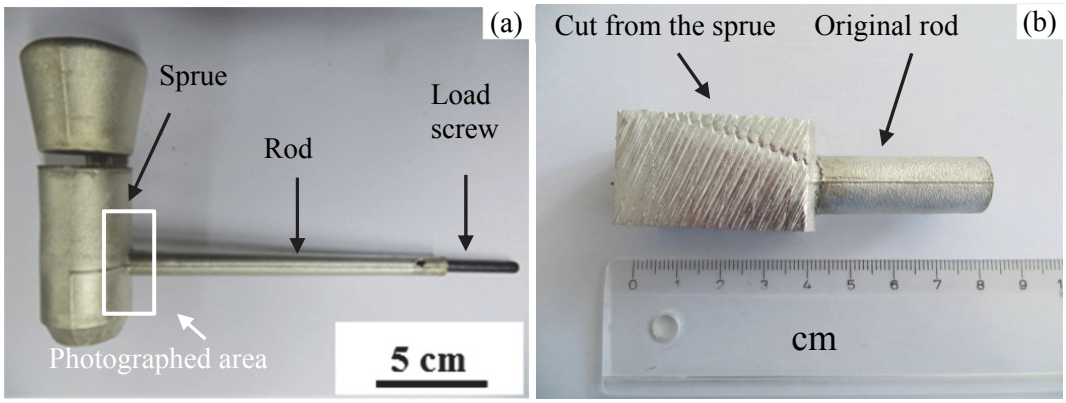

Fig. 4-3 Photographs of (a) the CRC mold casting, (b) sample for X-ray tomography machined out of the casting

The hot tears were then observed more in detail with X-ray micro-tomography. The hot tear was evaluated in a 3D X-ray tube-based high resolution tomography (nanotom® s – phoenix, GE Measurement & Control Solutions, Germany). The 3D volume reconstruction was made from the 2D projections (with a filtered back projection algorithm) using datos|x2.0 reconstruction software (phoenix, GE Measurement & Control Solutions, Germany). The resolution achieved after reconstruction of the volume in the interesting region was about 20

μm. Further data processing, including normalization and alignment of the 3D-data sets, the segmentation and characterization of the crack volume were done using the software IDL 8.1 (Exelis Visual Information Solutions, Inc., Germany). The complete CRC mould castings and the sample machined out for the X-ray experiments are shown in Fig. 4-3. The samples for the tomography consisted of both rod and a machined portion of cubic from the sprue of the castings so as to have the crack in the middle, Fig. 4-3 (b). The diameter of the rod was around 12 mm whereas the cubic portion from the sprue was machined to the smallest possible size without affecting the morphology of the tear to obtain the best tomography resolution. The crack volume of samples was calculated based on the 3D volume reconstruction results. The average crack volume of a minimum two samples was calculated for each alloy.

4.1.5 Characterization of microstructure and fracture surface

The microstructures and tear morphology of the cross-section of the region near the tear were investigated by optical microscopy (OM) and scanning electron microscopy (SEM). The samples were cold mounted, ground with SiC abrasive paper (grits size from 120, 500, 800, 1200, to 2500), polished with water free OPS and 1 μm diamond suspension. Then they were chemically etched in a solution of 8 g picric acid, 5 ml acetic acid, 10 ml distilled water, and 100 ml ethanol for around 5 s. Optical microscopy was performed with a LEICA DMI5000 M microscopy. Scanning electron microscopy was performed with a Zeiss Ultra 55 SEM equipped with Energy Dispersive X-ray Spectroscopy (EDX). The fracture surface of castings with a severe tear was also observed by SEM. X-ray diffraction (XRD) was carried out with a diffractometer (Siemens D5000, Germany) equipped with Cu Kα radiation to identify the constituent phases at the hot tearing area. The XRD measurement was performed at 40 kV and a tube current of 40 mA over the 2θ ranging from 10^0 to 90^0, using a step size of 0.01^o with a counting time of 5 s at each step.

4.1.6 Residual strain measurement

Neutron diffraction is proved to be a useful technique to analyse the residual strain/stress in magnesium alloys [70]. As the formation of hot tears will release the residual strain, thus in this work, residual strain in the castings with a tiny crack or no visible cracks was measured by neutron diffractometer STRESS-SPEC at FRM II (Heinz Maier-Leibnitz Zentrum, Garching, Germany).

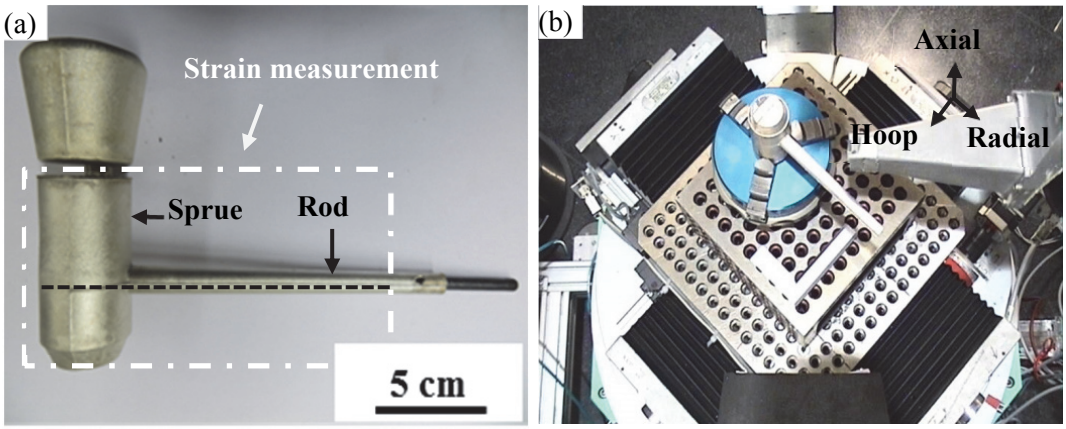

Fig. 4-4 (a) Macroscopic picture of casting for residual strain measurement; (b) instrument setup at STRESS-SPEC for the axial direction strain scanning.

Fig. 4-4 shows the photographs of CRC mould cast sample marked with the portion used for the residual strain measurement and the neutron diffraction instrument. The measurements were performed at room temperature. A wavelength of 0.147 nm provided by Si (400) monochromator was selected to measure the position variations of diffraction peaks from (211) and (203) planes of Mg. In a hexagonal system, these planes are written as $(21\bar{3}1)$ and $(20\bar{2}3)$, respectively. The sampling volume 3×3×2 mm^3 was controlled using a primary slit of 3×3 mm^2 and a radial collimator with FWHM (full width of half maximum) = 2 mm. Due to relatively large grains of the cast ingot, the sample was oscillated around Ω angle with amplitude of ± 5°, which ensured that more grains were subjected to the sampling volume. A cubic sample with a volume of 8 mm^3cut from the sprue was used as the stress-free reference.

Triaxial strain scanning (radial, hoop, and axial, as illustrated in Fig. 4-4 (b)) was carried out with a step size of 4 mm through the central line of sprue and rod. The lattice strain (ε_{hkl}) for the (21.1) and (20.3) reflection at a constant wavelength was calculated by,

$$\varepsilon_{hkl} = \frac{d_{hkl} - d_{hkl}^0}{d_{hkl}^0} = \frac{\sin\theta_{hkl}^0}{\sin\theta_{hkl}} - 1 \qquad 4\text{-}1$$

where d_{hkl} is the lattice spacing of *hkl* planes in the residual stressed materials and θ_{hkl} the corresponding diffraction angle, d_{hkl}^0 is the lattice spacing of *hkl* planes in the stress-free materials and θ_{hkl}^0 the corresponding diffraction angle.

4.2 Numerical simulation by ProCAST

4.2.1 Geometry and mesh

The model includes four assembled parts: mould, casting ingot, graphite stopper, and load screw, as shown in Fig. 4-5. All the dimensions are given in mm.

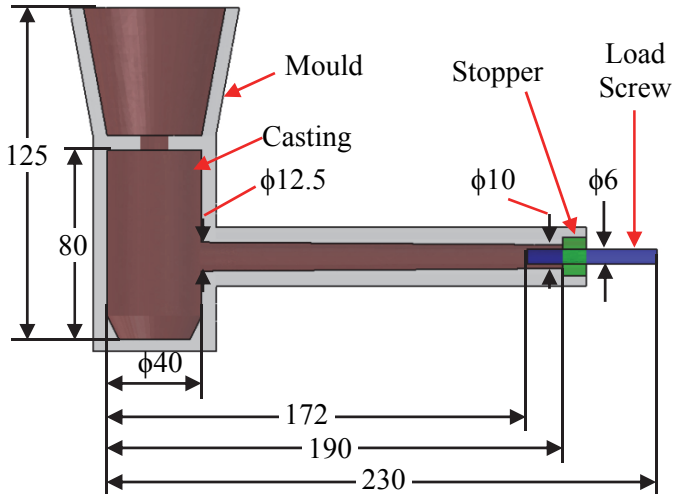

Fig. 4-5 Geometry of the model used in ProCAST simulation, unit: mm.

The mesh generator Visual-Mesh was used to construct the computational grid of the casting and the mould. Construction of this mesh is important, as it determines the accuracy of the computations and the time required for modeling. Fig. 4-6 shows the computational mesh of the casting and mould. Four node linear tetrahedral finite-elements were chosen for the ingot and the mould. A finer finite-element mesh was chosen for the ingot to increase the accuracy of the calculations, while a coarse mesh density was used for the mould.

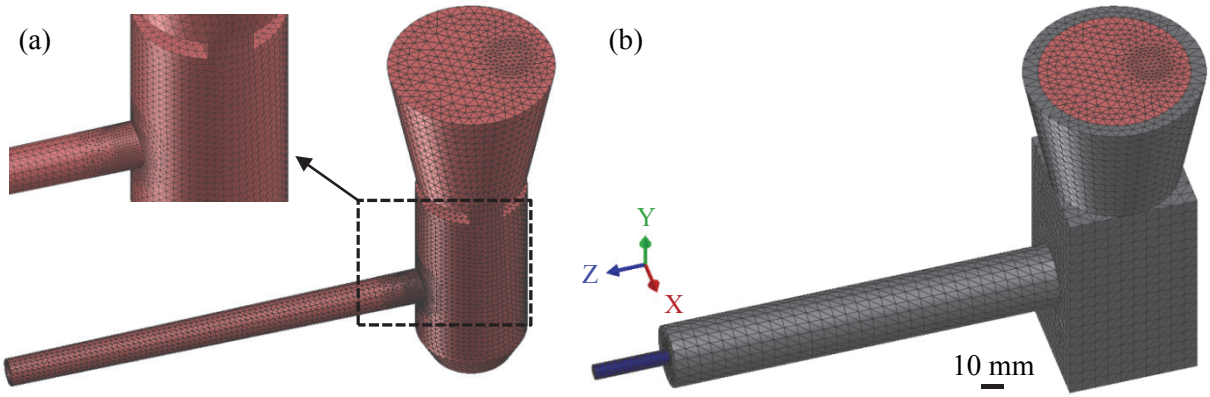

Fig. 4-6 Computational meshing of the casting and mould: (a) casting, (b) mould

4.2.2 Materials properties

The materials properties of the casting were computed using Scheil diffusion model for each alloy by ProCAST. ProCAST provided access to CompuTherm database to compute the materials properties of Mg alloys. It is possible to compute the thermal properties such as, solid fraction, density, viscosity, and thermal conductivity, based upon the chemical composition of the alloys. Besides the thermal properties, some stress properties can also be calculated automatically. The Young's modulus, the Poisson's ratio and the thermal expansion coefficient of Mg-Ca and Mg-Zn-Ca alloys were calculated based upon the phases obtained from the thermodynamic databases.

The material properties of the mould, load screw, and stopper were taken from the database of ProCAST. The mould and the load screw were assigned as H13 steel and the stopper was assigned as graphite.

4.2.3 Boundary and initial conditions

1. Volume manager: the intial filling of casting and the other three parts were set as 0.00% and 100.00%; the initial temperature of casting was set as 700 °C, either 250 °C or 450 °C was applied for the other three parts; the stress type for the casting was chosen as Linear-Elastic, the other three parts were set as rigid.
2. Interface HTC manager: the heat transfer coefficient between casting and mould was set as 500 W/(m^2·K)
3. Process condition manager: zero displacement was applied for the Z direction at the end of the rod, and zero displacements in all directions were assigned for the other parts.
4. Gravity definition: a gravity of 9.8 m/s^2 is applied to the ingot at the -Y Axis.
5. Simulation parameters: the stress model activation was set as “ON”.

4.2.4 Simulation results analysis

Simulation performed for the hydrodynamics of the casting procedure (the filling of the mould with the alloy), crystallization and cooling of the casting, formation of stresses and strains in the casting were all executed simultaneously. The results of temperature, solid fraction and HTI fields were displayed with Visual-Viewer. The HTI was defined as accumulated elastic and plastic strain during a solid fraction of 0.5-0.99 [92].

5 Results

5.1 Hot tearing of Mg-xCa binary alloy

5.1.1 Chemical composition

As trace elements might affect the HTS of Mg alloys, chemical compositions of as cast hot tearing samples were measured. Chemical compositions at different mould temperatures are listed in Table 5-1 and Table 5-2. The measured compositions were close to the nominal composition, and trace elements content was rare.

Table 5-1 Chemical compositions of Mg-xCa alloys at T_{mould} = 250 ^{0}C, in wt.%

Alloy	Ca	Fe	Cu	Ni	Mg
Mg-0.1Ca	0.08	0.0059	0.0018	0.0016	Bal.
Mg-0.2Ca	0.20	0.0056	0.0017	0.0015	Bal.
Mg-0.5Ca	0.53	0.0037	0.0017	0.0013	Bal.
Mg-1Ca	0.84	0.0042	0.0016	0.0013	Bal.
Mg-2Ca	1.91	0.0041	0.0016	0.0011	Bal.

Table 5-2 Chemical compositions of Mg-xCa alloys at T_{mould} = 450 ^{0}C, in wt.%

Alloy	Ca	Fe	Cu	Ni	Mg
Mg-0.1Ca	0.08	0.0052	0.0019	0.0014	Bal.
Mg-0.2Ca	0.19	0.0052	0.0018	0.0013	Bal.
Mg-0.5Ca	0.47	0.0059	0.0016	0.0014	Bal.
Mg-1Ca	0.99	0.0067	0.0017	0.0014	Bal.
Mg-2Ca	1.93	0.0072	0.0019	0.0015	Bal.

5.1.2 Experimental hot tearing tendency

5.1.2.1 Force-temperature-time curves

The as recorded force-temperature-time curves for Mg-xCa alloys at T_{mould} = 250 ^{0}C are shown in Fig. 5-1. The T_i and f_{si} of all the alloys were determined using the method described in section 4.1.3. For instance, the hot tear initiated at 596 °C for Mg-0.1Ca alloy (Fig. 5-1 (a)), and the corresponding solid fraction (f_{si}) was 0.989. Hot tearing occurred at a relatively high temperature in Mg-0.5Ca and Mg-1Ca alloys.

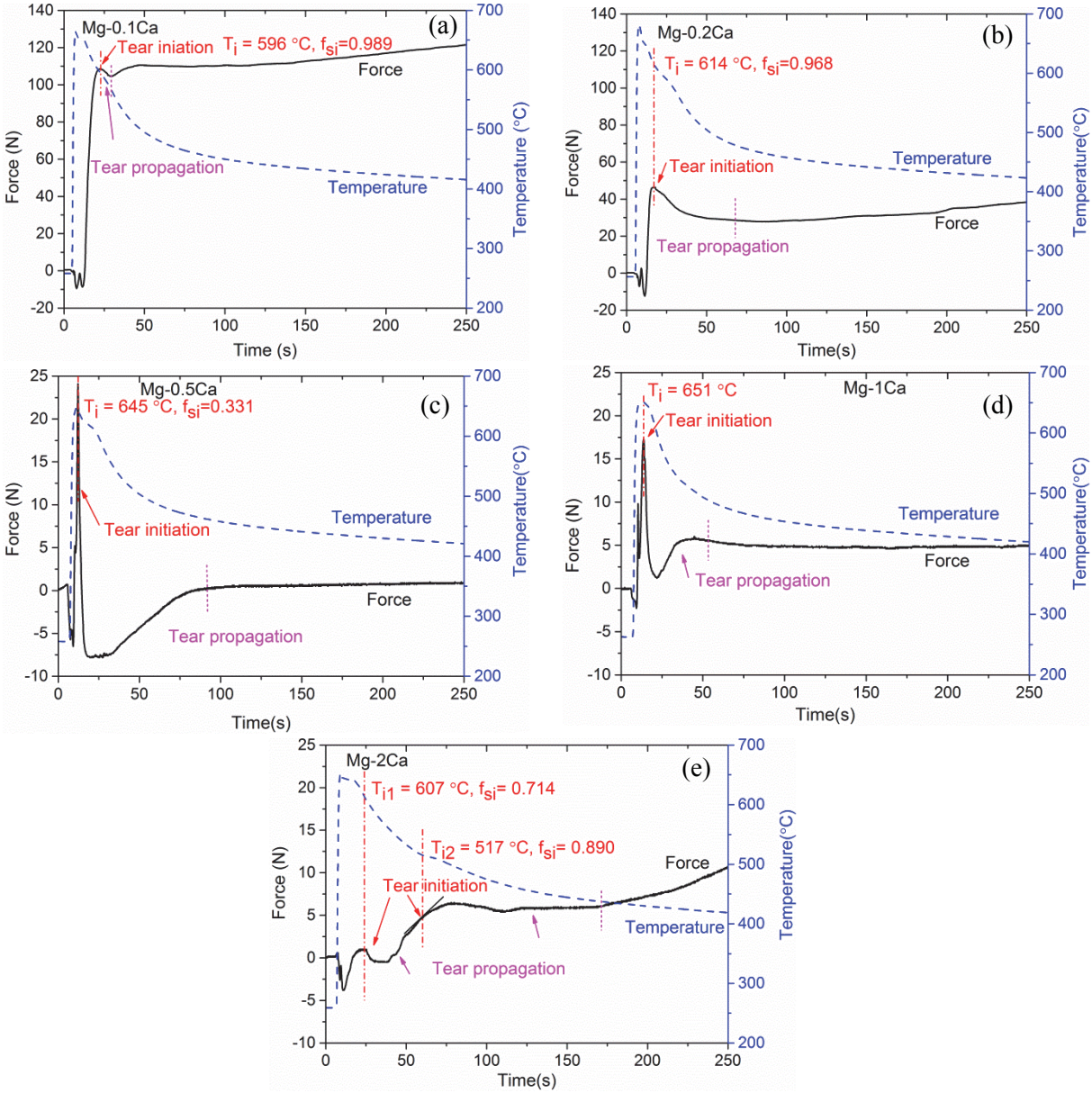

Fig. 5-1 Force-temperature-time curves of Mg-xCa alloys cast at T_{mould} = 250 ^{0}C (a) Mg-0.1Ca, (b) Mg-0.2Ca, (c) Mg-0.5Ca, (d) Mg-1Ca, and (e) Mg-2Ca

The high T_i is probably due to their high HTS. As shown in Fig. 4-1 (b), the thermocouple (TC1) was located in the centre of the junction. As a result, the recorded temperature was localized. According to the solidification sequence, the outer region of the junction area solidifies much faster than the centre region. Due to the wide solidification ranges in Mg-0.5Ca (131 ^{o}C) and Mg-1Ca (129 ^{o}C), it is highly possible that the crack initiated at the outer region, while the centre region still had a relatively low solid fraction. The high HTS is also evidenced at the last stage of the force development curve. At stage (IV), the force increment was stopped or became slow in Mg-0.5Ca and Mg-1Ca alloys, indicating that the hot cracking either was severe or even the rod portion of the casting was completely broken. Interestingly,

two force drops were observed for Mg-2Ca alloy, indicating that the hot tear initiated more than once in this alloy. Cao et al. [6] also observed multiple -force drops for Mg-Al alloys [17].

As mentioned previously, the end of the force drop is generally considered as the termination of crack propagation. However, for Mg-0.5Ca and Mg-1Ca alloys, the point where the contraction force plateaus (stops to increase) is regarded as the termination of tear propagation. The plateau in force indicates that the sample is totally broken. Thus, the commencement of the plateau should be considered as the end of the crack propagation.

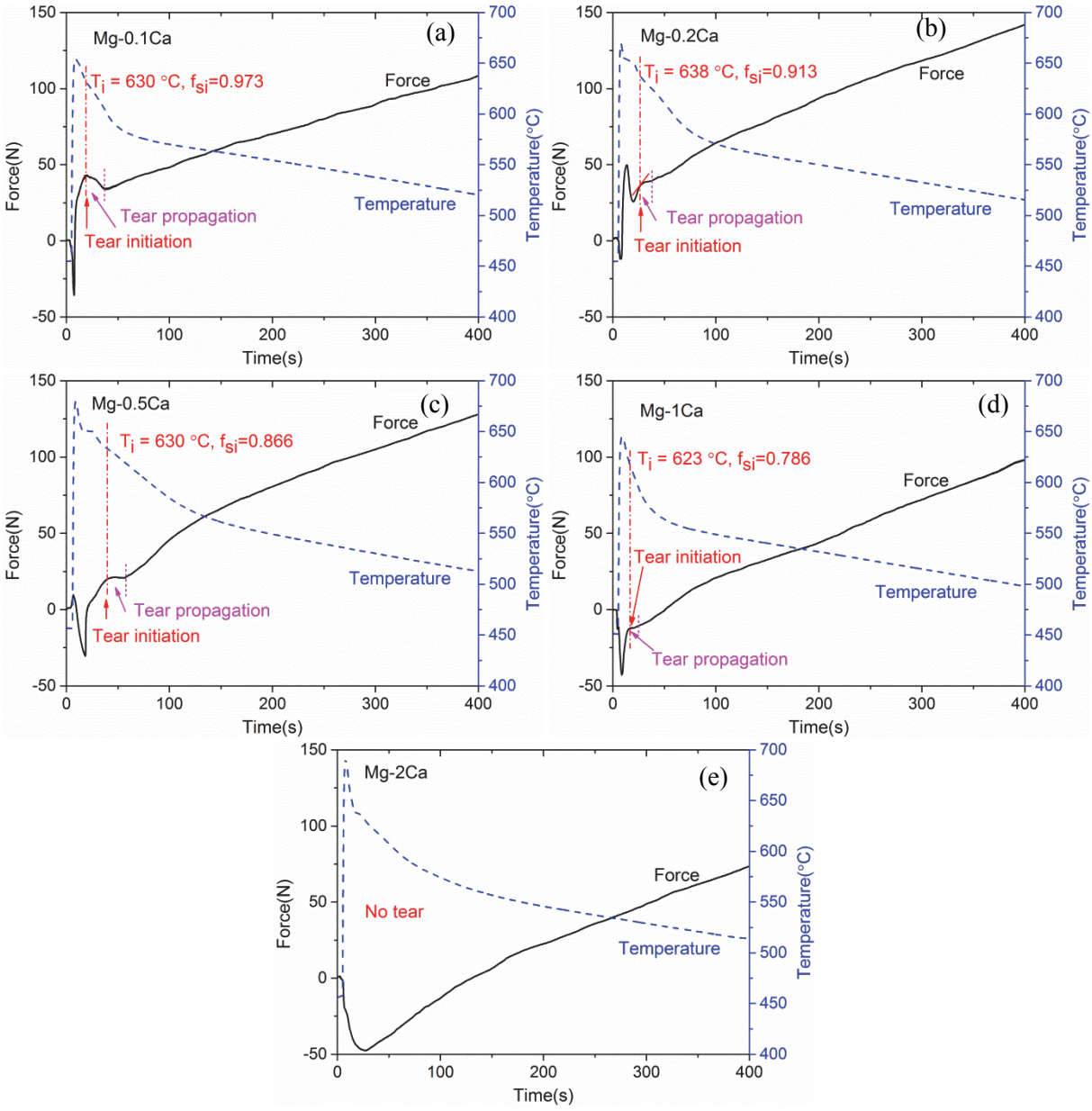

Fig. 5-2 Force-temperature-time curves of Mg-xCa alloys cast at T_{mould} = 450 ^{0}C (a) Mg-0.1Ca, (b) Mg-0.2Ca, (c) Mg-0.5Ca, (d) Mg-1Ca, and (e) Mg-2Ca

Force-temperature-time curves of Mg-xCa alloys cast at T_{mould} = 450 ^{0}C are shown in Fig. 5-2. For some alloys, the force drop is not so evident, which is due to both the simultaneous contribution of contraction force and and tear initiation (i.e. tension and compression). Instead, a sudden force increment change or a small force plateau is visible on the force curve. Therefore, as reported by Huang et al. [16] and Wang et al. [19], it is reasonable to consider the beginning of the sudden force increment change as the hot tearing initiation. Based on this principle, hot tearing initiation temperature of Mg-0.2Ca, Mg-0.5Ca, and Mg-1Ca was determined as 638 ^{0}C, 630 ^{0}C, and 623 ^{0}C, respectively. The end of the plateau or the beginning of the linear force increase was regarded as the termination of crack propagation. For Mg-2Ca alloy, the curve displayed no force drop, indicating no tear initiation.

Comparing the curves at both mould temperatures, it can be found that the force release was much lower for alloys cast at T_{mould} = 450 ^{0}C than that of alloys cast at T_{mould} = 250 ^{0}C. This indicated that high mould temperature decreased the HTS of Mg-xCa alloys. This phenomenon is also evidenced in Mg-Zn [18], Mg-Al [8], Mg-Gd [20], and Mg-Y [19] binary alloys.

5.1.2.2 Macro observation

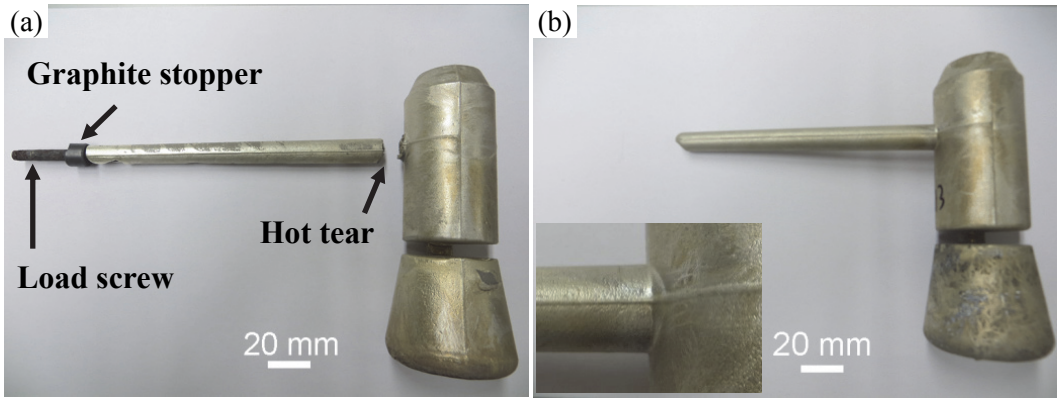

Fig. 5-3 Macro pictures of the entire casting of Mg-1Ca cast at T_{mould} = 250 ^{0}C (a) with shrinkage constraint, (b) without shrinkage constraint

Hot tears were initially examined visually on the casting surfaces upon removel from the mould. Generally, the tear occurred at the sprue-rod junction, as shown in Fig. 5-3 (a). At the end of the rod portion, part of the load screw was embedded in the casting. During solidification, the load screw was covered by the solidified alloy, and the rod was therefore unable to contract in the axial direction freely. This constrained shrinkage led to hot tearing. In comparison, Fig. 5-3 (b) shows a non-constrained casting. Both the constrained and non-constrained castings have the same composition and cast condition. The enlarged picture (as

inserted at the left corner) of the junction area clearly shows no visible crack for the non-constrained casting. The combined results demonstrate that the constrained shrinkage plays a key role on the hot tearing behaviour.

Mould temperatures	Mg-0.1Ca	Mg-0.2Ca	Mg-0.5Ca	Mg-1Ca	Mg-2Ca
250 ºC				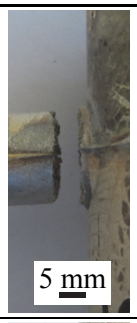	
450 ºC		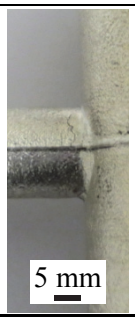			

Fig. 5-4 Macro observations of the hot tears of Mg-xCa alloys cast at T_{mould} = 250 ^{0}C and T_{mould} = 450 ^{0}C

Fig. 5-4 shows the photographs of the hot cracks in various alloy castings. It is clear that Ca content had a significant influence on the macro appearance of hot tears. Only a minor crack was observed in Mg-0.1Ca alloy whereas relatively severe cracking occurred in Mg-0.2Ca alloy at T_{mould} = 250 ^{0}C. Higher HTS was observed in both Mg-0.5Ca and Mg-1Ca alloys as the rod portion of the castings was completely detached from the sprue. The above observations are in good agreement with the conclusions drawn from the force curves recorded during the hot tearing experiments as the force curves for Mg-0.5Ca and Mg-1Ca alloys became a plateau (Fig. 5-1 (c) and (d)). Multiple-cracks were observed in Mg-2Ca alloy, however, in general, the severity reduced with 2 wt. % Ca addition. The multiple cracks can also be correlated with the mutil force drops observed in the force curve for Mg-2Ca alloy shown in Fig. 5-1 (e).

Hot tearing susceptibility of Mg-Ca alloys siginificantly drops as the mould temperature increases to 450 ^{0}C. Only fine tears are visible at the junction area of Mg-0.1Ca, Mg-0.2Ca, Mg-0.5Ca, and Mg-1Ca alloys. It is worth noting that for Mg-0.5Ca and Mg-1Ca alloys cast at T_{mould} = 450 ^{0}C, tears sometimes appeared in the middle of the rod. This will be further discussed in detail later.

5.1.2.3 X-ray tomography

X-ray tomography is proved a useful technique to observe the crack morphology and to evaluate the crack volume quantitatively [19, 20]. Fig. 5-5 shows the X-ray tomography photographs of longitudinal cross section (mid plane section) of Mg-0.1Ca, Mg-0.2Ca, and Mg-2Ca alloy castings. The cross section of steel tube used for protecting the thermocouple also appeared in the X-ray, as marked in Fig. 5-5 (a).The hot tears are indicated by black arrows.

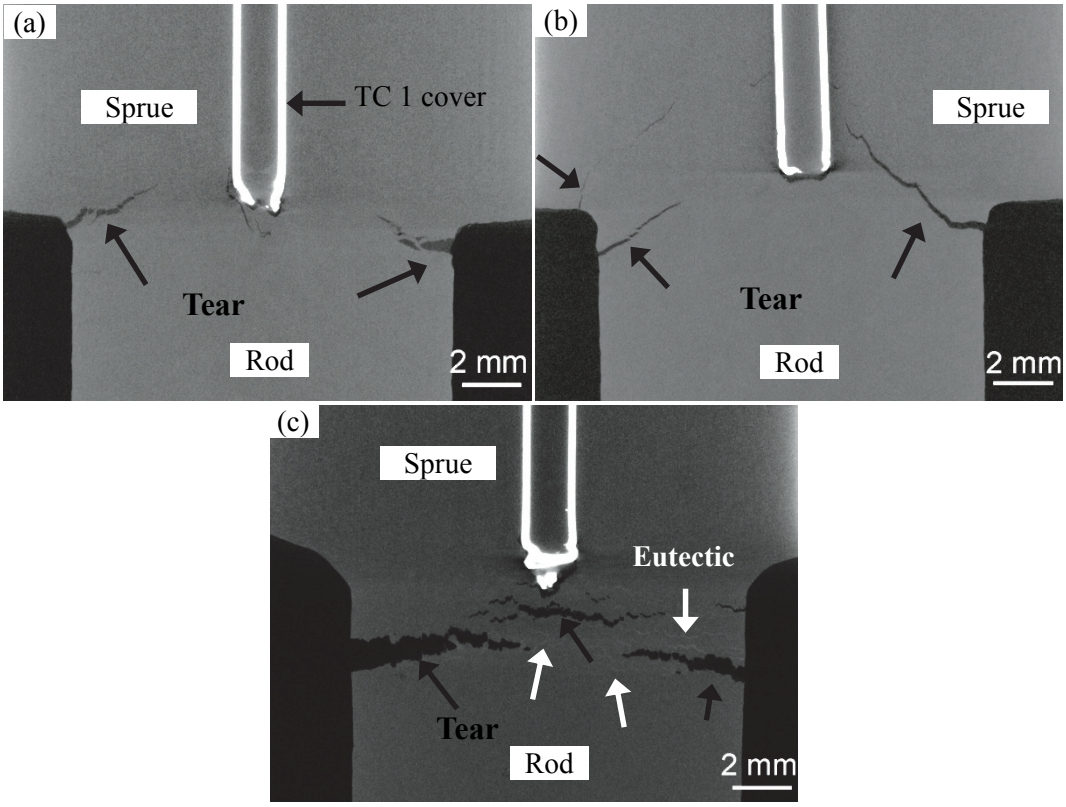

Fig. 5-5 X-ray tomography cross sections of Mg-Ca alloys cast at T_{mould} = 250 ^{0}C, (a) Mg-0.1Ca, (b) Mg-0.2Ca, (c) Mg-2Ca

As shown in Fig. 5-5, the hot tears in the Mg-0.1Ca and Mg-0.2Ca alloys were initiated at the sprue-rod junction and propagated towards the sprue from the junction, while the hot tear of Mg-2Ca alloy mainly propagated perpendicular to the contraction direction (along the radial direction of the rod). In addition, Mg-2Ca exhibited complex tear morphology, several

secondary micro-tears were observed in the junction area and river-type grey patterns were also observed near the main tears, as indicated by white arrows in Fig. 5-5 (c). These patterns show brighter color (gray) than the matrix (dark grey), demonstrating that these patterns contained high amount of solute element, Ca. Appearance of similar grey patterns were also reported in CRC mould cast high Gd and Y containing Mg-Gd and Mg-Y alloys, respectively, and were identified as eutectic or second phase [19, 20]. Due to the low content of Ca, these grey patterns were not obvious in Mg-0.1Ca and Mg-0.2Ca alloys.

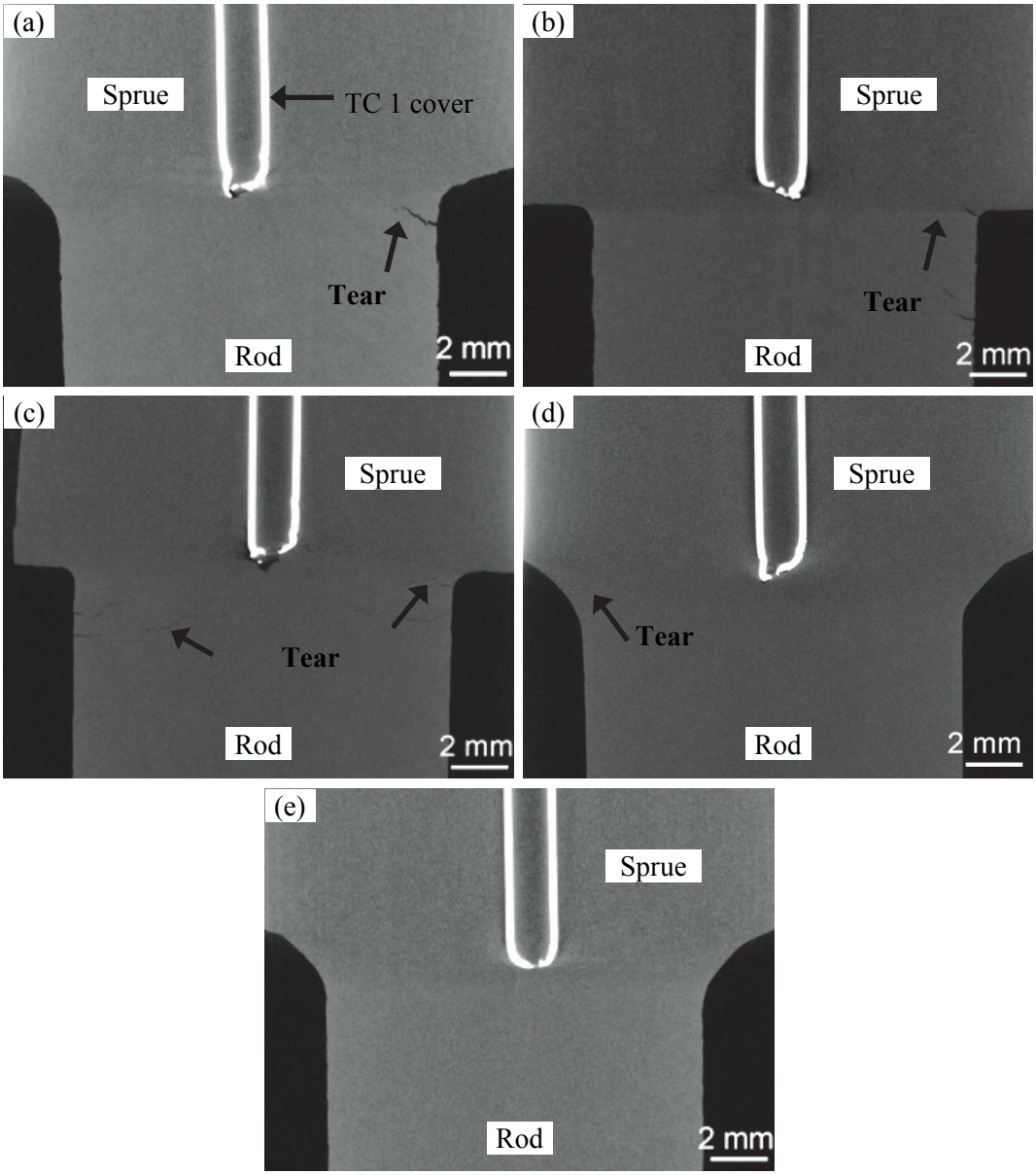

Fig. 5-6 X-ray tomography cross sections of alloys cast at T_{mould} = 450 ^{0}C, (a) Mg-0.1Ca, (b) Mg-0.2Ca, (c) Mg-0.5Ca, (d) Mg-1Ca, and (e) Mg-2Ca

Fig. 5-6 displays the X-ray tomography images of longitudinal cross section (mid plane section) of Mg-Ca alloys cast at T_{mould} = 450 ^{0}C. Fine tears can be found for Mg-0.1Ca,

Mg-0.2Ca, Mg-0.5Ca, and Mg-1Ca alloys. No tear in Mg-2Ca alloy is found, which is in good agreement with the above-mentioned force-temperature-time curves that no force drop is detected. No eutectic patterns are observed for all the alloys cast at the high mould temperature.

In order to quantitatively evaluate the severity of hot tears, crack volume was introduced as a hot tearing indicator [8]. The crack volumes measured by X-ray tomography of Mg-Ca alloys are shown in Fig. 5-7. The crack volume for Mg-0.5Ca and Mg-1Ca alloys at T_{mould} = 250 ^{0}C are displayed with dashed line as the rod portion of castings were completely broken. Measured crack volumes at T_{mould} = 450 ^{0}C show a relatively low value (less than 1 mm^3). For Mg-2Ca, crack volume is measure as 0, since no hot crack was present. At both mould temperatures, the hot crack volume increased with the Ca content, reaching a maximum between Mg-0.5Ca and Mg-1Ca, and then decreased with further increase in Ca addition.

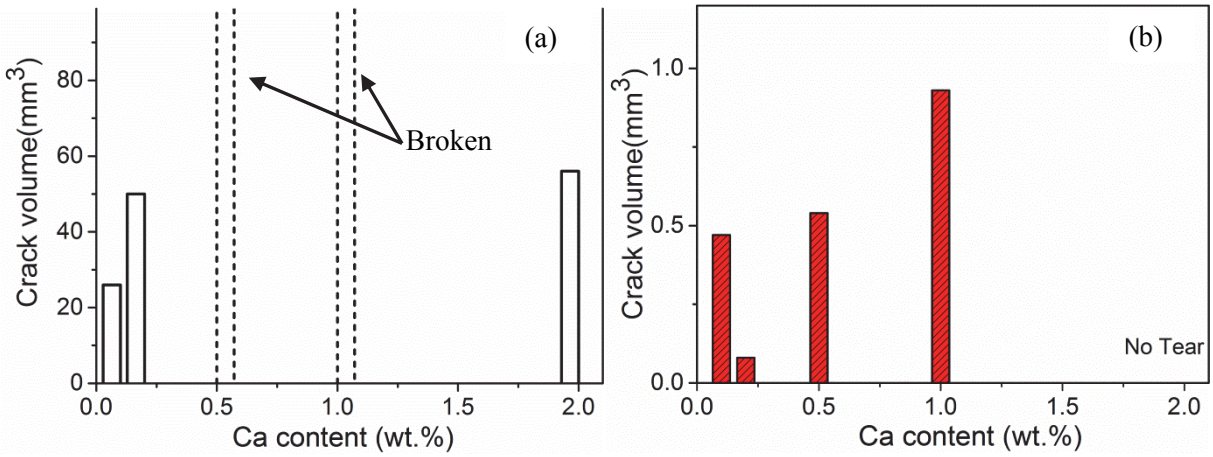

Fig. 5-7 Crack volume of Mg-Ca alloys measured by X-ray tomography (a) T_{mould} = 250 ^{0}C, (b) T_{mould} = 450 ^{0}C

5.1.2.4 Micro observation

Fig. 5-8 shows the optical microstructures on the longitudinal sections of the Mg-Ca alloys cast at T_{mould} = 250 ^{0}C. All the samples were cut from the regions near the junctions. As the rod portion of the casting of both Mg-0.5Ca and Mg-1Ca alloys were completely broken, the tear morphologies in the rod part near the fractured region were analysed and shown in Fig. 5-8 (c) and (d). A wider tear was found in Mg-0.2Ca alloy compared with Mg-0.1Ca alloy. Both Mg-0.1Ca and Mg-0.2Ca alloys showed a columnar grain structure at the tear region, whereas the other three alloys exhibited an equiaxed grain structure. In addition, there was no micro tear near the major tear in Mg-0.1Ca and Mg-0.2Ca alloys, while few micro tears near the major tear were evidenced in Mg-2Ca alloy and near the fractured region of Mg-0.5Ca and

Mg-1Ca alloy castings. The figures suggest that all the tears mainly propagated along grain boundaries.

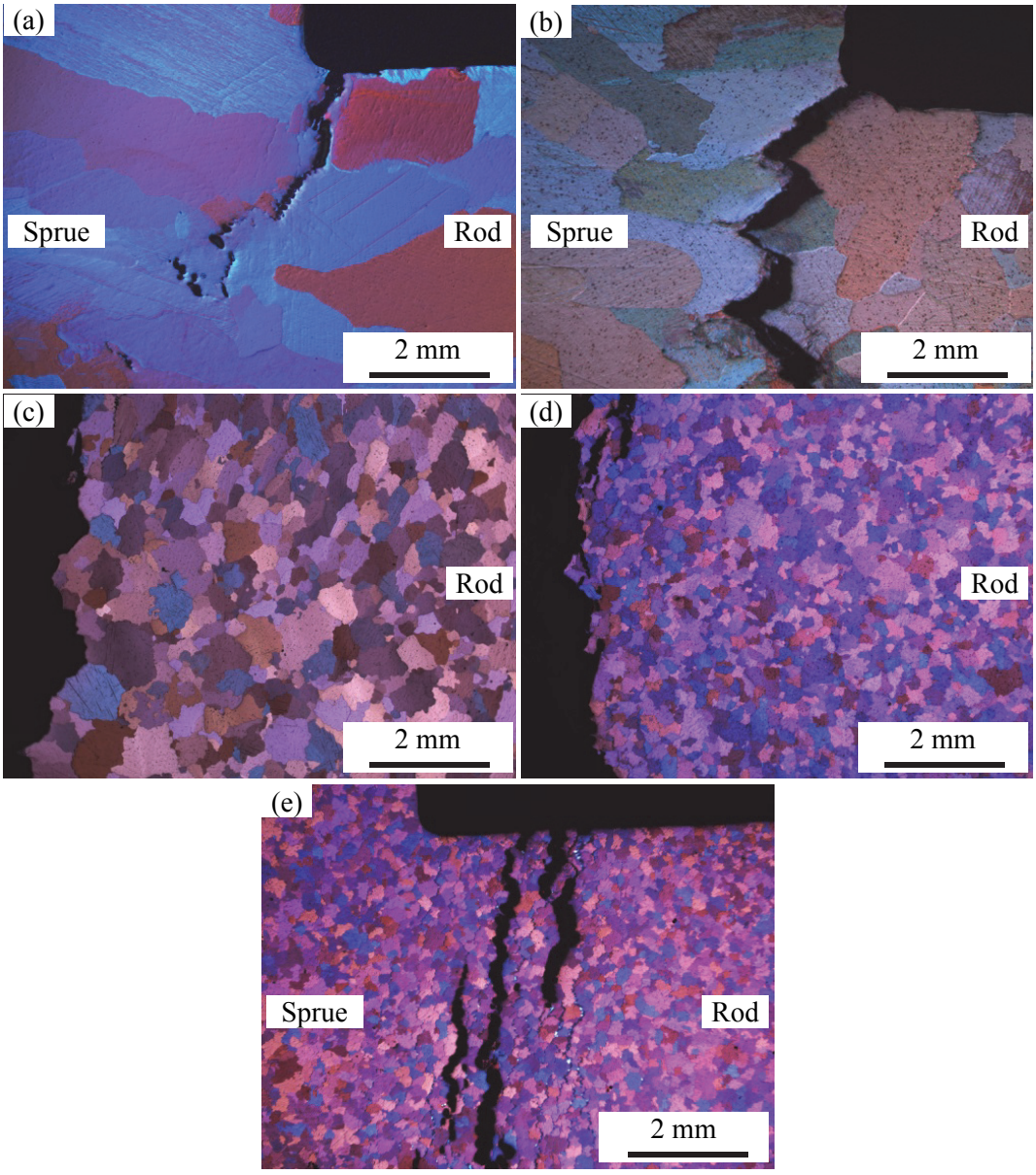

Fig. 5-8 Optical microstructures of alloys cast at T_{mould} = 250 ^{0}C showing the crack path in (a) Mg-0.1Ca, (b) Mg-0.2Ca, (c) Mg-0.5Ca, (d) Mg-1Ca, and (e) Mg-2Ca

Optical microstructures of Mg-Ca alloys cast at T_{mould} = 450 ^{0}C are shown in Fig. 5-9. In comparison with Mg-Ca alloys cast at T_{mould} = 250 ^{0}C, tears were much smaller at a high initial mould temperature. Similarly, the tears mainly propagated along the grain boundaries. No microstructural tears were evidenced in Mg-2Ca alloy.

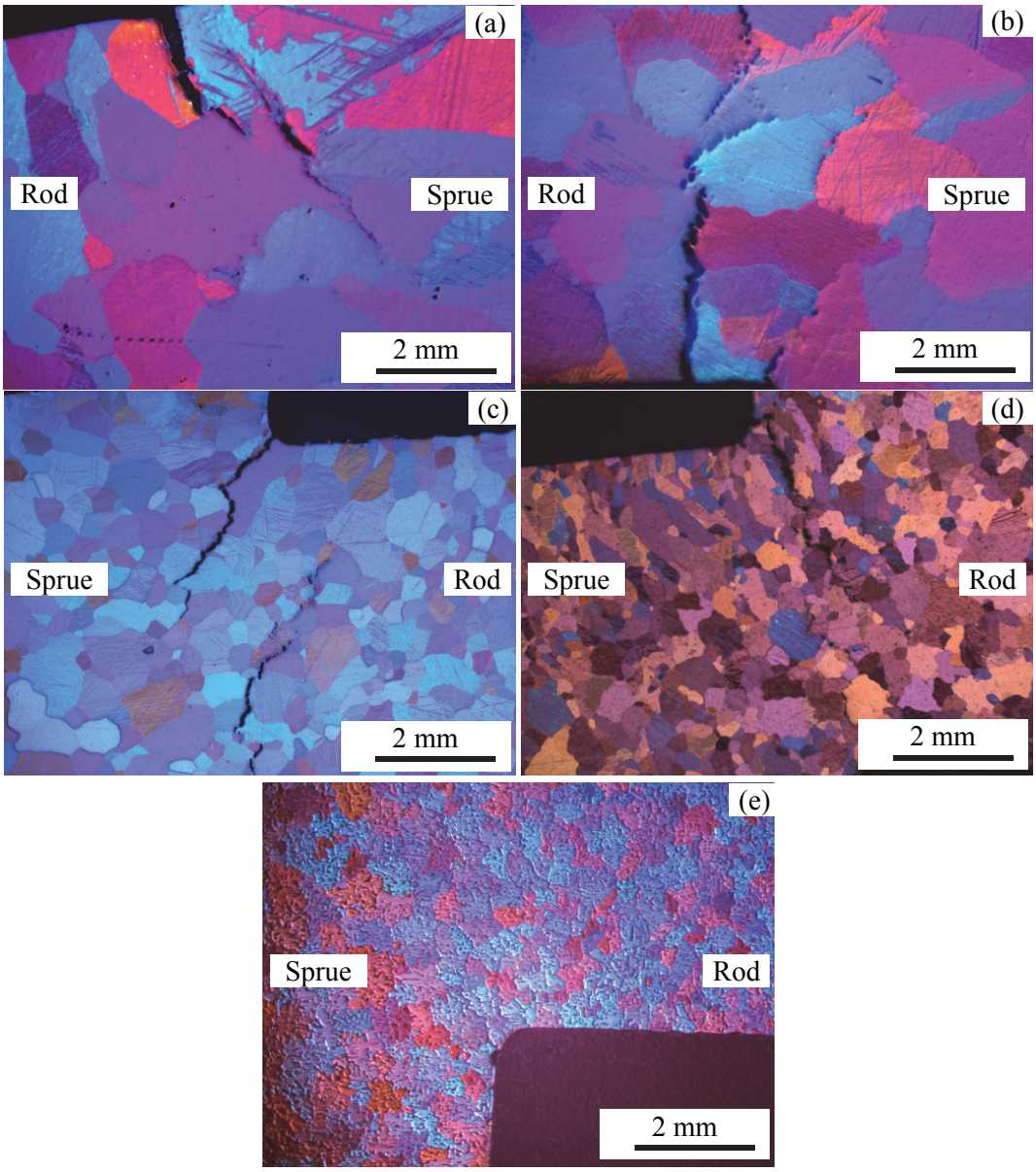

Fig. 5-9 Optical microstructures of alloys cast at T_{mould} = 450 ^{0}C showing the crack path in (a) Mg-0.1Ca, (b) Mg-0.2Ca, (c) Mg-0.5Ca, (d) Mg-1Ca, and (e) Mg-2Ca

5.1.2.5 Eutectic distribution

The presence of eutectic at the hot spot (near the tear) of all the alloy castings at T_{mould} = 250 ^{0}C, except Mg-0.1Ca alloy (microstructure is not shown), was seen as shown in Fig. 5-10. The absence of eutectic in Mg-0.1Ca alloy was due to its lower percentage of solute. The eutectic regions are indicated with white arrows in Fig. 5-10. A typical eutectic microstructure and the corresponding EDX analysis are shown in Fig. 5-10 (e) and (f). High content of Ca in the light grey region confirmed that it was eutectic (Mg+Mg_2Ca). The tears (black colour or bright white colour) are marked with black arrows in the Mg-0.5Ca (Fig. 5-10 (b)), Mg-1Ca (Fig. 5-10 (c)), and Mg-2Ca (Fig. 5-10 (d)) alloys. It is obvious that the amount of eutectic increased with increase in Ca content. Eutectic has a great impact on hot tearing behavior of

Mg alloys. Generally, large amount of eutectic liquid can fill the hot tear due to its high fluidity, which is also known as tear healing [23].

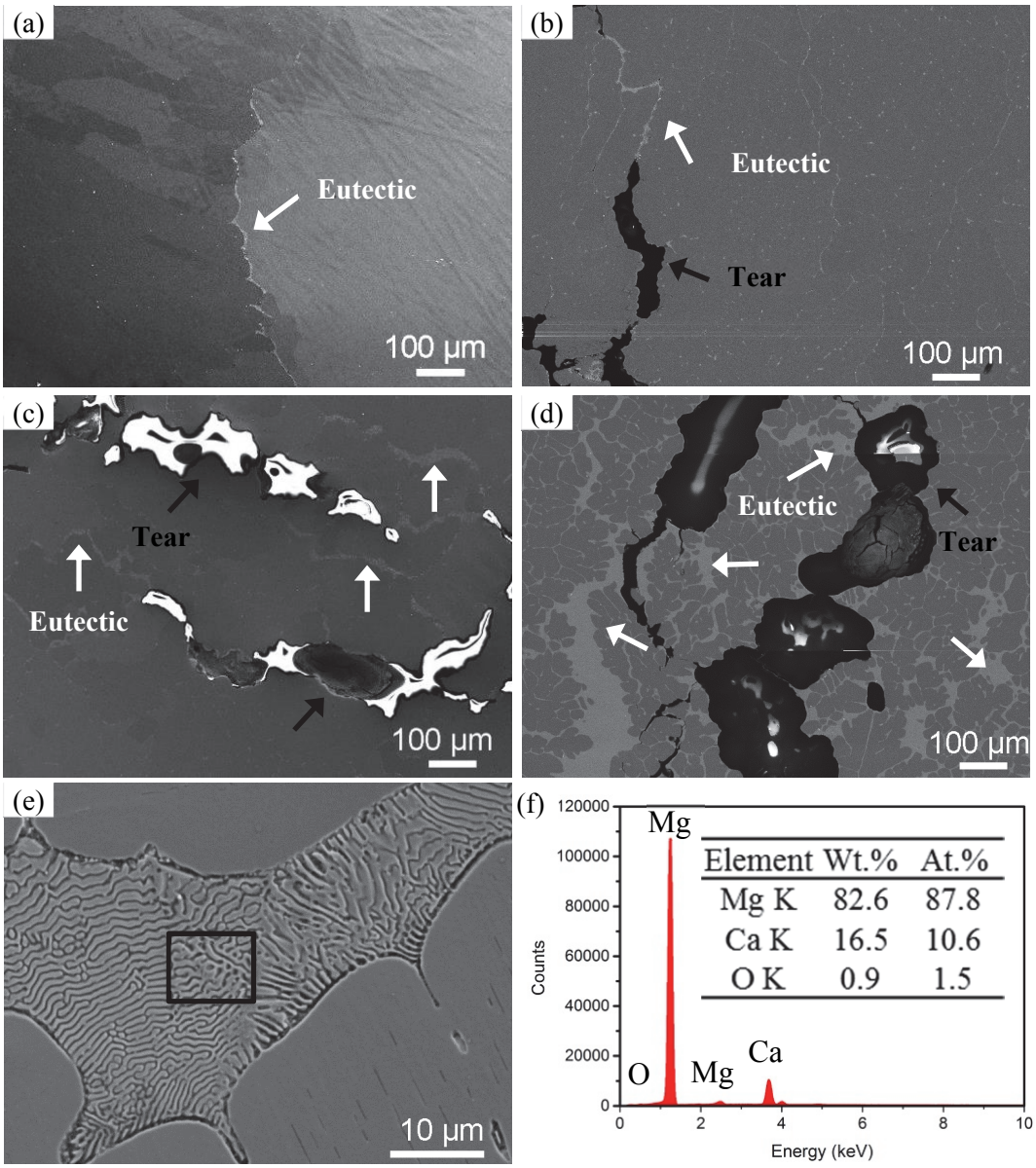

Fig. 5-10 Eutectic distribution near the hot tear, (a) Mg-0.2Ca, (b) Mg-0.5Ca, (c) Mg-1Ca, (d) Mg-2Ca, (e) enlarged eutectic microstructure of Mg-1Ca, and (f) EDX analysis of the eutectic (area marked with black box in (e))

5.1.2.6 Fracture surfaces

The fracture surfaces of Mg-0.2Ca, Mg-0.5Ca, Mg-1Ca, and Mg-2Ca alloys are shown in Fig. 5-11. The fracture surface of Mg-0.2Ca alloy was different from other alloys as it showed columnar dendritic grain morphology, while Mg-0.5 Ca, Mg-1Ca, and Mg-2Ca alloys had a granular grain structure. The columnar grains are more detrimental to hot tearing than

granular grains when they were subjected to a tensile stress perpendicular to the growth direction [13].

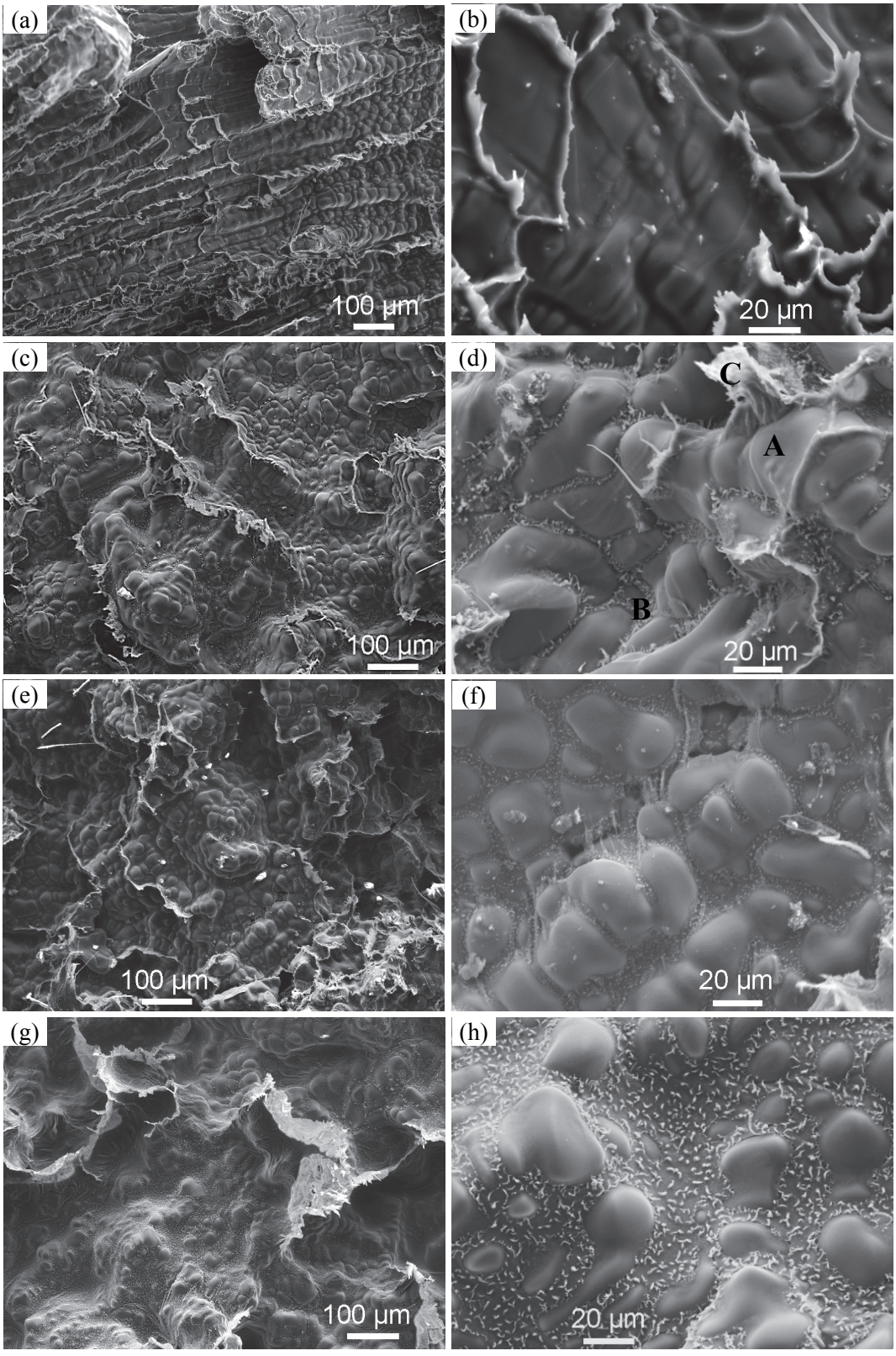

Fig. 5-11 Fracture surfaces of alloys cast at T_{mould} = 250 ^{0}C, (a), (b) Mg-0.2Ca, (c), (d) Mg-0.5Ca, (e), (f) Mg-1Ca, and (g), (h) Mg-2Ca

Fracture surfaces of the other three alloys appeared similar. They all showed typical hot tearing fracture surfaces, which consisted of dendritic grains covered by thin layer of eutectic liquid, precipitates (tiny white particles) located at grain or dendritic boundaries, and torn liquid films, marked as A, B, and C in Fig. 5-11 (d), respectively. EDX analysis results of these regions are listed in Table 5-3. The Ca content was high at point B and C. Interestingly, the torn liquid film was also evidenced in Mg-0.2Ca alloy (Fig. 5-11 (b)). The grains in Mg-2Ca alloy were completely covered by a thick film, indicating that a large amount of interdendritic liquid was present at the time of hot tearing [5]. This is in good agreement with the speculated low solid fraction (f_{si}= 0.714) from the recorded temperature and force vs time curve (Fig. 5-1 (e)). In all four alloys, no transgranular fractures were observed. The cracks mainly propagated along grain boundaries.

Table 5-3 EDX analysis results for regions A, B and C marked on the fracture surfaces of Mg-0.5Ca (Fig. 5-11 (d))

Regions	Ca		Mg		O	
	Wt.%	At.%	Wt.%	At.%	Wt.%	At.%
A (dendritic grain)	0.7	0.4	97.7	97.1	1.6	2.5
B (intermetallic)	20.5	12.5	64.7	64.9	14.8	22.6
C (liquid film)	11.1	6.2	63.7	58.6	25.2	35.2

5.1.2.7 Tears at middle of the rod

As mentioned in section 5.1.2.2, the tears of Mg-0.5Ca and Mg-1Ca alloys cast at a high mould temperature sometimes occurred in the middle of the rod, as shown in Fig. 5-12. No such middle tear was ever found in the samples cast at a low mould temperature, nor in Mg-0.1Ca, Mg-0.2Ca, and Mg-2Ca when cast at T_{mould} = 450 ^{0}C. In addition, the tears occurred frequently at the middle position. Three Mg-0.5Ca samples of six (in total) and two Mg-1Ca samples of six suffered from this middle tear. Moreover, the location of the tear seems random, as it was not always at the same place, as shown in Fig. 5-12. The middle tearing is also found occasionally for Mg-Al-Sr alloys, which might be due to a high tendency to stick to the wall of the mould during casting [24].

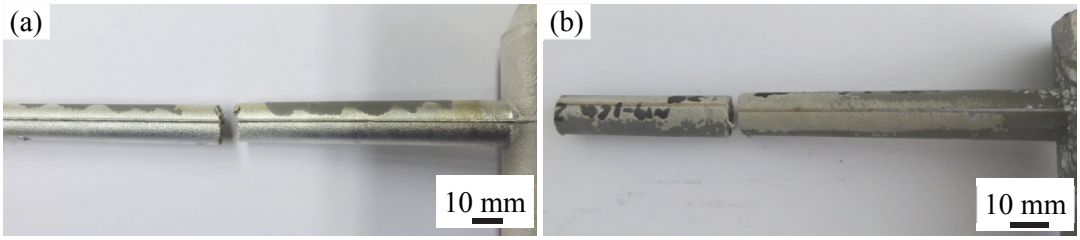

Fig. 5-12 Macro pictures show middle tear of alloys cast at T_{mould} = 450 ^{0}C, (a) Mg-0.5Ca, (b) Mg-1Ca

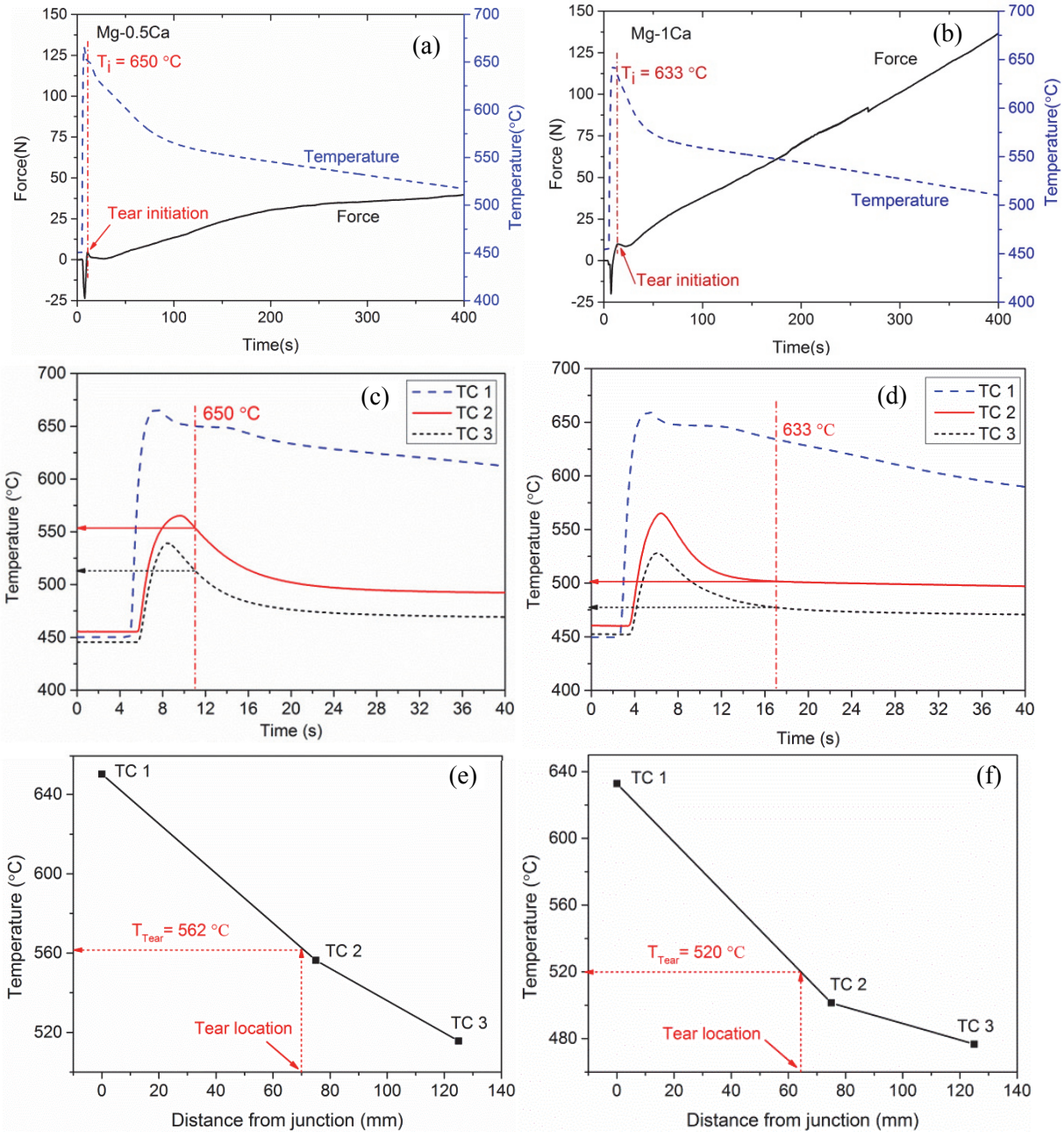

Fig. 5-13 Force-temperature-time curves of alloys show middle tear, (a) Mg-0.5Ca, (b) Mg-1Ca; cooling curves at three thermal couple position, (c) Mg-0.5Ca, (d) Mg-1Ca; estimating hot tearing initiation temperature, (e) Mg-0.5Ca, (f) Mg-1Ca

In order to clarify this, the tears were characterized in detail. First of all, force-temperature-time curves were investigated, as shown in Fig. 5-13 (a) and (b). Hot tearing initiation temperatures at sprue-rod junction are 650 °C and 633 °C for Mg-0.5Ca and Mg-1Ca, respectively. Considering that the tear occured in the middle of the rod, the temperature recorded at TC 1 is not the real temperature at the tearing location. Thus, a brief estimation method is introduced [24], as shown in Fig. 5-13. The temperature recorded at TC 1, TC 2, and TC 3 is compared in Fig. 5-13 (c) and (d). Three temperatures at tear initiation point can be read from the curves. By plotting these temperatures against the distance from the junction (Fig. 5-13 (e) and (f)), the tear initiation temperature at the tear position can be estimated. The middle tear initiation temperature is estimated to be 562 °C and 520 °C for Mg-0.5Ca and Mg-1Ca, respectively. The corresponding solid fraction is 0.962 for Mg-0.5Ca and 0.945 for Mg-1Ca, respectively.

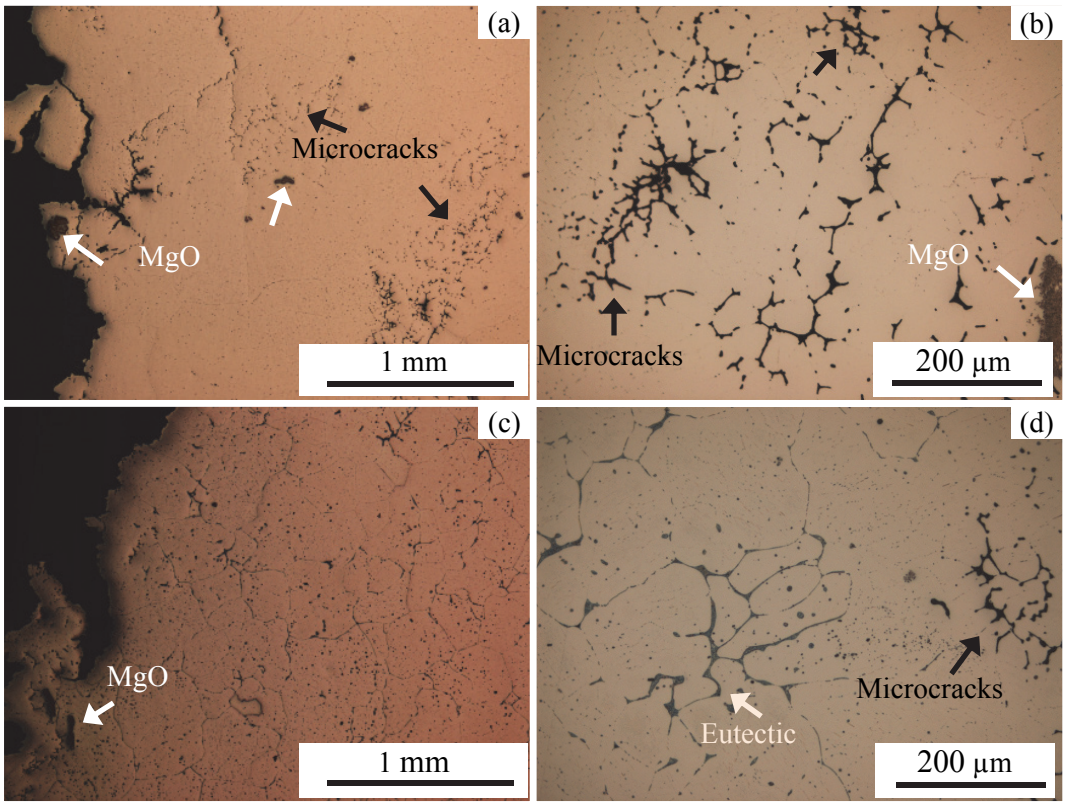

Fig. 5-14 Optical microstructures of middle tears for the alloys cast at T_{mould} = 450 °C (a), (b) Mg-0.5Ca; (c) (d) Mg-1Ca

Optical microstructures near the real tear region are shown in Fig. 5-14. Unlike the tear morphology at the sprue-rod junction area (Fig. 5-9), some MgO inclusions can be observed in both Mg-0.5Ca and Mg-1Ca alloys. Additionally, agglomeration of microcracks is evident in both alloys. Several microcrack agglomerates can be found near the main tear. Most of the

agglomerates are noncontinuous and randomly distributed, which is the main difference between the microcracks found on the tear surfaces of the sprue-rod junction (Fig. 5-9). For Mg-1Ca alloys, eutectic can be found (Fig. 5-14 (d)). The eutectic is also randomly distributed and appeared near the microtears. Such randomly distributed eutectic was likely due to the refilling of the microcracks. The prescense of such microtears and eutectic indicates that the region is under strain.

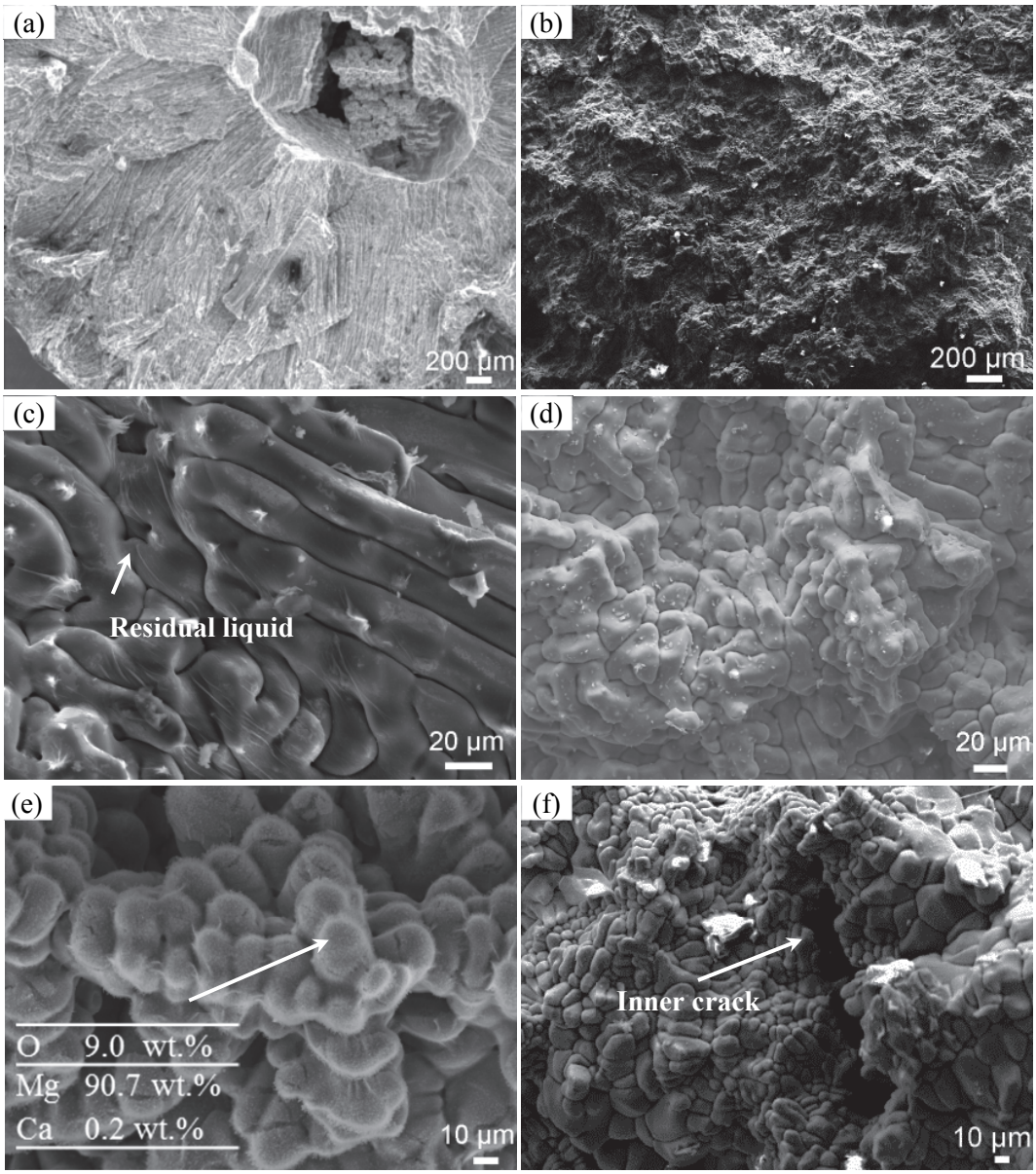

Fig. 5-15 Fracture surfaces of middle tear of the rod for (a), (c), and (e) Mg-0.5Ca; (b), (d), and (f) Mg-1Ca

In order to further understand the formation mechanisms for these middle tears, fracture surfaces at these locations for both alloys are observed. As shown in Fig. 5-15 (a) and (b), Mg-0.5Ca alloy mainly consists of columnar grains and Mg-1Ca mainly composes of

equiaxed grains. Higher magnification of dendritic grain morphology can be seen in Fig. 5-15 (c) and (d). Traces of residual liquid can be found on the surface of dendrites in Mg-0.5Ca alloy, indicating the tear is hot tear, as confirmed by the force curve. A large pore is present on the fracture surface of Mg-0.5Ca alloy (Fig. 5-15 (a)). Higher magnification of the defect (Fig. 5-15 (e)) showed a nappy layer was on top of the dendritic grain. The EDX analysis showed that the top layer contained quite high amount of oxygen (EDX results were listed in the table, as inserted in Fig. 5-15 (e)). Thus, the layer might be MgO inclusions. The microcrack is also found in Mg-1Ca alloy, as shown in Fig. 5-15 (f).

5.1.3 Numerical simulation

5.1.3.1 Solidification simulation

The filling and solidification procedures of Mg-0.5Ca alloy with an initial mould temperature of 250 °C were simulated by ProCAST. Fig. 5-16 shows the simulated temperature and solid fraction distribution on the mid-plane slice in the YZ direction. Temperature and solid fraction at different total solid fractions are displayed: (a) a total solid fraction around 0, (b) a total solid fraction around 0.4, (c) a total solid fraction around 0.9, and (d) a total solid fraction of 1. It is clear that the solidification started at the end of the rod portion and gradually proceeded to the centre of the sprue. Relatively large temperature gradients are observed in the casting.

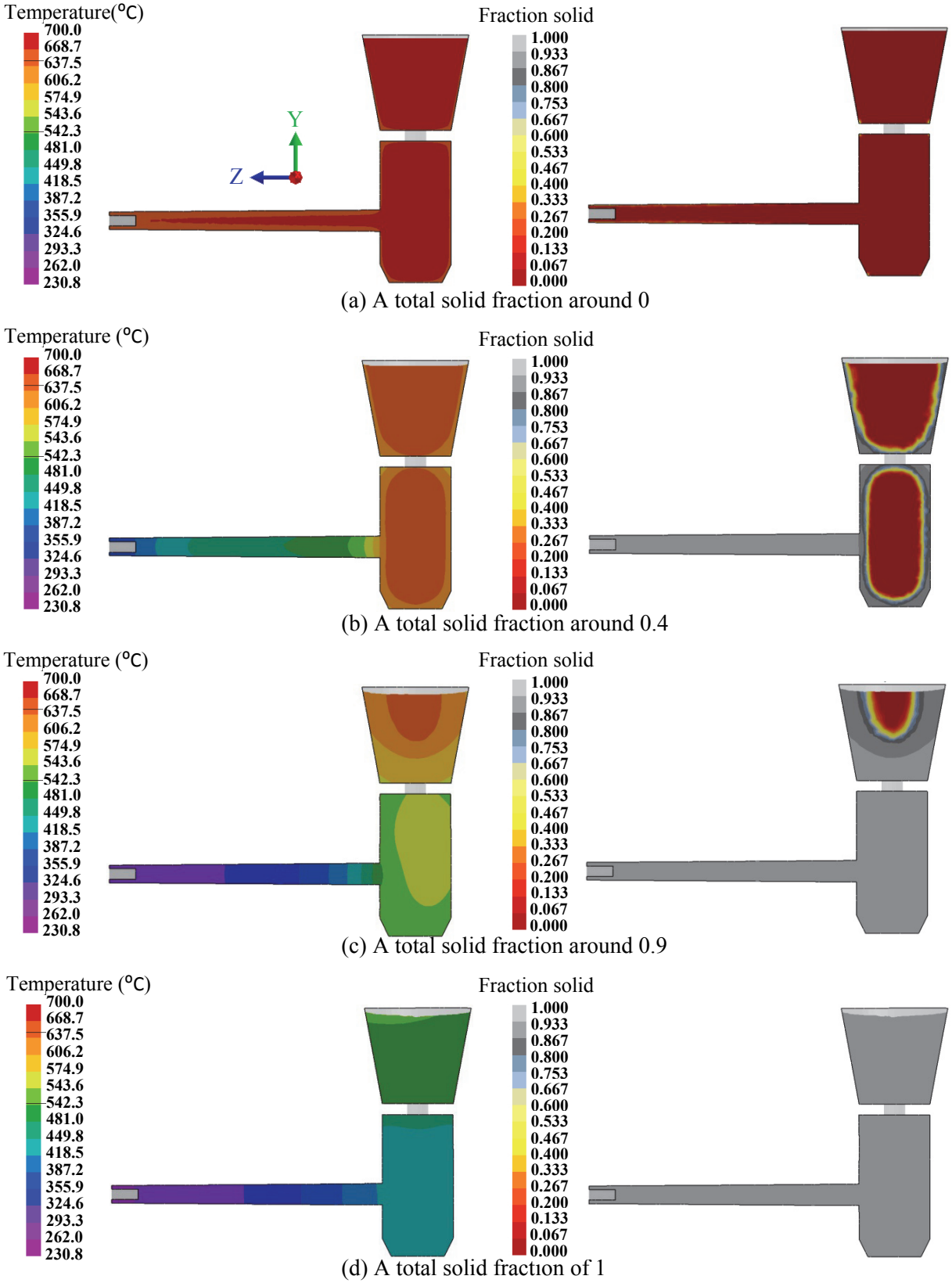

(a) A total solid fraction around 0

(b) A total solid fraction around 0.4

(c) A total solid fraction around 0.9

(d) A total solid fraction of 1

Fig. 5-16 Predicted temperature and solid fraction fields for the Mg-0.5Ca alloy with an initial mould temperature of 250 °C.

5.1.3.2 Hot tearing indicator

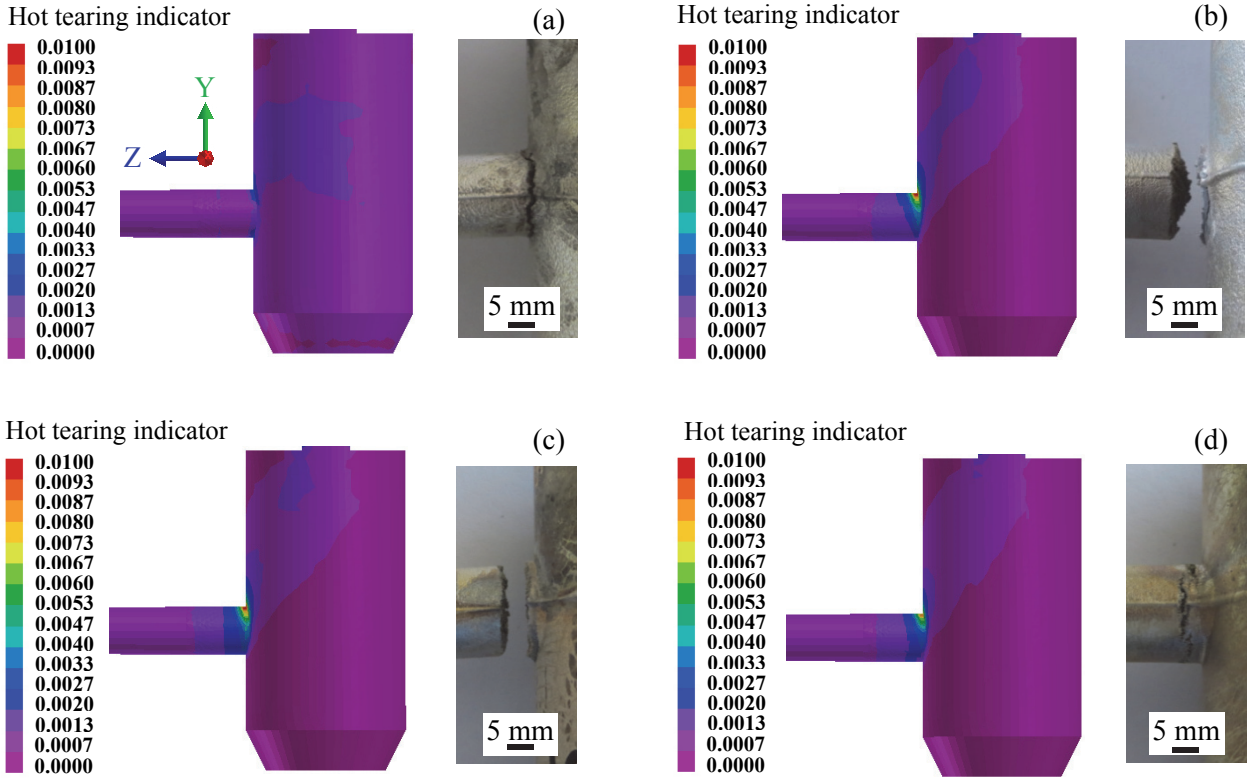

Fig. 5-17 Simulated HTI of snapshot view and experimental macro hot tears of Mg-Ca alloys at a mould temperature of 250 ^{0}C, (a) Mg-0.2Ca, (b) Mg-0.5Ca, (c) Mg-1Ca, and (d) Mg-2Ca

The simulated HTI of snapshot view at the YZ direction and the experimental macro tears of Mg-Ca alloys at an initial mould temperature of 250 ^{0}C are compared in Fig. 5-17. Simulation results indicate that the sprue-rod junctions are most susceptible to hot tearing, which agrees with the actual location of hot tearing. From the view of snapshot, HTI of Mg-0.2Ca alloy is low. The HTI of both Mg-0.5Ca and Mg-1Ca are higher than that of Mg-0.2Ca and Mg-2Ca alloys. However, the HTI of Mg-0.2Ca from the view of the centre slice shows high hot tearing susceptibility at the sprue-rod junction, as shown in Fig. 5-18 (a). Extremely high HTI at a triangle area at the sprue-rod junction is observed from the centre slice of Mg-0.2Ca. The HTI distribution for Mg-2Ca alloy at the snapshot and centre slice show similar resluts (Fig. 5-18). By comparing the micro tear morphologies (X-ray tomography) with the HTI distribution, it is found again that the experimental tear location agrees well with that from the simulation.

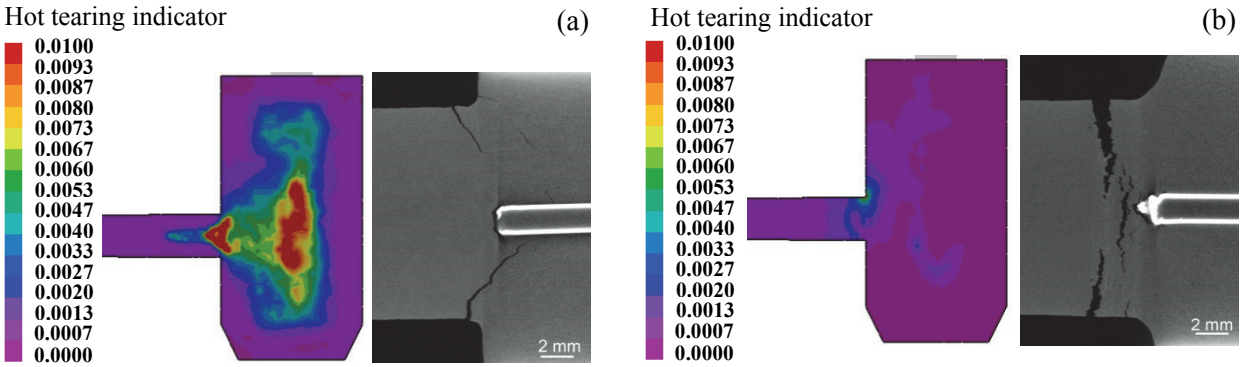

Fig. 5-18 Simulated HTI at centre slice of YZ direction and experimental 3D-X ray tomography photographies of Mg-Ca alloys at a mould temperature of 250 ^{0}C, (a) Mg-0.2Ca and (b) Mg-2Ca

5.2 Hot tearing of Mg-0.5Ca-xZn ternary alloy

5.2.1 Chemical composition

Mould temperature was not found to have an effect on chemical composition. Thus only the compositions of Mg-0.5Ca-xZn alloys cast at T_{mould} = 250 ^{0}C are listed in Table 5-4. The measured compositions are close to the nominal composition, and the trace elements are relatively low. The real Zr content is only 0.24 wt.%, which is much lower than the norminal Zr content of 0.5 wt.%. Therefore, the alloy is written as Mg-0.5Ca-4Zn-0.2Zr.

Table 5-4 Chemical compositions of Mg-0.5Ca-xZn alloys at T_{mould} = 250 ^{0}C, in wt.%

Alloy	Ca	Zn	Zr	Fe	Mn	Si	Mg
Mg-0.5Ca-0.5Zn	0.44	0.42	<0,0006	0.0044	0.0394	0.0145	Bal.
Mg-0.5Ca-1.5Zn	0.43	1.43	<0,0006	0.00502	0.038	0.0167	Bal.
Mg-0.5Ca-4Zn	0.39	4.13	<0,0006	0.00509	0.0353	0.0179	Bal.
Mg-0.5Ca-6Zn	0.38	6.20	<0,0006	0.0063	0.0387	0.0164	Bal.
Mg-0.5Ca-4Zn-0.2Zr	0.42	3.84	0.24	0.00288	0.0384	0.00553	Bal.

5.2.2 Experimental hot tearing tendency

5.2.2.1 Force-temperature-time curves

The as-recorded force-temperature-time curves of Mg-0.5Ca-xZn alloys cast at a mould temperature of 250 °C are displayed in Fig. 5-19. The overall force-temperature-time curves of Mg-0.5Ca-xZn alloys with the same range of force, time, and temperature are displayed in Fig. 5-19 (a), (c), (e), and (g). It is found that the force curve of Mg-0.5Ca-0.5Zn (Fig. 5-19

(a)) displays a flat line after the termination of tear propagation. The observation indicates that the sample is completely broken. Two hot tearing initiation points can be found on the curve of Mg-0.5Ca-6Zn alloy, as shown in Fig. 5-19 (g). This reveals that more than one tear initiated during the solidification process.

In order to determine whether the tear initiation and propagation occurred at an early stage of sonidification, curves with a smaller time range are shown in Fig. 5-19 (b), (d), (f), and (h), respectively. Hot tearing initiation and propagation termination is determined by the method described in section 5.1.2.1, as marked on the firgure. However, no typical force increase (stage II) and force drop (stage III) are observed for Mg-0.5Ca-1.5Zn and Mg-0.5Ca-4Zn alloys in Fig. 5-19 (d) and (f), respectively. It is found during the long force drop (Fig. 5-19 (d) and (f)), at a certain point, the force starts to decreases faster than before. The faster force drop is attributed to stress relaxation, thus the point is defined as hot tearing initiation. Similar determination of hot tearing initiation can also be found elseshere [101]. In addition, all the four Mg-0.5Ca-xZn alloys show a low f_{si}, especially Mg-0.5Ca-4Zn. This could be the due to a similar reason as that for low f_{si} in Mg-0.5Ca and Mg-1Ca cast at mould temperature of 250 °C.

Fig. 5-20 shows force-temperature-time curves of Mg-0.5Ca-xZn alloys cast at a mould temperature of 450 °C. All the force drops are obvious on the force curves. It should be noted that T_i and f_{si} values for Mg-0.5Ca-4Zn alloy were only estimated as the tear in this alloy occurred at the rear end of the rod portion and not at the sprue-rod junction (image of the tear position is shown in section 5.2.2.2. The estimation method is described in detail in section 5.1.2.7. According to the force curve, the initiation of force drop occurred when the recorded temperatures at TC 1, TC 2, and TC 3 were 484 ^{0}C, 419 ^{0}C and 398 ^{0}C, respectively. The length of the whole rod was 150 mm. The distance from TC 2 to TC 1 (junction, hot spot) was 75 mm, and distance from TC 3 to TC 1 was 125 mm. The tear was observed at 131 mm away from TC 1. By plotting the temperature against position (distance to the sprue-rod junction), the temperature at the tear location was estimated as 396 ^{0}C. The temperature prediction using the above method was believed to be reasonable in other investigation [24]

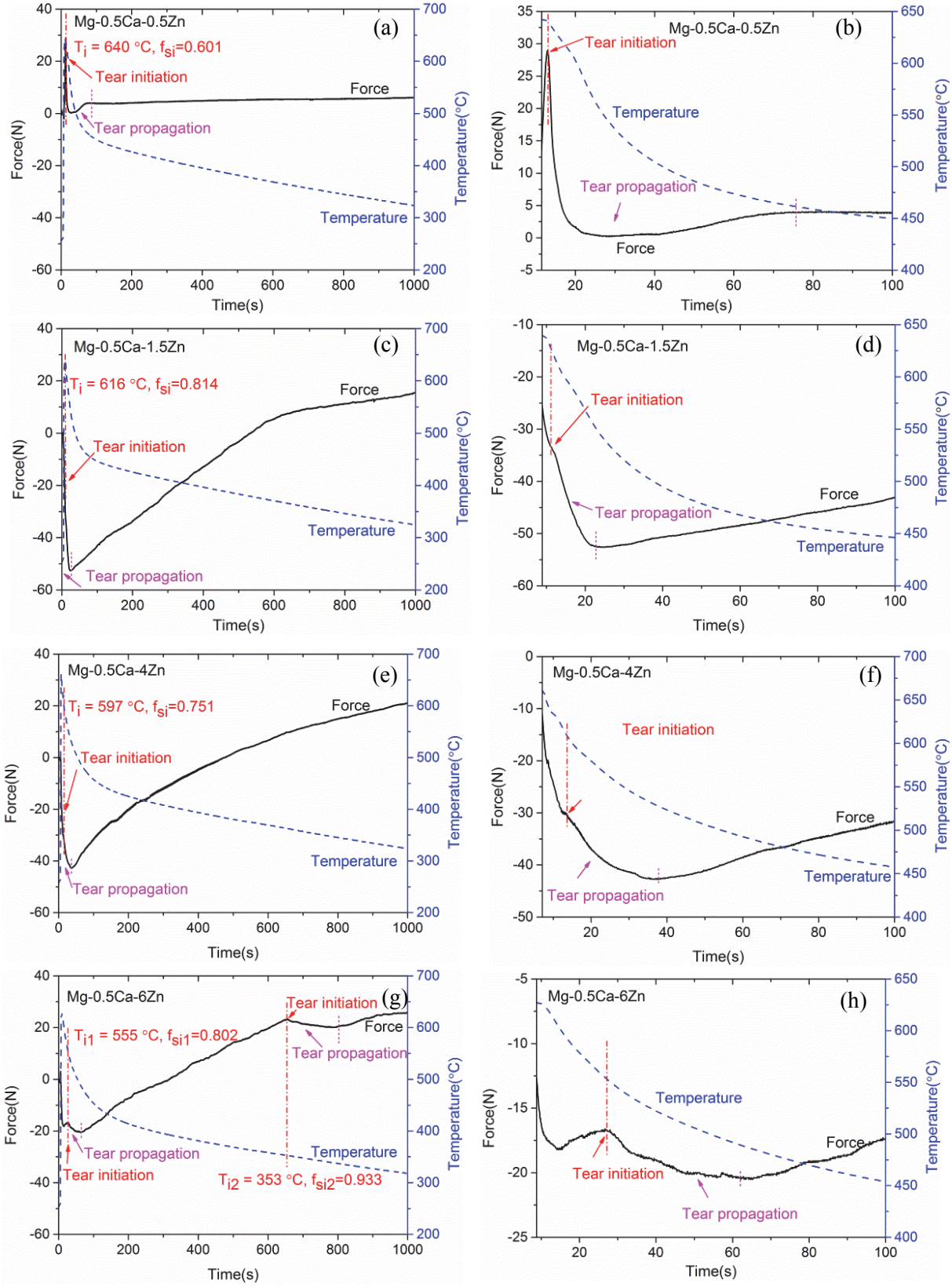

Fig. 5-19 Force-temperature-time curves of Mg-0.5Ca-xZn alloys cast at T_{mould} = 250 ^{0}C, (a), (b) Mg-0.5Ca-0.5Zn, (c), (d) Mg-0.5Ca-1.5Zn, (e), (f) Mg-0.5Ca-4Zn, and (g), (h) Mg-0.5Ca-6Zn

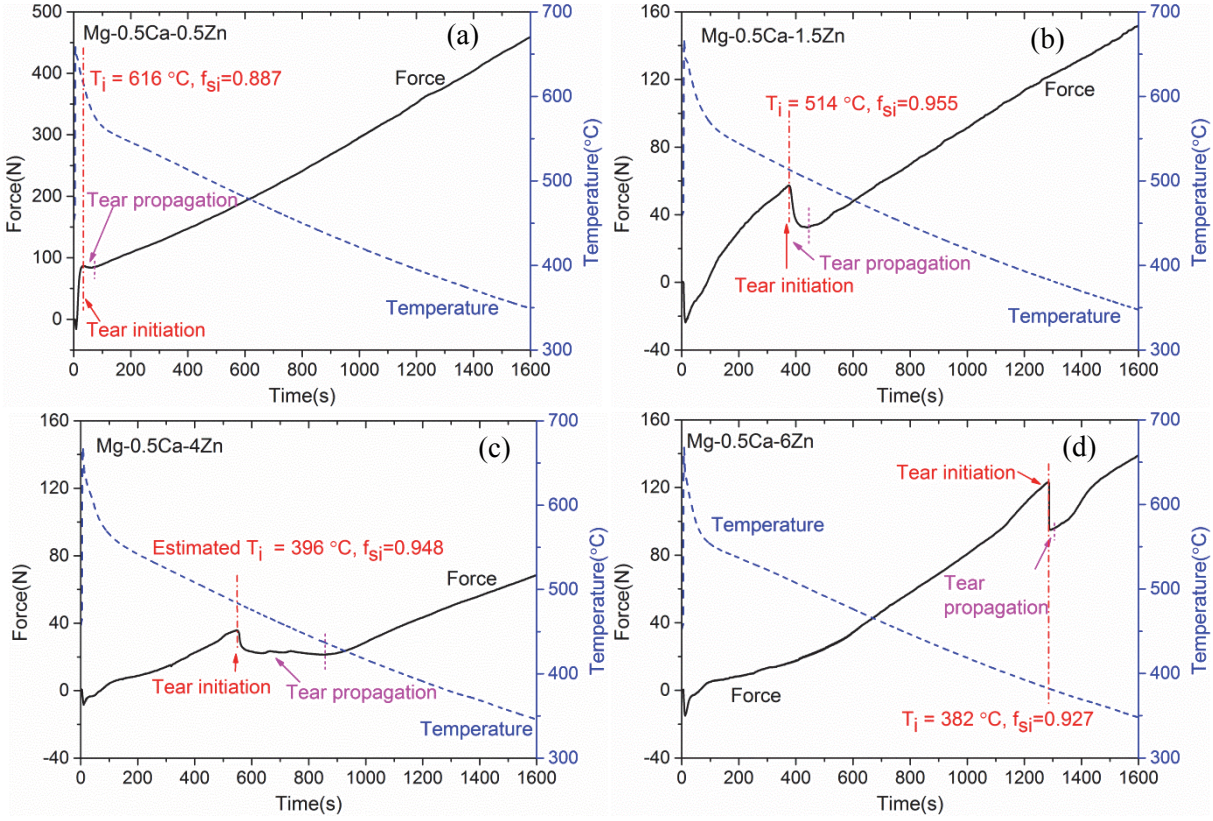

Fig. 5-20 Force-temperature-time curves of Mg-0.5Ca-xZn alloys cast at T_{mould} = 450 ^{0}C, (a) Mg-0.5Ca-0.5Zn, (b) Mg-0.5Ca-1.5Zn, (c) Mg-0.5Ca-4Zn, and (d) Mg-0.5Ca-6Zn

As shown in Fig. 5-20, the final force value (at a time of 1600 s) for Mg-0.5Ca-0.5Zn alloy (460 N) was significantly higher than those of the other three ternary alloys (all below 160 N). This suggests that the tear size of Mg-0.5Ca-0.5Zn alloys was smaller than that of Mg-0.5Ca-1.5Zn, Mg-0.5Ca-4Zn, and Mg-0.5Ca-6Zn alloys, and that they had the lower HTS. The smaller tear size, the larger force built up observed during cooling. This is because only the tear-free parts contribute to the accumulated contract force. Thus, it is expected that the as-recorded final force can inversely reflect the size of hot tears and consequently the HTS [8]. However, if the final force values of alloys are low and close to each other, this cannot be used to estimate the tear size. For instance, the final forces for Mg-0.5Ca-xZn alloys cast at T_{mould} = 250 ^{0}C were lower than 40 N and quite close to each other, and cannot be used to estimate the tear volume.

5.2.2.2 Macro observation

Macro pictures of hot tears of Mg-0.5Ca-xZn at both mould temperatures are shown in Fig. 5-21. At a mould temperature of 250 ^{0}C, Mg-0.5Ca-0.5Zn, Mg-0.5Ca-1.5Zn, and Mg-0.5Ca-4Zn alloys were completely broken. Mg-0.5Ca-6Zn alloy exhibited multi tears,

which agrees with the mutil force drops on the force-temperature-time curve. Among the studied alloys, only Mg-0.5Ca-6Zn alloy did not break suggesting that it had the lowest HTS.

Mould temperatures	Mg-0.5Ca-0.5Zn	Mg-0.5Ca-1.5Zn	Mg-0.5Ca-4Zn	Mg-0.5Ca-6Zn
250 °C				
450 °C			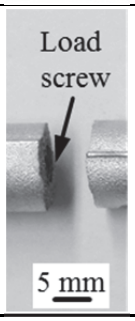	

Fig. 5-21 Macro photographs of the hot tears for Mg-0.5Ca-xZn alloys cast at T_{mould} = 250 ^{0}C and T_{mould} = 450 ^{0}C

When the mould temperature was 450 ^{0}C, only fine tears were observed in Mg-0.5Ca-0.5Zn alloy, which agreed well with the higher final force values on the force-temperature-time curves (Fig. 5-20). The severity of hot tears of Mg-0.5Ca-0.5Zn, and Mg-0.5Ca-6Zn alloys became less sever in comparison to the tears at a mould temperature of 250 ^{0}C. On the other hand, castings of Mg-0.5Ca-1.5Zn and Mg-0.5Ca-4Zn were completely broken, showing a high HTS even at the higher mould temperature. The hot tear in Mg-0.5Ca-4Zn alloy was observed away from the sprue-rod junction, at the load screw (the location of load screw shown in Fig. 4-1), as marked in Fig. 5-21.

5.2.2.3 X-ray tomography

Fig. 5-22 shows the X-ray tomography images of longitudinal cross section at the mid plane of Mg-0.5Ca-6Zn alloy cast at different mould temperatures. Most alloys investigated in this study were broken completely, thus only Mg-0.5Ca-6Zn alloy was analysed with X-ray tomography technique. The main tear located away from the exact sprue-rod junction for Mg-0.5Ca-6Zn alloy cast at T_{mould} = 250 ^{0}C whereas it was at the junction at the higher mould

temperature. Moreover, Mg-0.5Ca-6Zn alloy showed a severe tear at the lower mould temperature than that at the higher mould temperature. The quantified tear volumes at T_{mould} = 250 ^{0}C and T_{mould} = 450 ^{0}C were 81.73 mm^3 and 48.49 mm^3, respectively.

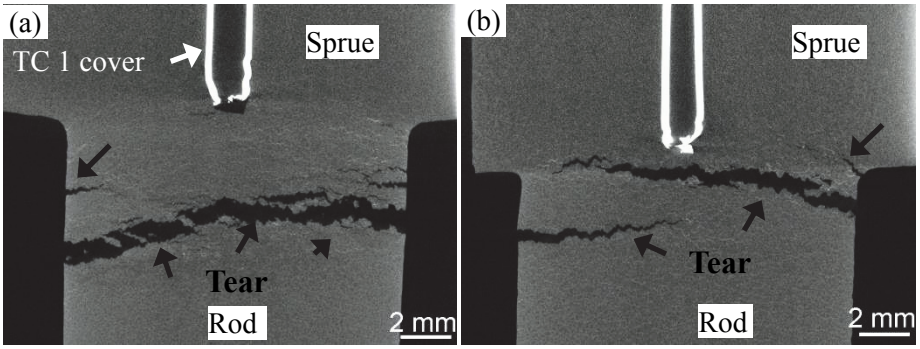

Fig. 5-22 X-ray tomography cross sections of Mg-0.5Ca-6Zn alloys cast at different mould temperatures, (a) T_{mould} = 250 ^{0}C, (b) T_{mould} = 450 ^{0}C

5.2.2.4 Micro observation

The optical microstructures on the longitudinal sections of the Mg-0.5Ca-xZn alloys cast at a mould temperature of 250 ^{0}C are shown in Fig. 5-23. The samples were cut from the regions near the junctions. As the casting of Mg-0.5Ca-0.5Zn, Mg-0.5Ca-1.5Zn, and Mg-0.5Ca-4Zn alloys were completely broken, the tear morphologies in the rod part near the fractured region were analysed and shown in Fig. 5-23 (a), (b), and (c), respectively. Both sprue and rod parts of Mg-0.5Ca-6Zn were shown in Fig. 5-23 (d), and complex tear morphologies were observed. All the tears were seen to propagate mainly along grain boundaries.

Similarly, samples were prepared from Mg-0.5Ca-xZn alloys cast at T_{mould} = 450 ^{0}C and the resultant microstructures are shown in Fig. 5-24. Only fine tears were found at the sprue-rod junction for Mg-0.5Ca-0.5Zn alloy. The tear morphology sample of Mg-0.5Ca-4Zn was taken from the rod portion attached to the sprue. The grain size of the tear region was smaller than that of the sprue-rod junction area. The tear width of Mg-0.5Ca-6Zn cast at T_{mould} = 450 ^{0}C was smaller than that cast at T_{mould} = 250 ^{0}C, which confirmed again that a higher mould temperature improved the resistance to hot tearing. All the tears of alloys cast at a high mould temperature also mainly propagated along grain boundaries irrespective of tear location.

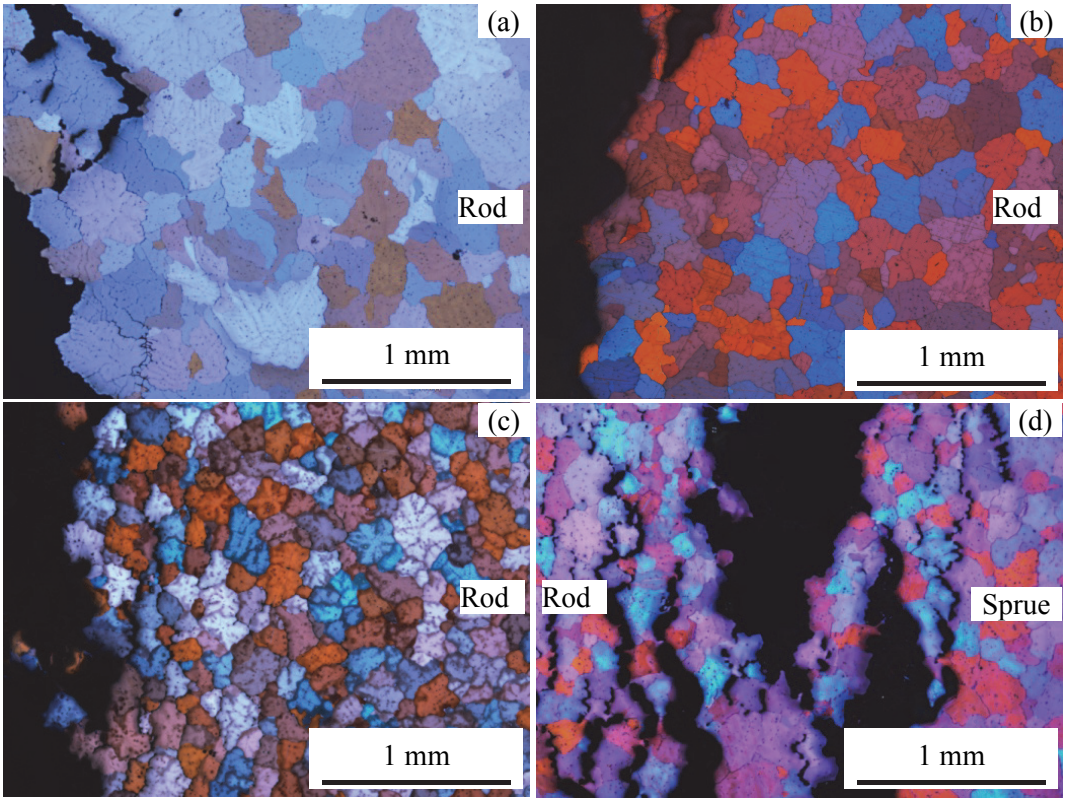

Fig. 5-23 Optical microstructures of tears for the alloys cast at T_{mould} = 250 ^{0}C, (a) Mg-0.5Ca-0.5Zn, (b) Mg-0.5Ca-1.5Zn, (c) Mg-0.5Ca-4Zn, and (d) Mg-0.5Ca-6Zn

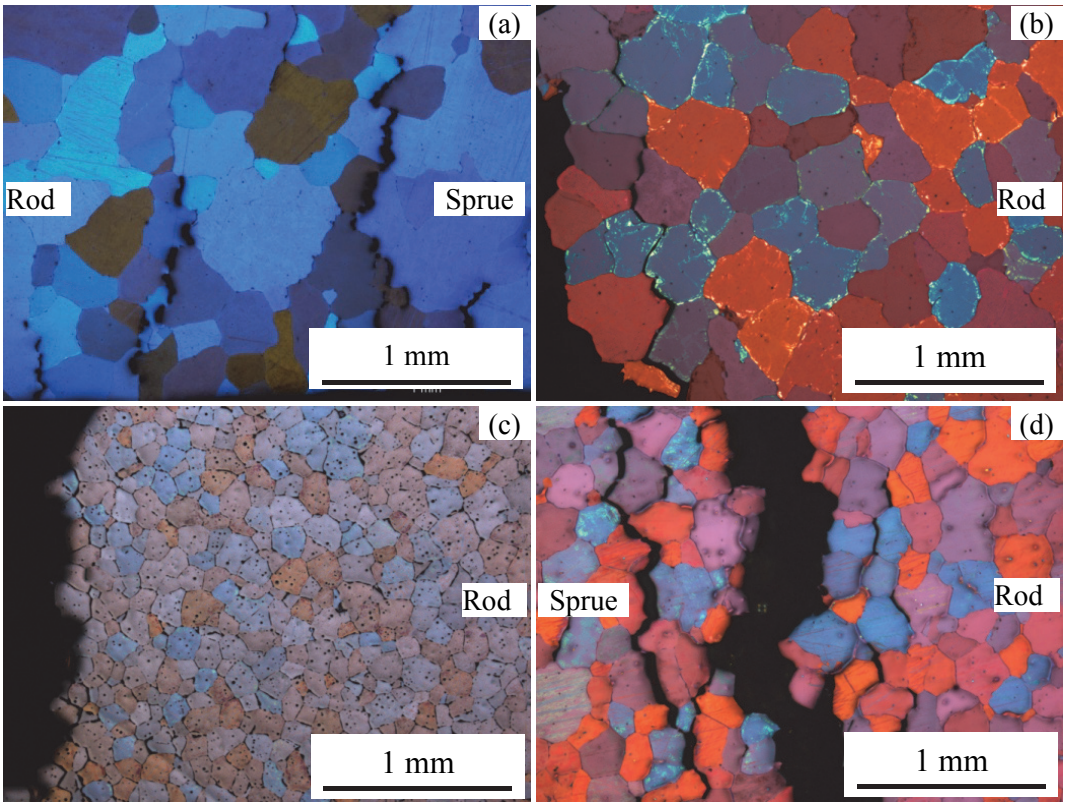

Fig. 5-24 Optical microstructures of tears for the alloys cast at T_{mould} = 450 ^{0}C, (a) Mg-0.5Ca-0.5Zn, (b) Mg-0.5Ca-1.5Zn, (c) Mg-0.5Ca-4Zn, and (d) Mg-0.5Ca-6Zn

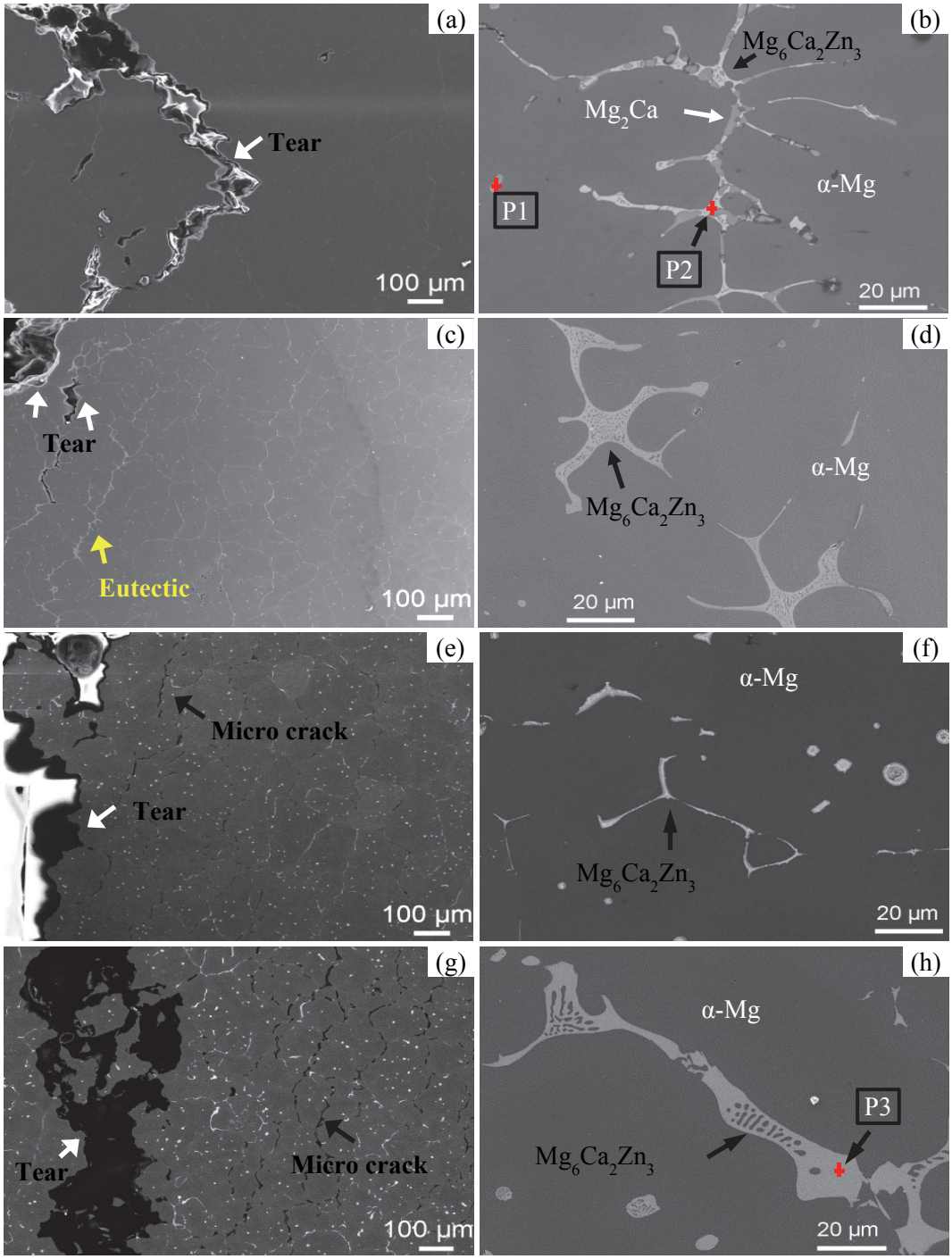

Fig. 5-25 Microstructures near the tear region of alloys cast at T_{mould} = 250 ^{0}C, (a), (b) Mg-0.5Ca-0.5Zn, (c), (d) Mg-0.5Ca-1.5Zn, (e), (f) Mg-0.5Ca-4Zn, and (g), (h) Mg-0.5Ca-6Zn

Generally, second phases as well as eutectic distribution near the tear region was interesting for hot tearing investigation. Thus, the SEM micrographs of the tear region for Mg-0.5Ca-xZn alloys cast at T_{mould} = 250 ^{0}C were taken and shown in Fig. 5-25. The amount of second phases was seen to increase with the increase in Zn content. The EDX anlysis of the second phases was carried out and the results are listed in Table 5-5. Mg-0.5Ca-0.5Zn contains both Mg_2Ca and $Mg_6Ca_2Zn_3$ phases and the other three alloys contain mainly the ternary

$Mg_6Ca_2Zn_3$ phase. In addition, MgZn is evident only in the Mg-0.5Ca-6Zn alloy. Some small eutectic $Mg_6Ca_2Zn_3$ was only evidenced in Mg-0.5Ca-1.5Zn alloy. Interestingly, some secondary microcracks were found near the main tear for the Mg-0.5Ca-4Zn and Mg-0.5Ca-6Zn alloys. However, no such microcracks were evident in the Mg-0.5Ca-0.5Zn and Mg-0.5Ca-1.5Zn alloys.

Table 5-5 EDX results of Mg-0.5Ca-xZn alloys at points marked in Fig. 5-25

Points	Ca		Zn		Mg		O	
	Wt.%	At.%	Wt.%	At.%	Wt.%	At.%	Wt.%	At.%
1 (Mg_2Ca)	12.3	8.0	3.2	1.3	83.7	89.4	0.8	1.3
2 ($Mg_6Ca_2Zn_3$)	19.6	14.3	16.0	7.2	63.1	76.1	1.3	2.5
3 (MgZn)	2.6	2.8	17.5	7.4	78.8	89.0	1.1	1.9

The detailed distribution of the microcracks for Mg-0.5Ca-4Zn and Mg-0.5Ca-6Zn are shown in Fig. 5-26. These microcracks were found mainly at the rod portion of the junction. Formation of such microcracks may results in a smaller main tear (i.e., the casting of Mg-0.5Ca-6Zn is not completely broken) due to the stress relaxation. It is reported that such stress relaxation can also contribute to the formation of microposity, which results in the reduced effective tearing strain [102]. The stress relief prevented further stress concentration at the junction area, which led to a small primary tear.

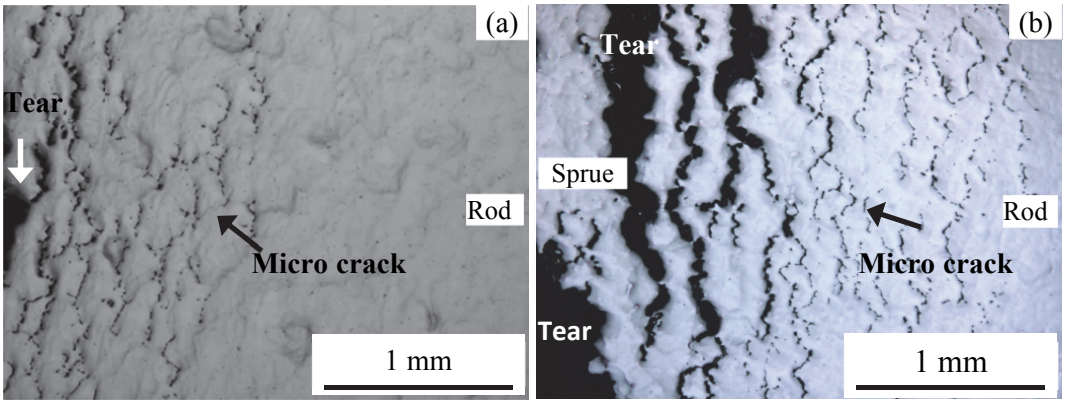

Fig. 5-26 Microtears distribution of the alloys cast at T_{mould} = 250 ^{0}C, (a) Mg-0.5Ca-4Zn, (b) Mg-0.5Ca-6Zn

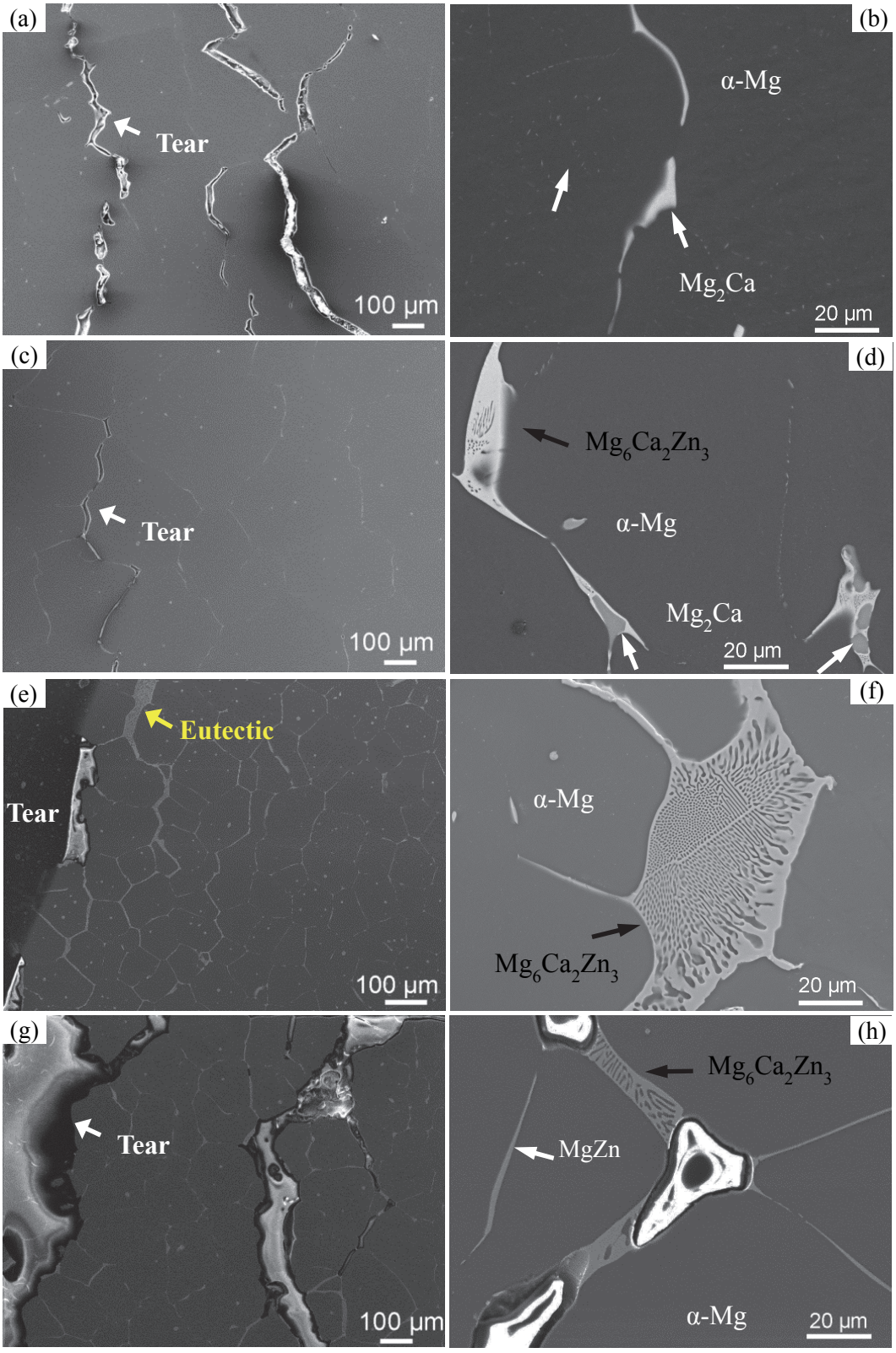

Fig. 5-27 Microstructures near the tear region of alloys cast at T_{mould} = 450 ^{0}C, (a), (b) Mg-0.5Ca-0.5Zn, (c), (d) Mg-0.5Ca-1.5Zn, (e), (f) Mg-0.5Ca-4Zn, and (g), (h) Mg-0.5Ca-6Zn

Fig. 5-27 displays the microstructures near the tear region of Mg-0.5Ca-xZn alloys cast at T_{mould} = 450 ^{0}C. The microstructures were similar with those of alloys cast at low mould

temperature. No siginificant eutectic segregation near the tears was found for Mg-0.5Ca-0.5Zn, Mg-0.5Ca-1.5Zn, and Mg-0.5Ca-6Zn alloys. Few eutectic regions were found near the tear region for the Mg-0.5Ca-4Zn alloy. The eutectic was mainly composed of primary Mg and the ternary $Mg_6Ca_2Zn_3$ phase. Further, Mg_2Ca is evident in the Mg-0.5Ca-1.5Zn alloy at the high mould temperature.

5.2.2.5 Fracture surfaces

Typical hot tearing fracture surfaces were observed for the Mg-0.5Ca-xZn alloys cast at T_{mould} = 250 ^{0}C, as shown in Fig. 5-28. The fracture surfaces from both the centre and edge region were observed and they were quite different. Firstly, the fracture surfaces at the centre region mainly consisted of dendritic grain and torn liquid film. However, the torn liquid film was not found at the edge region. Secondly, micro pores between dendritic grains were found at the edge region for all the four alloys. The micro pores at the centre region were only found for the Mg-0.5Ca-4Zn and Mg-0.5Ca-6Zn alloys. This agreed well with the previously shown micro secondary crack in Fig. 5-26.

Fig. 5-29 shows the fracture surfaces of the Mg-0.5Ca-1.5Zn and Mg-0.5Ca-4Zn alloys cast at T_{mould} = 450 ^{0}C. Only the fracture surface from the centre region is shown. Both fracture surfaces contained liquid film, which confirmed that they are hot tears. Although tears of Mg-0.5Ca-4Zn alloys occurred at the interface between alloy and load screw, liquid film still existed. Additionally, the torn liquid film on fracture surface of Mg-0.5Ca-1.5Zn was more than that of Mg-0.5Ca-4Zn. Dendrites are observed on the fracture surface at the sprue-rod junction (Fig. 5-29 (a)) and they are not seen on the fracture surface at the load screw (Fig. 5-29 (b)). In addition, the fracture surface at the load screw looks more like the cleavage surface, indicating its brittleness. Thus, there is a likelihood that the crack at the load screw is “cold crack” with some microtears (due to the presence of liquid flim) initiated above the solidiu temperature.

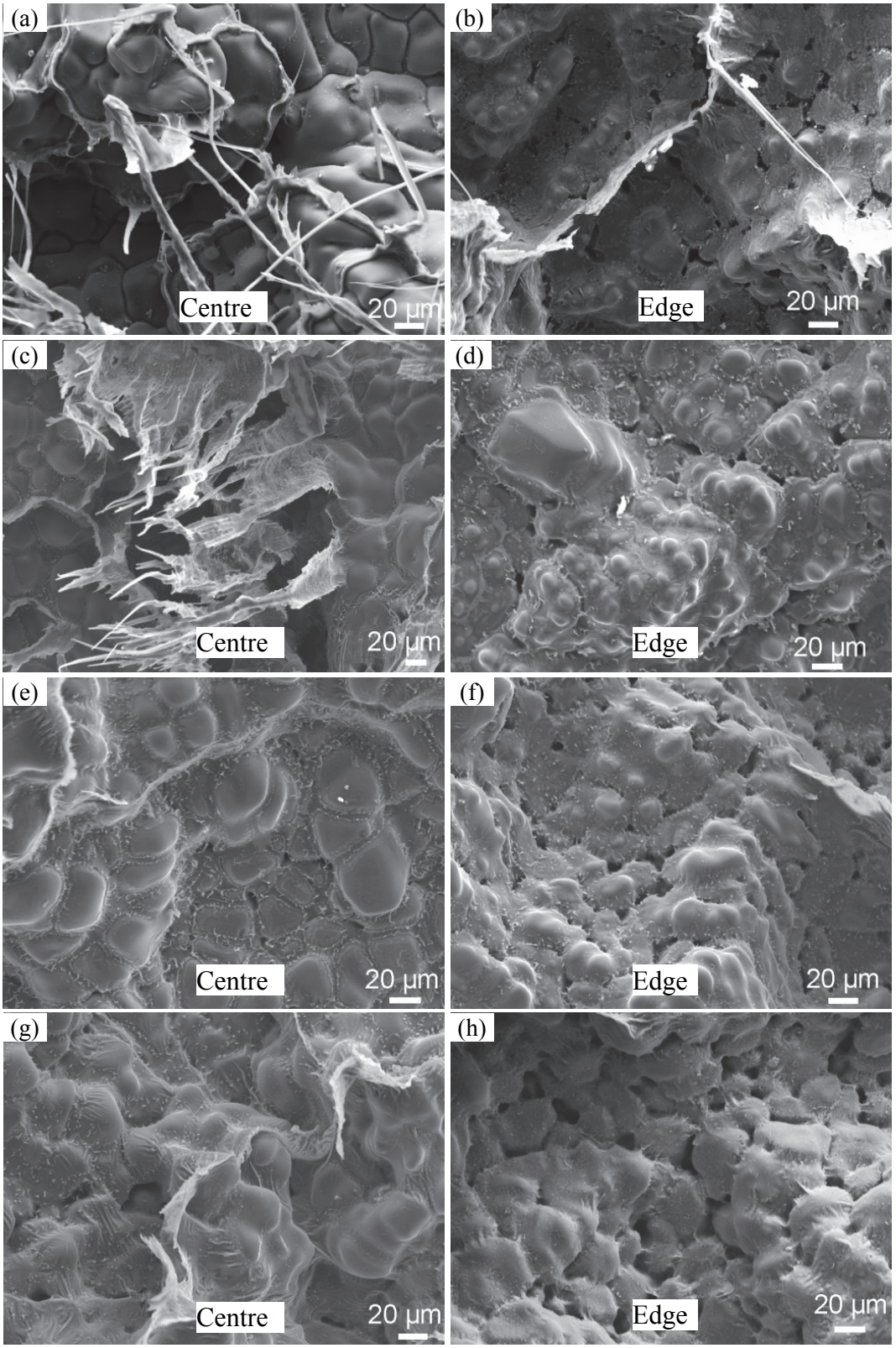

Fig. 5-28 Fracture surfaces of alloys cast at T_{mould} = 250 ^{0}C, (a), (b) Mg-0.5Ca-0.5Zn, (c) (d) Mg-0.5Ca-1.5Zn, (e), (f) Mg-0.5Ca-4Zn, and (g), (h) Mg-0.5Ca-6Zn

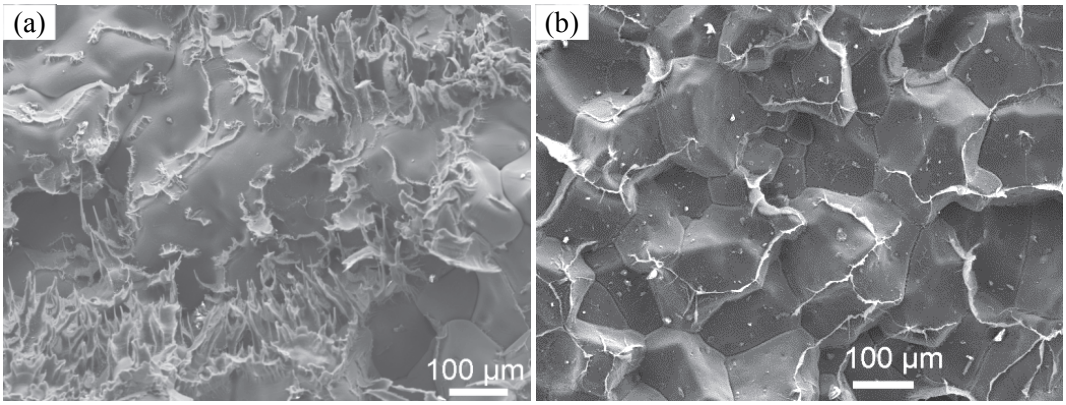

Fig. 5-29 Fracture surfaces of alloys cast at T_{mould} = 450 ^{0}C, (a) Mg-0.5Ca-1.5Zn, and (b) Mg-0.5Ca-4Zn

5.2.3 Hot tearing behaviour of Mg-0.5Ca-4Zn-0.2Zr alloys

Fig. 5-30 shows the effect of Zr addition on the hot tearing behaviour of Mg-0.5Ca-4Zn alloys. The addition of Zr was found to decrease the HTS at both mould temperatures. At a mould temperature of 250 ^{0}C, the addition of Zr resulted in a severe tear instead of completely broken at the sprue-rod junction. As the mould temperature increases to 450 ^{0}C, at both sprue-rod junction and load screw region, no visible tear were observed in the Zr containing alloy.

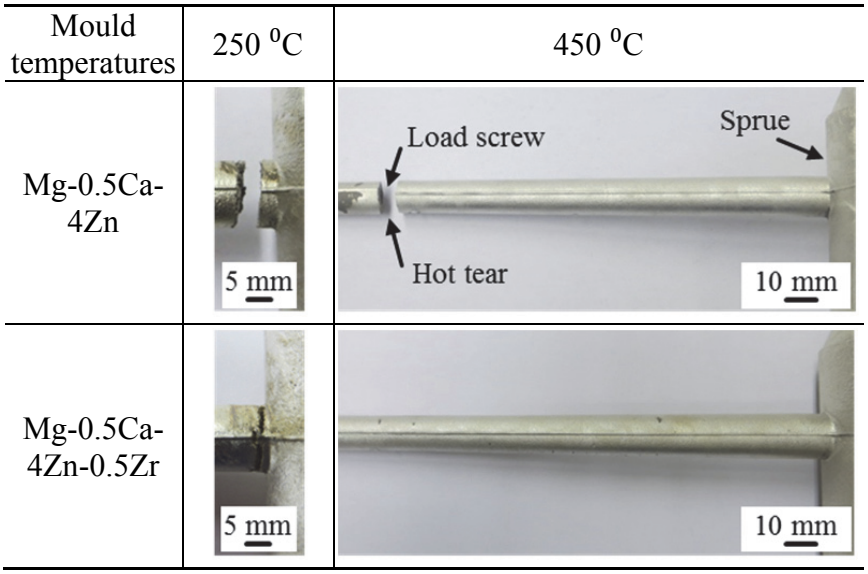

Fig. 5-30 Macro pictures of the hot tears of Mg-0.5Ca-4Zn and Mg-0.5Ca-4Zn-0.2Zr at both mould temperatures

The improved hot tearing resistance with the addition of Zr was mainly due to grain refinement. Grain morphologies of alloys with or without Zr addition are compared in Fig. 5-31. The grain size was significantly refined with the addition of Zr at both the mould temperatures. The grain size decreased from 126±57 µm to 70±30 µm with the Zr addition at a mould temperature of 250 ^{0}C. At a higher mould temperature of 450 ^{0}C, the grain size was

also refined from 149±74 µm to 64±28 µm for Zr free and Zr containing alloys. Zirconium is known as a very efficient grain refiner for Al-free Mg alloys [103-105]. According to Pandat software, 0.2 wt.% Zr (actual composition) has little impact on the freezing range (FR) of Mg-0.5Ca-4Zn alloy. The calculated FR of Mg-0.5Ca-4Zn and Mg-0.5Ca-4Zn-0.5Zr with Pandat Software are 341 ^{0}C and 342 ^{0}C, respectively. Therefore, only the grain refinement was responsible for the decreased HTS. An improvement in hot tearing resistance by grain refinement was also reported in Al alloys [106].

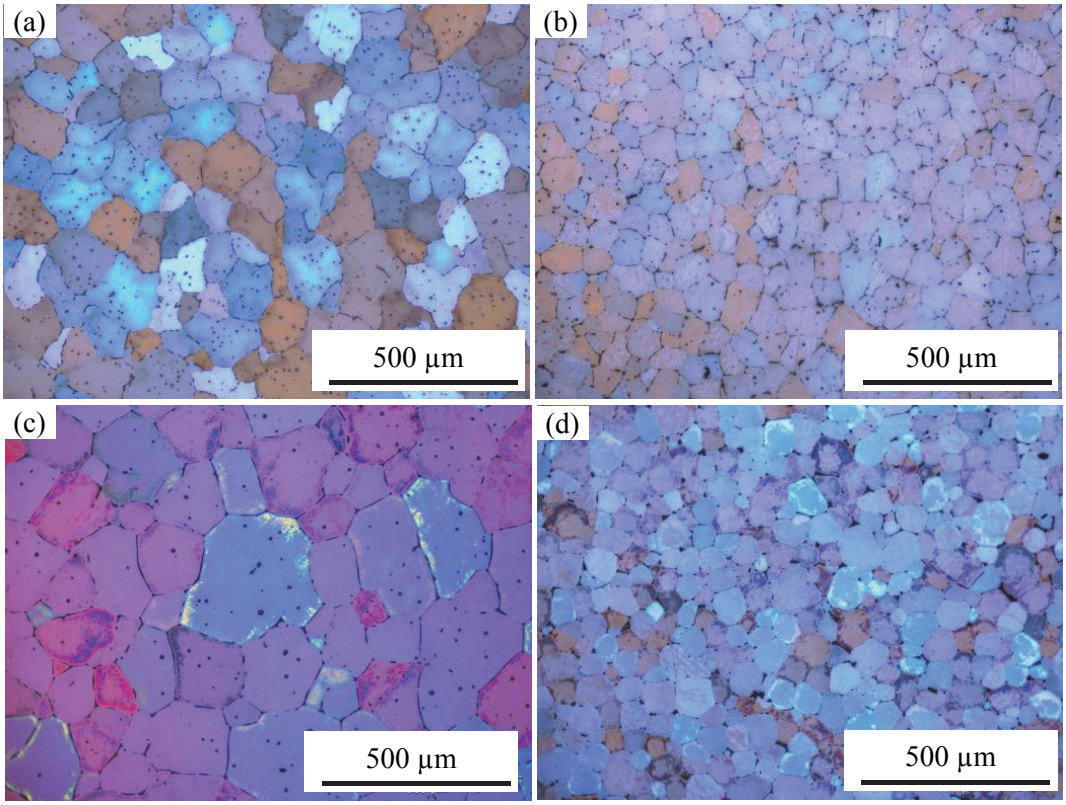

Fig. 5-31 Optical microstructures of alloys cast at T_{mould} = 250 ^{0}C, (a) Mg-0.5Ca-4Zn, (b) Mg-0.5Ca-4Zn-0.2Zr, alloys cast at T_{mould} = 450 ^{0}C, (c) Mg-0.5Ca-4Zn, (d) Mg-0.5Ca-4Zn-0.2Zr,

5.2.4 Numerical simulation of hot tearing tendency

The HTI simulations are compared with the experimental results for Mg-0.5Ca-xZn alloys at a mould temperature of 250 ^{0}C, as shown in Fig. 5-32. The high HTI of all Mg-0.5Ca-xZn alloys appears at the sprue-rod junction. Besides, with increasing the Zn content, the simulated susceptible hot tearing area deviates away from the exact junction. The experimental hot tears of alloys with a high Zn content also occurred away from the exact sprue-rod junction. Thus, the HTI simulation successfully predicts the susceptible hot tearing area.

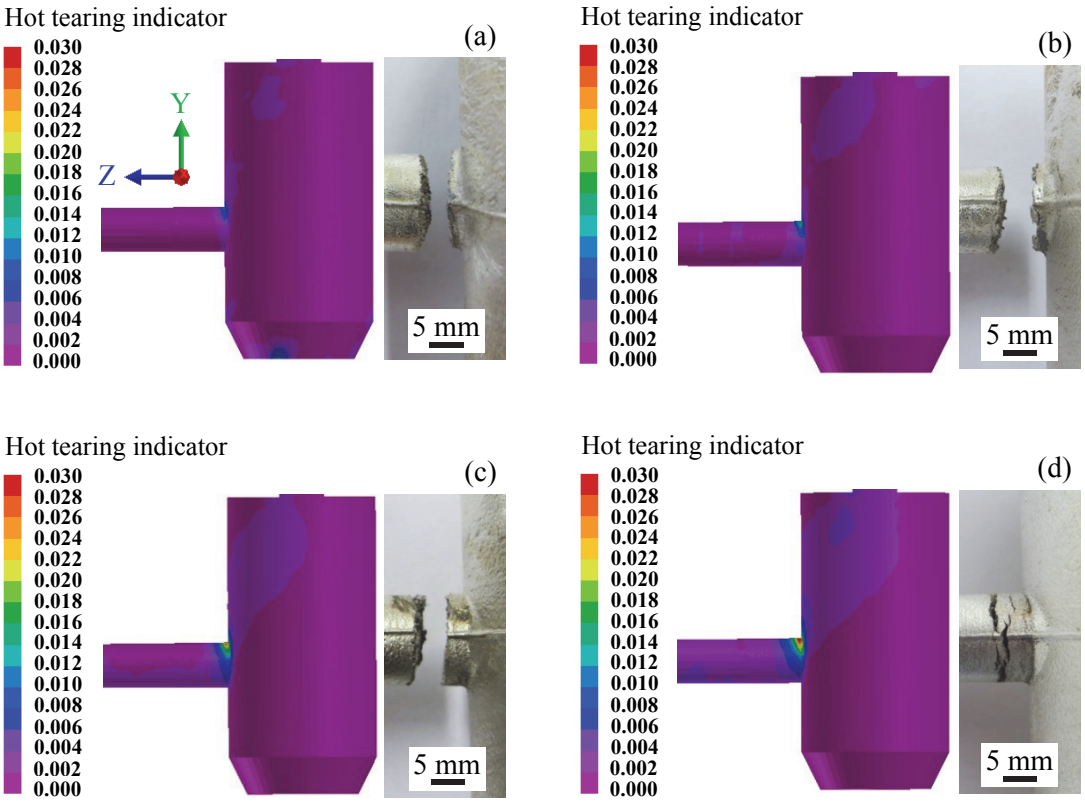

Fig. 5-32 Simulated HTI of snapshot view and experimental hot tears of alloys cast at T_{mould} = 250 ^{0}C, (a) Mg-0.5Ca-0.5Zn, (b) Mg-0.5Ca-1.5Zn, (c) Mg-0.5Ca-4Zn, and (d) Mg-0.5Ca-6Zn

5.3 Hot tearing of Mg-2Ca-xZn ternary alloy

5.3.1 Chemical composition

Chemical compositions of Mg-2Ca-xZn alloys at T_{mould} = 250 ^{0}C are listed in Table 5-6. The measured compositions are close to the nominal composition, and the trace elements are relatively low.

Table 5-6 Chemical compositions of Mg-2Ca-xZn alloys at T_{mould} = 250 ^{0}C, in wt.%

Alloy	Ca	Zn	Fe	Mn	Si	Mg
Mg-2Ca-0.5Zn	1.98	0.51	0.00437	0.0394	0.0123	Bal.
Mg-2Ca-1.5Zn	1.94	1.49	0.00449	0.0381	0.0133	Bal.
Mg-2Ca-4Zn	1.72	4.07	0.00665	0.0420	0.0160	Bal.
Mg-2Ca-6Zn	1.64	6.49	0.00548	0.0371	0.0143	Bal.

5.3.2 Experimental hot tearing tendency

5.3.2.1 Force-temperature-time curves

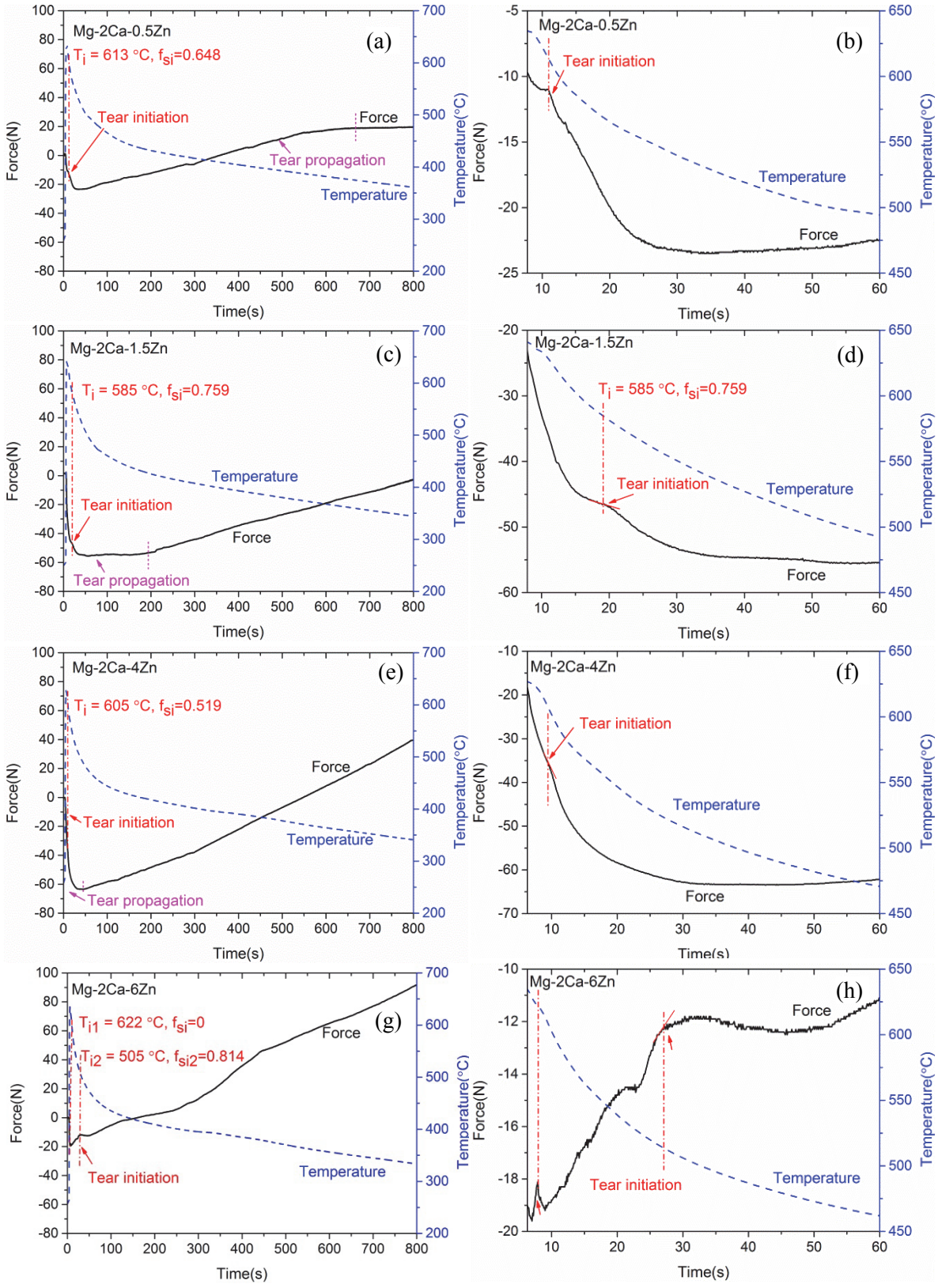

Fig. 5-33 Force-temperature-time curves of Mg-2Ca-xZn alloys cast at T_{mould} = 250 ^{0}C (a), (b) Mg-2Ca-0.5Zn, (c), (d) Mg-2Ca-1.5Zn, (e), (f) Mg-2Ca-4Zn, and (g), (h) Mg-2Ca-6Zn

The as-recorded force-temperature-time curves of Mg-2Ca-xZn at a mould temperature of 250 ^{0}C are displayed in Fig. 5-33. The determination of hot tearing initiation is shown in detail in Fig. 5-33 (b), (d), (f), and (h). By comparing the overall force-temperature-time curves, it is observed that Mg-2Ca-0.5Zn alloy displays a rough plateau after the termination of crack propagation. This observation indicates that the Mg-2Ca-0.5Zn sample was completely broken (severe HTS). Moreover, multiple force drops in the force curve of Mg-2Ca-6Zn alloy are noticed. In addition, the f_{si} is found lower than 0.9 for all the Mg-2Ca-xZn alloys. The f_{si} of Mg-2Ca-0.5Zn, Mg-2Ca-1.5Zn, Mg-2Ca-4Zn, and Mg-2Ca-6Zn alloys are 0.648, 0.759, 0.519, and 0.814, respectively.

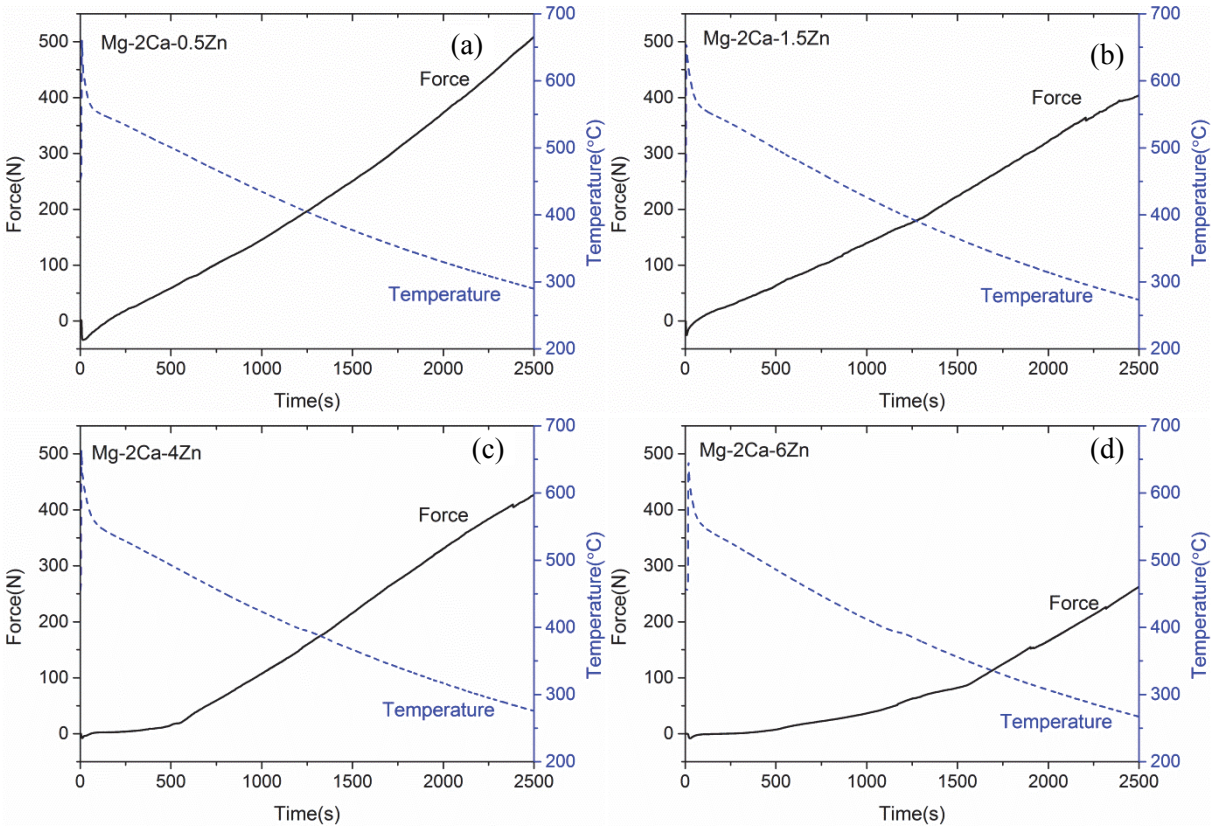

Fig. 5-34 Force-temperature-time curves of Mg-2Ca-xZn alloys cast at T_{mould} = 450 ^{0}C (a) Mg-2Ca-0.5Zn, (b) Mg-2Ca-1.5Zn, (c) Mg-2Ca-4Zn, and (d) Mg-2Ca-6Zn

Fig. 5-34 shows the force-temperature-time curves of Mg-2Ca-xZn alloys cast at the mould temperature of 450 ^{0}C. No force drops are evident on the curves for all four alloys, indicating that no tear occurred in these alloys. The force increase for Mg-2Ca-6Zn alloy is slower than that for other three alloys, which is attributed to its larger freezing range (FR). According to the thermodynamic calculations using the Pandat software, the FR of Mg-2Ca-(0.5-4) Zn alloys are in the range of 244-234 ^{0}C whereas the FR of Mg-2Ca-6Zn is 327 ^{0}C. According to the software, the solidification ends with a binary MgZn phase in Mg-2Ca-6Zn alloy which

results in a solidus temperature (T_s) as low as 294 ^{0}C. On the other hand, the T_s of the other alloys are 394 ^{0}C as in these cases the solidification ends with ternary $Mg_6Ca_2Zn_3$ phase. Hence, Mg-2Ca-6Zn alloy has longer solidification time. As a result, the force increment seems slow at the early stage of solidification for Mg-2Ca-6Zn alloy.

5.3.2.2 Macro observation

Mould temperatures	Mg-2Ca-0.5Zn	Mg-2Ca-1.5Zn	Mg-2Ca-4Zn	Mg-2Ca-6Zn
250 °C	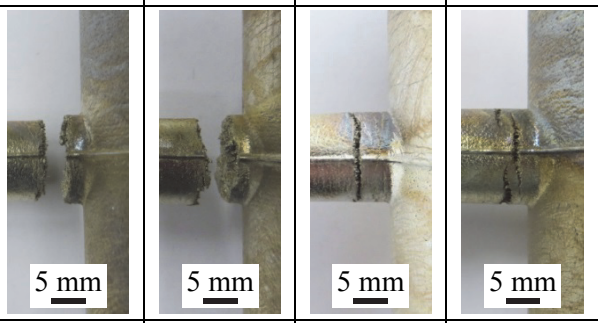			
450 °C	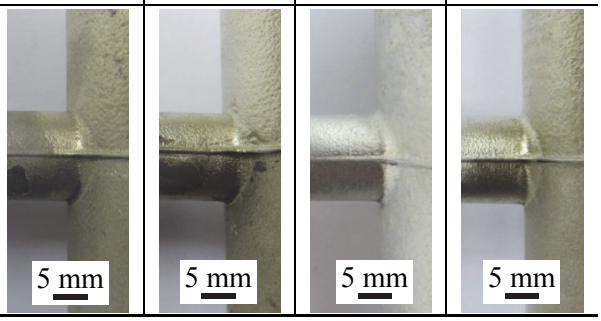			

Fig. 5-35 Macro observations of the hot tears of Mg-2Ca-xZn alloys cast at T_{mould} = 250 ^{0}C and T_{mould} = 450 ^{0}C

Macro photographs of hot tears in Mg-2Ca and Mg-2Ca-xZn alloy samples cast at both mould temperatures are shown Fig. 5-35. The influence of Zn content on the hot tearing of Mg-Ca-Zn alloys can be seen clearly at the mould temperature of 250 ^{0}C. As the Zn content increases the HTS of Mg-Ca-Zn alloy increases up to 1.5% Zn and then decreases. The peak severity occurs at 0.5 to 1.5% Zn content as the rod portions of the Mg-2Ca-0.5Zn and Mg-2Ca-1.5Zn alloys castings are completely broken. Mg-2Ca-6Zn alloy exhibits multiple cracking, which agrees well with the multiple force drops in the force-temperature-time curves (Fig. 5-33 (g)). In addition, the tear location has moved away from the sprue at a high Zn content. This observation may explain why the predicted f_{si} using the force-temperature-time curves is lower than 0.9. The recorded temperature was from the centre of sprue-rod junction area, and hence the calculated f_{si} is the solid fraction at the sprue-rod junction, not at

the exact location of tearing. As the tear occurred away from the junction, the actual tear initiation temperature must be slightly lower than the measured value and hence the corresponding solid fraction must be higher. No visible tears are observed for all the alloys when the mould temperature increased to 450 ^{0}C, indicating that increasing the initial mould temperature is an effective way to enhance the resistance to hot tearing.

5.3.2.3 X-ray tomography

X-ray tomography photographs taken at the longitudinal cross section (mid plane section) of Mg-2Ca-4Zn and Mg-2Ca-6Zn alloys samples cast at T_{mould} = 250 ^{0}C are shown in Fig. 5-36. There are few white areas (marked with white arrows) near the tear locations in Mg-2Ca-4Zn and Mg-2Ca-6Zn alloys. These white areas are eutectic, which can refill the previously formed tears.

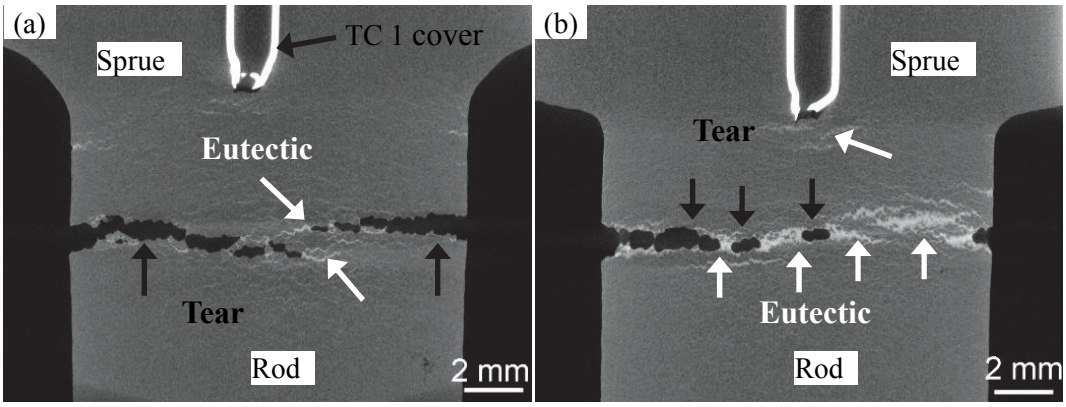

Fig. 5-36 X-ray tomography photographs of the alloys cast at T_{mould} = 250 ^{0}C, (a) Mg-2Ca-4Zn, and (b) Mg-2Ca-6Zn

Fig. 5-37 shows X-ray tomography photographs of Mg-2Ca-xZn alloys cast at T_{mould} = 450 ^{0}C. Only fine tear are evidenct at the sprue-rod junction in Mg-2Ca-0.5Zn, Mg-2Ca-1.5Zn, and Mg-2Ca-4Zn, as marked with red arrows. Interestingly, the microstructures are homogeneous in all the alloys cast at the high mould temperature of 450 ^{0}C: as no eutectic segregation is observed around the sprue-rod junction area.

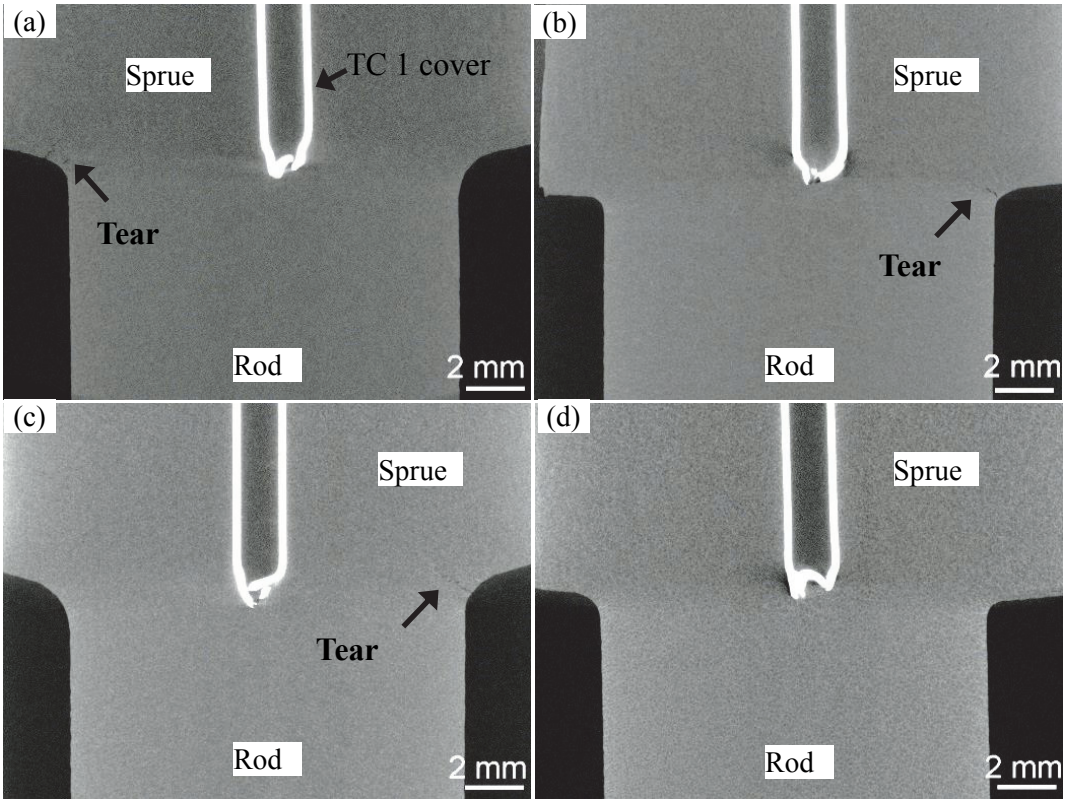

Fig. 5-37 X-ray tomography photographs of the alloys cast at T_{mould} = 450 ^{0}C, (a) Mg-2Ca-0.5Zn, (b) Mg-2Ca-1.5Zn, (c) Mg-2Ca-4Zn, and (d) Mg-2Ca-6Zn

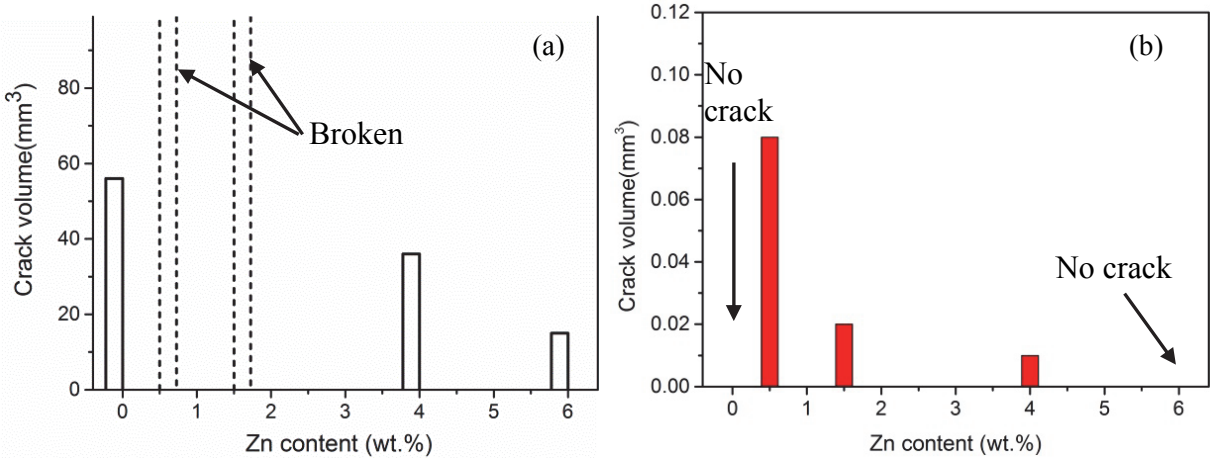

Fig. 5-38 Crack volumes of Mg-2Ca-xZn alloys cast at different mould temperatures, (a) T_{mould} = 250 ^{0}C and (b) T_{mould} = 450 ^{0}C.

The measured crack volumes are shown in Fig. 5-38. As Mg-2Ca-0.5Zn and Mg-2Ca-1.5Zn alloys samples were completely broken, the crack volumes are displayed with dashed column in Fig. 5-38 (a). It is clear that with the increment in Zn content, the HTS of Mg-2Ca-xZn alloys firstly increases up to 1.5% Zn and then decreases with further Zn addition. In general, the crack volumes of alloys cast at T_{mould} = 450 ^{0}C are relatively low (lower than 0.10 mm^3).

These results demonstrate again that casting at a higher mould temperature largely improves the hot tearing resistance of Mg-2Ca-xZn alloys. The measured crack volume for Mg-2Ca-6Zn alloy is zero at T_{mould} = 450 ^{0}C, indicating that no crack is observed by X-ray tomography.

5.3.2.4 Micro observation

Polarized optical tear morphologies at the hot spot of Mg-2Ca-xZn alloys at the mould temperature of 250 ^{0}C are shown in Fig. 5-39. It is obvious thet all the cracks propagate along the grain boundaries. It is worth noting that the grain sizes of Mg-2Ca-xZn alloys decreases with increasing Zn content. However, the grain refinement at the hot spot is not significant. All the four alloys show a dendritic structure at T_{mould} = 250 ^{0}C.

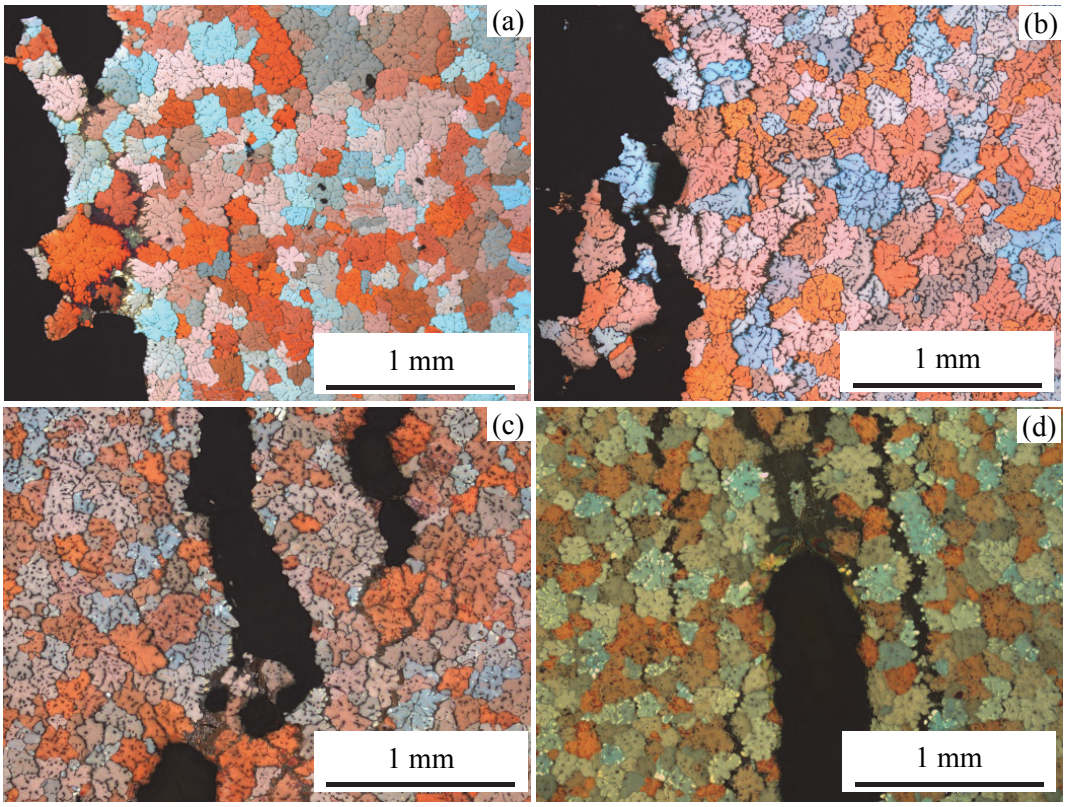

Fig. 5-39 Optical microstructures of tears for Mg-2Ca-xZn alloys cast at T_{mould} = 250 ^{0}C, (a) Mg-2Ca-0.5Zn, (b) Mg-2Ca-1.5Zn, (c) Mg-2Ca-4Zn, and (d) Mg-2Ca-6Zn

Fig. 5-40 displays the tear morphologies of Mg-2Ca-xZn alloy cast at T_{mould} = 450 ^{0}C. Fine cracks are evident in the Mg-2Ca-0.5Zn and Mg-2Ca-1.5Zn alloys (as indicated by white arrow). The tears are discontinuous and locate at the grain boundaries. In comparison with the microstructures of alloys at a mould temperature of 250 ^{0}C, the structures are less dendritic in nature at higher mould temperature (450^{o}C). This is because at a higher mould temperature, the solute has enough time to diffuse and hence well distributed.

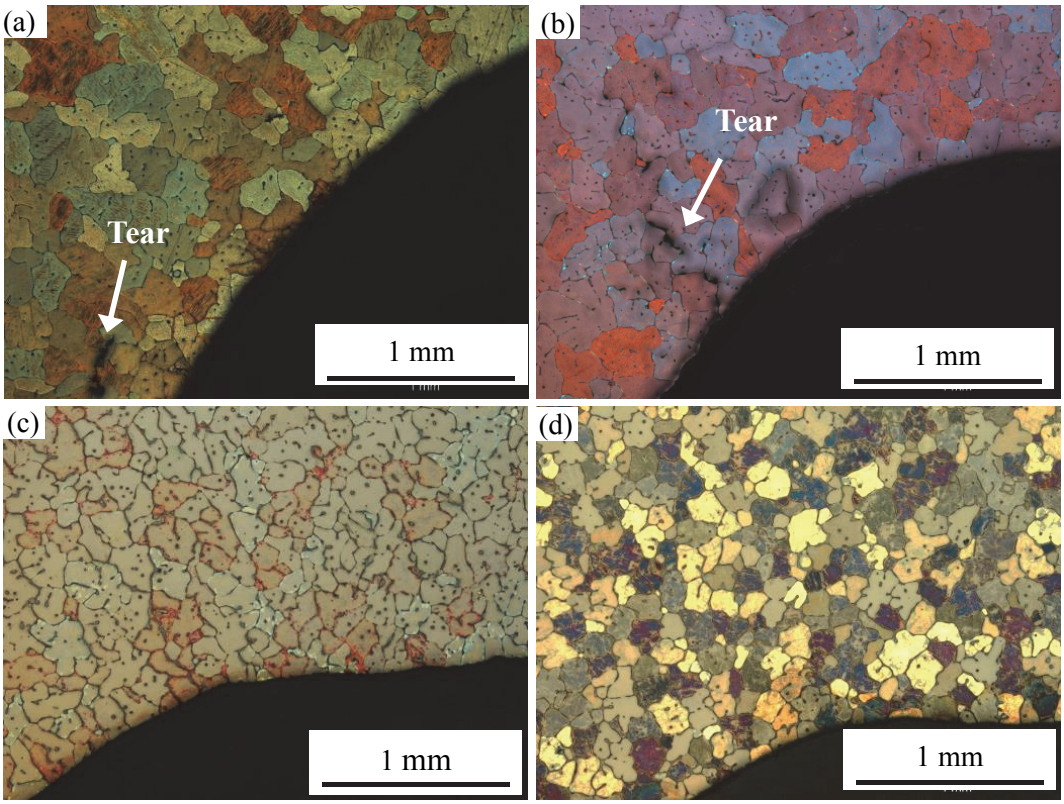

Fig. 5-40 Optical microstructures of tears for Mg-2Ca-xZn alloys cast at T_{mould} = 450 ^{0}C, (a) Mg-2Ca-0.5Zn, (b) Mg-2Ca-1.5Zn, (c) Mg-2Ca-4Zn, and (d) Mg-2Ca-6Zn

Microstructures near the main tear region of Mg-2Ca-xZn alloys cast at T_{mould} = 250 °C are shown in Fig. 5-41. Large eutectic structures are evident in all four alloys. According to the EDX results (Fig. 5-42), Mg_2Ca is the main second phase in the Mg-2Ca-0.5Zn alloy. As the Zn content increases to 1.5 wt.% and 4 wt.%, in addition to Mg_2Ca, ternary $Mg_6Ca_2Zn_3$ phases are also observed. However, only the $Mg_6Ca_2Zn_3$ phase is present as the second phase in Mg-2Ca-6Zn alloy. The solutes are highly segregated at the tearing area due to the non-equilibrium solidification that occurred.

Fig. 5-43 shows the XRD patterns of alloys cast at T_{mould} = 250 ^{0}C. The second phases were identified according to the standard PDF cards. The XRD results confirm that both Mg-2Ca-0.5Zn and Mg-2Ca-1.5Zn alloys contain primary Mg and Mg_2Ca phase. However, peaks for both Mg_2Ca and $Mg_6Ca_2Zn_3$ phases are detected in Mg-2Ca-4Zn alloy. The XRD pattern of Mg-2Ca-6Zn alloy consists of peaks for primary Mg and ternary $Mg_6Ca_2Zn_3$ phase. Although SEM observations indicated the presence of the ternary $Mg_6Ca_2Zn_3$ phase in Mg-2Ca-1.5Zn alloy, it is not detected by XRD, suggesting that the amount of $Mg_6Ca_2Zn_3$ in this alloy is below the detection limit of XRD.

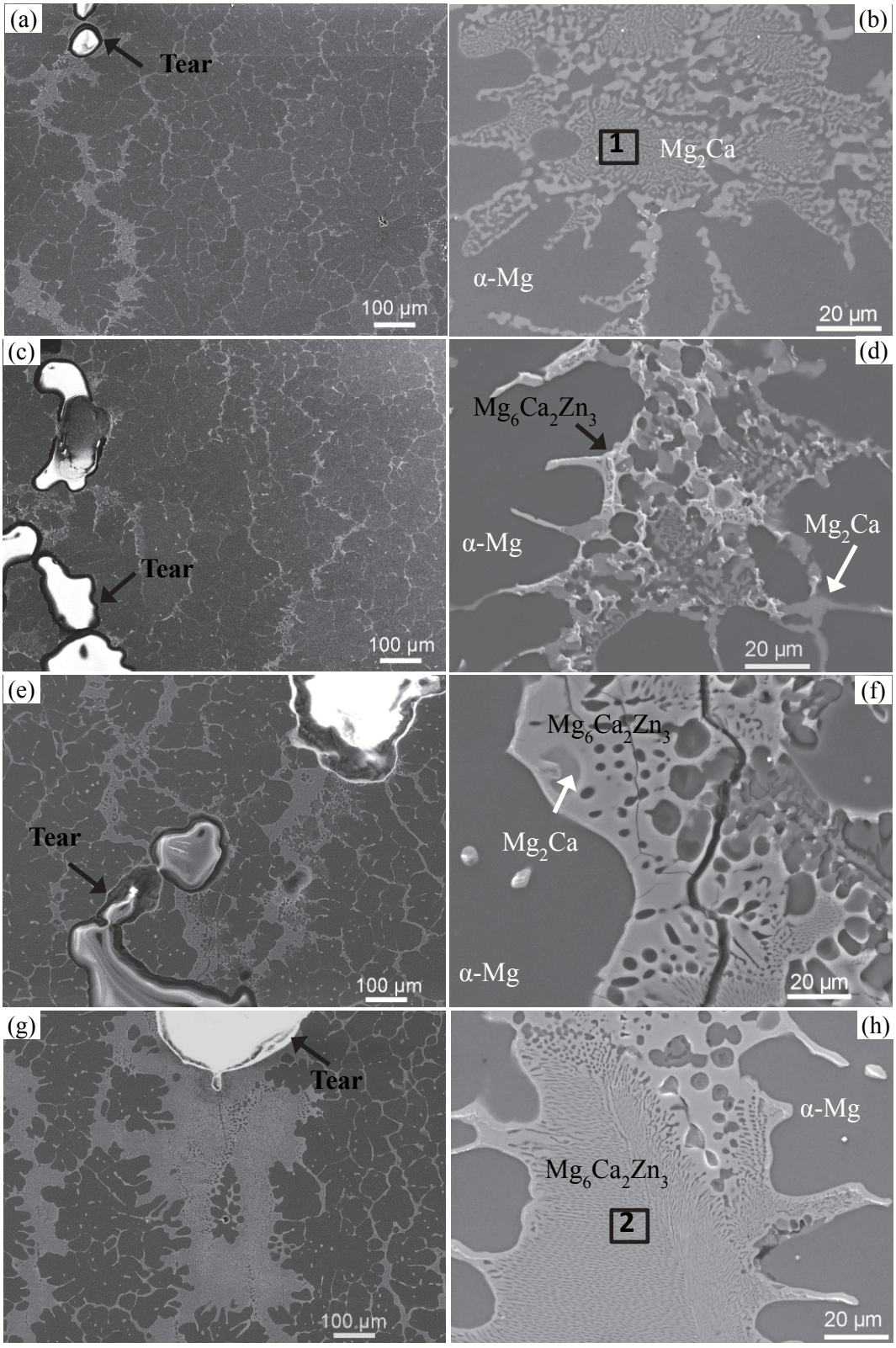

Fig. 5-41 Microstructures near the tear regions of Mg-2Ca-xZn alloys cast at T_{mould} = 250 °C, (a), (b) Mg-2Ca-0.5Zn; (c), (d) Mg-2Ca-1.5Zn; (e), (f) Mg-2Ca-4Zn; and (g), (h) Mg-2Ca-6Zn

The microstructures of the alloys cast at T_{mould} = 450 ^{o}C are displayed in Fig. 5-44, while the XRD patterns of the Mg-2Ca-xZn alloys cast at T_{mould} = 450 ^{o}C are shown in Fig. 5-45. These microstructures are different from that of the alloys cast at T_{mould} = 250 ^{0}C in several ways. Firstly, the volume of eutectic or second phase at the hot spot is much less than that observed at the lower mould temperature. This indicates that the solute segregation at the high mould temperature, 450 °C, is lower than that at the low mould temperature, 250 °C, which is likely due to the homogenous distribution of solute at a low cooling rate (high initial mould temperature). Secondly, more Mg_2Ca particles are found in the Mg-2Ca-0.5Zn, Mg-2Ca-1.5Zn, and Mg-2Ca-4Zn alloys. Finally, more $Mg_6Ca_2Zn_3$ is observed in the Mg-2Ca-1.5Zn alloy, as detected by XRD.

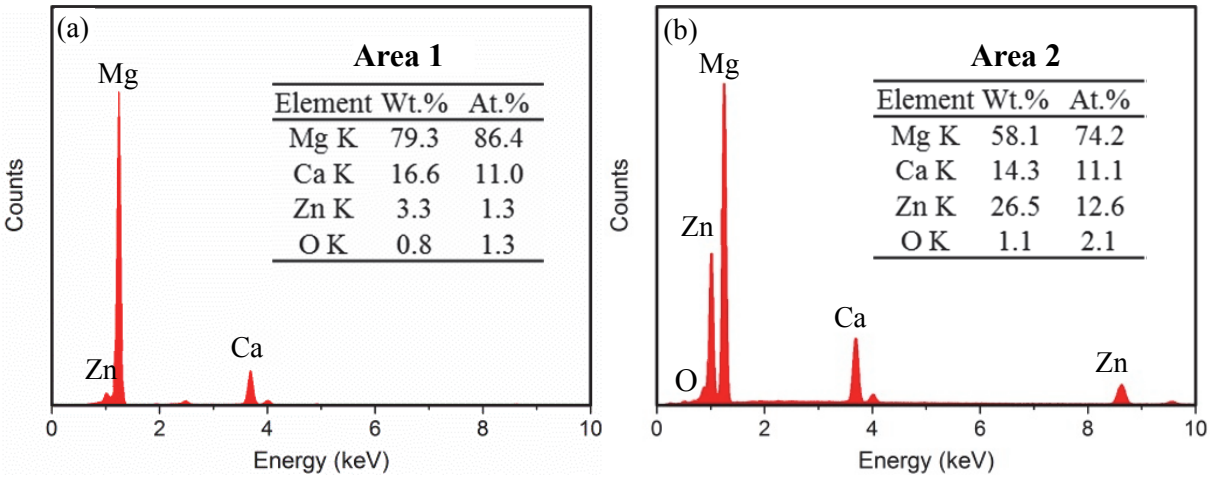

Fig. 5-42 EDX analysis of Mg-2Ca-xZn alloys, (a) area 1 (Mg_2Ca) in Fig. 5-41 (b); (b) area 2 ($Mg_6Ca_2Zn_3$) in Fig. 5-41 (h)

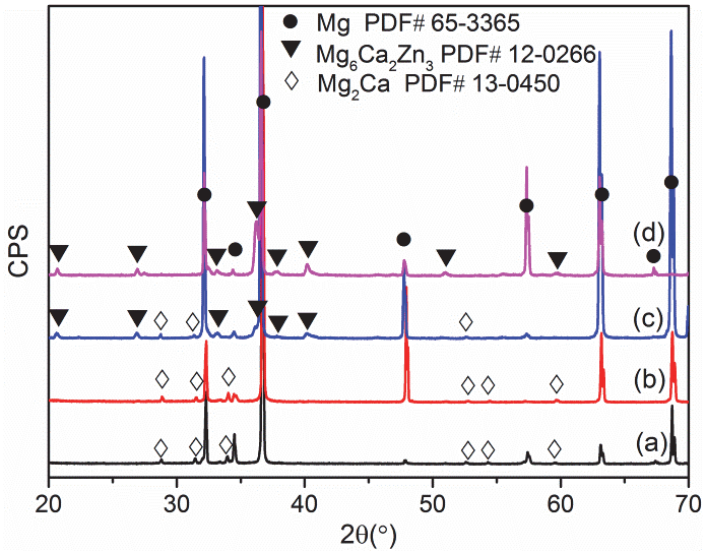

Fig. 5-43 XRD patterns of alloys cast at T_{mould} = 250 ^{0}C, (a) Mg-2Ca-0.5Zn, (b) Mg-2Ca-1.5Zn, (c) Mg-2Ca-4Zn, and (d) Mg-2Ca-6Zn

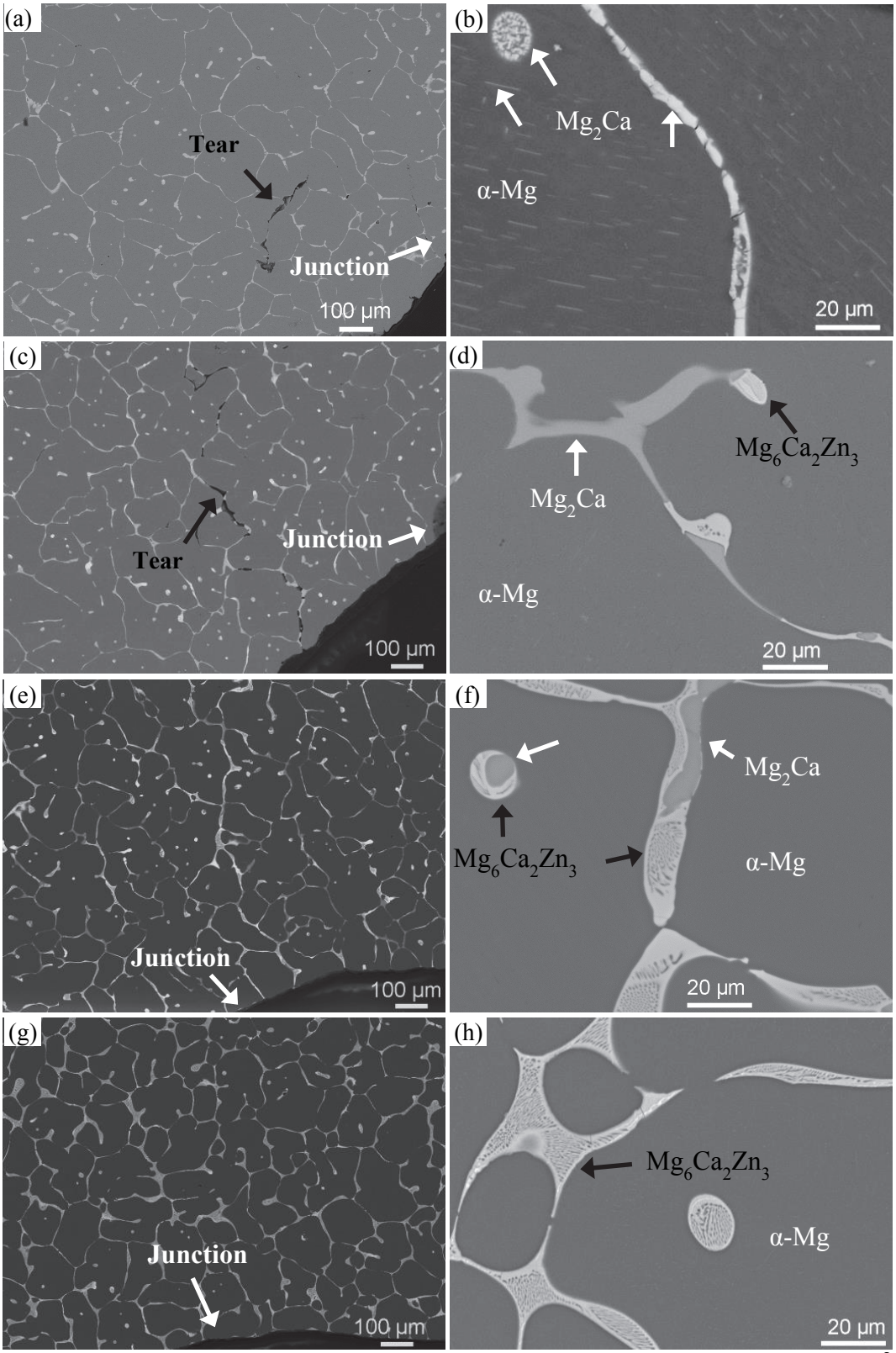

Fig. 5-44 Microstructures at the sprue-rod junctions of alloys cast at T_{mould} = 450 ^{0}C, (a) Mg-2Ca-0.5Zn; (b) Mg-2Ca-1.5Zn; (c) Mg-2Ca-4Zn; and (d) Mg-2Ca-6Zn. The phase indicated by the black arrows is $Mg_6Ca_2Zn_3$ and Mg_2Ca by the white arrows

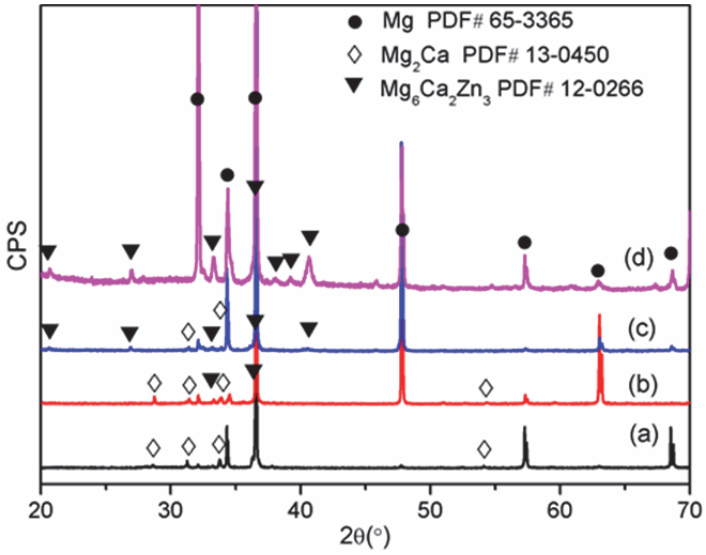

Fig. 5-45 XRD patterns of alloys cast at T_{mould} = 450 ^{0}C, (a) Mg-2Ca-0.5Zn, (b) Mg-2Ca-1.5Zn, (c) Mg-2Ca-4Zn, and (d) Mg-2Ca-6Zn

5.3.2.5 Eutectic distribution

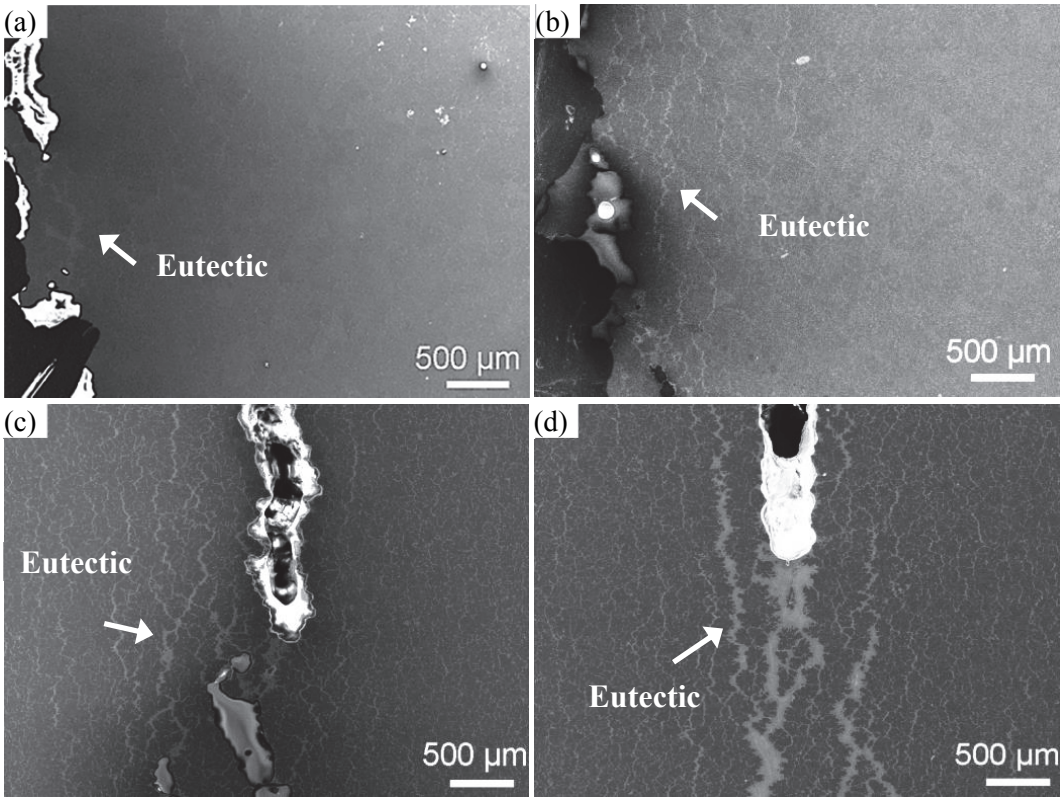

Fig. 5-46 Eutectic distribution at the hot spot for Mg-2Ca-xZn alloys cast at T_{mould} = 250 ^{0}C, (a) Mg-2Ca-0.5Zn, (b) Mg-2Ca-1.5Zn, (c) Mg-2Ca-4Zn, (d) Mg-2Ca-6Zn

As previously mentioned, the eutectic structure is evident only in the the Mg-2Ca-xZn alloys cast at T_{mould} = 250 ^{0}C. In order to further analyse its distribution, SEM was carried out near tear region and the resulting micrographs are shown in Fig. 5-46. As the microstructures of

Mg-2Ca-xZn alloys cast at T_{mould} = 450 ^{0}C are homogenous, only the microstructures of the alloys cast at T_{mould} = 250 ^{0}C are shown here. As proved previously, the river like structure with a slightly brighter colour than the matrix is confirmed as eutectic. Similar to the X-ray photographs, the eutectic in Mg-2Ca-0.5Zn and Mg-2Ca-1.5Zn alloys are not clearly visible in the SEM micrographs. Eutectic segregation is mainly found near the tears and its amount increases with increase in Zn content. The Mg-2Ca-6Zn alloy is seen to have a large amount of eutectic. The width of eutectic in front of the main crack tip is almost the same as the width of the tear.

5.3.2.6 Fracture surfaces

The observations of the fracture surfaces also help to understand the hot tearing behaviour of alloys. Typical hot tearing fracture surfaces are observed for Mg-2Ca-xZn alloys cast at T_{mould} = 250 ^{0}C (Fig. 5-47). Evidence of ruptured liquid films is seen in all the shown fracture surfaces, which clearly proves the fact that the liquid is present during tearing. Besides, dendrites are visible in all the fracture surfaces of Mg-2Ca-xZn alloys.

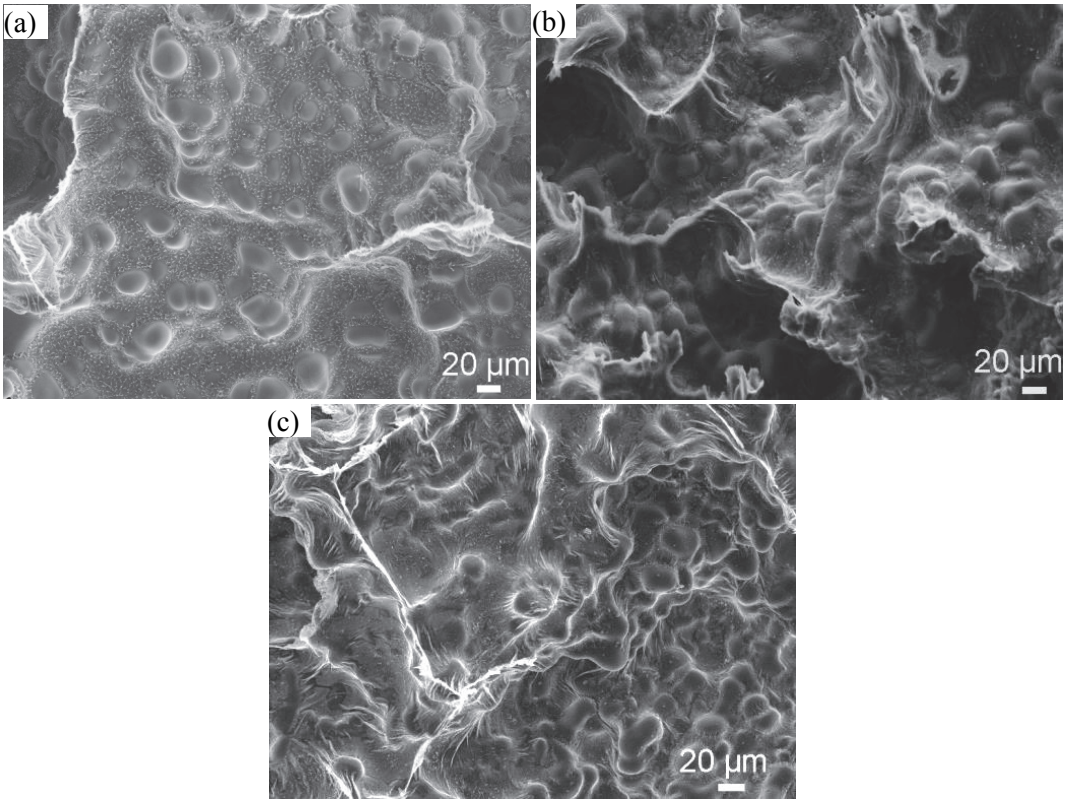

Fig. 5-47 Fracture surfaces of alloys cast at T_{mould} = 250 ^{0}C, (a) Mg-2Ca-0.5Zn, (b) Mg-2Ca-1.5Zn, and (c) Mg-2Ca-4Zn

5.3.2.7 Residual strain and residual stress at T_{mould} = 450 °C

Triaxial residual strains of Mg-2Ca-xZn alloys cast at T_{mould} = 450 ^{0}C are measured by neutron diffraction. The resulting residual strain properties for the (203) reflection are shown in Fig. 5-48. The position "0" along the X- axis represents the sprue-rod junction. It needs to be pointed out that all the fine tears of the tested alloys occurred at the sprue-rod junction, as shown in Fig. 5-37.

Four essential features can be observed for strain distribution profiles. Firstly, the residual strains vary significantly and have a large error bar (uncertainty) in Mg-2Ca-0.5Zn (Fig. 5-48 (a)) and Mg-2Ca-1.5Zn (Fig. 5-48 (b)). On the contrary, the residual strains seem stable in the Mg-2Ca-4Zn and Mg-2Ca-6Zn alloys. As a result, the following discussion will mainly focus on the Mg-2Ca-4Zn and Mg-2Ca-6Zn alloys. Secondly, a higher magnitude of residual strain was seen at the sprue portion (position below 0), while a lower magnitude was observed at the rod portion (position above 0). Thirdly, the magnitude of residual strain on the sprue part is higher that on the rod part in both Mg-2Ca-4Zn and Mg-2Ca-6Zn alloys. Fourthly, a strain relief in the radial direction near the junction was observed for the Mg-2Ca-4Zn alloy. No such strain relief in the radial direction was observed for the Mg-2Ca-6Zn alloy, as the radial strain remained tensile from -12 mm to 0 mm.

The calculated triaxial residual stresses for the (203) and (211) reflections of Mg-2Ca-4Zn and Mg-2Ca-6Zn alloys are displayed in Fig. 5-49. In both alloys, the triaxial residual stresses for the (203) reflections were mainly compressive while for the (211) reflections the stresses were tensile. All the residual stresses were in the range of -80 MPa to 60 MPa.

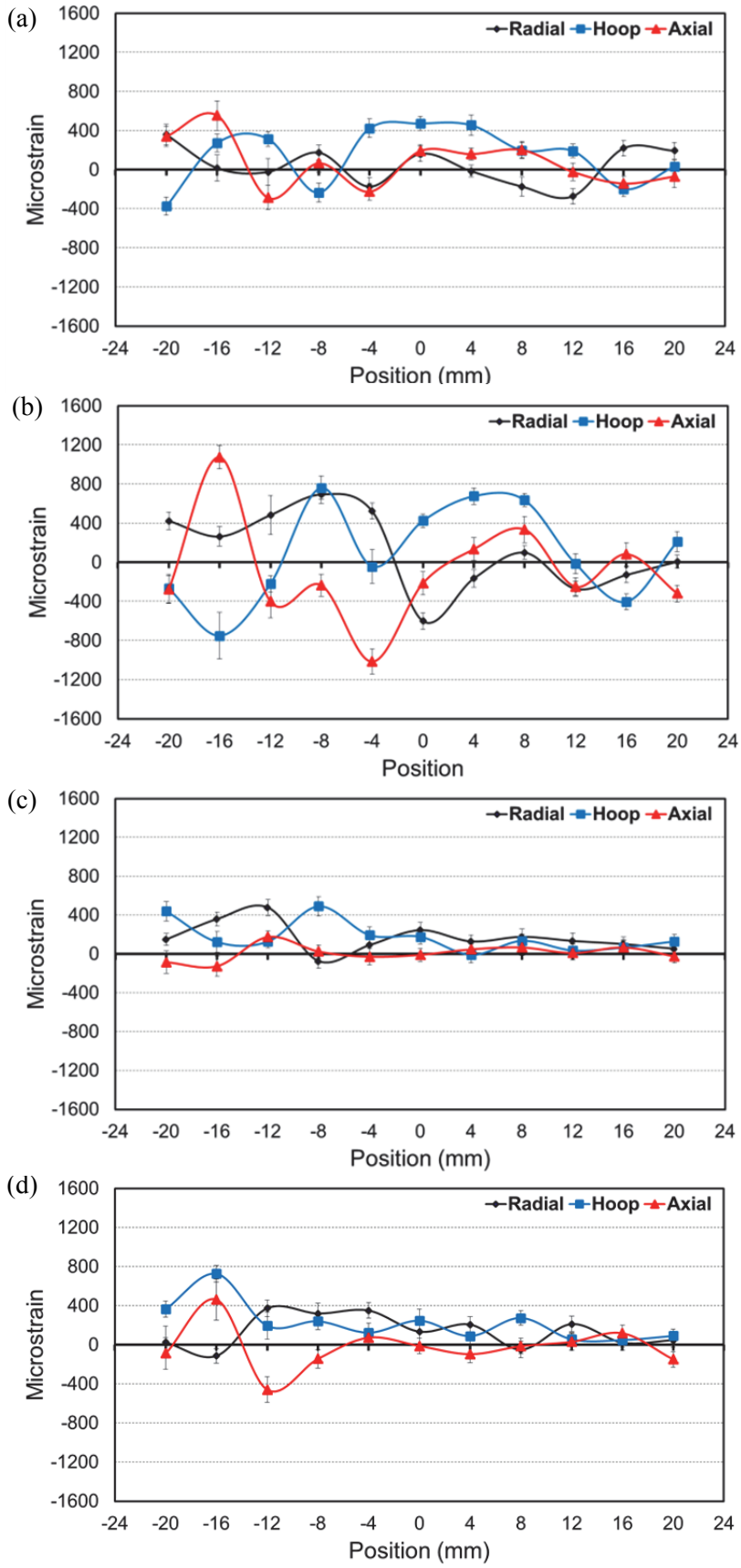

Fig. 5-48 Residual strain distributions of alloys cast at T_{mould} = 450 ^{0}C for the (203) refelection, (a) Mg-2Ca-0.5Zn, (b) Mg-2Ca-1.5Zn, (c) Mg-2Ca-4Zn, and (d) Mg-2Ca-6Zn

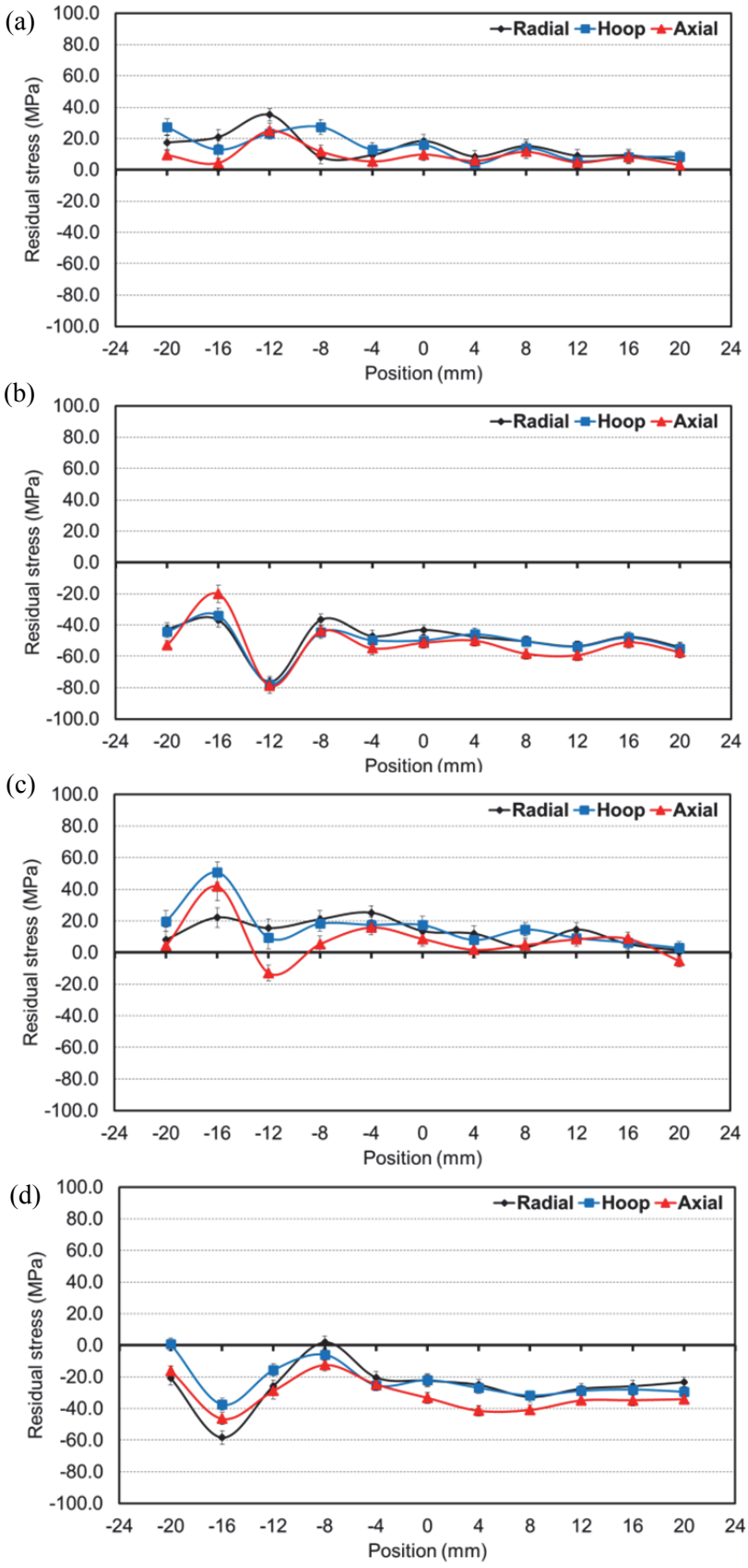

Fig. 5-49 Residual stress distributions of alloys cast at T_{mould} = 450 ^{0}C of Mg-2Ca-4Zn alloy, (a) (203) refelection, (b) (211) refelection, and Mg-2Ca-6Zn alloy, (c) (203) refelection, (d) (211) refelection.

5.4 Hot tearing of Mg-xCa-4Zn ternary alloy

5.4.1 Chemical composition

Table 5-7 show the chemical compositions of Mg-0.2Ca-4Zn and Mg-1Ca-4Zn alloys cast at T_{mould} = 250 ^{0}C. The actual compositions are similar to the nominal composition.

Table 5-7 Chemical compositions of Mg-xCa-4Zn alloys at T_{mould} = 250 ^{0}C, in wt.%

Alloy	Ca	Zn	Fe	Mn	Si	Mg
Mg-0.2Ca-4Zn	0.17	3.96	0.00544	0.0361	0.0147	Bal.
Mg-1Ca-4Zn	0.84	4.16	0.00616	0.0410	0.0162	Bal.

5.4.2 Experimental hot tearing tendency

5.4.2.1 Force-temperature-time curves

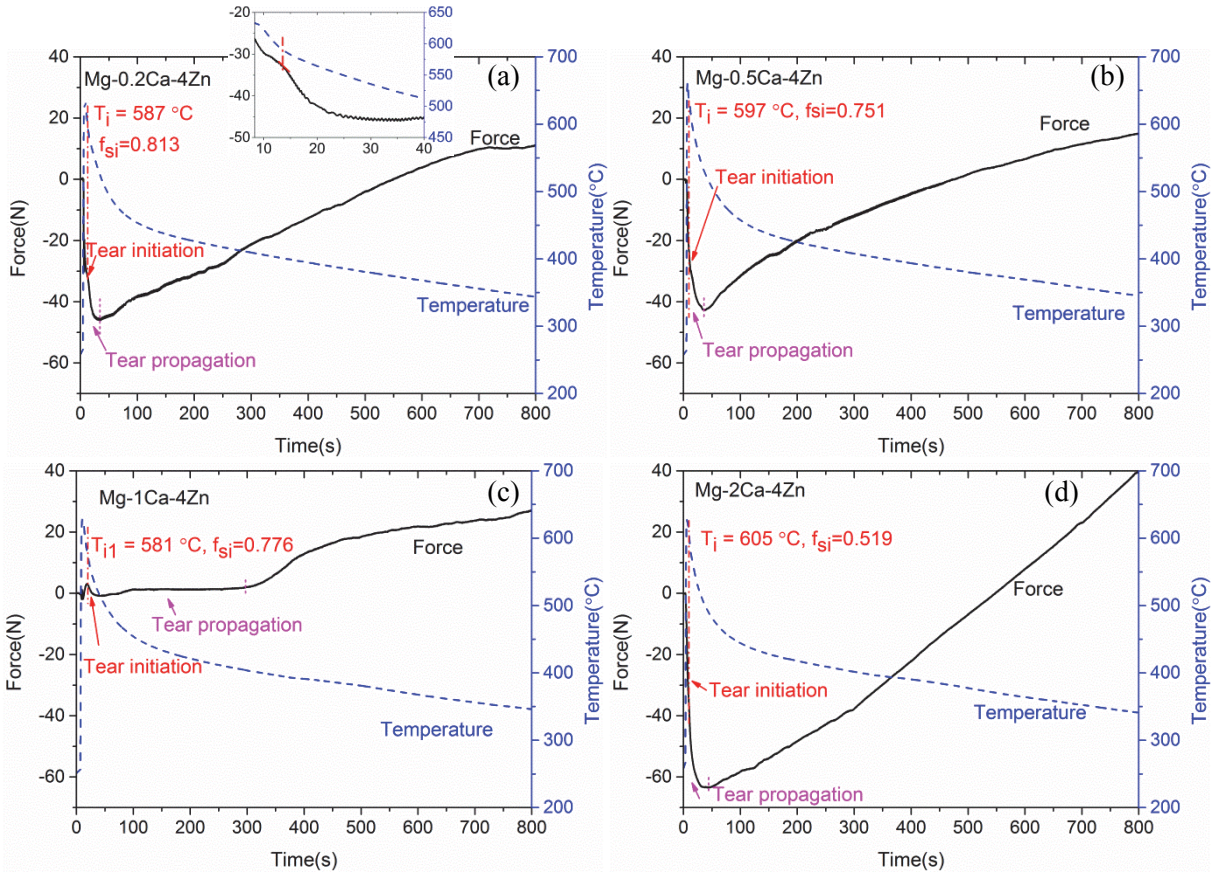

Fig. 5-50 Force-temperature-time curves of Mg-xCa-4Zn alloys cast at T_{mould} = 250 ^{0}C, (a) Mg-0.2Ca-4Zn, (b) Mg-0.5Ca-4Zn, (c) Mg-1Ca-4Zn, and (d) Mg-2Ca-4Zn

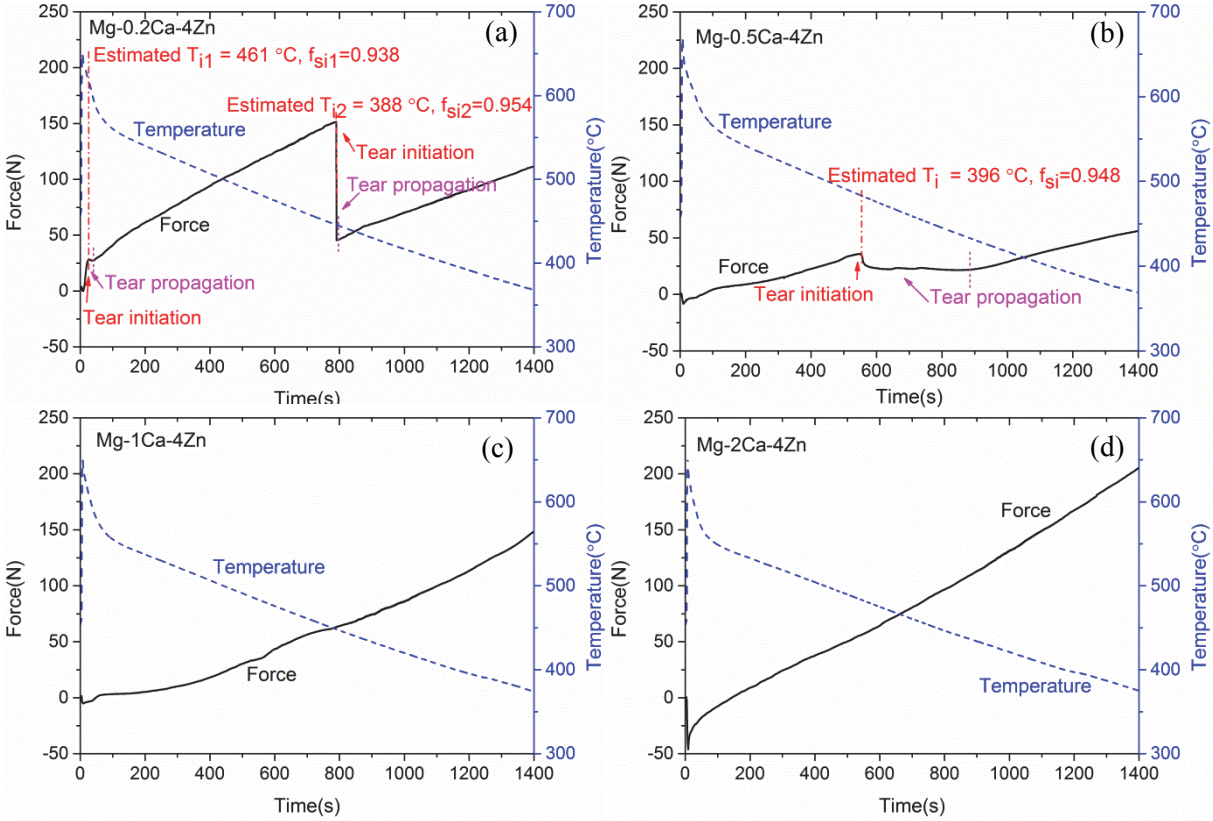

Fig. 5-51 Force-temperature-time curves of Mg-xCa-4Zn alloys cast at T_{mould} = 450 ^{0}C, (a) Mg-0.2Ca-4Zn, (b) Mg-0.5Ca-4Zn, (c) Mg-1Ca-4Zn, and (d) Mg-2Ca-4Zn

Force-temperature-time curves of Mg-xCa-4Zn alloys cast at both mould temperatures are shown in Fig. 5-50 and Fig. 5-51. The tear initiation and propagation information are marked on the figures. Similar to the other ternary Mg-Ca-Zn alloys, the f_{si} is not high for Mg-xCa-4Zn alloys cast at T_{mould} = 250 ^{0}C. As the initial mould temperature increased to 450 ^{0}C, the tears of Mg-0.2Ca-4Zn and Mg-0.5Ca-4Zn alloys occurred near the load screw, thus the T_i and f_{si} of these two alloys were estimated using the method mentioned in section 5.1.2.7. No typical force drop nor force increment change was observed for Mg-1Ca-4Zn and Mg-2Ca-4Zn, indicating that no hot tearing occurred.

5.4.2.2 Macro observation

Fig. 5-52 displays macro images of the hot tears in the Mg-xCa-4Zn alloys cast at both mould temperatures. The influence of Ca content on the hot tearing of Mg-Ca-Zn alloys can be seen clearly at the mould temperature of 250^{0}C. As the Ca content increases the HTS of Mg-Ca-Zn alloy increases up to 0.5% Ca and then decreases. The peak severity occurs at 0.5% Ca content as the rod portions of the Mg-0.5Ca-4Zn castings are completely broken. In addition, the tear location has moved away from the exact sprue-rod junction to the rod part at a high Ca content. Similarly, the tearing also occurred away from the junction for the Mg-0.5Ca-xZn

and Mg-2Ca-xZn alloys. This may explain why the predicted f_{si} using the force-temperature-time curves is low. No visible tears are observed for Mg-1Ca-4Zn and Mg-2Ca-4Zn alloys when the mould temperature increased to 450 ^{0}C, confirming that increasing the initial mould temperature effectively enhances the resistance to hot tearing. However, hot tears of Mg-0.2Ca-4Zn and Mg-0.5Ca-4Zn appeared near the load screw on the rod portion.

Mould temperatures	Mg-0.2Ca-4Zn	Mg-0.5Ca-4Zn	Mg-1Ca-4Zn	Mg-2Ca-4Zn
250 °C		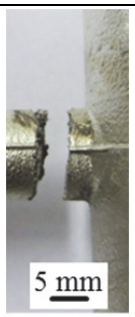	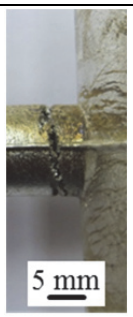	
450 °C	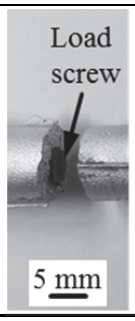	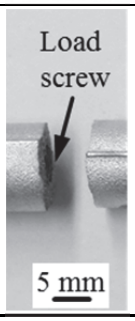		

Fig. 5-52 Macro observations of the hot tears of Mg-xCa-4Zn alloys cast at T_{mould} = 250 ^{0}C and T_{mould} = 450 ^{0}C

5.4.2.3 X-ray tomography

X-ray tomography photographs taken at the longitudinal cross section (mid plane section) of Mg-xCa-4Zn alloys cast at T_{mould}=250 ^{0}C and T_{mould}= 450 ^{0}C are shown in Fig. 5-53 and Fig. 5-54, respectively. There are a few white areas (marked with white arrows) near the tear locations in Mg-1Ca-4Zn and Mg-2Ca-4Zn alloys at T_{mould}= 250 ^{0}C. These white areas are eutectic, as verified previously. Only fine tears are evident at the sprue-rod junction in Mg-1Ca-4Zn and Mg-2Ca-4Zn alloys at T_{mould}= 450 ^{0}C. Interestingly, the microstructures are homogeneous in all the alloys cast at the high mould temperature 450 °C, as no eutectic segregation is observed around the sprue-rod junction area.

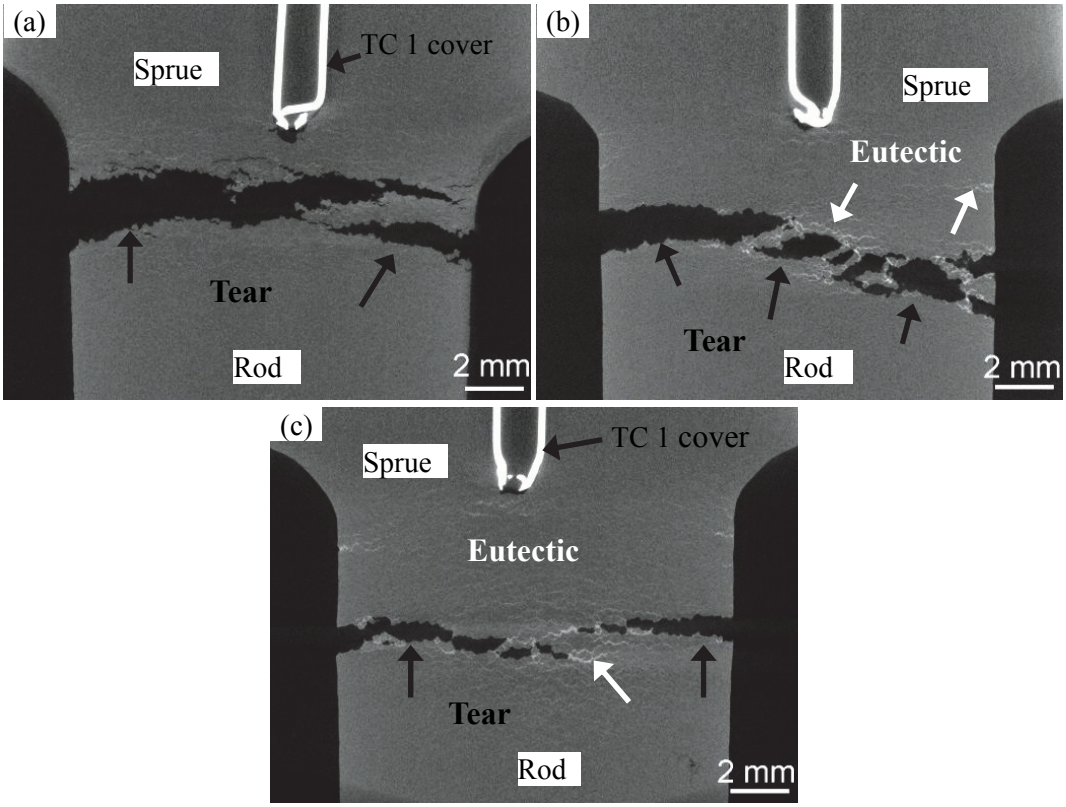

Fig. 5-53 X-ray tomography photographs of the Mg-xCa-4Zn alloys cast at T_{mould}=250 ^{0}C, (a) Mg-0.2Ca-4Zn, (b) Mg-1Ca-4Zn, and (c) Mg-2Ca-4Zn

The measured crack volumes of Mg-xCa-4Zn alloys are given in Fig. 5-55. For those alloys with a completely broken tear, the crack volume is displayed with dashed columns. As can be seen from both pictures and crack volumes, HTS at T_{mould} = 250 ^{0}C increases with Ca content, reaches a maximum at Mg-0.5Ca-4Zn, and then decreases with further Ca addition.

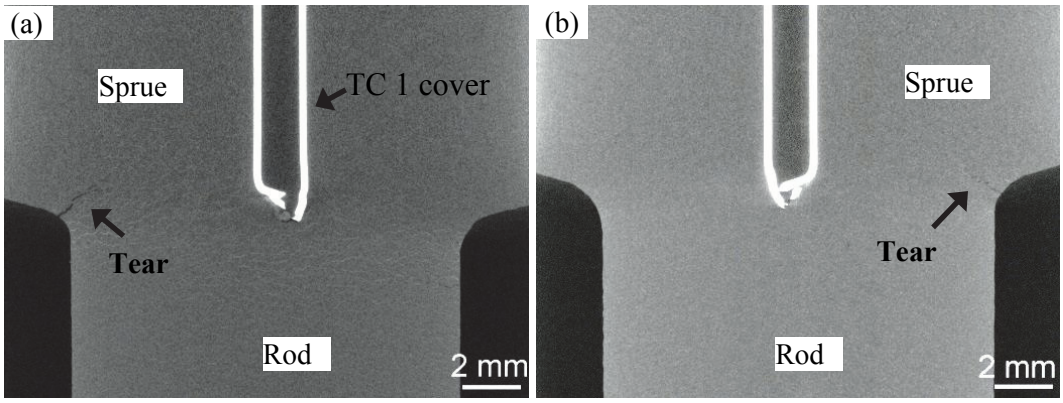

Fig. 5-54 X-ray tomography photographs of the Mg-xCa-4Zn alloys cast at T_{mould} = 450 ^{0}C, (a) Mg-1Ca-4Zn, and (b) Mg-2Ca-4Zn

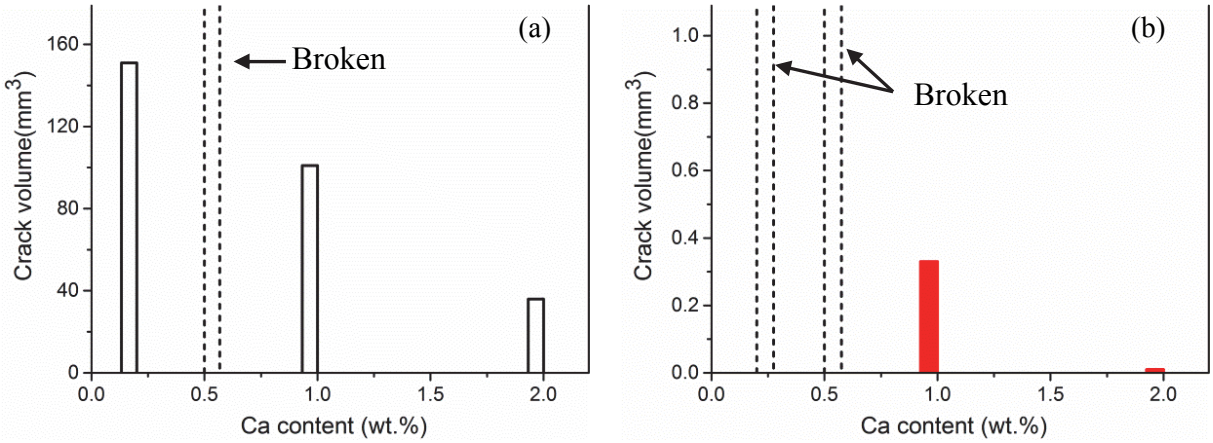

Fig. 5-55 Crack volumes of Mg-xCa-4Znalloys cast at different mould temperature, (a) T_{mould} = 250 ^{0}C and (b) T_{mould} = 450 ^{0}C

5.4.2.4 Micro observation

Polarized optical tear morphologies at the hot spot of Mg-xCa-4Zn alloys at both mould temperatures are shown in Fig. 5-56 and Fig. 5-57. It is obvious that all the tears, including the tears near the load screw, propagate along the grain boundaries. It is worth noting that the grain sizes of Mg-xCa-4Zn alloys decreases with increasing Ca content. However, the grain refinement at the hot spot is not significant.

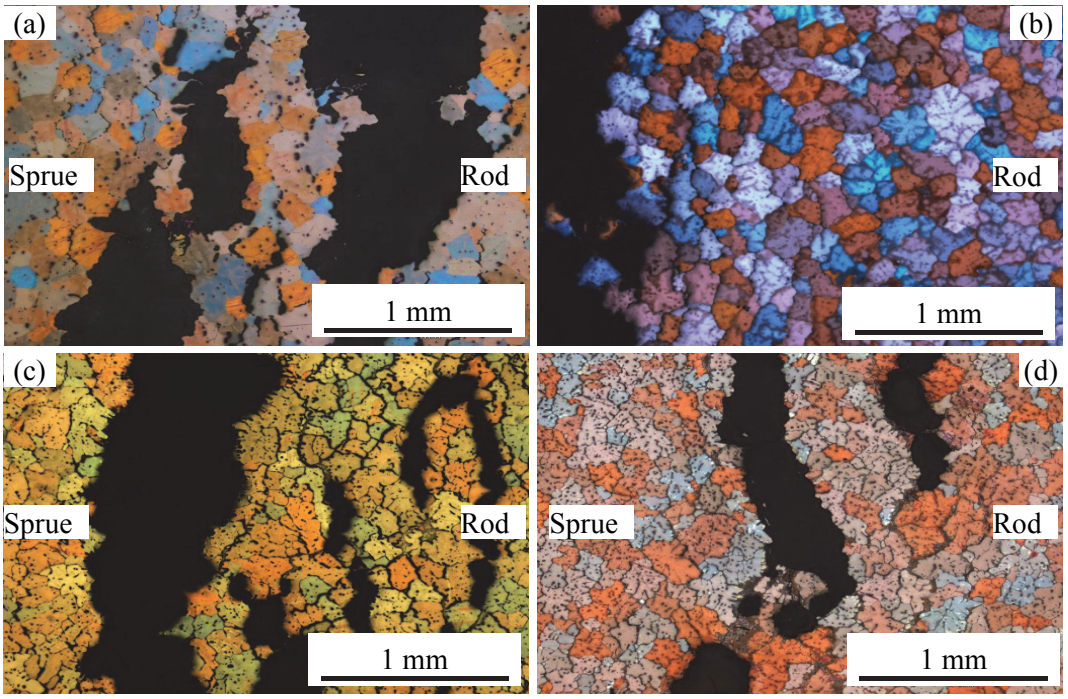

Fig. 5-56 Optical microstructures of tears for the Mg-xCa-4Zn alloys cast at T_{mould} = 250 ^{0}C, (a) Mg-0.2Ca-4Zn, (b) Mg-0.5Ca-4Zn, (c) Mg-1Ca-4Zn, and (d) Mg-2Ca-4Zn

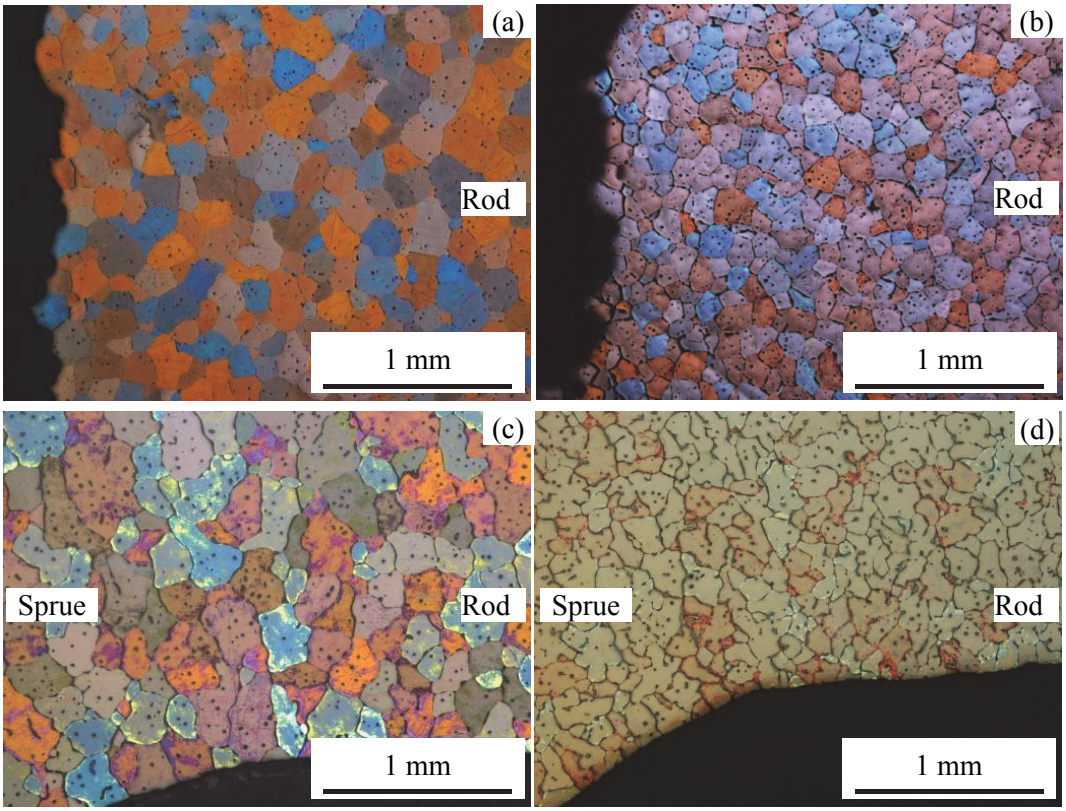

Fig. 5-57 Optical microstructures of tears for the Mg-xCa-4Zn alloys cast at T_{mould} = 450 ^{0}C, (a) Mg-0.2Ca-4Zn, (b) Mg-0.5Ca-4Zn, (c) Mg-1Ca-4Zn, and (d) Mg-2Ca-4Zn

Microstructures near the main tear region of the Mg-xCa-4Zn alloys cast at T_{mould} = 250 °C are shown in Fig. 5-58. Large eutectic structures are evident in high Ca containing alloys, such as Mg-1Ca-4Zn and Mg-2Ca-4Zn. The Mg-2Ca-4Zn alloy displays more eutectic than the Mg-1Ca-4Zn alloy. $Mg_6Ca_2Zn_3$ is the main second phase for all the Mg-xCa-4Zn alloys, while a small amount of MgZn is evident in Mg-0.2Ca-4Zn and Mg_2Ca is observed in Mg-2Ca-4Zn alloy.

Microstructures near the main tear region of Mg-xCa-4Zn alloys cast at T_{mould} = 450 °C are shown Fig. 5-59. No eutectic is observed near the tear region of Mg-0.2Ca-4Zn alloy. In addition, no eutectic segregation is found at the sprue-rod junction in Mg-1Ca-4Zn and Mg-2Ca-4Zn alloys at the high initial mould temperature.

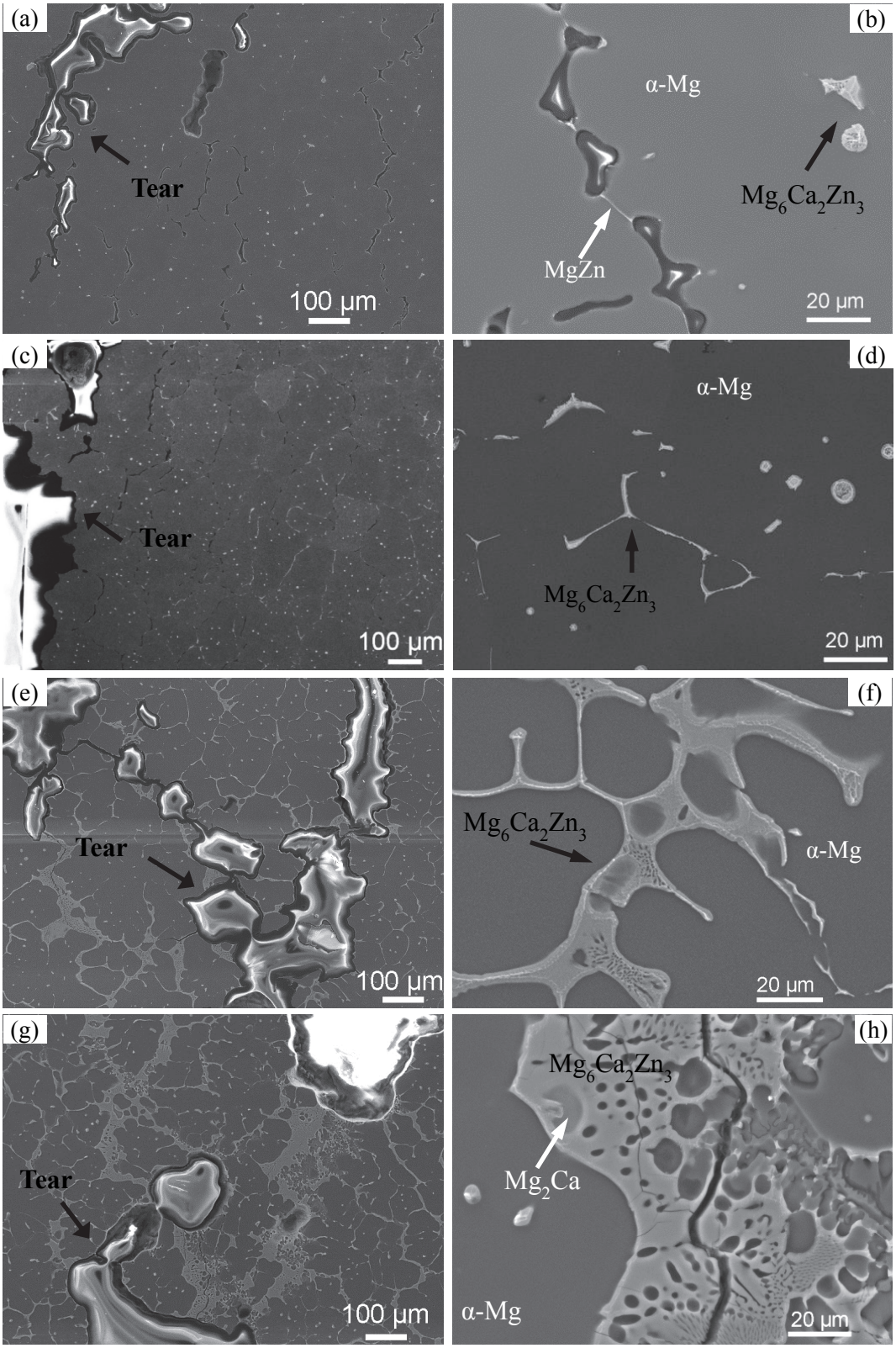

Fig. 5-58 Microstructures near the tear regions of Mg-xCa-4Zn alloys cast at T_{mould} = 250 °C, (a), (b) Mg-0.2Ca-4Zn, (c), (d) Mg-0.5Ca-4Zn, (e), (f) Mg-1Ca-4Zn, and (g), (h) Mg-2Ca-4Zn

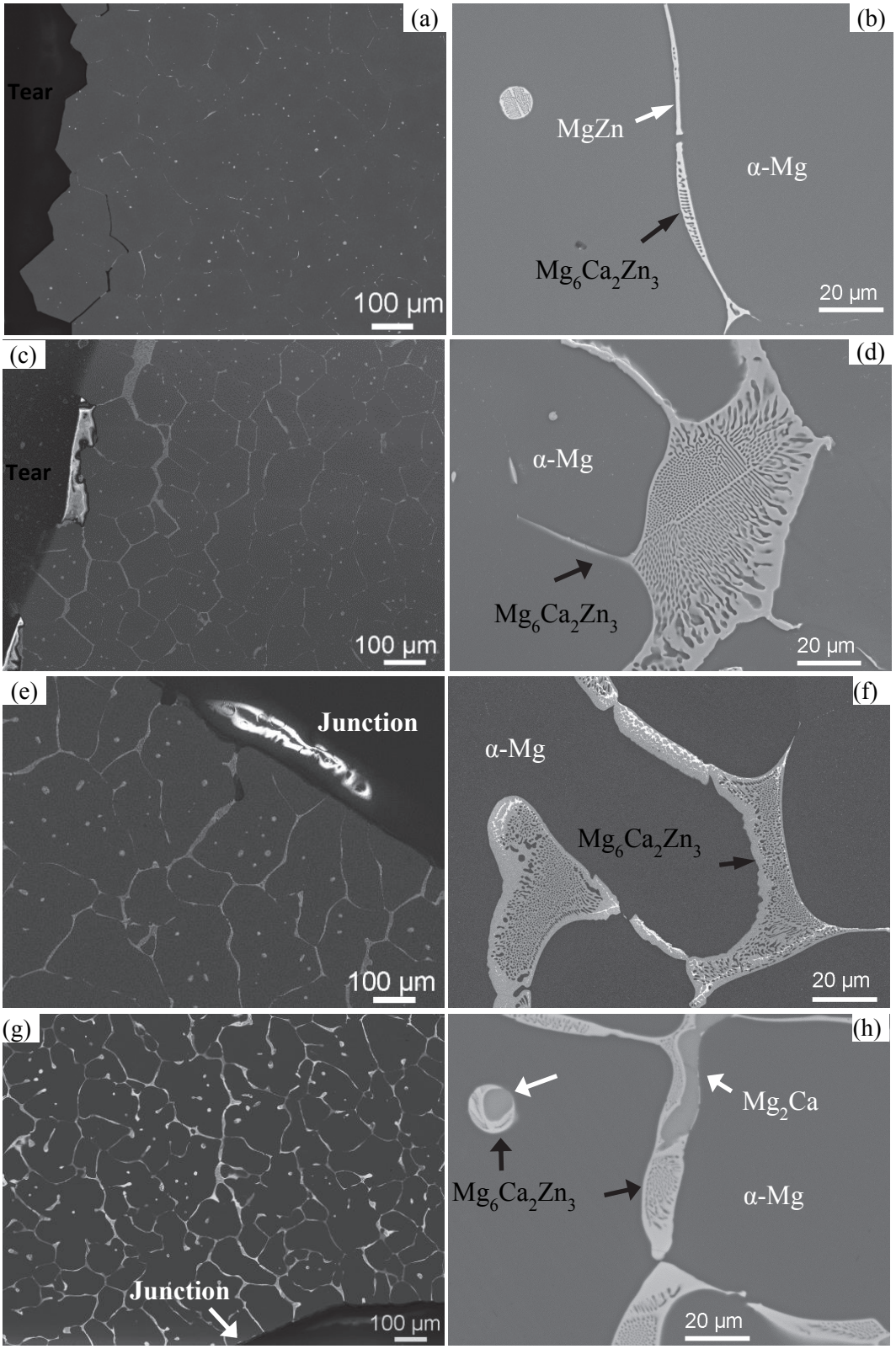

Fig. 5-59 SEM microstructures of tears for the alloys cast at T_{mould} = 450 ^{0}C, (a) Mg-0.2Ca-4Zn, (b) Mg-0.5Ca-4Zn, (c) Mg-1Ca-4Zn, and (d) Mg-2Ca-4Zn

5.4.2.5 Fracture surfaces

Fracture surfaces of Mg-xCa-4Zn alloys cast at T_{mould} = 250 ^{0}C are shown in Fig. 5-60. The fracture surfaces are similar to other fracture surfaces those of Mg-0.5Ca-xZn and Mg-2Ca-xZn alloys. The surfaces consist of ruptured liquid film, dendritic grain and precipitates. The presence of ruptured liquid film confirms that they are hot tears.

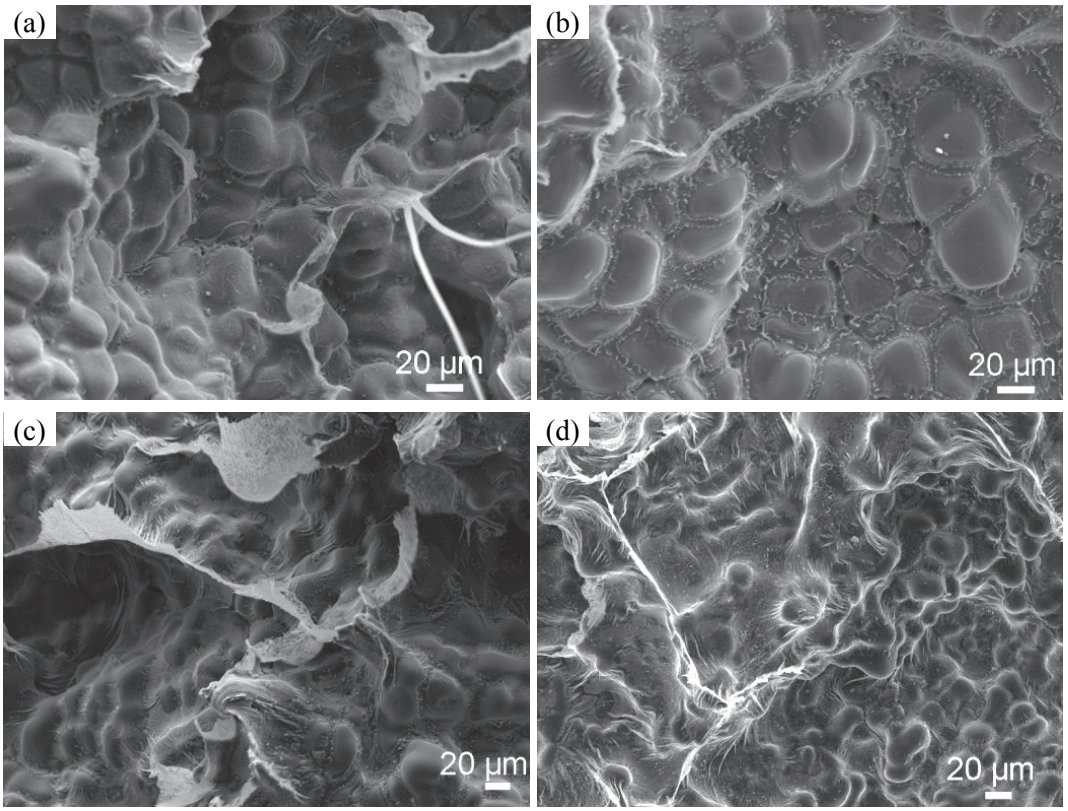

Fig. 5-60 Fracture surfaces of alloys cast at T_{mould} = 250 ^{0}C, (a) Mg-0.2Ca-4Zn, (b) Mg-0.5Ca-4Zn, (c) Mg-1Ca-4Zn, and Mg-2Ca-4Zn

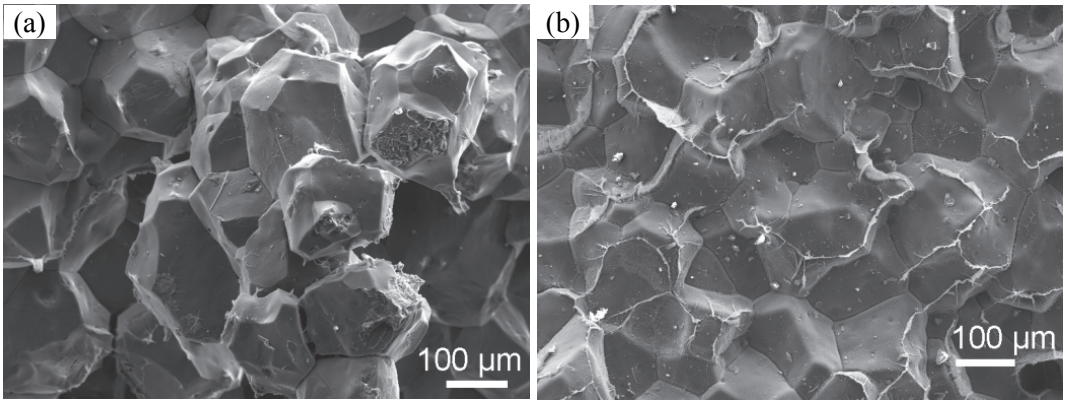

Fig. 5-61 Fracture surfaces of alloys cast at T_{mould} = 450 ^{0}C, (a) Mg-0.2Ca-4Zn, and (b) Mg-0.5Ca-4Zn

Fracture surfaces of Mg-0.2Ca-4Zn and Mg-0.5Ca-4Zn alloys cast at T_{mould} = 450 ^{o}C is shown in Fig. 5-61. As described previously in section 5.2.2.5, the fracture surface of the

Mg-0.5Ca-4Zn alloy contains no dendrties and looks like cleavage surface. It is found that the Mg-0.2Ca-4Zn alloy shows the similar fracture surface. It needs to be pointed out that the tears in both Mg-0.2Ca-4Zn and Mg-0.5Ca-4Zn alloys appear near the load screw. Therefore, the cracks near the load screw are likely “cold cracks” with some microtears intiated above the solidus temperature.

6 Discussion

6.1 Hot tearing behaviour of Mg-Ca binary alloys

6.1.1 Comparison with thermodynamic prediction

Among all the criteria listed in the literature review, T. W. Clyne and G. J. Davies' model was chosen to predict the HTS of Mg-xCa alloys. Clyne and Davies [40] suggested that hot tearing occurs near the end of solidification when the solid fraction is between 0.90 and 0.99. Prediction of hot tearing susceptibility (HTS) based on this solid fraction range has been successfully used for many alloys, such as Al-Mg, Al-Zn, Al-Si, Mg-Y, and Mg-Zn [18, 19, 40]. Therefore, Clyne and Davies' model was chosen to predict the compositional dependence on HTS in Mg-Ca alloys.

In order to calculate the crack susceptibility coefficient (CSC), it is necessary to obtain the solid fraction as a function of time during solidification. The thermodynamic calculations in this research were carried out using Pandat software including PanEngine module based on thermodynamic database PanMg 8.0. The solidification path was calculated using Scheil model. Detailed description about the thermodynamic calculations for the prediction of hot tear using the above model can also be found elsewhere [19].

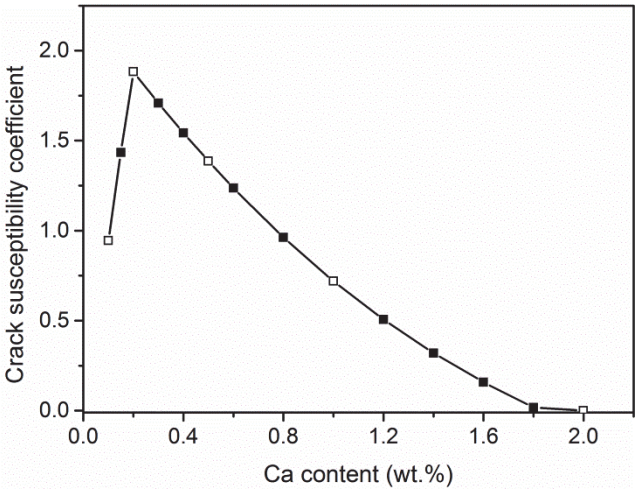

Fig. 6-1 Predicted crack susceptibility coefficient of Mg-Ca alloys from Clyne and Davis' model. The data points with open bullets correspond to the compositions of the investigated alloys.

From the thermodynamic calculations point of view, CSC is an indicator to evaluate HTS. While in the experiments, the parameter ''crack volume'' was selected as an indicator to

evaluate the HTS. Both of them are practically useful to evaluate the impact of composition of primary alloying element on the hot tearing susceptibility of alloys. CSC of Mg-Y and Mg-Zn alloys predicted from thermodynamic calculations were found to be in good agreement with that their corresponding HTS derived from the crack volume obtained from the experiment [18, 19]. Hence, in the present study, Clyne and Davies' thermodynamic model was used to predict the compositional dependence on hot tearing of Mg-Ca alloys and presented in Fig. 6-1.

Similar to the crack volume curve (Fig. 5-7) the predicted CSC (Fig. 6-1) curve also show that the HTS of Mg-Ca alloys changes with Ca content and follows "Λ" shape (HTS firstly increases with increasing the content of solutes and then decreases with further increasing the content). However, in the investigated composition range, there is a discrepancy in the peak susceptibility between them. As shown in Fig. 6-1, the predicted maximum hot tearing susceptibility of Mg-Ca alloys occurs at 0.2 wt. % Ca. The experimental results indicated that both Mg-0.5Ca and Mg-1Ca alloys had a higher HTS than Mg-0.2Ca alloy (Fig. 5-3). Thus, the Ca content for the peak susceptibility differed between prediction and experimental results.

The inconsistency of peak susceptibility is caused by the limitations of the Clyne and Davis' model in three ways. Firstly, in their model, the definition of vulnerable period during which the hot tearing occurs was not defined accurately. They defined this period ($0.9 < fs < 0.99$) only based on the previous experimental results. Recent experimental evidence has shown that, the hot tearing may initiate with a solid fraction less than 0.9 [18, 68]. In the present study, hot tearing also occurred at a solid fraction lower than 0.9, in Mg-0.5Ca, Mg-1Ca and Mg-2Ca alloys (Fig. 5-1). In a simplified version of the Clyne and Davies' CSC model, the upper limit of fs was set as 0.98 instead of 0.99 [22, 107]. Because at $fs \geq 0.98$ the structure develops considerable strength and solid-state creep can compensate the strain caused by thermal contraction [7]. Secondly, the Clyne and Davies' model uses a fixed equation to estimate the cooling rate which was simplified based on the situation of heat flow [40]. They did not incorporate the influence of mold temperature in their equation. Thirdly, their calculation of HTS was only based on the thermodynamics. They did not consider the influences of microstructures and materials properties on HTS. In fact, both the initiation and propagation of hot tearing depend not only on the microstructures but also on the semi-solid mechanical properties of investigated alloys.

Similar inconsistency of peak susceptibility between prediction and experiments are also evidenced in Mg-Al and Mg-Y alloys [17, 19]. For instance, the predicted CSC peak occurs at 1.5 wt.% Y, while the experimental ‘‘crack volume’’ peak observed at 0.9 wt. % Y in the binary Mg-Y alloys [19]. Wang et al. [19] suggested that as the vulnerable temperature intervals for both Mg-1.5Y and Mg-0.9Y alloys are close, their CSC values are also close. Moreover, the microstructural observations in their study demonstrated that Mg-0.9Y exhibited a coarser grain size compared to that of Mg-1.5Y alloy. Therefore, this grain refinement was suggested as the reason for the low HTS observed for Mg-1.5Y alloy in the experiments.

However, the inconsistency of peak susceptibility between prediction and experiments of Mg-Ca alloys in the present study was not due to grain refinement, as Mg-0.5Ca (323 ± 291 μm) and Mg-1Ca (172 ± 83 μm) alloys had grain sizes smaller than that of Mg-0.2Ca (1206 ± 1222 μm) alloy, as shown in Fig. 5-8. Besides, the columnar grain morphology in Mg-0.2Ca alloy should result in a higher HTS than the equiaxed grain morphology in Mg-0.5Ca and Mg-1Ca alloys [108]. It may be expected that brittle intermetallic in Mg-Ca alloys played an important role in influencing the HTS peak susceptibility inconsistency. Recently, the influence of type and morphology of eutectic on the hot tearing response of Al-Mg-Si-Fe alloys was reported [109]. The influence of brittle intermetallic on HTS for Mg-Ca alloys will be discussed in more detail in the following sections.

6.1.2 Effect of Ca on HTS of Mg-Ca binary alloys

Effect of alloy composition on HTS for binary Mg alloys has been extensively studied [18-20, 68]. As like previous studies, the present results also demonstrate that the effect of primary alloying composition on HTS follows the so called “Λ” shape. Generally, the HTS of alloys is affected by alloying composition in the following ways: susceptible freezing range (ΔT_s, temperature range of a solid fraction between 0.9 and 0.99), amount of eutectic liquid (f_e, eutectic liquid at eutectic temperature), and amount of intermetallic (f_i, such as Mg_2Ca). All these parameters for the binary Mg-Ca alloys are listed in Table 6-1.

In general, a large susceptible freezing range (vulnerable intervals) leads to severe hot tearing owing to the fact that the alloy spend longer time in the vulnerable region during solidification [19]. The susceptible temperature range ΔT_s (Table 6-1) reaches a maximum at 0.2 wt.% Ca, and decreases with further Ca addition. Consequently, the HTS calculated based on the ΔT_s also follows the “Λ” shape. Based on the values of ΔT_s, Mg-0.2Ca alloy should have the highest HTS whereas Mg-2Ca alloy should have no or minimal hot tearing.

Table 6-1 Susceptible freezing range, eutectic liquid fraction, and intermetallic fraction of Mg-Ca alloys

	Mg-0.1Ca	Mg-0.2Ca	Mg-0.5Ca	Mg-1Ca	Mg-2Ca
ΔT_s (°C)	55.7	123	105	69.7	0
f_e	0.0052	0.011	0.027	0.054	0.110
f_i	0.0016	0.0032	0.0082	0.0167	0.0339

The amount of eutectic liquid is also regarded as one of the most important factors to influencing hot tearing. The eutectic liquid of Mg-Ca alloys continuously increases with increasing Ca content. Generally, the fluidity of the melt increases with the amount of low melting point eutectic liquid [19]. Such high fluidity facilitates tear healing, which results in an improved hot tearing resistance. In other words, Mg-Ca alloys with a high amount of eutectic liquid such as Mg-2Ca alloy should have a low HTS.

The amount of intermetallic is another important parameter affecting the HTS of Mg-Ca alloys. In the non-equilibrium solidification process, intermetallic may form at some region due to the local segregation of solutes while the rest of the melt is still in the semi-solid state. These intermetallics may act as nuclei for hot tearing initiation near the solidus [19]. The effect of intermetallic (Mg_2Ca) on HTS for Mg-Ca alloys may be more obvious than that for other binary Mg alloys, because Mg_2Ca is highly brittle in nature. This brittle intermetallic (Mg_2Ca) leads to an extremely poor ductility for Mg-Ca alloys. The elongation of Mg-Ca alloys decreases dramatically with increasing the Ca content in both as-cast and extruded conditions [76, 83, 110]. Mg-Ca alloys show a zero elongation with a Ca content higher than 2 wt.% in as-cast condition [111]. It might be argued that the poor ductility at room temperature is not directly related to the hot tearing behavior that occurs above the solidus temperature. However, high strength aluminum alloys susceptible to cold cracking due to their low ductility and fracture toughness, are also found to prone to hot tearing [112]. Therefore, Mg-Ca alloys with a poor ductility (more intermetallic) are more prone to hot tearing than alloys with a better ductility. Moreover, addition of Ca increases the die sticking problems of Mg alloys [74]. In the present study, it is severe die sticking problem was encountered with high Ca containing Mg-Ca alloys during casting. The die sticking is likely to act as a restraint and result in high HTS. The high HTS of Mg-0.5Ca and Mg-1Ca might be due to the poor ductility and high die sticking tendency. Actually, the real Ca content was much higher than

the nominal Ca content at the hot spot (at which the tear occurs) where the amount of eutectic was found to be high (Fig. 5-10 (f)). Consequently, the hot spot area was more "brittle" than expected (the normal nominal content) due to the large amount of intermetallic. A high amount of eutectic (Fig. 5-5 (c)) distributed mainly at the junction area (hot spot). However, a straightforward correlation of any of these discussed parameters to hot tearing behavior of an alloy is not possible as it is a complex phenomenon.

Based on the above discussions, the discrepancy between CSC prediction and experimental HTS ("crack volume") can be further clarified. Mg-0.2Ca alloy exhibits the largest ΔT_s and hence, highest CSC value, however, it contained a small amount of brittle intermetallic. Therefore, Mg-0.2Ca alloy showed lower HTS than Mg-0.5Ca and Mg-1Ca alloys. On the other hand, Mg-2Ca alloy showed a relatively large crack volume (Fig. 5-7) despite that ΔT_s for Mg-2Ca is zero and predicted CSC being minimum. The possible reason for this discrepancy was the presence of a high content of brittle intermetallic (Mg_2Ca) that might have influenced the final crack volume.

6.1.3 Tearing in the middle of the rod at T_{mould} = 450 ^{0}C

Occasionally, tearing occurred in the middle of the rod in Mg-0.5Ca and Mg-1Ca alloys cast at T_{mould} = 450 ^{0}C (Fig. 5-12). However, as mentioned earlier, the "middle tearing" behaviour is not evident in other Mg-Ca alloys cast at T_{mould} = 450 ^{0}C nor in alloys (including Mg-0.5Ca and Mg-1Ca) cast at T_{mould} = 250 ^{0}C.

It is proposed that the "middle tearing" behaviour is due to the defects, such as oxide inclusions and randomly distributed microcracks. Tears at sprue -rod junction did not display the presence of MgO inclusions. Thus, tears at the middle were likely due to the agglomeration of MgO inclusions, which nucleated hot tearing. At the high mould temperature (450 ^{0}C), Mg-0.5Ca and Mg-1Ca alloys were easily oxidized and the oxide inclusions were introduced in the casting. The "middle tearing" is also likely due to the prescence of bifilms. According to John Campbell, the bifilm can randomly locate in the casting due to the chaotic of the surface turbulent [113]. Such randomly distributed bifilm agrees well with the randomly distributed microcracks and the "middle cracking" locations. Besides, the bifilm shown in John Campbell's book [113] looks similar with the microcracks shown in Fig. 5-14. With the prescence of bifilms at grain boundary, the material is weakened and easy to initiate hot tearing. It is reported that defects in casting can act as a stress concentrator, which can easily trigger the hot tearing [112]. In other words, hot tearing is easy to initiate with the presence of such defects. In addition, Mg-0.5Ca and Mg-1Ca showed a

high HTS at a mould temperature of 250 ^{0}C (Fig. 5-7), which makes them more susceptible to casting defects in the middle of the rod.

6.1.4 Effect of mould temperature

Mould temperature plays an important role on HTS of Mg-xCa alloys. The crack volumes at different mould temperatures clearly demonstrate that high mould temperature greatly improves the hot tearing resistance of Mg-xCa binary alloys. Generally, high mould temperature improves the hot tearing resistance due to a reduction in thermal gradient and better compensation of strain [14]. During solidification, thermal gradients within the melt may result in regions of localized strain. Hot tearing occurs only if such accumulated thermal strain exceeds a critical value of strain in the casting [6, 114]. Normally, a lower cooling rate results in a smaller thermal gradient. With a lower cooling rate (high initial mould temperature), the solidification is closer to an equilibrium state, which results in lower contraction strain. Such low contraction strain leads to low HTS.

Experimental cooling curves (temperature-time) of Mg-Ca alloys are displayed in Fig. 5-1 and Fig. 5-2. The cooling curves of Mg-2Ca alloy at different mould temperatures are compared in Fig. 6-2. Cooling rate in this study is defined as the temperature change during the entire solidification range (i.e. from the liquidus to solidus) divided by the corresponding solidification time. The calculated cooling rates of alloys are around 4.25 ± 0.28 ^{0}C/s and 0.44 ± 0.03 ^{0}C/s at T_{mould}=250 ^{0}C and T_{mould}=450 ^{0}C, respectively. Thus, the significantly decreased cooling rate leads to the highly improved hot tearing resistance at T_{mould} = 450 ^{0}C.

As solidification of a casting at a high initial mould temperature takes a longer time, the accumulated contraction strain can be better accommodated through microscopic movements of the dendrite cells or liquid metal [66]. The long solidification time provides adequate time to compensate for the accumulated strain. However, the time for compensation may not be sufficient during a faster solidification process (low initial mould temperature). In addition, due to the slower cooling at a high initial mould temperature, the solutes distributed uniformly. This is evidenced in the microstructures of Mg-Ca alloys cast at both mould temperatures (Fig. 5-5, Fig. 5-6, and Fig. 5-10), as solute segregation was only observed in alloys cast a T_{mould} = 250 ^{0}C. Such solute segration leads to the large amount of eutectic and is likely to result in high HTS, as strain may concentrate on the solute segregated region. Especially in the brittle intermetallic (such as Mg_2Ca) containing eutectic, the solute segregated region is prone to hot tearing. In other words, no such solute segregation is

observed in alloys cast at high initial mould temperature and hence, hot tearing severity decreases.

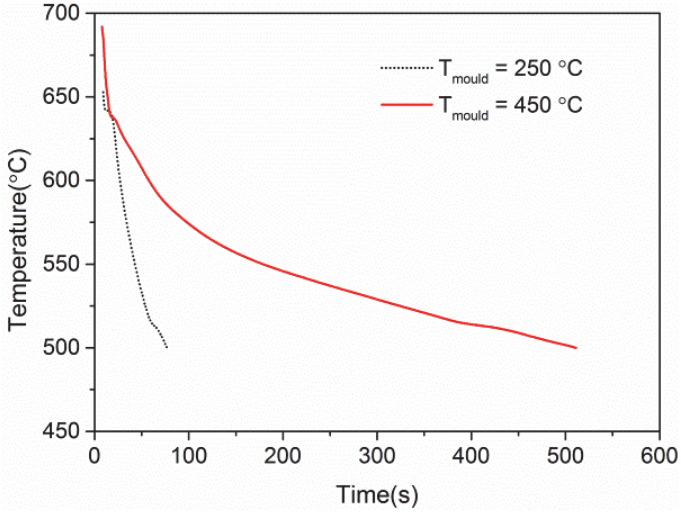

Fig. 6-2 Experimental cooling curves of Mg-2Ca cast at different mould temperatures

6.2 Hot tearing behaviour of Mg-Ca-Zn alloys

6.2.1 Effect of Zn and Ca content on hot tearing behaviour of Mg-Ca-Zn alloys

Generally, the HTS of alloys is affected by alloy composition in the following ways: the length of susceptible freezing range (ΔT_s, temperature range of a solid fraction (f_s) between 0.9 and 0.99) and the amount of eutectic liquid (f_{le}, eutectic liquid at eutectic temperature).

6.2.1.1 Susceptible freezing range

Fig. 6-3 (a) shows the solidification curves of Mg-0.5Ca-xZn alloys calculated by Pandat Software with scheil model. The addition of Zn largely widens the FR of Mg-0.5Ca-xZn alloys. The solidus temperature of Mg-0.5Ca, Mg-0.5Ca-0.5Zn, and Mg-0.5Ca-(1.5-6) Zn is 517 ^{0}C, 394 ^{0}C, and 294 ^{0}C, respectively, as listed in Table 6-2. Similarly, the solid fraction vs. temperature curves of the Mg-2Ca-xZn and Mg-xCa-4Zn alloys are shown in Fig. 6-3 (b) and (c). The calculated FR and ΔT_s are listed in Table 6-2. The addition of Zn to Mg-2Ca alloys also widens the freezing range of the Mg-2Ca-xZn alloys. The solidus temperature of Mg-2Ca, Mg-2Ca-(0.5-4) Zn, and Mg-2Ca-6Zn is 517 ^{0}C, 394 ^{0}C, and 294 ^{0}C, respectively. Moreover, Mg-2Ca-xZn alloys show a lower FR than that of Mg-0.5Ca-xZn alloys. Solidus temperature of Mg-(0.2-1) Ca-4Zn and Mg-2Ca-4Zn is 294 ^{0}C and 394 ^{0}C, respectively. Freezing range decreases with increase in Ca content in Mg-xCa-4Zn alloys.

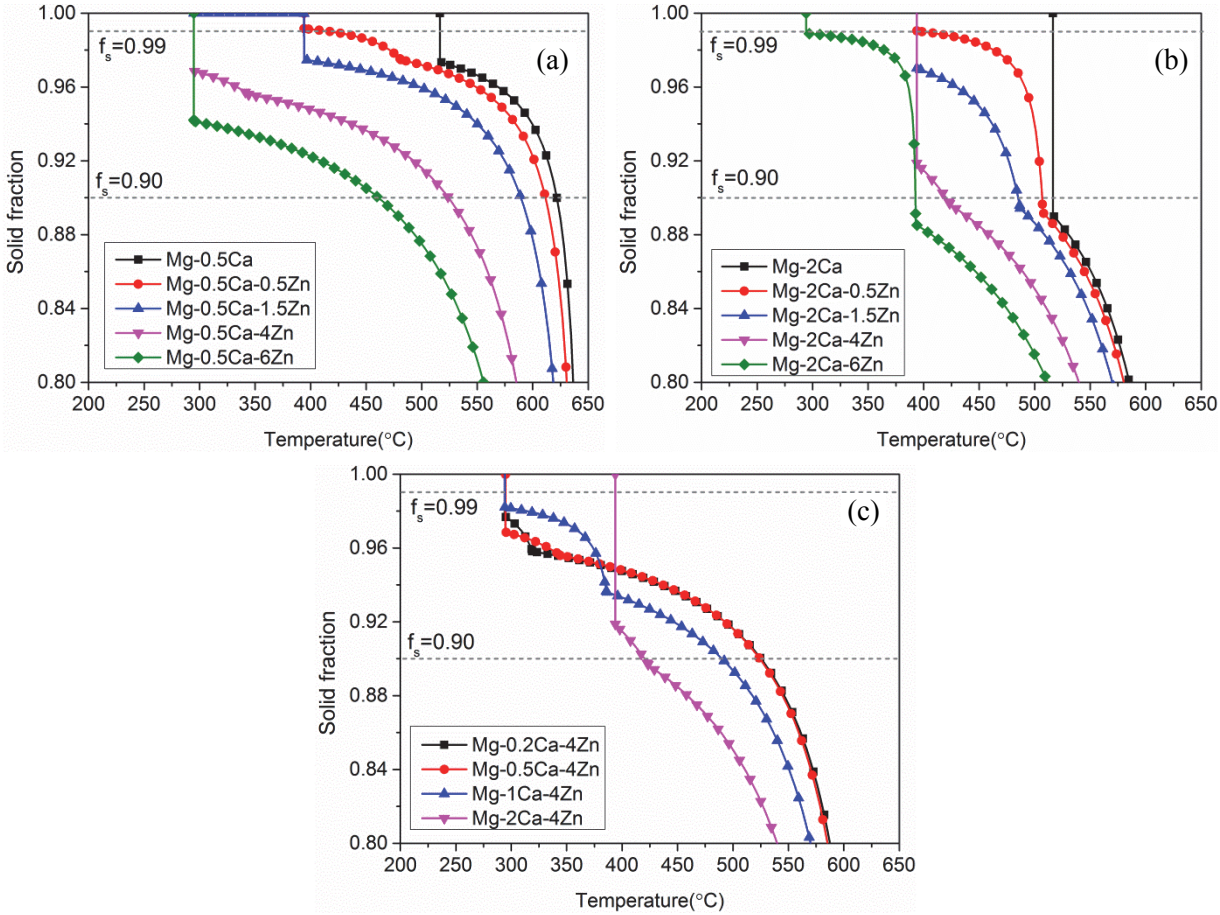

Fig. 6-3 Solid fraction as a function of temperature for alloys calculated with Pandat Software, (a) Mg-0.5Ca-xZn alloys, (b) Mg-2Ca-xZn alloys, and (c) Mg-xCa-4Zn alloys

The susceptible temperature range (ΔT_s) of ternary Mg-Ca-Zn alloys was also calculated and listed in Table 6-2. For better visibility, the susceptible temperature ranges are plotted in Fig. 6-4. It is well established that HTS is extremely sensitive to ΔT_s [10]. During f_s= 0.9-0.99, interdendritic separation occurs, which requires the liquid to be distributed as an interdendritic film. If the remaining liquid is not sufficient to accommodate the separation, a hot tear forms. Thus, at this temperature range, the casting is most susceptible to hot tearing.

In this study, ΔT_s of Mg-0.5Ca-xZn alloys increases with increasing Zn content and reaches a maximum of 228 ^{0}C at Mg-0.5Ca-4Zn. With further addition of Zn to 6 wt.%, the ΔT_s drops to 165 ^{0}C. The ΔT_s of Mg-2Ca-xZn alloys significantly increases with 0.5% Zn, then decreases marginally with increasing Zn content until 4% Zn. Then, further increase in the Zn content increases the ΔT_s (Mg-2Ca-6Zn). It is also noticed that Mg-2Ca-xZn alloys have a lower ΔT_s than that of Mg-0.5Ca-xZn alloys with a fixed Zn content. The ΔT_s of Mg-xCa-4Zn alloys gradually decreases with Ca content, as shown in Fig. 6-4 (b).

Table 6-2 Calculated temperature (in ^{0}C) at different solid fraction with Scheil model of Mg-Ca-Zn alloys, T_l: liquidus temperature, T_s: solidus temperature, FR: freezing range, $T_{0.9}$: temperature at f_s=0.9, $T_{0.99}$: temperature at f_s=0.99, and ΔT_s: $T_{0.9}$ -$T_{0.99}$

	T_l	T_s	FR	$T_{0.9}$	$T_{0.99}$	ΔT_s
Mg-0.5Ca	647	517	130	622	517	105
Mg-0.5Ca-0.5Zn	646	394	252	611	415	196
Mg-0.5Ca-1.5Zn	643	295	348	589	394	195
Mg-0.5Ca-4Zn	636	295	341	523	295	228
Mg-0.5Ca-6Zn	629	295	334	460	295	165
Mg-2Ca	639	517	122	517	517	0
Mg-2Ca-0.5Zn	638	394	244	507	404	103
Mg-2Ca-1.5Zn	635	394	241	486	394	92
Mg-2Ca-4Zn	628	394	234	424	394	30
Mg-2Ca-6Zn	622	295	327	394	344	50
Mg-0.2Ca-4Zn	637	295	342	535	295	240
Mg-1Ca-4Zn	633	295	338	497	295	202

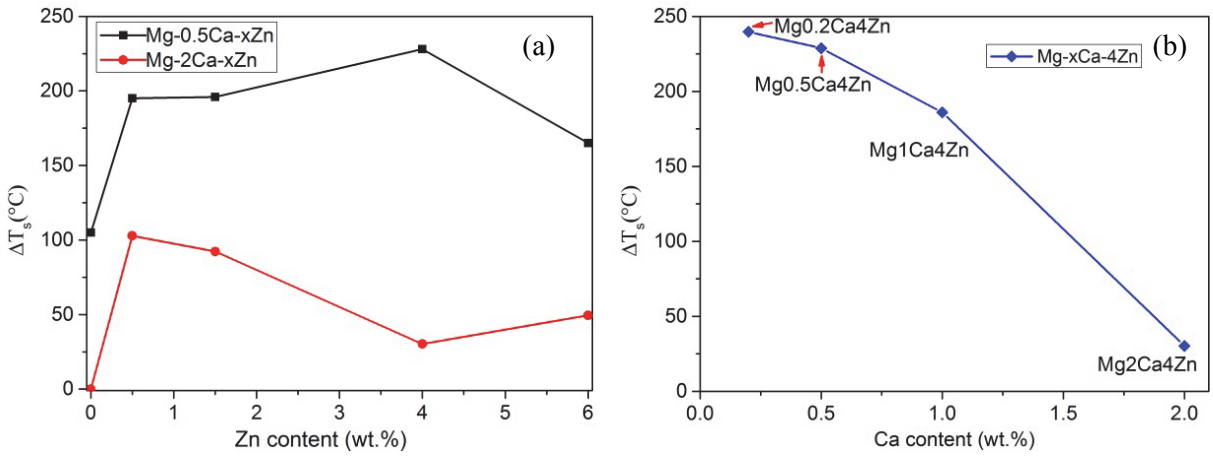

Fig. 6-4 Susceptible temperature ranges of (a) Mg-0.5Ca-(0-6) Zn and Mg-2Ca-(0-6) Zn alloys, (b) Mg-(0-2) Ca-4Zn alloys

Quantified crack volumes are used to evaluate the HTS of ternary Mg-Ca-Zn alloys: large crack volumes indicate a high HTS. In addition, a good correlation between ΔT_s and HTS is also found: a large ΔT_s results in a high HTS. A good correlation between experimental HTS and susceptible temperature range (vulnerable temperature range) is established in Mg-Y alloys [19]. The crack volumes of ternary Mg-Ca-Zn alloys (cast at T_{mould}=250 ^{0}C) are plotted

against ΔT_s for the alloys in Fig. 6-5. However, some discrepancies between large ΔT_s and high HTS are found. For instance, despite the slightly higher ΔT_s compared to that of the Mg-2Ca-4Zn alloy, the Mg-2Ca-6Zn alloy has a lower crack volume. Similarly, the Mg-0.2Ca-4Zn alloy has a slightly higher ΔT_s compared with that of the Mg-0.5Ca-4Zn alloy, but the Mg-0.2Ca-4Zn alloy has a lower crack volume. This discrepancy indicates that hot tearing is a complex phenomenon and ΔT_s is not the only underlying factor influencing hot tear formation.

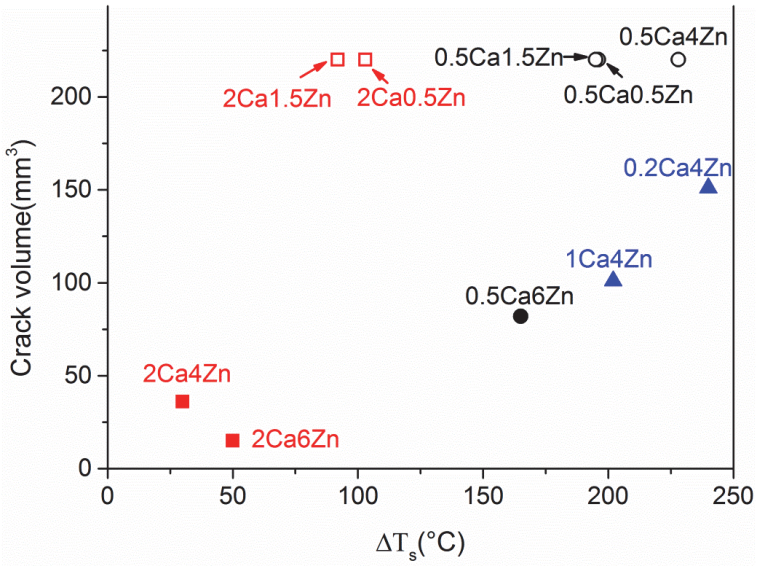

Fig. 6-5 Correlation between ΔT_s and crack volumes of ternary Mg-Ca-Zn alloys (Crack volume data are from T_{mould} = 250 ^{0}C, completely broken tears are displayed as hallow circle or box)

6.2.1.2 Liquid healing

Amount of eutectic liquid (f_{le}) plays an important role on HTS. After hot tears nucleate, the regions near them have a negative pressure. The negative pressure can suck back the eutectic liquid, and healing of hot cracks may occur [16]. Liquid healing is evidenced in Mg-Y and Mg-Gd binary alloys, especially at a high content of solute [19, 64]. It is found that the more f_{le} is present, the more likely the solidifying alloy can accommodate the rising tension and heal the cracks [23].

Table 6-3 Calculated eutectic liquid (f_{le}) of Mg-0.5Ca-xZn-(0.2Zr) alloys

	Mg-0.5Ca	Mg-0.5Ca-0.5Zn	Mg-0.5Ca-1.5Zn	Mg-0.5Ca-4Zn	Mg-0.5Ca-6Zn	Mg-0.5Ca-4Zn-0.2Zr
f_{le}	0.027	0.008	0.0001	0.032	0.058	0.032

The calculated f_{le} of Mg-0.5Ca-xZn-(0.2Zr) alloys is listed in Table 6-3. The Mg-0.5Ca, Mg-0.5Ca-4Zn, Mg-0.5Ca-6Zn, and Mg-0.5Ca-4Zn-0.2Zr alloys have a high f_{le}. However, a large amount of eutectic near the main tear area was only evidenced in the Mg-0.5Ca and Mg-0.5Ca-4Zn-0.2Zr alloys, as shown in Fig. 6-6 (a) and (g), respectively. Crack refilling by wide eutectic was obviously observed in the the Mg-0.5Ca and Mg-0.5Ca-4Zn-0.2Zr alloys. However, much less eutectic was found in Mg-0.5Ca-4Zn and Mg-0.5Ca-6Zn alloys. Interestingly, a large amount of torn liquid film was found on the fracture surfaces of the Mg-0.5Ca-4Zn (Fig. 6-6 (d)) and Mg-0.5Ca-6Zn (Fig. 6-6 (f)) alloys. Thus, it is suggested that the high amount of eutectic liquid in the Mg-0.5Ca-4Zn and Mg-0.5Ca-6Zn alloys might form the liquid film rather than eutectic. This indicated cracking healing with eutectic of these two alloys was less efficient. Additionally, the large amount of liquid film revealed that the remaining liquid was unable to flow into the tear area, thereby suggesting poor feeding of eutectic liquid in the Mg-0.5Ca-4Zn and Mg-0.5Ca-6Zn alloys.

Large amount of devoiced eutectic segregation is mainly in Mg-2Ca-xZn alloys cast at T_{mould}=250 ^{0}C. The following discussion is based on the liquid healing of cracks in Mg-2Ca-xZn alloys cast at T_{mould}=250 ^{0}C.

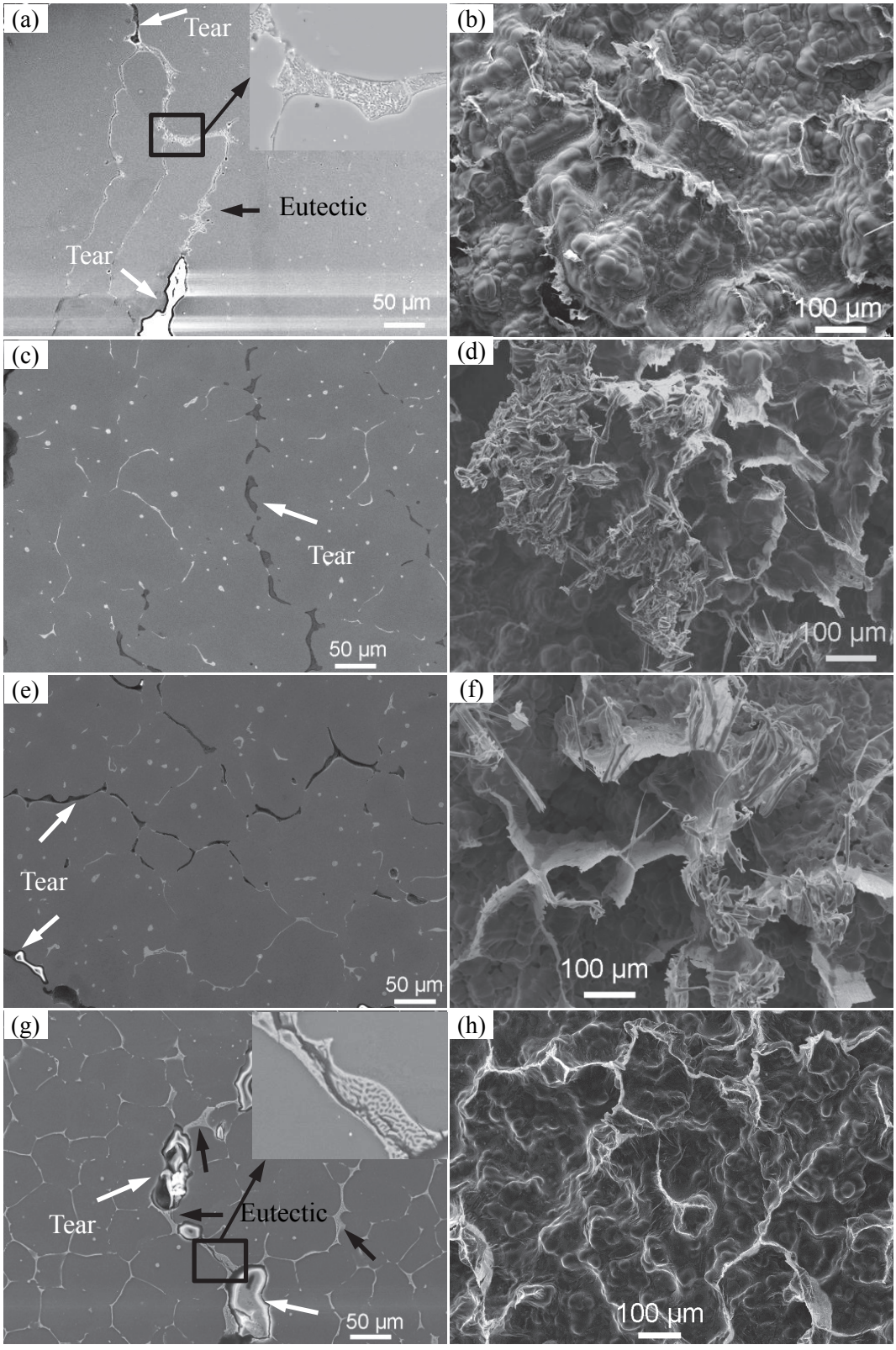

Fig. 6-6 Cross section of hot tears and fracture surface of alloys cast at T_{mould} = 250 ^{0}C, (a), (b) Mg-0.5Ca, (c), (d) Mg-0.5Ca-4Zn, (e), (f) Mg-0.5Ca-6Zn, and (g), (h) Mg-0.5Ca-4Zn-0.2Zr

In fact, eutectic structure is mainly observed near the tears instead of the exact junctions of sprue and rod part in Mg-2Ca-xZn alloys. Its existence at these specific locations indicates that the formation of eutectic and tear is somehow related. After the hot tears occur, the regions near them have a negative pressure. This negative pressure can suck back the liquid, and the cracks can be refilled [19]. Many previous investigations have shown that the liquid eutectic can completely or partially heal the previously formed hot cracks in binary Mg-Al, Mg-Zn and Mg-Y alloys [14, 19, 20]. Wang et al. [19] and Srinivasan et al. [20] have observed the presence of eutectic near the crack regions in Mg-Y and Mg-Gd alloys respectively and suggested that the cracks can be healed partially or completely by eutectic liquid during solidification.

The quantity of eutectic liquid available for the crack healing is also regarded as one of the most important factors to influence the final hot tearing. The f_{le} of Mg-2Ca-xZn alloys calculated using Pandat thermodynamic software and Scheil solidification model, are listed in Table 6-4. The f_{le} for Mg-2Ca-6Zn alloy is found to be relatively low. However, both X-ray tomography studies and SEM analyses confirm that Mg-2Ca-6Zn contains maximum eutectic among all the alloys. Thus, it is proposed that the liquid fraction (f_{lt}) at the onset of $Mg_6Ca_2Zn_3$ formation is the proper "eutectic liquid" for Mg-2Ca-xZn alloys. The f_{lt} is not applied to Mg-0.5Ca-xZn alloys, because much less eutectic is found near the tears than that in Mg-2Ca-xZn alloys. In other words, it is believed that the formation of $Mg_6Ca_2Zn_3$ phase takes part in the crack healing. The f_{lt} for Mg-2Ca-6Zn is 0.111, which is the largest among all (Table 6-4). The f_{lt} value for Mg-2Ca-xZn alloys increases with increase in Zn content, which agrees well with the SEM analysis. The proposal is further supported by the following experimental observations. Firstly, the crack initiation of Mg-2Ca-6Zn occurs before the formation of $Mg_6Ca_2Zn_3$ phase during solidification. According to the force curves, crack initiated at 505 ^{0}C whereas the onset of $Mg_6Ca_2Zn_3$ formation occurs at 394 ^{0}C (calculated by Pandat) for Mg-2Ca-6Zn alloy. Thus, the eutectic liquid of $Mg_6Ca_2Zn_3$ refills the crack and thus heals the cracks. Secondly, the SEM results confirm that the eutectic structure of Mg-2Ca-6Zn alloy mainly consists of $Mg_6Ca_2Zn_3$ phase and α-Mg.

Table 6-4 Calculated fraction of eutectic liquid (f_{le}), fraction of liquid at the onset of $Mg_6Ca_2Zn_3$ formation (f_{lt}) in Mg-2Ca-xZn alloys

	Mg-2Ca	Mg-2Ca-0.5Zn	Mg-2Ca-1.5Zn	Mg-2Ca-4Zn	Mg-2Ca-6Zn
f_{le}	0.110	0.009	0.029	0.079	0.007
f_{lt}	-	0.009	0.029	0.079	0.111

As the Mg-2Ca-6Zn alloy has the maximum eutectic among all, it is expected to exhibit the best crack healing ability among all. As a result, although ΔT_s of the Mg-2Ca-6Zn alloy is slightly larger than that of the Mg-2Ca-4Zn alloy, the final crack volume (HTS) of Mg-2Ca-6Zn is less than that of the Mg-2Ca-4Zn alloy.

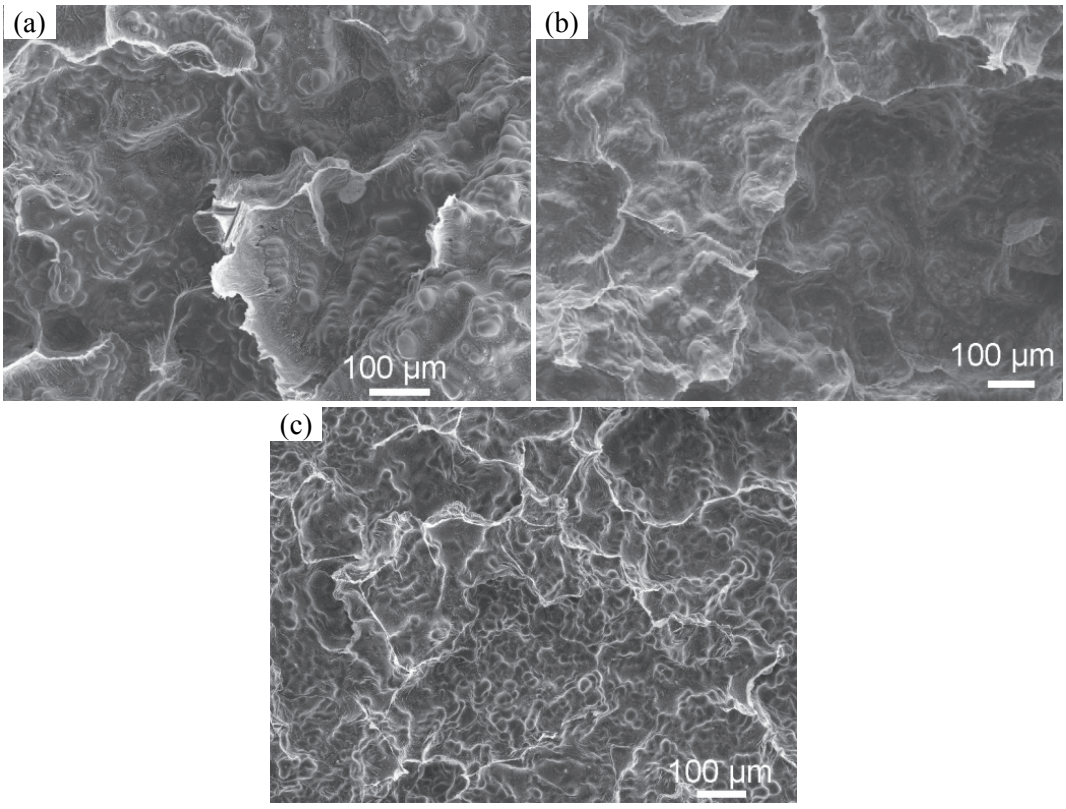

Fig. 6-7 Fracture surface of alloys cast at T_{mould} = 250 ^{0}C, (a) Mg-2Ca-0.5Zn, (b) Mg-2Ca-1.5Zn, and (c) Mg-2Ca-4Zn

It is found that most of the eutectic liquid formed eutectic rather than liquid film in Mg-2Ca-xZn alloys. A small amount of torn liquid film is observed on the low magnified fracture surfaces of Mg-2Ca-4Zn alloys, as shown in Fig. 6-7. Thus, it is demonstrated again that healing by eutectic liquid is effective in Mg-2Ca-xZn alloys.

Table 6-5 shows the calculated f_{le} and f_{lt} for Mg-xCa-4Zn alloys. The f_{le} of Mg-1Ca-4Zn is low compare to that of the other Mg-xCa-4Zn alloys. However, both X-ray tomography and SEM analyses comfirm that the Mg-1Ca-4Zn alloy contains a certain amount of eutectic. Thus, the concept of f_{lt} is also applied to Mg-xCa-4Zn alloys, as listed in Table 6-5. Thus, the higher f_{lt} explains the reason that more eutectic is found in the Mg-1Ca-4Zn alloy than that of the Mg-0.2Ca-4Zn and Mg-0.5Ca-4Zn alloys.

Table 6-5 Calculated fraction of eutectic liquid (f_{le}), fraction of liquid at the onset of $Mg_6Ca_2Zn_3$ formation (f_{lt}) in Mg-xCa-4Zn alloys

	Mg-0.2Ca-4Zn	Mg-0.5Ca-4Zn	Mg-1Ca-4Zn	Mg-2Ca-4Zn
f_{le}	0.023	0.032	0.015	0.079
f_{lt}	0.023	0.044	0.062	0.079

Eutectic is found mainly in the Mg-1Ca-4Zn and Mg-2Ca-4Zn alloys and torn liquid film agglomeration is mainly observed in Mg-0.2Ca-4Zn and Mg-0.5Ca-4Zn alloys, as shown in Fig. 5-58 and Fig. 6-8. This inidicates that the Mg-1Ca-4Zn and Mg-2Ca-4Zn alloys provide better eutectic liquid healing than the Mg-0.2Ca-4Zn and Mg-0.5Ca-4Zn alloys.

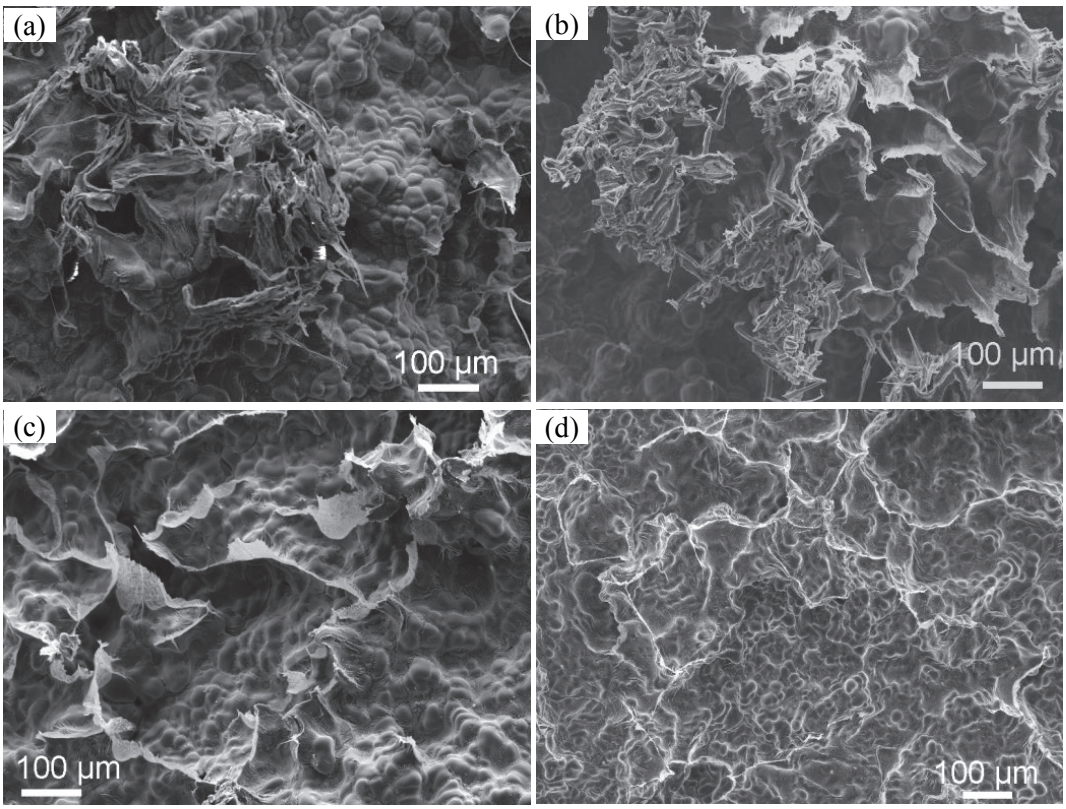

Fig. 6-8 Fracture surface of Mg-xCa-4Zn alloys cast at T_{mould} = 250 ^{0}C, (a) Mg-0.2Ca-4Zn, (b) Mg-0.5Ca-4Zn, (c) Mg-1Ca-4Zn, and (d) Mg-2Ca-4Zn

In summary, eutectic healing is mainly found in high Ca containing ternary Mg-Ca-Zn alloys, such as in Mg-1Ca-4Zn and Mg-2Ca-xZn alloys. Large amount of torn liquid film agglomeration is observed on the fracture surfaces of low Ca containing Mg-Ca-Zn alloys, such as Mg-0.2Ca-4Zn and Mg-0.5Ca-xZn alloys. Besides, the addition of Zr facilitates the formation of eutectic. According to the force-temperature-time curves (Fig. 5-19, Fig. 5-33, and Fig. 5-50) of all the ternary alloys cast at T_{mould} = 250 ^{0}C, all the hot tearing initiated at a

low solid fraction. In other words, large amount of liquid exists at the moment of the hot tearing initiation. The residual liquid forms either liquid film or eutectic that heals the hot tear.

6.2.1.3 Intermetallics

The second phases may play an important role in influencing the initiation of hot tearing [115]. The second phases with low melting points may decrease the solidus temperature of the alloy, thereby prolonging the liquid film stage where hot tearing is likely to occur. Moreover, the brittle second phases with higher melting points may contribute to the fracture of the interconnected coherent solid network in the critical temperature range. The presence of second phases may also influence the properties of the inter-dendritic liquid that is present in the hot tear region, (i.e., wettability).

As proved in Mg-2Ca-xZn alloys, the ternary phase $Mg_6Ca_2Zn_3$ takes part in the eutectic healing. Besides, as mentioned earlier, the brittle intermetallic Mg_2Ca is partly responsible for the high HTS of Mg-Ca alloys. Thus, the formation of second phases in ternary Mg-Ca-Zn alloys also helps to understand the hot tearing behaviour.

It is reported that the type and amount of second phases in ternary Mg-Ca-Zn alloys highly depends on the Zn/Ca atomic ratio and solidification conditions. As reported by Bakhsheshi-Rad et al. [116], the intermetallics are Mg_2Ca and $Mg_6Ca_2Zn_3$ for Mg-Ca-Zn alloys with Zn/Ca atomic ratio below 1.23, $Mg_6Ca_2Zn_3$ for Zn/Ca ratio between 1.23 and 7.38, and $Mg_6Ca_2Zn_3$ and $Mg_{51}Zn_{20}$ for Zn/Ca ratio above 7.38. The $Mg_{51}Zn_{20}$ phase transforms through eutectoidal decomposition to α-Mg and MgZn at room temperature [117]. However, the MgZn phase is not observed in the provided SEM microstructure or in the XRD patterns in Bakhsheshi-Rad's research [116], probably due to the small amount of MgZn. A recent paper by Naghdi et al. [117] reveals that the MgZn phase exists in the as-cast Mg-0.5Ca-4Zn alloy with a Zn/Ca atomic ratio of 4.93. The microstructure shows that the MgZn phase is surrounded by the ternary $Mg_6Ca_2Zn_3$ phase. Naghdi et al. [117] stated that the different solidification conditions is responsible for the inconsistency.

The Zn/Ca atomic ratio as well as the second phase for this study is listed in Table 6-6. It is found that Mg_2Ca is the main second phase in alloys with a Zn/Ca atomic ratio below 0.62; Mg_2Ca and $Mg_6Ca_2Zn_3$ in alloys with Zn/Ca atomic ratio between 0.46 and 1.85; $Mg_6Ca_2Zn_3$ in alloys with Zn/Ca atomic ratio between 1.85 and 4.93; and $Mg_6Ca_2Zn_3$ and MgZn in alloys with Zn/Ca atomic ratio above 7.83. In addition, the second phases also dependend on the initial mould temperature. For instance, Mg_2Ca is found in the Mg-0.5Ca-1.5Zn alloy cast at high initial mould temperature, but not in the alloy cast at low mould temperature. In this

study, due to the solidification sequence, both Zn and Ca enriches near the tearing region, especially at a low initial mould temperature. Thus, the solidification conditions are different from both those in Bakhsheshi-Rad and Naghdi's research.

Table 6-6 Zn/Ca atomic ratio and experimeatal intermetallics near the tear region of Mg-Ca-Zn alloys

Alloys	Zn/Ca atomic ratio	Intermetallics in the experiments			
		SEM+EDX (T_{mould} = 250 °C)	SEM+EDX (T_{mould} = 450 °C)	XRD (T_{mould} = 250 °C)	XRD (T_{mould} = 450 °C)
Mg0.5Ca0.5Zn	0.62	Mg_2Ca+$Mg_6Ca_2Zn_3$	Mg_2Ca	-	-
Mg0.5Ca1.5Zn	1.85	$Mg_6Ca_2Zn_3$	Mg_2Ca+$Mg_6Ca_2Zn_3$	-	-
Mg0.5Ca4Zn	4.93	$Mg_6Ca_2Zn_3$	$Mg_6Ca_2Zn_3$	-	-
Mg0.5Ca6Zn	7.38	$Mg_6Ca_2Zn_3$+MgZn	$Mg_6Ca_2Zn_3$+MgZn	-	-
Mg2Ca0.5Zn	0.15	Mg_2Ca	Mg_2Ca	Mg_2Ca	Mg_2Ca
Mg2Ca1.5Zn	0.46	Mg_2Ca+$Mg_6Ca_2Zn_3$	Mg_2Ca+$Mg_6Ca_2Zn_3$	Mg_2Ca	Mg_2Ca+$Mg_6Ca_2Zn_3$
Mg2Ca4Zn	1.23	Mg_2Ca+$Mg_6Ca_2Zn_3$	Mg_2Ca+$Mg_6Ca_2Zn_3$	Mg_2Ca+$Mg_6Ca_2Zn_3$	Mg_2Ca+$Mg_6Ca_2Zn_3$
Mg2Ca6Zn	1.85	$Mg_6Ca_2Zn_3$	$Mg_6Ca_2Zn_3$	$Mg_6Ca_2Zn_3$	$Mg_6Ca_2Zn_3$
Mg0.2Ca4Zn	12.33	$Mg_6Ca_2Zn_3$+MgZn	$Mg_6Ca_2Zn_3$+MgZn	-	-
Mg1Ca4Zn	2.46	$Mg_6Ca_2Zn_3$	$Mg_6Ca_2Zn_3$	-	-

6.2.2 Residual strain

Hot tearing is a strain involved phenomenon. Therefore, the measurement of residual strain distribution helps to understand the mechanism of hot tearing. Neutron diffraction for strain analysis is preferred because of its high penetration depth and flexible gauge volume choices for coarse grained as-cast ingots [70].

The large strain variation in the Mg-2Ca-0.5Zn and Mg-2Ca-1.5Zn alloys might be due to their large grain sizes. This is further supported by the larger strain error in the sprue portion than in the rod portion in the Mg-2Ca-4Zn and Mg-2Ca-6Zn alloys. The sprue portion exhibited a coarser grain structure with respect to the rod portion. Low variation of strain was also found in grain refined aluminium-copper alloyB206, while high variation of strain was found in unrefined B206 alloy [118].

The higher magnitude of residual strain on the sprue portion than that in the rod portion was likely due to the strain relief upon removel of load cell. After the casting cooled to around 100 ^{0}C, it was taken out from the mould and thus the restriction from the load cell was also removed. Such removel led to the strain relief on the rod portion but on the sprue part. Therefore, the resulted residual strain is lower in the rod portion.

As mentioned earlier, the strain relief along the radial direction was observed in Mg-2Ca-4Zn alloys. This is because the casting contraction was restricted by the load cell in the radial direction (Fig. 4-4) and formation of fine tears (Fig. 5-37 (c)) would therefore result in relief along this direction. In contrast, in the case of Mg-2Ca-6Zn alloy, the lack of hot tear at the sprue-rod junction (Fig. 5-37 (d)) resulted in, no observed strain relief along the radial direction for this alloy.

Another interesting finding is that the developed residual stresses can either be tensile or compressive, which depends on the measured planes. It is clear that under a certain stress some planes will be subjected to tensile stress and some will be under compressive stress. According to the plane distribution of α-Mg (hexagonal, P63/mmc), it is possible to develop a tensile stress on the (211) plane and compressive stress on the (203) plane. Bichler et al. [93] also found that the developed residual strain varies from different reflections in AZ91D alloy.

6.2.3 Tearing at load screw at T_{mould} = 450 ^{0}C

Tearing of ternary Mg-Ca-Zn alloys sometimes occurs at the load screw on the rod at an initial mould temperature of 450 ^{0}C. No such tearing is found in the alloys cast at a mould temperature of 250 ^{0}C. Both Mg-0.2Ca-4Zn and Mg-0.5Ca-4Zn alloys were prone to tearing at the load screw. Tearing at load screw is also evident in the Mg-0.5Ca-1.5Zn, Mg-0.5Ca-6Zn, and Mg-1Ca-4Zn alloys. However, the probability of "load screw tearing" in the Mg-0.5Ca-1.5Zn, Mg-0.5Ca-6Zn, and Mg-1Ca-4Zn alloys is lower than that of Mg-0.2Ca-4Zn and Mg-0.5Ca-4Zn alloys.

The occurrence of the tear near the load screw might be due to the relatively low solidus temperature and high HTS of these alloys. First of all, due to different thermal conductivity between steel (load screw) and Mg alloys, the interface between the load screw and the casting is another stress concentrator in addition to the sprue-rod junction. Small cracks can be observed at the interface for those alloys with hot tears at the sprue-rod junction. These small cracks proved that the interface was a "weak" place for hot tearing. Then, the long solidification duration enables the hot tearing to occur at the interface. The solidus temperatures (T_s) of all those alloys with "load screw tearing" are 294 ^{0}C, as listed in Table

6-2. With a mould temperature of 450 ^{0}C, it took quite a long time to accomplish the solidification. In other words, the time spent at the interface is long, which made the "weak" interface susceptible to hot tearing. With a high HTS of these alloys, once the accumulated strain exceeds the stress limit of the interface, hot tearing initiates [6]. For those alloys with a lower HTS than these "load screw tearing" alloys, the accumulated stress is not high enough to break at the interface. Consequently, the main hot tear appeared at the sprue-rod junction and only small tears can be observed at the interface. Additionally, as the thermal stresses released at the interface, no visible tear can be observed at the sprue-rod junction of these "load screw tearing" alloys.

6.2.4 Effect of mould temperature

As previously mentioned, a high mould temperature decreases the HTS of binary Mg-Ca alloys. It is also reported that high initial mould temperatures decreases the HTS of ternary Mg-Zn-Y [9] and AZ91D [15] alloys. In this study, it is found that an increase in mould temperature improves the hot tearing resistance of some ternary Mg-Ca-Zn alloys, such as Mg-2Ca-xZn, Mg-0.5Ca-0.5Zn, and Mg-1Ca-4Zn. As for other ternary Mg-Ca-Zn alloys, the castings still exhibit a high HTS at the high mould temperature of 450 ^{0}C. For instance, the Mg-0.2Ca-4Zn, Mg-0.5Ca-1.5Zn, and Mg-0.5Ca-4Zn alloys were completely broken at the high mould temperature.

As explained earlier in section 6.1.4, the improvement of hot tearing resistance at a high initial mould temperature is highly related to cooling rate. Thus, the cooling rates of ternary Mg-Ca-Zn alloys at different mould tempertures were calculated and listed in Table 6-7. According to the calculation, the cooling rate depends on both the mould temperature and the solidification range. Generally, high mould temperature and large FR result in low cooling rate.

In this study, the experimental cooling rates of those alloys with the same T_s (almost the same FR) are close. The T_s of Mg-0.5Ca-1.5Zn, Mg-0.5Ca-4Zn, Mg-0.5Ca-6Zn, Mg-2Ca-6Zn, Mg-0.2Ca-4Zn, and Mg-1Ca-4Zn alloys is 294 ^{0}C, whereas the cooling rate of these alloys are around 0.26 ^{0}C/s and 0.16 ^{0}C/s at T_{mould}=250 ^{0}C and T_{mould}=450 ^{0}C, respectively. All the cooling rates of those alloys with a T_s = 394 ^{0}C are higher than the cooling rates of alloys with a T_s = 294 ^{0}C, especially at a low mould temperature. Moreover, cooling rates of those alloys with high T_s of 394^{0}C rapidly decrease with increase in initial mould temperature. For instance, as the mould temperature increases from 250 ^{0}C to 450 ^{0}C, the cooling rate of the Mg-0.5Ca-0.5Zn alloy drops from 0.59 ± 0.05 ^{0}C/s to 0.22 ± 0.01 ^{0}C/s. However, the cooling

rates of the alloys with T_s = 294 ^{0}C does not decrease significantly with increase in the mould temperature. For instance, the cooling rates of Mg-0.5Ca-1.5Zn alloy decreases from 0.26 ± 0.02 ^{0}C/s to 0.16 ± 0.01 ^{0}C/s.

Table 6-7 Cooling rates, T_s, FR and ranking of whether high mould temperatures decreases the HTS of Mg-Ca-Zn ternary alloys.

	Cooling rates at 250 ^{0}C (^{0}C/s)	Cooling rates at 450 ^{0}C (^{0}C/s)	Ts (^{0}C)	FR (^{0}C)	High mould temperature decreases HTS?
Mg-0.5Ca-0.5Zn	0.59±0.05	0.22±0.01	394	252	Yes
Mg-0.5Ca-1.5Zn	0.26±0.02	0.16±0.01	294	348	No
Mg-0.5Ca-4Zn	0.26±0.01	0.16±0.01	294	341	No
Mg-0.5Ca-6Zn	0.26±0.01	0.16±0.01	294	334	Yes
Mg-2Ca-0.5Zn	0.50±0.01	0.18±0.01	394	244	Yes
Mg-2Ca-1.5Zn	0.57±0.05	0.18±0.01	394	241	Yes
Mg-2Ca-4Zn	0.65±0.01	0.19±0.01	394	234	Yes
Mg-2Ca-6Zn	0.25±0.02	0.15±0.01	294	327	Yes
Mg-0.2Ca-4Zn	0.26±0.01	0.16±0.01	294	342	No
Mg-1Ca-4Zn	0.25±0.01	0.15±0.01	294	338	Yes

The high mould temperature effectively improves the hot tearing resistance of thoses alloys with evidently decreased cooling rates between two mould temperatures. The ranking of whether high mould teamperature decreases the HTS of alloys is listed in Table 6-7. HTS of Mg-Ca-Zn alloys with T_s of 394 ^{0}C (cooling rates evidently decreased) all decreased at the high initial mould temperature. It is found that increasing the mould temperature does not always improve the hot tearing resistance of the alloys with a low T_s, 294 ^{0}C. The detailed mechanisms of reduction in HTS at a high intial mould temperature can be found in section 6.1.4.

6.2.5 Effect of grain refinement

The reduced HTS of Mg-0.5Ca-4Zn-0.2Zr is mainly due to grain refinement. The solidification curves of Mg-0.5Ca-4Zn and Mg-0.5Ca-4Zn-0.2Zr alloys are compared in Fig. 6-9. A similar solidification path is observed for these two alloys. The FR of the Mg-0.5Ca-4Zn and Mg-0.5Ca-4Zn-0.2Zr alloys are 341 ^{0}C and 342 ^{0}C, respectively. The ΔT_s of both the alloys are 228 ^{0}C. In other words, susceptible freezing range has little impact on the different hot tearing behaviours between Mg-0.5Ca-4Zn and Mg-0.5Ca-4Zn-0.2Zr alloys.

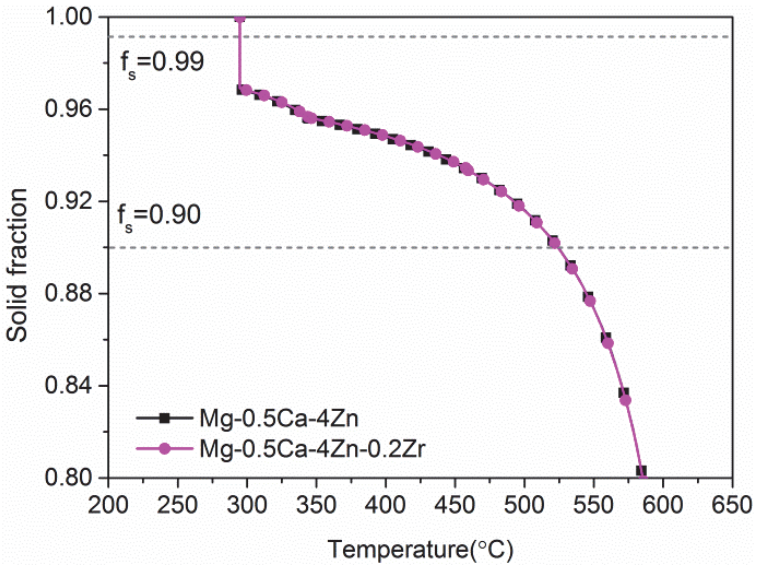

Fig. 6-9 Solid fraction as a function of temperature for Mg-0.5Ca-4Zn and Mg-0.5Ca-4Zn-0.2Zr alloys calculated with Pandat Software

Grain refinement delays the onset of strength development and prolongs mass feeding [63]. The duration of bulk liquid feeding was enhanced for the refined casting conditions and thus, hot tearing severity was reduced [118]. Moreover, this refined grain size is better for the accommodation of deformation caused by the solidification schrinkage. In the grain refined alloy, the eutectic liquid distributed uniformly at the grain boundary, which was easy for feeding. This is evidenced in the tear microstructure and fracture surfaces shown in Fig. 6-6. With addition of Zr, much less ruptured liquid metal is found on the fracture surface, as shown in Fig. 6-6. This indicates Zr-containing alloy exhibits a better compensation of strain than that of Zr free alloy. Futhermore, the local strain at the grain boundaries was smaller in the refined alloy than that in the non-refined alloy. In castings with the same shape and prepared under the same condition (the same mould temperature), the total stain is the same. The total strain spreads out in the entire casting. As there are more grain boundaries in the grain refined casting, the local strain at each grain boundary is smaller. The local strain beared in the grain refined castings is small and hence, the HTS is reduced.

6.3 Hot tearing mechanisms

6.3.1 Solidification and hot tearing

Hot tearing is defined as failure occurring in the mushy zone of a freezing alloy, i.e. at solid fraction f_s <1. Thus, the understanding of the whole solidification process in alloys is essential for the investigation of hot tearing behavior. According to Eskin et al.'s [7] investigations, four stages of solidification characterize the permeability of the solid network

(Fig. 6-10). (1) Mass feeding, in which both the liquid and solid can freely move. (2) Inter-dendritic feeding, in which the dendrites start to form a solid skeleton and the liquid must flow through the dendritic network. (3) Inter-dendritic separation, in which the liquid network becomes fragmented, and pores form or hot tearing may occur. (4) Inter-dendritic bridging, in which the ingot has developed a considerable strength and solid-state creep compensates further contraction. The last two stages are important for hot tearing. With the increase in the solid fraction, the permeability of the solid network becomes very low. The liquid feeding ceases when the solid fraction increases to a critical value. Meanwhile, it is considered by Eskin et al [7] that the hindered feeding of the solid phase by the liquid is the main cause of hot tearing.

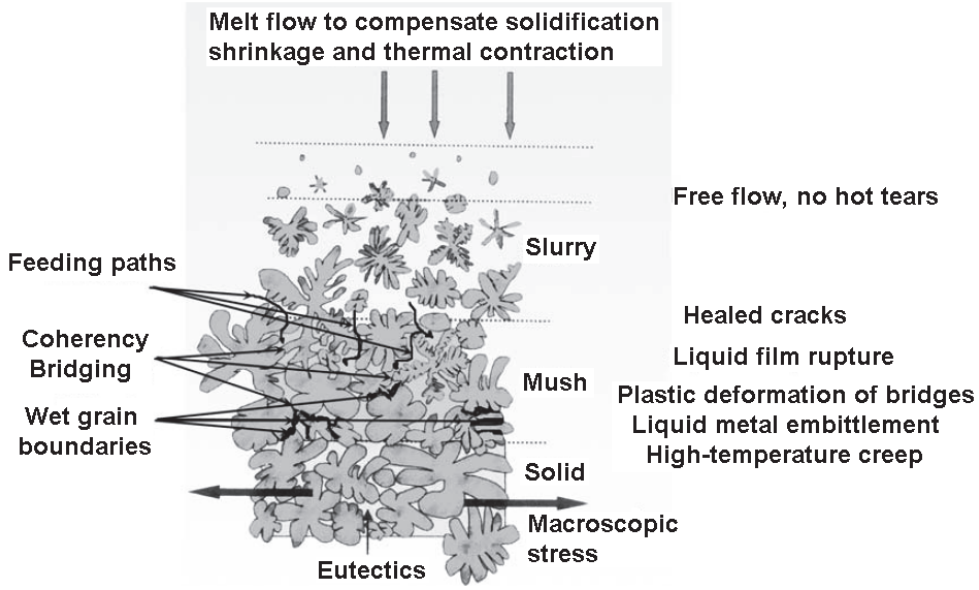

Fig. 6-10 Schematic of different length scales of equiaxed dendritic solidification [7]

6.3.2 Tear initiation and propagation

6.3.2.1 Liquid film rupture

Torn liquid films were evident on the fracture surfaces in binary Mg-Ca and ternary Mg-Ca-Zn alloys. Thus, liquid film rupture is considered as one of the tearing mechanisms in this study. Liquid film theory was firstly introduced by Pellini et al. [114]. They found that a thin continuous liquid film exists at the junction area of the solidified dendrites at the late stage of solidification. During solidification, as the dendrites grow and come into contact, a coherent network forms. At this time, there is a thin continuous liquid film remaining between the solidified dendrites. As solidification further proceeds, the film becomes thinner and thinner. In the meantime, highly concentrated contraction forces can build up in the liquid

film region. Once the contraction strain is high enough and reaches the deformation limit, the hot tearing initiates along the liquid films.

The optical microstructural observations of binary Mg-Ca alloys confirmed that the hot tears were located at the grain boundaries. Besides, the ruptured liquid films observed on all the fracture surfaces suggested that the crack propagation occurred with tearing of liquid film. These liquid films were located mainly at the grain boundaries. In addition, the hot tearing curves showed that the solid fraction corresponding to the tearing initiation was quite low for the Mg-0.5Ca, Mg-1Ca, and Mg-2Ca alloys. At the later stage of solidification, the grains or dendrites are covered by a small amount of remaining liquid with a lower melting temperature. With further solidification proceeding, the dendrites grow and try to coalesce. In the meantime, the remained liquid becomes rare and the thin liquid film starts to distribute at the grain or dendritic boundaries. Under the accumulated thermal strain and stress, hot tearing nucleation may occur at such thin liquid films. If the hot tearing initiates after the grains coalesce (at a higher solid fraction), the fractured grain bridges or grain plastic deformation should be evidenced on the fracture surface [119]. However, no such features were observed on the fracture surfaces of investigated Mg-Ca alloys. Therefore, it is most probable that the liquid film at the grain boundaries was responsible for the initiation of hot tearing in Mg-Ca alloys. Ruptured liquid film between two grains on the fracture surface of was observed in the Mg-0.5Ca alloy, as shown in Fig. 6-11. A thin area of ruptured liquid film between the two sides of the crack is evident, as marked with arrows. It seems that the thin liquid film fractured under tension in the direction of the arrows.

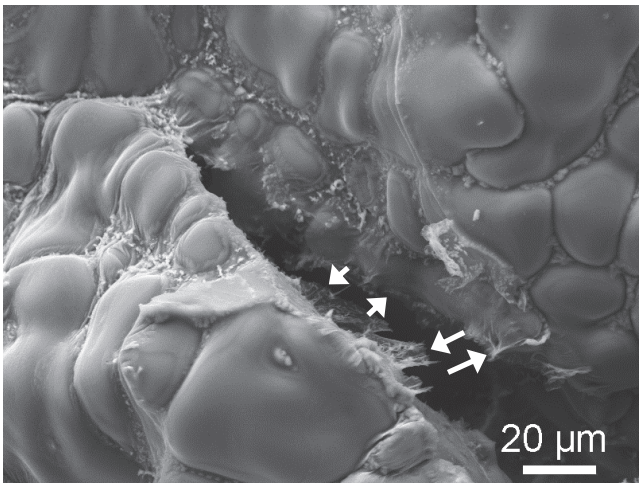

Fig. 6-11 Liquid film on the fracture surface of Mg-0.5Ca alloy cast at T_{mould} = 250 ^{0}C

Torn liquid film is also found on all the fracture surfaces at both mould temperatures in all the ternary Mg-Ca-Zn alloys. Therefore, it is proposed that liquid film rupture is also one of the

hot tearing mechanisms for the ternary Mg-Ca-Zn alloys. It is found that the amount of torn liquid film is composition dependent. As mentioned in section 6.2.1.2, large amount of ruptured liquid film clusters are evidenced on the fracture surfaces of Mg-0.5Ca-xZn and Mg-0.2Ca-4Zn alloys. Thus, for these alloys, liquid film rupture is considered as the main hot tearing mechanism. However, the amount of ruptured liquid film was found much less in the Mg-2Ca-xZn and Mg-1Ca-4Zn alloys. Thus, for these alloys, liquid film rupture can only be regarded as one of the hot tearing mechanisms.

6.3.2.2 Rupture of solid bridging

After the coherent network forms, solid bridges between the adjacent dendrites appear. Thus, the strength of the casting begins to develop. If this can occur to a sufficient extent, the strength of the casting might be high enough to prevent the inter-dendritic separation. Hence, no hot tearing would occur. On the contrary, if the contraction force exceeds the strength built up from solid bridging, hot tearing forms.

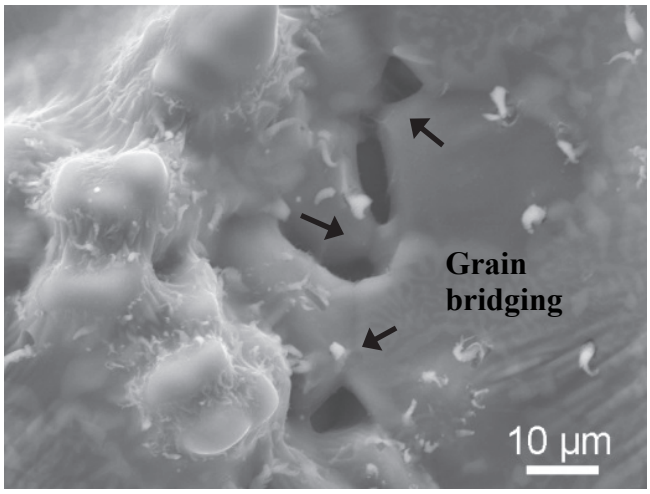

Fig. 6-12 Evidence of grain bridging on fracture surface of Mg-2Ca-0.5Zn alloy cast at T_{mould} = 250 ^{0}C

Inner cracks with grain bridging and gaps between grains or dendritic grains are observed on the fracture surface of the Mg-2Ca-0.5Zn alloy, as shown in Fig. 6-12 (d). These gaps can either grow to a continuous tear or be filled by eutectic. If the contraction force exceeds the strength built up from solid bridging, it is easy for the formed gap (crack) to propagate through the neighbouring grain bridge (liquid metal embrittlement of solid bridges [7]). If the strength built up through grain bridging is high enough to resist the crack propagation, no continuous tear will form. On the other hand, these early formed gaps might be filled with eutectic, which depends on the amount of available eutectic liquid and feeding conditions.

Therefore, based on the observations of fracture surfaces, liquid metal embrittlement of solid bridges is considered as another possible tearing propagation mechanism.

6.3.2.3 Tear propagation

In the present study, two types of tearing propagation were found for Mg-Ca alloys: (i) crack propagation along the dendritic and grain boundaries by liquid film rupture and (ii) crack propagation across the brittle eutectic region. Actually, the second tearing propagation is not typical of hot tear propagation. This will be explained in more detail in the following parts. As the hot tear nucleates at the liquid film, it propagates through the liquid film, as shown in Fig. 6-11.

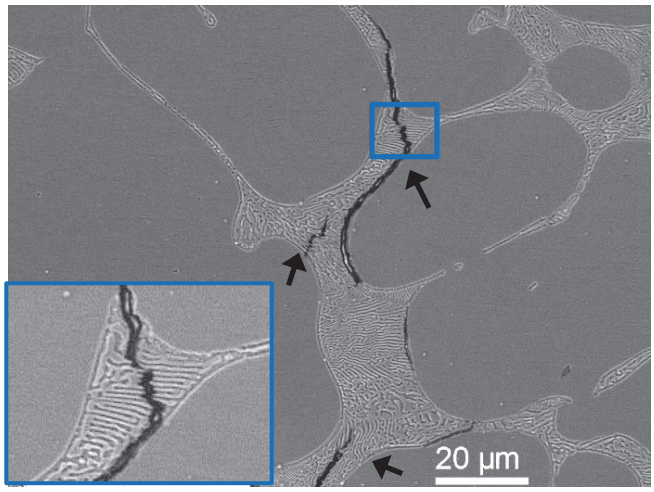

Fig. 6-13 Tear propagates through the eutectic in Mg-2Ca alloy T_{mould} = 250 ^{0}C

Interestingly, crack propagation through the eutectic was evidenced in Mg-2Ca alloy, as shown in Fig. 6-13. The propagation of a crack through eutectic indicated that the eutectic in Mg-Ca alloys is brittle. This phenomenon can also be observed in an SEM micrograph at lower magnification (Fig. 5-10 (d)). The crack propagation through eutectic demonstrates two following viewpoints. The first possibility is that the cracking occurred below the solidus temperature, because the eutectic formed at the end of solidification. According to the tear propagation information shown in Fig. 5-1, the crack propagation of Mg-2Ca alloy terminated at 439 ^{o}C, which is below the solidus temperature. Normally, this kind of cracking is called “cold cracking”. The other possibility is that the brittleness of the intermetallics in Mg-Ca alloys, especially alloys with high content of eutectics, at high temperatures facilitated the propagation of the already formed hot tears. The crack propagation through the eutectic was only evidenced in Mg-2Ca alloy, which contained the largest amount of brittle intermetallic among the studied alloys.

Tear propagation through the eutectic or second phase is also observed in ternary Mg-Ca-Zn alloys, especially in those alloys with large amount of eutectic at the hot spot, as shown in Fig. 6-14. Similar to the tears found for binary Mg-Ca alloys, all the tears found across the eutectic in the Mg-2Ca-4Zn, Mg-2Ca-6Zn and Mg-1Ca-4Zn alloys are fine tears.

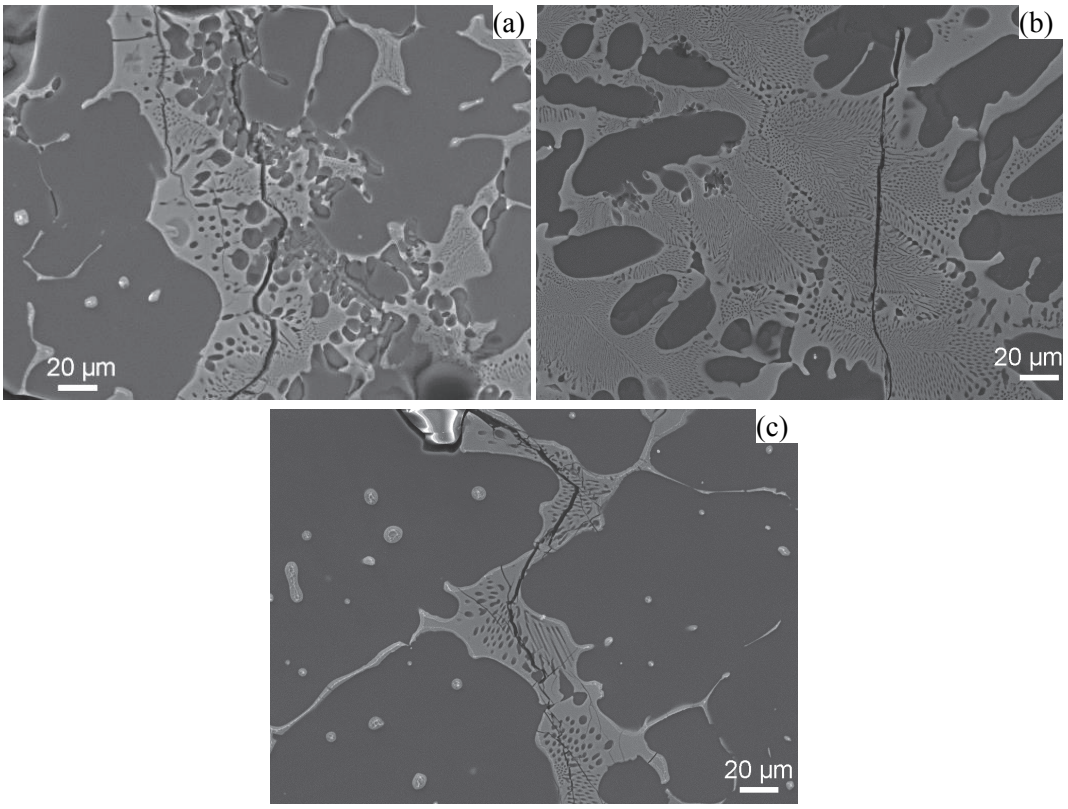

Fig. 6-14 Tear propagates through the eutectic at T_{mould} = 250 ^{0}C in (a) Mg-2Ca-4Zn, (b) Mg-2Ca-6Zn, and (c) Mg-1Ca-4Zn

6.3.3 Tear healing

As mentioned previously, there is liquid remaining after inter-dendritic separation takes places during solidification. If the remaining liquid of eutectic composition is able to flow into the separation gap, it will then solidify into solid eutectic at the eutectic temperature. Thus, the hot tears or interdendritic gaps can be refilled and healed. Detailed liquid healing description can be found in the previous sections. It is concluded that liquid heal of hot tear mainly occures in high Ca-containing alloys cast at a low mould temperature (250 ^{0}C).

The tear healing by eutectic refilling was observed in binary Mg-Ca alloys (Fig. 6-15). For the alloys with low amount of eutectic such as Mg-0.2Ca and Mg-0.5Ca, only the smaller tears (with a small width) were effectively healed. On the other hand, even in the case of Mg-1Ca and Mg-2Ca alloys, the larger tears were healed partially since these alloys contain a higher content of Ca, and in turn greater amount of eutectic (Fig. 5-10 (c) and (d)).

In ternary Mg-Ca-Zn alloys, tearing healing by eutectic is also evidenced, especially in the high Ca containing alloys, such as Mg-1Ca-4Zn and Mg-2Ca-xZn. The typical tear healing of the Mg-2Ca-4Zn and Mg-2Ca-6Zn alloys is shown in Fig. 6-16. Large lamellar eutectic were located either between two tears or in front of the tear. This kind of large lamellar eutectic can effectively "heal" the previously formed hot tear.

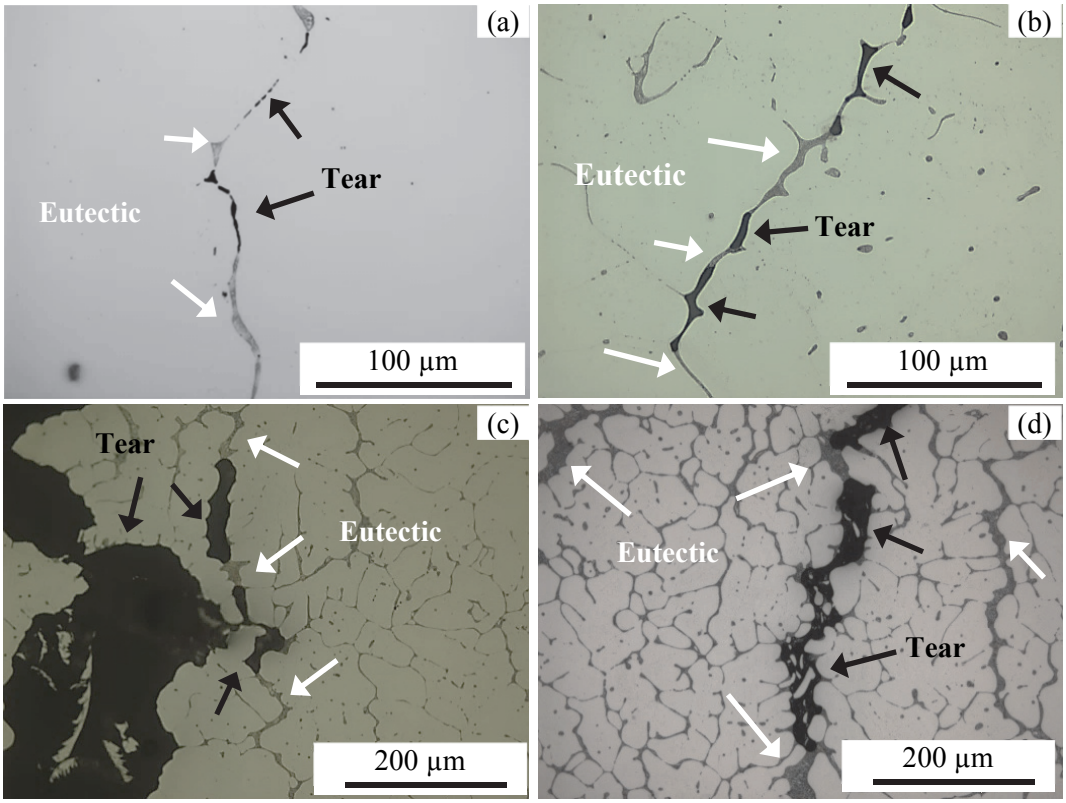

Fig. 6-15 Tear healing of alloys cast at T_{mould} = 250 ^{0}C, (a) Mg-0.2Ca, (b) Mg-0.5Ca, (c) Mg-1Ca, and (d) Mg-2Ca

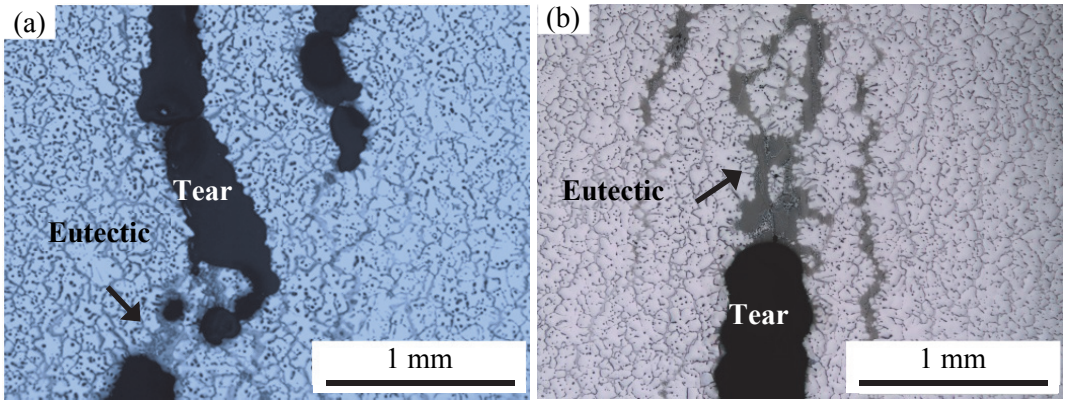

Fig. 6-16 Tear healing of alloys cast at T_{mould} = 250 ^{0}C, (a) Mg-2Ca-4Zn and (b) Mg-2Ca-6Zn

6.3.4 Micropores

Micropores were observed either at the edge or in the centre on the fracture surfaces of both binary Mg-Ca and ternary Mg-Ca-Zn alloys. In this study, it is proposed that the exsistence of micropores proves the alloy has a high HTS.

For Mg-Ca binary alloys, the highest HTS measured for Mg-0.5Ca and Mg-1Ca alloys can further be supported by the observations on the fracture surface of hot tears. The existence of micropores on the fracture surface for Mg-0.5Ca and Mg-1Ca alloys is observed (Fig. 6-17), which are not detected in other Mg-Ca binary alloys. During the casting practice, the solidification initiates from the outside region of the casting due to the fact that the melt first contacts with the colder mould (250°C). After the outer region solidifies, the thermal strains also first accumulate at such regions. On the other hand, the melt fluidity of these two alloys with a small amount of eutectic is not so high. As a result, pores may initiate at the outer region. The earlier formation of these pores at the outer region possibly results in the formation of hot tears at such places in these two alloys. These tears then possibly propagate inward toward the centre of the casting with solidification proceeding, which could lead to the complete rupture of the casting for these two alloys.

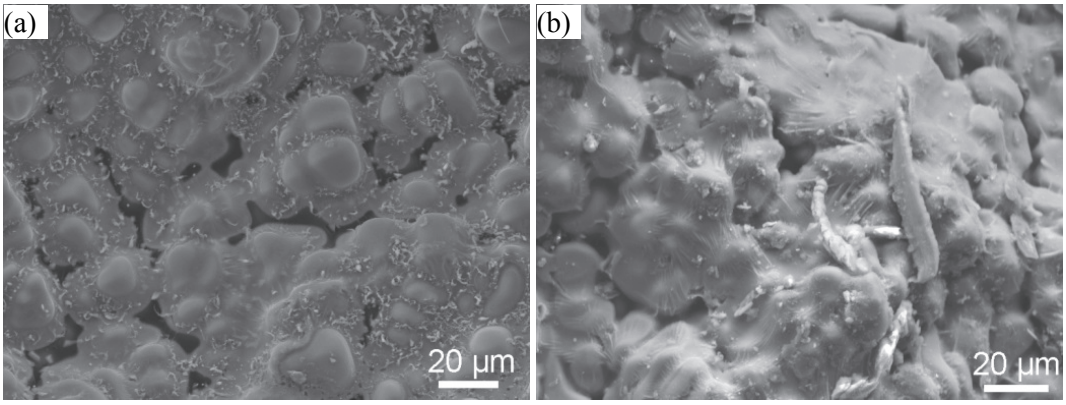

Fig. 6-17 Micro pores at the edge of fracture surface of (a) Mg-0.5Ca and (b) Mg-1Ca, both alloys are cast at T_{mould} = 250 ^{0}C

Micropores at the edge on fracture surface are also evidenced for some of the ternary Mg-Ca-Zn alloys, such as Mg-0.5Ca-xZn (Fig. 5-28) and Mg-0.2Ca-4Zn (Fig. 6-18) at a mould temperature of 250 ^{0}C. Micropores at the edge are not found for the Mg-2Ca-xZn and Mg-1Ca-4Zn alloys. As illustrated in Mg-Ca binary alloys, the existence of the pores at the edge indicated a high HTS of Mg-0.5Ca and Mg-1Ca. Similarly, those ternary Mg-Ca-Zn alloys with micropores at the edge also exhibit a high HTS. It is worth noting that micro pores

are also evidenced in the centre of the hot spot for the Mg-0.5Ca-4Zn and Mg-0.5Ca-6Zn alloys (Fig. 5-28).

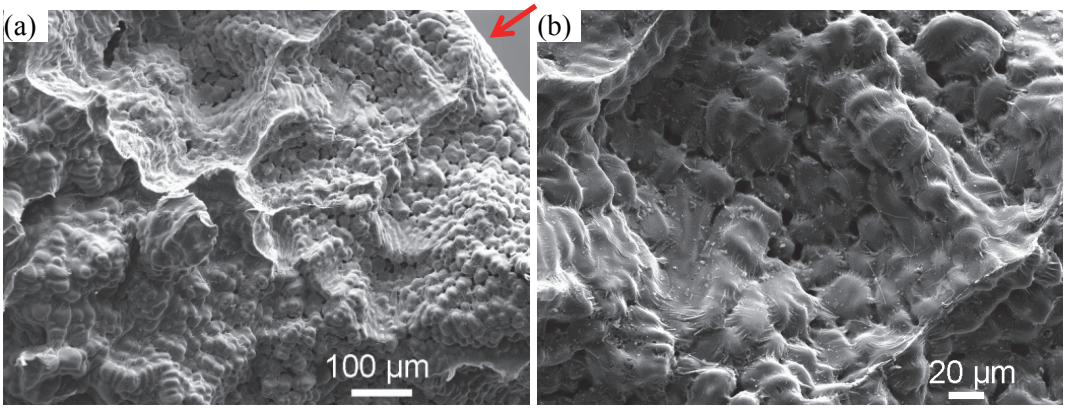

Fig. 6-18 Micro pores at the edge of fracture surface of (a) Mg-0.2Ca-4Zn cast at T_{mould} = 250 ^{0}C and (b) enlarged pore structures.

The formation of the micropores at the edge might be explained as follows. Due to the cooling conditions, the solidification started from the edge (outer region, close to the “cold” mould) to the centre. Thus, small thermal contraction force might generate between the edge and the centre. This thermal contraction force is much lower than the contraction force between the rod and the sprue. Thus, the small contraction force might lead to the formation of micropores in the edge area.

7 Summary

The hot tearing behaviour of Mg-Ca and Mg-Ca-Zn alloys were investigated with an instrumented constrained rod casting (CRC) mould apparatus. The crack volume, measured with X-ray micro-tomography technique, is used as an index for the hot tearing susceptibility (HTS) of alloys. The tearing mechanisms are also discussed. The following conclusions are drawn:

1. Clyne and Davies' thermodynamic model was chosen to predict the compositional dependence on HTS in binary Mg-Ca alloys. The predicted HTS of Mg-Ca alloys first increased with Ca content, reached a maximum at 0.2wt.% Ca, and then decreased with further increasing in the content of Ca to 2 wt.%, hence following the "Λ" shape. The CRC experimental results also show that the curve of HTS as a function of Ca content follows a typical "Λ" shape. However, the prediction and the experimental results display a discrepancy in the peak susceptibility: prediction showed that the peak susceptibility occurs at 0.2wt.% Ca, whereas the peak susceptibility occurred at 0.5 and 1 wt.% Ca in the CRC experiments.

2. The CRC instrument was successfully used to evaluate the HTS of binary Mg-Ca and ternary Mg-Ca-Zn alloys. When hot tearing initiates, force drop or sudden change of force increment is observed on the force-temperature-time curves. Solid fraction corresponding to the tearing initiation (f_{si}) for binary Mg-0.5Ca and Mg-1Ca alloys cast at T_{mould} = 250 °C was relatively low, which was due to their high HTS. The hot tearing in binary Mg-Ca-Zn alloys initiates at a solid fraction range from 0.519 to 0.955, depending on composition and initial mould temperature. The constraint from the load screw plays a key role in hot tearing. Most hears occurred at the exact sprue-rod junction (i.e. hot spot region). Some tears in the ternary alloys cast at T_{mould} = 250 °C tend to occur on the rod portion about 1-5 mm away from the exact sprue-rod junction. Due to the presense of oxide inclusions, tears in Mg-0.5Ca and Mg-1Ca alloys cast at T_{mould} = 450 °C sometimes occurred in the middle of the rod. Tears in some ternary Mg-Ca-Zn alloys cast at T_{mould} = 450 °C were observed at the load screw. This is owing to the stress concentration at the load screw, the long solidification time and the high HTS of those alloys.

3. The initiation and propagation of hot tearing are influenced by mould temperature, grain size, freezing range, and amount of eutectic/second phase. The increment in mould

temperature from 250 to 450 ^{0}C significantly reduces the HTS of binary Mg-Ca alloys and ternary Mg-Ca-Zn alloys. High initial mould temperature reduces the cooling rate resulting in a small thermal gradient and low strain rate imposed on the solidifying casting. Refined grain size (Zr addition), narrow freezing range and large amount of eutectic lead to a small HTS. High amount of remaining liquid at the time of hot tearing might result in a large quantity of either liquid film agglomerates or large lamellar eutectic near the hot tears. Only the large lamellar eutectic was able to heal the previously formed tears. Eutectic healing does not always occur at the final eutectic temperature for ternary alloys due to insufficient amount of liquid. It also happens when some phases form before the final eutectic temperature.

4. The simulation of HTS for binary Mg-Ca alloys and ternary Mg-Ca-Zn alloys using HTI based on the accumulated elastic and plastic strain at the last stages of solidification by ProCAST software is in good agreement with the experimental tear location.

5. The hot tears initiate at the grain boundaries and propagate along the grain boundaries through thin film rupture and rupture of solid bridges. Micropores were observed either at the edge or in the centre on the fracture surfaces of both binary Mg-Ca and ternary Mg-Ca-Zn alloys. The existence of micropores proves the alloy has a high HTS.

Outlook:

- This thesis has predicted the hot tearing tendency of binary alloys based on Clyne and Davies' model. The predicted tendencies correlated well with experimental results. However, there is still disrepency in the peak susceptibility between the prediction and experimental results. Moreover, the Clyne and Davies' model is not capable of predicting hot tearing susceptibility in multi-component system. Thus, it is necessary to modify the Clyne and Davies' model or develop a new hot tearing creterion.

- Future work should improve hot tearing theories. The theories may lead to establishment of new predicted models that can be evaluable to all alloy systems.

- A standard hot tearing test system needs to be established and developed which is applicable to all casting alloys and types. In order to quantify the hot tearing tendency, a consistent approach should be agreed upon.

- New techniques (i.e. *in situ* tomography) should be introduced in the investigation of hot tearing behaviour.

8 Acknowledgements

I gratefully acknowledge the financial support of the Chinese Science Council (CSC).

This thesis would not have been finished without the contribution of the following people that I would like to acknowledge sincerely.

I would like to thank my supervisor Prof. Dr. Karl Ulrich Kainer for all of his help and guidance during my research. I also specially thank Prof. Dr. Babette Tonn for her agreement to be the chief reviewer of this work and her valuable suggestions to complete this study.

I sincerely want to thank Dr. Norbert Hort and Dr. Yuanding Huang for their scientific and fruitful discussions during this work. I learned a lot from the discussions on hot teaing of magnesium alloys with them.

Many thanks also to Dr. Francesco D'Elia and Dr. Zhi Wang for their helps in experiments, results analysis, and valuable discussions.

I would like to thank Dr. Amirthalingam Srinivasan and Dr. Chamini Mendis for their helpful discussion and English improvement. Moreover, experiments help from Dr. Felix Beckmann and Dr. Jie Cheng is also greately acknowledged.

Many thanks to Mr. Günter Meister, Mr. Gert Wiese, Mrs. Petra Fischer and Mrs. Sabine Schubert for their excellent technical help. I also gratitude all the staffs of WZP group for their assistance and the great working atmosphere during my stay.

Finally, I would like to thank my parents and all my friends. Without their support, encouragement, and patience, I would not have come so far!

9 References

[1] A. Luo. Magnesium: Current and potential automotive applications. JOM: Journal of Minerals, Metals and Materials Society. 2002;54:42-48.

[2] H. E. Friedrich, B. L. Mordike. Magnesium technology. Germany: Springer Berlin Heidelberg; 2006.

[3] L. Katgerman, D. G. Eskin. In search of the prediction of hot cracking in aluminium alloys. Hot Cracking Phenomena in Welds II. Berlin: Springer Berlin Heidelberg; 2008. p. 11-26.

[4] Z. S. Zhen, N. Hort, Y. D. Huang, O. Utke, N. Petri, K. U. Kainer. Hot tearing behaviour of binary Mg–1Al alloy using a contraction force measuring method. International Journal of Cast Metals Research. 2009;22:331-334.

[5] G. Cao, C. Zhang, H. Cao, Y. A. Chang, S. Kou. Hot-tearing susceptibility of ternary Mg-Al-Sr alloy castings. Metallurgical and Materials Transactions A. 2010;41:706-716.

[6] D. G. Eskin, Suyitno, L. Katgerman. Mechanical properties in the semi-solid state and hot tearing of aluminium alloys. Progress In Materials Science. 2004;49:629-711.

[7] D. G. Eskin, L. Katgerman. A quest for a new hot tearing criterion. Metallurgical and Materials Transactions A. 2007;38:1511-1519.

[8] Z. Zhen, N. Hort, Y. Huang, N. Petri, O. Utke, K. U. Kainer. Quantitative determination on hot tearing in Mg-Al binary alloys. Materials Science Forum. 2009;618-619:533-540.

[9] Z. Wang, J. Song, Y. Huang, A. Srinivasan, Z. Liu, K. Kainer, et al. An investigation on hot tearing of Mg-4.5Zn-(0.5Zr) alloys with Y additions. Metallurgical and Materials Transactions A. 2015;46:2108-2118.

[10] T. W. Clyne, G. J. Davies. Comparison between experimental data and theoretical predictions relating to dependence of solidification cracking on composition. Solidification and casting of metals. London: Metals society; 1979. p. 275-278.

[11] M. Rappaz, J. M. Drezet, M. Gremaud. A new hot tearing criterion. Metallurgical and Materials Transactions A. 1999;30:449-455.

[12] D. Viano, D. StJohn, J. Grandfield, C. Cáceres. Hot tearing in aluminium-copper alloys. In: H. Kvande, editor. California: TMS; 2005. p. 895-899.

[13] M. Easton, H. Wang, J. Grandfield, D. StJohn, E. Sweet. An analysis of the effect of grain refinement on the hot tearing of aluminium alloys. Materials Forum. 2004;28:224-229.

[14] S. Li. Hot tearing in cast aluminum alloys: Measures and effects of process variables [Doctoral thesis]. Worcester, America: Worcester Polytechnic Institute; 2010.

[15] H. Huang, P. Fu, Y. Wang, L. Peng, H. Jiang. Effect of pouring and mold temperatures on hot tearing susceptibility of AZ91D and Mg–3Nd–0.2Zn–Zr Mg alloys. Transactions of Nonferrous Metals Society of China. 2014;24:922-929.

[16] Y. D. Huang, Z. Wang, A. Srinivasan, K. U. Kainer, N. Hort. Metallurgical characterization of hot tearing curves recorded during solidification of magnesium alloys. Acta Physica Polonica A. 2012;122:497-500.

[17] G. Cao, S. Kou. Hot cracking of binary Mg–Al alloy castings. Materials Science and Engineering: A. 2006;417:230-238.

[18] L. Zhou, Y. D. Huang, P. L. Mao, K. U. Kainer, Z. Liu, N. Hort. Influence of composition on hot tearing in binary Mg–Zn alloys. International Journal of Cast Metals Research. 2011;24:170-176.

[19] Z. Wang, Y. D. Huang, A. Srinivasan, Z. Liu, F. Beckmann, K. U. Kainer, et al. Hot tearing susceptibility of binary Mg–Y alloy castings. Materials & Design. 2013;47:90-100.

[20] A. Srinivasan, Z. Wang, Y. D. Huang, F. Beckmann, K. Kainer, N. Hort. Hot tearing characteristics of binary Mg-Gd alloy castings. Metallurgical and Materials Transactions A. 2013;44:2285-2298.

[21] Z. Wang, Y. D. Huang, A. Srinivasan, Z. Liu, K. U. Kainer, N. Hort. Influences of Y additions on the hot tearing susceptibility of Mg-1.5wt.%Zn alloys. Materials Science Forum. 2013;765:306-310.

[22] P. Gunde, A. Schiffl, P. J. Uggowitzer. Influence of yttrium additions on the hot tearing susceptibility of magnesium–zinc alloys. Materials Science and Engineering: A. 2010;527:7074-7079.

[23] G. Cao, S. Kou. Hot tearing of ternary Mg-Al-Ca alloy castings. Metallurgical and Materials Transactions A. 2006;37:3647-3663.

[24] G. Cao, I. Haygood, S. Kou. Onset of hot tearing in ternary Mg-Al-Sr alloy castings. Metallurgical and Materials Transactions A. 2010;41:2139-2150.

[25] L. Zhou, Y. D. Huang, P. L. Mao, K. U. Kainer, Z. Liu, N. Hort. Investigations on hot Ttearing of Mg-Zn-(Al) alloys. In: W. H. Sillekens, S. R. Agnew, N. R. Neelameggham, S. N. Mathaudhu, editors. John Wiley & Sons; 2011. p. 125-130.

[26] Y. Wang, Q. Wang, G. Wu, Y. Zhu, W. Ding. Hot-tearing susceptibility of Mg–9Al–xZn alloy. Materials Letters. 2002;57:929-934.

[27] W. Zheng, S. Li, B. Tang, D. Zeng, X. Guo. Effect of rare earths on hot cracking resistant property of Mg-Al alloys. Journal of Rare Earths. 2006;24:346-351.

[28] Y. Wang, Q. Wang, G. Wu, Y. Zhu, W. Ding. Hot tearing susceptibility of Mg-9Al-xZn alloy. Materials Letters. 2002;57:929–934.

[29] S. Li, B. Tang, X. Y. Jin, D. B. Zeng. An investigation on hot-cracking mechanism of Sr addition into Mg–6Al–0.5Mn alloy. Journal of Materials Science. 2012;47:2000-2004.

[30] Q. D. Wang, W. D. Chen, X. Q. Zeng, Y. Z. Lu, W. J. Ding, Y. P. Zhu, et al. Effects of Ca addition on the microstructure and mechanical properties of AZ91 magnesium alloy. Journal of Materials Science. 2001;36:3035-3040.

[31] A. A. Luo, M. P. Balogh, B. R. Powell. Creep and microstructure of magnesium-aluminum-calcium based alloys. Metallurgical and Materials Transactions A. 2002;33:567-574.

[32] W. C. Kim, J. G. Kim, J. Y. Lee, H. K. Seok. Influence of Ca on the corrosion properties of magnesium for biomaterials. Materials Letters. 2008;62:4146-4148.

[33] Y. Wan, G. Xiong, H. Luo, F. He, Y. Huang, X. Zhou. Preparation and characterization of a new biomedical magnesium-calcium alloy. Materials & Design. 2008;29:2034-2037.

[34] H. R. Bakhsheshi-Rad, M. H. Idris, M. R. Abdul-Kadir. Synthesis and in vitro degradation evaluation of the nano-HA/MgF2 and DCPD/MgF2 composite coating on biodegradable Mg–Ca–Zn alloy. Surface and Coatings Technology. 2013;222:79-89.

[35] L. B. Tong, M. Y. Zheng, X. S. Hu, K. Wu, S. W. Xu, S. Kamado, et al. Influence of ECAP routes on microstructure and mechanical properties of Mg–Zn–Ca alloy. Materials Science and Engineering: A. 2010;527:4250-4256.

[36] B. Zhang, Y. Hou, X. Wang, Y. Wang, L. Geng. Mechanical properties, degradation performance and cytotoxicity of Mg–Zn–Ca biomedical alloys with different compositions. Materials Science and Engineering: C. 2011;31:1667-1673.

[37] B. P. Zhang, Y. Wang, L. Geng. Research on Mg-Zn-Ca alloy as degradable biomaterial. In: R. Pignatello, editor. Biomaterials - Physics and Chemistry: InTech; 2011. p. 183-204.

[38] Y. Sun, B. Zhang, Y. Wang, L. Geng, X. Jiao. Preparation and characterization of a new biomedical Mg–Zn–Ca alloy. Materials & Design. 2012;34:58-64.

[39] X. Gao, S. M. Zhu, B. C. Muddle, J. F. Nie. Precipitation-hardened Mg–Ca–Zn alloys with superior creep resistance. Scripta Materialia. 2005;53:1321-1326.

[40] T. W. Clyne, G. J. Davies. The influence of composition on solidification cracking in binary alloy systems. Brit Foundryman. 1981;74:65-73.

[41] T. W. Clyne, G. J. Davies. A quantitative solidification cracking test for castings and an evaluation of cracking in aluminium-magnesium alloys. British Foundryman. 1975;68:238-244.

[42] L. Katgerman. A mathematical model for hot cracking of aluminum alloys during D.C. Casting. JOM: Journal of Minerals, Metals and Materials Society. 1982;34:46-49.

[43] M. Braccini, C. L. Martin , M. Suery, Y. Brechet. Relation between mushy yone rheology and hot tearing phenomena in Al-Cu. Modeling of Casting, Welding and Advanced Solidification Processes IX. Aachen, Germany: Shaker Verlag GmbH; 2000. p. 18-24.

[44] J. F. Grandfield, C. J. Davidson, J. A. Taylor. Application of a new hot tearing analysis to horizontal direct chili cast magnesium alloy AZ91. Light Metals 2001. 2001:895-901.

[45] Suyitno, W.H.Kool, L. Katgerman. Micro-mechanical model of hot tearing at triple junctions in DC casting. Materials Science Forum. 2002;396-402:179-184.

[46] Suyitno, W. H. Kool, L. Katgerman. Hot tearing criteria evaluation for direct-chill casting of an Al-4.5 Pct Cu alloy. Metallurgical and Materials Transactions A. 2005;36:1537-1546.

[47] L. Zhou, Y. D. Huang, P. L. Mao, K. U. Kainer, Z. Liu, N. Hort. Influence of composition on hot tearing in binary Mg-Zn alloys. International Journal of Cast Metals Research. 2011;24:170-176.

[48] A. R. E. Singer, P. H. Jennings. Hot-shortness of some aluminium-iron-silicon alloys of high purity. Journal of the Institute of Metals. 1946;73:273-284.

[49] P. H. Jennings, A. R. E. Singer, W. I. Pumphrey. Hot-shortness of some high-purity alloys in the systems aluminium copper silicon and aluminium magnesium silicon. Journal of the Institute of Metals. 1948;74:227-246.

[50] D. Warrington, D. G. McCartney. Hot-cracking in aluminium alloys 7050 and 7010-a comparative study. Cast Metals. 1991;3:202-208.

[51] J. M. Drezet, M. Rappaz. Study of hot tearing in aluminum alloys using the ring mold test. In: B. G. Thomas, C.Beckermann, editors. Modeling of casting, welding, and advanced solidification process VIII. San Antonio, Texas, USA 1998. p. 883-890.

[52] D. M. Viano. Hot tearing in aluminium alloys [Doctoral thesis]. Australia: University of Queensland; 2011.

[53] S. S. Li, B. Tang, X. Y. Jin, D. B. Zeng. An investigation on hot-cracking mechanism of Sr addition into Mg-6Al-0.5Mn alloy. Journal of Materials Science. 2012;47:2000-2004.

[54] Z. Zhen, O. Utke, W. Punessen, N. Hort, K. U. Kainer. Vorrichtung zur Bestimmung der Heißrissempfindlichkeit von metallischen Schmelzen. In: E. PATENTANMELDUNG, editor. Germany2008.

[55] S. Li, D. Apelian, K. Sadayappan. Hot tearing in cast Al alloys: mechanisms and process controls. Transactions of the American Foundry Society. 2012;120:149-155.

[56] S. Instone, D. StJohn, J. Grandfield. New apparatus for characterising tensile strength development and hot cracking in the mushy zone. International Journal of Cast Metals Research. 2000;12:441-456.

[57] I. Farup, J. M. Drezet, M. Rappaz. IN situ observation of hot tearing formation in succinonitrile acetone. Acta Materialia. 2001;49:1261-1269.

[58] C. Davidson, D. Viano, L. Lu, D. StJohn. Observation of crack initiation during hot tearing. International Journal of Cast Metals Research. 2006;19:59-65.

[59] A. B. Phillion, R. W. Hamilton, D. Fuloria, A. C. L. Leung, P. Rockett, T. Connolley, et al. In situ X-ray observation of semi-solid deformation and failure in Al–Cu alloys. Acta Materialia. 2011;59:1436-1444.

[60] M. Sistaninia, S. Terzi, A. B. Phillion, J. M. Drezet, M. Rappaz. 3-D granular modeling and in situ X-ray tomographic imaging: A comparative study of hot tearing formation and semi-solid deformation in Al–Cu alloys. Acta Materialia. 2013;61:3831-3841.

[61] C. Puncreobutr, P. D. Lee, K. M. Kareh, T. Connolley, J. L. Fife, A. B. Phillion. Influence of Fe-rich intermetallics on solidification defects in Al–Si–Cu alloys. Acta Materialia. 2014;68:42-51.

[62] H. R. Abedi, A. Zarei-Hanzaki, S. M. Fatemi-Varzaneh, A. A. Roostaei. The semi-solid tensile deformation behavior of wrought AZ31 magnesium alloy. Materials & Design. 2010;31:4386-4391.

[63] M. Easton, J. Grandfield, D. StJohn, B. Rinderer. The effect of grain refinement and cooling rate on the hot tearing of wrought aluminium alloys. Materials Science Forum. 2006;519-521:1675-1680.

[64] A. Srinivasan, Z. Wang, Y. D. Huang, F. Beckmann, K. U. Kainer, N. Hort. Hot tearing susceptibility of magnesium-gadolinium binary alloys. Transactions of the Indian Institute of Metals. 2012;65:701-706.

[65] L. Bichler, A. Elsayed, K. Lee, C. Ravindran. Influence of mold and pouring temperatures on hot tearing susceptibility of AZ91D magnesium alloy. International Journal of Metalcasting. 2008;2:43-56.

[66] Z. Wang, Y. Huang, A. Srinivasan, Z. Liu, F. Beckmann, K. Kainer, et al. Experimental and numerical analysis of hot tearing susceptibility for Mg–Y alloys. Journal of Materials Science. 2014;49:353-362.

[67] Z. Wang, Y. D. Huang, Z. Zhen, Z. Liu, K. U. Kainer, N. Hort. Hot tearing of magnesium alloys. International Magnesium Association 70th Annual World Magnesium Conference. Xian, China 2013. p. 53-63.

[68] Z. Zhen, N. Hort, O. Utke, Y. Huang, N. Petri, K. U. Kainer. Investigations on hot tearing of Mg-Al binary alloys by using a new quantitative method. In: E. A. Nyberg, S. R. Agnew, N. R. Neelameggham, M. O. Pekguleryuz, editors. TMS Wiley; 2009. p. 105-110.

[69] M. G. Pokorny. Prediction of hot tear formation for binary magnesium-aluminium alloys in a permanent mold [Master thesis]. America: University of Iowa; 2009.

[70] W. Gan, Y. Huang, Z. Wang, N. Hort, M. Hofmann. Residual stresses near the hot sprues of as-cast Mg-Zn alloys investigated by STRESS-SPEC neutron diffractometer. Materials Science Forum. 2014;768-769:428-432.

[71] Z. Wang, Y. D. Huang, A. Srinivasan, Z. Liu, K. U. Kainer, N. Hort. Prediction of hot tearing tendency for binary Mg-Y alloys. In: J.T. Cieslinski, J. A. Szymczyk, editors. Developments in mechanical engineering. Strasund, Germany 2012. p. 191-197

[72] Y. Wang, B. Sun, Q. Wang, Y. Zhu, W. Ding. An understanding of hot tearing mechanism in AZ91 magnesium alloy. Materials Letters. 2002;53:35-39.

[73] M. Pekguleryuz, P. Labelle, D. Argo, E. Baril. Magnesium diecasting alloy AJ62X with superior creep resistance, ductility and diecastability. In: H. I. Kaplan, editor. TMS2003. p. 201-206.

[74] B. R. Powell, A. A. Luo, B. L. Tiwari, V. Rezhets. The die castability of calcium-containing magnesium alloys: Thin-wall computer case. Magnesium Technology 2002. 2002:123-129.

[75] B. Tang, S.-S. Li, X.-S. Wang, D.-B. Zeng, R. Wu. Effect of Ca/Sr composite addition into AZ91D alloy on hot-crack mechanism. Scripta Materialia. 2005;53:1077-1082.

[76] Z. J. Li, X. N. Gu, S. Q. Lou, Y. F. Zheng. The development of binary Mg-Ca alloys for use as biodegradable materials within bone. Biomaterials. 2008;29:1329-1344.

[77] D. Q. Tan, X. X. Yang, Y. J. Zhan, D. F. Xiao. On ignition point of Mg-Ca alloy under nitrogen atmosphere. China Foundry. 2011;8:282-285.

[78] D. B. Lee. High temperature oxidation of AZ31+0.3 wt.% Ca and AZ31+0.3 wt.%CaO magnesium alloys. Corrosion Science. 2013;70:243-251.

[79] D. H. StJohn, M. Qian, M. A. Easton, P. Cao, Z. Hildebrand. Grain refinement of magnesium alloys. Metallurgical and Materials Transactions A. 2005;36:1669-1679.

[80] P. Li, B. Tang, E. G. Kandalova. Microstructure and properties of AZ91D alloy with Ca additions. Materials Letters. 2005;59:671-675.

[81] B. Zhang, Y. Wang, L. Geng, C. Lu. Effects of calcium on texture and mechanical properties of hot-extruded Mg–Zn–Ca alloys. Materials Science and Engineering: A. 2012;539:56-60.

[82] L. B. Tong, M. Y. Zheng, L. R. Cheng, S. Kamado, H. J. Zhang. Effect of extrusion ratio on microstructure, texture and mechanical properties of indirectly extruded Mg–Zn–Ca alloy. Materials Science and Engineering: A. 2013;569:48-53.

[83] M. Salahshoor, Y. B. Guo. Biodegradable orthopedic magnesium-calcium (MgCa) alloys, processing, and corrosion performance. Materials. 2012;5:135-155.

[84] H. Somekawa, T. Mukai. High strength and fracture toughness balance on the extruded Mg–Ca–Zn alloy. Materials Science and Engineering: A. 2007;459:366-370.

[85] G. Levi, S. Avraham, A. Zilberov, M. Bamberger. Solidification, solution treatment and age hardening of a Mg–1.6 wt.% Ca–3.2 wt.% Zn alloy. Acta Materialia. 2006;54:523-530.

[86] J. F. Nie, B. C. Muddle. Precipitation hardening of Mg-Ca(-Zn) alloys. Scripta Materialia. 1997;37:1475-1481.

[87] L. B. Tong, M. Y. Zheng, S. W. Xu, S. Kamado, Y. Z. Du, X. S. Hu, et al. Effect of Mn addition on microstructure, texture and mechanical properties of Mg–Zn–Ca alloy. Materials Science and Engineering: A. 2011;528:3741-3747.

[88] J. H. Gao, S. K. Guan, Z. W. Ren, Y. F. Sun, S. J. Zhu, B. Wang. Homogeneous corrosion of high pressure torsion treated Mg–Zn–Ca alloy in simulated body fluid. Materials Letters. 2011;65:691-693.

[89] E. W. Postek, R. W. Lewis, D. T. Gethin. Finite element modelling of the squeeze casting process. International Journal of Numerical Methods For Heat & Fluid Flow. 2008;18:325-355.

[90] N. Hatami, R. Babaei, M. Dadashzadeh, P. Davami. Modeling of hot tearing formation during solidification. Journal of Materials Processing Technology. 2008;205:506-513.

[91] J. Z. Zhu, J. Guo, M. T. Samonds. Numerical modeling of hot tearing formation in metal casting and its validations. International Journal For Numerical Methods In Engineering. 2011;87:289-308.

[92] ESI Group Inc. ProCAST 2030.0 User Manual. 2013.

[93] L. Bichler, C. Ravindran. New developments in assessing hot tearing in magnesium alloy castings. Materials & Design. 2010;31:S17-S23.

[94] M. Pokorny, C. Monroe, C. Beckermann, L. Bichler, C. Ravindran. Prediction of hot tear formation in a magnesium alloy permanent mold casting. International Journal of Metalcasting. 2008;2:41-53.

[95] S. Hadzic, E. S. Kelty, C. Sommitsch. Prediction and validation of hot tearing in permanent mold steel casting using a viscoplastic damage model. Computer methods in materials science. 2013;13:36-42.

[96] S. Norouzi, A. Shams, H. Farhangi, A. Darvish. The temperature range in the simulation of residual stress and hot tearing during investment casting. World Academy of Science, Engineering and Technology. 2009;58:283-289.

[97] M. G. Pokorny, C. A. Monroe, C. Beckermann, Z. Zhen, N. Hort. Simulation of stresses during casting of binary magnesium aluminum alloys. TMS magnesium technology2010. p. 401-407.

[98] C. A. Monroe, C. Beckermann, J. Klinkhammer. Simulation of deformation and hot tear formation using a visco-plastic model with damage. TMS 2009. p. 313-320.

[99] M. Sistaninia, A. B. Phillion, J. M. Drezet, M. Rappaz. A 3-D coupled hydromechanical granular model for simulating the constitutive behavior of metallic alloys during solidification. Acta Materialia. 2012;60:6793-6803.

[100] W. M. van Haaften, W. H. Kool, L. Katgerman. Hot tearing studies in AA5182. Journal of Materials Engineering And Performance. 2002;11:537-543.

[101] F. D'Elia, C. Ravindran, D. Sediako, K. U. Kainer, N. Hort. Hot tearing mechanisms of B206 aluminum–copper alloy. Materials & Design. 2014;64:44-55.

[102] M. M'Hamdi, A. Mo, H. Fjær. TearSim: A two-phase model addressing hot tearing formation during aluminum direct chill casting. Metallurgical and Materials Transactions A. 2006;37:3069-3083.

[103] M. Qian, A. Das. Grain refinement of magnesium alloys by zirconium: Formation of equiaxed grains. Scripta Materialia. 2006;54:881-886.

[104] M. Sun, M. A. Easton, D. H. StJohn, G. H. Wu, T. B. Abbott, W. J. Ding. Grain refinement of magnesium alloys by Mg-Zr master alloys: The role of alloy chemistry and Zr particle number density. Advanced Engineering Materials. 2013;15:373-378.

[105] D. H. Stjohn, M. A. Easton, M. Qian, J. A. Taylor. Grain refinement of magnesium alloys: A review of recent research, theoretical developments, and their application. Metallurgical and Materials Transactions A. 2013;44:2935-2949.

[106] S. Lin, C. Aliravci, M. O. Pekguleryuz. Hot-tear susceptibility of aluminum wrought alloys and the effect of grain refining. Metallurgical and Materials Transactions A. 2007;38:1056-1068.

[107] M. A. Easton, M. A. Gibson, S. M. Zhu, T. B. Abbott. An a priori hot-tearing indicator applied to die-cast magnesium-rare earth alloys. Metallurgical and Materials Transactions A. 2014;45:3586-3595.

[108] S. M. Li, K. Sadayappan, D. Apelian. Role of grain refinement in the hot tearing of cast Al-Cu alloy. Metallurgical and Materials Transactions B. 2013;44:614-623.

[109] L. Sweet, M. A. Easton, J. A. Taylor, J. F. Grandfield, C. J. Davidson, L. M. Lu, et al. Hot tear susceptibility of Al-Mg-Si-Fe alloys with varying iron contents. Metallurgical and Materials Transactions A. 2013;44a:5396-5407.

[110] I. Antoniac, M. Dinu. Microstructural and mechanical features of Mg-Ca alloys. 2011 E-Health and Bioengineering Conference (Ehb). 2011.

[111] Y. S. Jeong, W. J. Kim. Enhancement of mechanical properties and corrosion resistance of Mg–Ca alloys through microstructural refinement by indirect extrusion. Corrosion Science. 2014;82:392-403.

[112] John F. Grandfield, Dmitry G. Eskin, I. F. Brainbridge. Direct-chill casting of light alloys New Jersey: Wiley; 2013.

[113] J. Campbell. Casting. Second ed. Great Britain: Elsevier Science Ltd.; 2003.

[114] W. S. Pellini. Strain theory of hot tearing. Foundry. 1952;80:125-199.

[115] Z. Wang. Hot tearing of Mg-Y and Mg-Y-Zn alloys [Doctoral thesis]. Germany: Clausthal University of Technology; 2014.

[116] H. R. Bakhsheshi-Rad, M. R. Abdul-Kadir, M. H. Idris, S. Farahany. Relationship between the corrosion behavior and the thermal characteristics and microstructure of Mg–0.5Ca–xZn alloys. Corrosion Science. 2012;64:184-197.

[117] F. Naghdi, R. Mahmudi. The microstructure and creep characteristics of cast Mg–4Zn–0.5Ca and Mg–4Zn–0.5Ca–2RE alloys. Materials Science and Engineering: A. 2014;610:315-325.

[118] F. D'Elia, C. Ravindran, D. Sediako. Interplay among solidification, microstructure, residual strain and hot tearing in B206 aluminum alloy. Materials Science and Engineering: A. 2015;624:169-180.

[119] Suyitno, D. G. Eskin, L. Katgerman. Structure observations related to hot tearing of Al-Cu billets produced by direct-chill casting. Materials Science and Engineering A. 2006;420:1-7.

10 Publication list during doctoral study

Journal papers

- J. Song, Z. Wang, Y. D. Huang, A. Srinivasan, F. Beckmann, K. U. Kainer, N. Hort. Hot tearing susceptibility of Mg-Ca binary alloys. **Metallurgical and Materials Transactions A**, 2015, 46(12): 6003-6017.

- J. Song, Z. Wang, Y. D. Huang , A. Srinivasan , F. Beckmann , K. U. Kainer , N. Hort. Hot tearing characteristics of Mg–2Ca–xZn alloys. **Journal of Materials Science**, 2016, 51(5): 2687-2704.

- J. Song, Z. Wang, Y. D. Huang, A. Srinivasan, F. Beckmann, K. U. Kainer, N. Hort. Effect of Zn addition on hot tearing behaviour of Mg–0.5Ca–xZn alloys. **Materials & Design**, 2015, 87: 157-170

- Z. Wang, J. Song, Y. D. Huang, A. Srinivasan, Z. Liu, K. U. Kainer, N. Hort. An Investigation on Hot Tearing of Mg-4.5Zn-(0.5Zr) Alloys with Y Additions. **Metallurgical and Materials Transactions A**, 2015, 46(5): 2108-2118.

Conference contributions

- J. Song, Z. Wang, Y. D. Huang, K. U. Kainer, N. Hort. Influences of Ca Addition on the Hot Tearing Behaviour of Mg-4Zn-xCa Alloys, **The 10th International Conference on Magnesium Alloys and Their Applications**, Oct 11-16, 2015, Jeju, Korea **(Oral presentation, presented by colleague)**

- J. Song, H. Dieringa, Y. D. Huang, W. Gan, K. U. Kainer, N. Hort. Mechanical properties and microstructures of nano SiC reinforced ZE10 composites prepared with ultrasonic vibration. **Advanced Materials Research**, 2014, 1019: 169-176. **AMI Light Metals Conference 2014**, Oct. 15-17, 2014, Pilanesburg National Park, South Africa **(Oral presentation, speaker)**

- J. Song, Y. D. Huang, K. U. Kainer, W. Gan, N. Hort. Residual stresses of the as-cast Mg-xCa alloys with hot sprues by neutron diffraction. **9th European Conference on Residual Stresses (ECRS-9)**, Jul. 7-10, 2014, University of Technology of Troyes, France **(Poster, presented by colleague)**

Other conferences

- J. Song, Z. Wang, Y. D. Huang, K. U. Kainer, N. Hort. Influences of Zn Addition on the Hot Tearing Behaviour of Mg-0.5 wt. % Ca Alloy. **Junior Euromat 2014**, Jul. 21-25, 2014, Lausanne, Switzerland (**3 min Oral presentation + poster, speaker**).

- J. Song, Z. Wang, Y. D. Huang, K. U. Kainer, N. Hort. Hot tearing susceptibility of Mg-Ca alloys. **4th International Conference on Advances in Solidification Processes (ICASP-4),** Jul. 8-11, 2014, Old Windsor, UK (**Oral presentation, speaker**).

Curriculum Vitae

Personal information

First name: Jiangfeng

Last name: Song

Gender: Female

Date of birth: 18.03.1987

Email: songjf0303@gmail.com

Education

2012-2015 Doctoral Candidate at Institute of Metallurgy, Clausthal University of Technology, Germany

2009-2012 Master of Materials Science and Engineering, Central South University, China

2005-2009 Bachelor of Materials Chemistry, Central South University, China

Professional experience

2012-2015 Research assistant at Magnesium Innovation Centre, Helmholtz-Zentrum Geesthacht (HZG), Germany

Signature:

Date: